IONIC LIQUID ELECTROCHEMICAL PROCESSING OF REACTIVE METALS

by

JAMES VAUGHAN

M.A.Sc., The University of British Columbia, 2003
B.Eng., McGill University, 2001

A THESIS SUBMITTED IN PARTIAL FULFILLMENT OF
THE REQUIREMENTS FOR THE DEGREE OF

DOCTOR OF PHILOSOPHY

in

The Faculty of Graduate Studies

(Materials Engineering)

THE UNIVERSITY OF BRITISH COLUMBIA

November 2007

© James Vaughan, 2007

Abstract

Ionic liquids (ILs) were studied as solvents for electrochemical reactions with the intent to devise metallurgical processes for Al, Mg and Ti that are less energy intensive and operate at lower temperatures than current industrial practice. Tetra-alkyl phosphonium ILs are on the low end of the IL cost spectrum and are regarded as understudied compared with imidazolium and pyridinium ILs. They are also known to be more thermally stable.

The density, viscosity and conductivity of the phosphonium ILs and metal salt-IL mixtures were measured. The conductivity of the phosphonium ILs tested were found to be roughly an order of magnitude lower than imidazolium ILs; this is attributed to the relatively large cation size and localized charge. Linear density-temperature functions are presented. The viscosity and conductivity temperature relationship was modeled using the Vogel-Tamman-Fulcher (VTF) equation.

The electrochemical window of $AlCl_3$-$[P_{14,6,6,6}]Cl$ was studied on a Pt substrate over a wide range of $AlCl_3$ concentrations using cyclic voltammetry (CV). It was found that the tetra-alkyl phosphonium cation is on the order of 800 mV more electrochemically stable than the 1-ethyl-3-methyl imidazolium (EMI^+).

Cathodic and anodic polarization of Al in $AlCl_3$-$[P_{14,6,6,6}]Cl$ (X_{AlCl3} = 0.67) was studied at temperatures ranging from 347 to 423 K. The Butler-Volmer equation was fitted to the plots by varying the kinetic parameters. The cathodic reaction was found to be diffusion limited and the anodic reaction is limited by passivation at lower temperatures. The overpotential required for electrodissolution of Al was found to be higher than for electrodeposition.

Aluminium was electrodeposited using both an electrowinning setup (chlorine evolution anode reaction) and electrorefining setup (Al dissolution anode reaction). The deposits were characterized in terms of morphology, current efficiency and power consumption. A variety of deposit morphologies were observed ranging from smooth, to spherical to dendritic, and in some cases, the IL was occluded in the deposit. The current efficiency and power consumption were negatively impacted by the presence of H_2O and HCl present in the as-received ILs and by $Cl_2(g)$ generated by the anode reaction in the

case of the electrowinning setup. HCl was removed by cyclic polarization or corrosion of pure Al, resulting in current efficiencies above 90%. Aluminium was electrodeposited using the electrorefining setup with anode-cathode spacing of 2 mm at power consumption as low as 0.6 kWhr/kg-Al. This is very low compared with industrial Al electrorefining and Al electroplating using the National Bureau of Standards bath, which require 15-18 kWhr/kg-Al and 18 kWhr/kg-Al, respectively. However, due to low solution conductivity the power consumption increases significantly with increased anode-cathode spacing.

Titanium tetrachloride was found to be soluble in $[P_{14,6,6,6}]Cl$ and increases the conductivity of the solution. Attempts to reduce the Ti(IV) included corrosion of titanium metal, corrosion of magnesium metal powder and cathodic polarization. Despite a few attempts, the electro-deposition of Ti was not observed. At this point, titanium electrodeposition from phosphonium based ILs does not appear feasible.

Table of Contents

Abstract ..... **ii**
Table of Contents ..... **iv**
List of Tables ..... **vi**
List of Figures ..... **viii**
Abbreviations and Symbols ..... **xiii**
Acknowledgements ..... **xv**
Introduction **1**
Research Objectives **5**
Chapter 1 Literature Review ***6***
1.1 Ionic Liquids **6**
1.2 Aluminium **10**
1.3 Magnesium **25**
1.4 Titanium **36**
1.5 Electrodeposition of Reactive Metals **41**
Chapter 2 Physical Properties of Ionic Liquids ***52***
2.1 Experimental Aspects **52**
2.2 Density **61**
2.3 Viscosity **69**
2.4 Conductivity **78**
2.5 Summary **102**
Chapter 3 Electrochemistry ***107***
3.1 Experimental Aspects **107**
3.2 Cyclic Voltammograms **109**
3.3 Diffusion **116**
3.4 Potentiodynamic Polarization **121**
3.5 Electric Double Layer **129**
Chapter 4 Deposition of Aluminium ***131***
4.1 Experimental Aspects **132**
4.2 Potentiostatic Deposition **133**

4.3 Galvanostatic Deposition **139**
4.4 Mini Pilot Plant **142**
4.5 Summary **149**
Chapter 5 Reduction of Titanium ***153***
Chapter 6 Conclusions and Recommendations **158**
References **161**

List of Tables

Table 1 Standard reduction potentials of metals from aqueous acidic solutions (Bard 1985). 1
Table 2 Power consumption of industrial electrowinning operations 3
Table 3 The equilibrium constant for the primary dissociation of $AlCl_3$ in NaCl, BPC and MEIC. 9
Table 4 Aluminium oxide minerals (Frank 1997, Korbel 1999 and Websites: Webminerals and IAI). 12
Table 5 Conditions for aluminium electrowinning by the Hall-Héroult process. 14
Table 6 Waste for smelting and ancillary processes in North America (Richards, 1994, p. 394-96). 17
Table 7 Alternative processes investigated for aluminium production (Welch 1999, p. 26). 19
Table 8 Developments and history of magnesium production 25
Table 9 Magnesium-containing compounds (Andreassen 1997, p. 983). 27
Table 10 Typical magnesium ore compositions. 27
Table 11 Electrolyte composition, major components (Strelets 1977, p. 148 and 207). 30
Table 12 Electrolyte composition, minor components (Strelets, 1977 p. 207 and p. 248). 31
Table 13 Operating parameters of industrial magnesium electrolysers (Andreassen 1997, 990-993) 32
Table 14 Secondary magnesium material and recycling scenarios (Antrekowitsch 2002, p. 46). 34
Table 15 Typical impurities in crude magnesium (Strelets, 1977, p. 308). 34
Table 16 Methods of refining magnesium (Strelets, 1977, p. 312-315 and Antrekowitsch, 2002, p. 47) 35
Table 17 History of titanium production. 36
Table 18 Common titanium-containing minerals (Sibum 1997, p. 1134-1137). 37
Table 19 Typical compositions of rutile, ilmenite and upgraded ilmenite (UGI) ores (Noda 1988, p. 760 and Sibum 1997, p. 1137). 38
Table 20 Progress in Ti Sponge production at Osaka Titanium Co. (Noda, 1988, 759-60) 39
Table 21 Electrodeposition of Al from molten salts and ILs. 44
Table 22 Operating parameters of an NBS bath (Berkowitz 1972, p. 38) 45
Table 23 Electrodeposition of aluminium from solutions other than molten salts or ILs. 48
Table 24 Electrodeposition of solid magnesium. 49
Table 25 Electrodeposition of solid titanium 51
Table 26 Molecular weight (MW), purity, melting point (T_{mp}) and upper limit of the safe operating temperature in an air environment of phosphonium ionic liquids (Cytec Inc.). 52
Table 27 Ionic liquid metal impurity content. 53
Table 28 Known impurities (Cytec Inc., 2006). 54
Table 29 Methods to identify and remove impurities (Hilgers 2003, p. 25-27) 56
Table 30 Linear density functions for the neat ILs. 25 mL pyncometer used unless indicated otherwise.... 64
Table 31 Linear density functions for the chloroaluminate ILs, 10 mL pyncometer used. 66
Table 32 Ion volumes calculated by Jenkins (1999 and 2005) 67

Table 33 Summary of the VTF parameters used to fit the dynamic viscosity model of tetra-alkyl phosphonium ILs. 76
Table 34 Experimental error in the conductance measurements, based on 6 repeat experiments. 79
Table 35 Summary of the VTF parameters used to fit the equivalent conductivity model of neat tetra-alkyl phosphonium ILs. 85
Table 36 Summary of the VTF parameters used to model the equivalent conductivity $AlCl_3$-tetra-alkyl phosphonium chloride ILs. 93
Table 37 The conductivity and density of halo-aluminate ILs at 298 K. 98
Table 38 Conductivity of Al electroplating solutions near room temperature (Liao 1997). 98
Table 39 Conductivity of industrial electrowinning and refining solutions (Ettel, 1977) 99
Table 40 Solubility of metal salts $[P_{14,6,6,6}]^+$ ILs, colour indicated when noted. 101
Table 41 Summary of calculated glass transition temperatures (T_0). 103
Table 42 The electrochemical window of ILs. 114
Table 43 The diffusion coefficient of $Al_2Cl_7^-$. 119
Table 44 The diffusion of $[P_{14,6,6,6}]^+$ calculated using Equation 43 120
Table 45 The reactions considered in the modeling of the polarization curves. 123
Table 46 Model parameters for Figure 69. 124
Table 47 Diffusion boundary layer thickness as a function of temperature and parameters used in the calculations. 128
Table 48 Summary potentiostatic electrodeposition of Al on Cu plate (0.5 cm^2), pure Al plate CE. 138
Table 49 Deposition of aluminium from $[P_{14,6,6,6}]Cl$-$AlCl_3$ (X_{AlCl3} = 0.67), two anode setup, copper cathode, anode-cathode spacing was 2 mm. 139
Table 50 Potentiostatic deposition of Al from $[P_{14,6,6,6}]Cl$-$AlCl_3$ (X_{AlCl3} = 0.67), Al or DSA anodes (~6 cm^2 total), copper cathode (~1 cm^2), anode-cathode spacing = 2 mm, temperature = 395 +/- 2 K, solution purified by corrosion of pure Al. 144

List of Figures

Figure 1 Simplified flowsheet of a primary metal production using ionic liquids..... 4
Figure 2 Examples of tetra-alkyl phosphonium cations and anions that have been used by Cytec Inc. to make ionic liquids (Cytec Inc., 2006)..... 7
Figure 3 Structure of 1-butyl-3-methyl imidazolium chloride (BMIC)..... 8
Figure 4 Major operations involved in the production of aluminium..... 11
Figure 5 Hall-Héroult process Ettel diagram..... 15
Figure 6 Simplified Ettel diagram for a single cell version of ALCOA aluminum chloride electrolysis process..... 21
Figure 7 Major operations involved in the production of magnesium by electrolysis..... 26
Figure 8 Major operations involved in the production of magnesium by metallo-thermic reduction..... 26
Figure 9 Major operations involved in the production of titanium..... 37
Figure 10 Glass sublimation apparatus used to prepare the $AlCl_3$ for the purified $AlCl_3$-IL mixture..... 58
Figure 11 Corrosion rate of Al foil coupons (99.99% pure, 18 cm^2) in $AlCl_3$-$[P_{14,6,6,6}]$ (X_{AlCl3} = 0.67). The solution was stirred and heated to 373 or 388 K..... 59
Figure 12 Density measurement experimental set-up for the chloroaluminate ILs..... 62
Figure 13 Effect of anion type on the density of trihexyl(tetradecyl) phosphonium ILs..... 62
Figure 14 Effect of cation type on the density of phosphonium chloride ILs..... 63
Figure 15 Effect of cation alkyl chain symmetry on the density of phosphonium bromide ILs..... 63
Figure 16 The density functions of $[P_{14,6,6,6}]Cl$ plotted to the range of temperatures tested..... 64
Figure 17 The density of $[P_{14,6,6,6}]Cl$-$AlCl_3$ as a function of $AlCl_3$ concentration and temperature..... 65
Figure 18 The density of $[P_{14,4,4,4}]Cl$-$AlCl_3$ as a function of $AlCl_3$ concentration and temperature..... 66
Figure 19 Comparison of the measured density (298 K) with the calculated density..... 67
Figure 20 Viscosity measurement experimental set-up..... 69
Figure 21 An example of repeated viscosity experiments for $[P_{14,4,4,4}]Cl$, measured (kinematic) viscosity vs. temperature..... 70
Figure 22 Dynamic viscosity of phosphonium ILs as a function of temperature..... 71
Figure 23 Linear fit of VTF parameters, T_o adjusted to maximize linearity; B is the slope of the line..... 72
Figure 24 Effect of anion type on the dynamic viscosity of $[P_{14,6,6,6}]^+$ ILs as a function of absolute temperature..... 73
Figure 25 Effect of anion type on the activation energy of viscosity of $[P_{14,6,6,6}]^+$ ILs..... 73
Figure 26 Effect of alkyl chain length on the dynamic viscosity of tetra-alkyl phosphonium chloride ILs as a function of absolute temperature..... 74
Figure 27 Effect of alkyl chain length on the activation energy of viscosity of phosphonium chloride ILs. 74
Figure 28 Effect of tetra-alkyl phosphonium bromide cation symmetry on the viscosity as a function of temperature..... 75

Figure 29 Effect of alkyl symmetry on the activation energy of viscosity of phosphonium bromide ILs.... 75
Figure 30 Effect of toluene on the viscosity of $[P_{14,6,6,6}]Cl$. 76
Figure 31 Conductivity measurement experimental setup. 78
Figure 32 Effect of drying the ILs for 4 hours at 413 K on the conductivity of $[P_{14,6,6,6}]Br$ and $[P_{14,6,6,6}]Cl$. 80
Figure 33 VTF equation parameters for the neat ILs; T_0 was the variable to optimize a linear fit. 82
Figure 34 VTF equation parameters for the $AlCl_3$-IL mixtures; T_0 was the variable to optimize a linear fit. 82
Figure 35 Effect of anion type on the measured conductivity of $[P_{14,6,6,6}]^+$ ILs. 83
Figure 36 Effect of anion type on the equivalent conductivity of $[P_{14,6,6,6}]^+$ ILs 83
Figure 37 Effect of cation type on the measured conductivity of chloride phosphonium ILs. 84
Figure 38 Effect of cation type on the equivalent conductivity of phosphonium chloride ILs. 84
Figure 39 Effect of cation symmetry on the equivalent conductivity of tetra-alkyl phosphonium bromide ILs. 85
Figure 40 Effect of anion type on the activation energy of conductivity in $[P_{14,6,6,6}]^+$ ILs 86
Figure 41 Effect of cation type on the activation energy of conductivity in phosphonium chloride ILs. 86
Figure 42 Effect of cation symmetry on the activation energy of conductivity in phosphonium bromide ILs. 87
Figure 43 Measured conductivity of the $AlCl_3$-$[P_{14,6,6,6}]Cl$ system. 88
Figure 44 The effect of purification of $AlCl_3$-$[P_{14,6,6,6}]Cl$ ($X_{AlCl3} = 0.67$) on the solution conductivity. The $AlCl_3$ was sublimed and the solution was heated and exposed to high purity Al to remove H^+. 88
Figure 45 Equivalent conductivity of the $AlCl_3$-$[P_{14,6,6,6}]Cl$ system. 89
Figure 46 Effect of $AlCl_3$ and purification on the activation energy of conductivity in $AlCl_3$-$[P_{14,6,6,6}]Cl$ ILs. 89
Figure 47 Measured conductivity of the $AlBr_3$-$[P_{14,6,6,6}]Br$ system. 90
Figure 48 Measured conductivity of the $AlCl_3$-$[P_{14,4,4,4}]$ system. 91
Figure 49 Equivalent conductivity of the $AlCl_3$-$[P_{14,4,4,4}]$ system. 91
Figure 50 Effect of $AlCl_3$ on the activation energy of conductivity of $AlCl_3$-$[P_{14,4,4,4}]Cl$ ILs. 92
Figure 51 Measured conductivity of the $AlCl_3$-$[P_{4,4,4,4}]Cl$ system. 92
Figure 52 Effect of the addition of 1 wt. % NaCl to acidic and basic chloroaluminate melts. Note: The solubility of NaCl was low in both systems. 94
Figure 53 Measured conductivity of the $AlCl_3$-MEIC system. 95
Figure 54 The relationship between anion volume and the measured conductivity of $[P_{14,6,6,6}]^+$ ILs. 96
Figure 55 The relationship between anion volume and the equivalent conductivity of $[P_{14,6,6,6}]^+$ ILs. 96
Figure 56 The relationship between cation volume and the measured conductivity of phosphonium chloride ILs. 97

Figure 57 The relationship between cation volume and the equivalent conductivity of phosphonium chloride ILs. 97
Figure 58 Measured conductivity of metal salt-$[P_{14,6,6,6}]Cl$. Note: $MgCl_2$ was only slightly soluble. 100
Figure 59 Measured conductivity of the $FeCl_3$-$[P_{14,6,6,6}]Cl$ system. 100
Figure 60 Measured conductivity of the $TiCl_4$-$[P_{14,6,6,6}]Cl$ system. 101
Figure 61 Comparison of the densities of $[P_{14,6,6,6}]^+$ ILs with different anions. The measured density is at 298 K, the calculated density is based on the anion and cation volume calculations of Jenkins (1999) and the density at T_0 was estimated using extrapolating the density functions back to T_0. The average T_0 values from Table 41 were used. 105
Figure 62 The ratio of activation energy of viscosity to conductivity ($E_{a,\eta}/E_{a,\Lambda}$). 106
Figure 63 Electrochemical experiment setup. 108
Figure 64 Cyclic voltammograms of the $AlCl_3$-$[P_{14,6,6,6}]Cl$ with various concentrations of $AlCl_3$ at 373 K. Pt wire WE (0.096 cm^2), Pt foil CE (2 cm^2), Al wire RE, the WE-CE and WE-RE spacing was 1 mm. Scanning from OC (~ 0.7 V vs. Al wire) to +2 V to -3 V to +2 V). SR = 5 mV/s. The solutions were stirred using a magnetic stir-bar. 113
Figure 65 Cyclic voltammogram (2^{nd} cycle) depicting the stripping and deposition of aluminium on a copper wire substrate from $AlCl_3$-$[P_{14,6,6,6}]Cl$, 373 K, 25 mV/s scan rate. 114
Figure 66 Peak cathodic current as a function of temperature and scan rate. 0.67 X_{AlCl3} in $AlCl_3$-$[P_{14,6,6,6}]Cl$. The electrodes were: Al plate WE (0.72 cm^2), Al wire RE, and two Al plate CEs (6 cm^2). WE-CE spacing was 2 mm. WE-RE spacing was 1 mm. No stirring. 116
Figure 67 Peak cathodic current as a function of temperature and scan rate. 0.67 X_{AlCl3} in $AlCl_3$-$[P_{14,6,6,6}]Cl$. The electrodes were: Cu plate WE (0.4 cm^2), Al wire RE, and two Al plate CEs (6 cm^2). WE-CE spacing was 2 mm. WE-RE spacing was 1 mm. No stirring. 116
Figure 68 Calculated diffusion constants for $Al_2Cl_7^-$ in purified $AlCl_3$-$[P_{14,6,6,6}]$ (X_{AlCl3} = 0.67) 118
Figure 69 Potentiodynamic polarization curves of Al deposition (cathodic) and stripping (anodic) as a function of solution temperature. The solution was 0.67 X_{AlCl3} in $[P_{14,6,6,6}]Cl$. The electrodes were: Al plate working (1 cm^2) and counter (6 cm^2) electrode, Al wire reference electrode. SR = 1 mV/s. Current interrupt IR compensation was employed. No stirring. 122
Figure 70 Current contributions of hydrogen evolution and aluminium deposition/stripping to the model of the potentiodynamic polarization of Al in 0.67 X_{AlCl3} $AlCl_3$-$[P_{14,6,6,6}]Cl$ at 355 K. The electrodes were: Al plate working (1 cm^2) and counter (6 cm^2) electrode, Al wire reference electrode. SR = 1 mV/s. Current interrupt IR compensation was employed. No stirring. 124
Figure 71 Potentiodynamic polarization curves of Al deposition (cathodic) and stripping (anodic) as a function of solution temperature. The solution was 0.67 X_{AlCl3} in $AlCl_3$-$[P_{14,6,6,6}]Cl$. The solution was purified by removal of HCl by exposure to high purity Al and sublimation of the $AlCl_3$. The electrodes were: Al plate working (0.72 cm^2) and counter (6 cm^2) electrode, Al wire reference electrode. SR = 1 mV/s. Current interrupt IR compensation was employed. No stirring. 126

Figure 72 The effect of scan rate on the current density during the cathodic polarization of Al at 399 K. The solution was 0.67 X_{AlCl3} in $AlCl_3$-$[P_{14,6,6,6}]Cl$. The solution was purified by removal of HCl by exposure to high purity Al and sublimation of the $AlCl_3$. The electrodes were: Al plate working (0.72 cm^2) and counter (6 cm^2) electrode, Al wire reference electrode. Current interrupt IR compensation was employed. No stirring. 126
Figure 73 Diffusion limited cathodic current due to deposition of Al from cathodic potentiodynamic scans. $AlCl_3$-$[P_{14,6,6,6}]Cl$, X_{AlCl3} = 0.67. 127
Figure 74 Schematic of the cathode double layer during deposition of Al in Lewis acidic $AlCl_3$-$[P_{14,6,6,6}]Cl$. Note: the ions are not drawn to scale. 129
Figure 75 Schematic of the potential profile of the cathodic double layer during deposition of Al in an acidic $AlCl_3$-$[P_{14,6,6,6}]$ melt. The changes in potential and distances are not to scale. 130
Figure 76 Potentiostatic aluminium deposition from $AlCl_3$-$[P_{14,6,6,6}]Cl$, E = –1.1 V vs. Al/Al(III), 373 K, Cu wire WE (~0.3 cm^2), Al wire RE, GC CE (0.5 cm^2) 134
Figure 77 Secondary electron micrographs of Al electrowinning deposit, 2 hours at 373 K, -1.1 V vs. Al/Al(III), 0.66 X_{AlCl3} in $AlCl_3$-$[P_{14,6,6,6}]Cl$, EDS analysis spot is the cross (left) Higher magnification (right). 134
Figure 78 Cross sectioned Backscattered Electron Images of Al deposited on Cu wire, -1.1 V vs. Al/Al(III), in $AlCl_3$-$[P_{14,6,6,6}]Cl$ (X_{AlCl3} = 0.66) at 373 K, (left) 2 hours (right) 5 hours. 135
Figure 79 Potentiostatic deposition of Al from $AlCl_3$-$[P_{14,6,6,6}]Cl$ (X_{AlCl3} = 0.67) cathode potential set with respect to the Al CE, Anode-Cathode spacing was 3 or 4 mm, single Al plate anode (~4 cm^2), Cu plate cathode (0.5 cm^2). 136
Figure 80 SEM micrograph of aluminium electrorefining deposit from $AlCl_3$-$[P_{14,6,6,6}]Cl$ (X_{AlCl3} = 0.67) at 373 K. 23 hours at -0.75 V, 600X (left) 22 hours at -1.25 V, 1000X (right). 136
Figure 81 SEM micrograph of aluminium electrorefining deposit after 24 hours at -1.0 V vs. Al CE in $AlCl_3$-$[P_{14,6,6,6}]Cl$ (X_{AlCl3} = 0.67) at 373 K, 70X (left) 900X (right). 137
Figure 82 SEM micrographs of aluminium electrorefining deposit after 24 hours at -1.0 V vs. Al CE in $AlCl_3$-$[P_{14,6,6,6}]Cl$ (X_{AlCl3} = 0.67) at 388 K, 100X (left) 1000X (right). 137
Figure 83 SEM micrographs of aluminium electrorefining deposit after 22 hours at -1.0 V vs. Al CE at 373 K, $AlCl_3$-$[P_{14,6,6,6}]Cl$ (X_{AlCl3} = 0.6) 1000X (left), $AlCl_3$-$[P_{14,4,4,4}]Cl$ (X_{AlCl3} = 0.67) 800X (right). 137
Figure 84 Deposition 1, 200X (left), 1500X cross-section (right), 20 hours, 386 K 23 A/m^2. 140
Figure 85 Deposition 2, 200X (left), 800X (right), 20 hours, 400 K, 25 A/m^2. 140
Figure 86 Deposition 3, 200X (left), 800X (right), 4 hours, 427 K, 45 A/m^2. 140
Figure 87 Deposition 4, 200X (left), 1500X cross-section (right), 4 hours, 429 K, 40 A/m^2. 141
Figure 88 Deposition 5, 200X (left), 1500X cross-section (right), 4 hours, 429 K 48 A/m^2. 141
Figure 89 Deposition 6, 200X (left), 800X (right), 5.6 hours, 383 K 33 A/m^2. 141
Figure 90 Potentiostatic deposition of Al from $AlCl_3$-$[P_{14,6,6,6}]Cl$ (X_{AlCl3} = 0.67) cathode potential set with respect to the Al CE. All of the experiments were carried out using the same solution. Solution was

purified by removal of HCl by corrosion of pure Al and the $AlCl_3$ was sublimated. The temperature was 395 K +/- 2 K..... 143
Figure 91 Deposit 1, bulk deposit 200X (left), corner 60X (right), 5.2 hours, 395 K, 67.5 A/m^2. 145
Figure 92 Deposit 2, bulk deposit 200X (left), edge 200X (right), 12.4 hours, 395 K, 44.0 A/m^2. 145
Figure 93 Deposit 3, bulk deposit 200X (left), corner 100X (right), 20 hours, 395 K, 5.8 A/m^2. 146
Figure 94 Deposit 4, bulk deposit 200X (left), edge 200X (right), 20 hours, 395 K, 14.3 A/m^2. 146
Figure 95 Deposit 5, bulk deposit 200X (left), edge 200X (right), 20 hours, 395 K, 17.0 A/m^2. 146
Figure 96 Deposit 6, bulk deposit 200X (left), edge 200X (right), 22 hours, 395 K, 6.7 A/m^2. 147
Figure 97 Cross sections: Deposit 2 edge 1500X (left) Deposit 4 edge 4000X (right), The lighter colour is the copper plate..... 147
Figure 98 Cross sections: Deposit 3 corner 800X (left) Deposit 4 corner 1000X (right), The lighter colour is the copper plate..... 148
Figure 99 Ettel diagram for the electrodeposition of Al with an Al anode. The electrode spacing is 2 mm. The solution was $AlCl_3$-$[P_{14,6,6,6}]Cl$ (X_{AlCl3} = 0.67) at 395 K with a current density of 17 A/m^2. 150
Figure 100 Ettel diagram for the electrodeposition of Al with an Al anode. The electrode spacing is 1 cm. The solution was $AlCl_3$-$[P_{14,6,6,6}]Cl$ (X_{AlCl3} = 0.67) at 395 K with a current density of 17 A/m^2. 150
Figure 101 Ettel diagram for the electrodeposition of Al with an Al anode. The electrode spacing is 10 cm. The solution was $AlCl_3$-$[P_{14,6,6,6}]Cl$ (X_{AlCl3} = 0.67) at 395 K with a current density of 17 A/m^2. 150
Figure 102 Cathodic polarization of Cu in $TiCl_4$-$[P_{14,6,6,6}]$ (X_{TiCl4} = 0.33), solution stirred. Cu WE (0.5 cm^2), Ti CE (16 cm^2), Ti RE. WE-CE spacing = 2 mm. WE-RE spacing = 1 mm. Scan rate = 5 mV/s..... 154
Figure 103 Cathodic polarization of Cu in $TiCl_4$-$[P_{14,6,6,6}]$ (X_{TiCl4} = 0.5), solution stirred. Cu WE (0.7 cm^2), Ti CE (16 cm^2), Ti RE. WE-CE spacing = 2 mm. WE-RE spacing = 1 mm. Scan rate = 5 mV/s..... 154
Figure 104 Cathodic polarization of Cu in $TiCl_4$-$[P_{14,6,6,6}]$ (X_{TiCl4} = 0.33) after adding Mg powder. Cu WE (0.5 cm^2), Ti CE (16 cm^2), Ti RE. WE-CE spacing = 2 mm. WE-RE spacing = 1 mm. Scan rate = 5 mV/s, solution stirred. 155
Figure 105 Cyclic polarization of Ti plates (10 cm^2 each), Ti plate RE $TiCl_4$-$[P_{14,6,6,6}]$ (X_{TiCl4} = 0.5) after adding Mg powder, solution stirred. Scan rate = 50 mV/s, temperature = 373 K. 156
Figure 106 Cathodic polarization of Cu in $TiCl_4$-$[P_{14,6,6,6}]$ (X_{TiCl4} = 0.5) after adding Mg powder, solution stirred. Cu WE (0.5 cm^2), Ti CE (16 cm^2), Ti RE. WE-CE spacing = 2 mm. WE-RE spacing = 1 mm. Scan rate = 5 mV/s, solution stirred. 156
Figure 107 Potentiostatic polarization of Cu (0.5 cm^2) at -2.5 V vs. Ti metal, in $TiCl_4$-$[P_{14,6,6,6}]$ (after adding Mg powder, Ti plate CE's (16 cm^2 total) at 413 K, solution stirred. 157

Abbreviations and Symbols

Abbreviations

A-C	Anode-cathode spacing (mm)
AN	Acetonitrile
avrg or avg	Indicates that an average value was used
BBIC	1-butyl-3-butyl imidazolium chloride
BEI	Backscattered Electron Image
BMIC	1-butyl-3-methyl imidazolium chloride
$BMITf_2N$	1-butyl-3-methylimidazolium bis(trifluoromethylsulfonyl)
BPC	Butyl pyridinium chloride
BTMAC	Benzyl-tri-methyl ammonium chloride
CD	Current density (A/m^2)
CE	Counter electrode
C.E.	Current efficiency (%)
C.I.	Current inefficiency (%)
C_o	Bulk concentration ($moles/m^3$)
CV	Cyclic voltammogram
d	Anode-cathode spacing (m)
$DMSO_2$	Dimethylsulfone $(CH_3)_2SO_2$
E	Potential (V)
E^o	Standard potential of a cell reaction when that reaction involves the oxidation of molecular hydrogen to solvated protons (V)
EDS	Energy Dispersive X-ray Analysis (EDX or EDAX)
E_{MF}	Electromotive force for an electrochemical reaction (V)
EMIC	1-ethyl-3-methyl imidazolium chloride
E.P.A.	Environmental Protection Agency (U.S.A.)
EPB	Ethyl pyridinium bromide
EPC	Ethyl pyridinium chloride
EW	Electrowinning
F	Faraday's constant (96485 C/mol)
GC	Glassy carbon
HMIC	1-hexyl-3-methylimidazolium chloride
$HMIPF_6$	1-hexyl-3-methylimidazolium hexafluorophosphate
I	Electric current (A)
ICF	Intermetallic compound formation
IL or ILs	Ionic liquid(s)
j	Current density (A/m^2)
M	Molarity, Moles of solute / Liter solution
MEIB	1-methyl-3-ethyl imidazolium bromide
MEIC	1-methyl-3-ethyl imidazolium chloride
MMC	Metal Matrix Composites
MMIC	1-methyl-3-methyl imidazolium chloride
MPC	Methyl pyridinium chloride

MW	Molecular weight (g/mol)
MX	Metal Salt
N_A	Avagadro's number ($6.02 \cdot 10^{23}$ $mole^{-1}$)
η_a or n_a	Anode overpotential (V)
η_c or n_c	Cathode overpotential (V)
NBS	National Bureau of Standards (U.S.A.)
$[N_{2,2,2,2}]^+$	Tetra-ethyl ammonium cation
OCP	Open circuit potential
$[P_{14,6,6,6}]^+$	Tetra-alkyl phosphonium cation, the four numbers (14,6,6,6) represent the number of carbon atoms in each of the four hydrocarbon chains. $[P_{14,6,6,6}]^+$ is trihexyl(tetradecyl) phosphonium.
P_{90}	Percent of a material passing through a given sieve size (80% for P_{80})
PPC	Propyl pyridinium chloride
R	Universal Gas Constant (8.314 J/(mole·K))
R	Organic chain or ring consisting of carbon and hydrogen, when in a chemical formula, e.g. R_4PCl.
R'	Organic chain or ring consisting of carbon and hydrogen different from R, e.g. $R'R_3PCl$.
RE	Reference electrode
STM	Scanning tunneling microscopy
t	Time (s)
T_0	Calculated theoretical glass transition temperature (K)
T_g	Experimentally measured glass transition temperature (K)
THF	Tetrahydrofuran (C_4H_8O)
TMPAC	Tri-methyl-phenyl ammonium chloride
U_E	Potential loss due to solution resistance (V)
U_H	Potential loss due to hardware (V)
UPD	Under potential deposition
VTF	Vogel-Tamman-Fulcher equation
X_{AlCl3}	Mole fraction aluminium chloride (or $AlBr_3$ or $TiCl_4$ etc.)
WE	Working electrode

Symbols

κ	Specific or measured conductivity (S/m)
δ	Diffusion layer boundary thickness (m)
Λ_m	Molar conductivity ($S \cdot m^2/mol$)
Λ	Equivalent conductivity ($S \cdot m^2/mol\text{-}eq$)
ρ	Density (kg/m^3)
η	Dynamic viscosity (Pa·s or cP, 1 cP = 0.001 Pa·s)
υ	Kinematic viscosity (cSt)
$\bar{e}$	Electron

Acknowledgements

This research was made possible by the financial support of the Electrometallurgy Consortium and the Natural Sciences and Engineering Research Council of Canada.

I like to acknowledge the many individuals who contributed to the work. My supervisor, David Dreisinger, provided all the necessary tools required to tackle this work along with the guidance and support that has allowed me to develop my technical proficiency as well as soft skills. This work was initiated by Jianming Lu; he was instrumental in establishing the scope of the project and made himself available to discuss many issues that arose. Bérend Wassink was also of great assistance, especially in the set-up and operation of the glove box and the design of the sublimation apparatus. Jana Haggins, Jack Tu and Herman Huang were undergraduate student researchers that contributed greatly to this thesis during their work terms. Alec Mitchell, Dave Dixon and Dan Bizzotto have contributed some of their ideas to this work. Akram Alfantazi was also supportive the work and I remained an honorary member of his corrosion group. The phosphonium ionic liquids used were donated by Cytec Inc. Al Robertson of Cytec answered ionic liquid related questions during our numerous email communications. David Creber of Alcan shared his understanding of current industrial Al, Mg and Ti production. Don Jenkins of the University of Warwick calculated the ion volumes that are presented in this thesis and discussed the significance of these values with me.

Last but not least, my family and friends who help directly by editing some of the things I write, but usually they help more by distracting me from the work occasionally so that I am able to let it go and return with a fresh mind.

The past year has been quite eventful as I was married to my lovely wife Jaclyn in December 2006. She deserves a special mention as she sees me every day and probably knows much more about ionic liquid electrochemistry than she ever really wanted to.

Introduction

Ionic liquids (ILs) are salts that are molten at temperatures below about 373 K. Since their discovery in the late 19th century, uses for these unique salts have been sought after. The use of ILs as a media to electro-deposit metals is of especially great interest as ILs exhibit large electrochemical operating windows similar to high-temperature molten salts, yet with a melting point and liquid temperature range more closely resembling solutions for hydrometallurgical electrowinning and electrorefining processes. The low melting point of the ILs is due to a relatively large organic cation that reduces the strong cation-anion interactions.

The main objective of this thesis was to study the deposition of reactive metals such as Al, Mg and Ti from ILs since they cannot be deposited from aqueous solutions.

The electrochemical reactivity of metals can be described by comparing their standard reduction potential (E^o). The lower, more negative, the E value is, the more reactive a metal is. Table 1 lists the standard reduction potentials for select metals in acidic aqueous solutions. The industrial production and refining methods of these metals are also noted.

Table 1 Standard reduction potentials of metals from aqueous acidic solutions (Bard 1985).

Reduction Reaction	E^o (V)	Industrial Reduction and Refining Methods
$Cu^{2+} + 2\bar{e} \rightarrow Cu$	0.34	Produced by aqueous electrowinning or smelting. Electrorefined in aqueous solutions.
$Ni^{2+} + 2\bar{e} \rightarrow Ni$	-0.26	Produced by smelting and/or aqueous electrowinning.
$Zn^{2+} + 2\bar{e} \rightarrow Zn$	-0.76	Produced by aqueous electrowinning or smelting.
$Ti^{2+} + 2\bar{e} \rightarrow Ti$	-1.63	Produced by magnesiothermic reduction. Refined (consolidated from sponge) using electron beam or electrode arc melting.
$Al^{3+} + 3\bar{e} \rightarrow Al$	-1.67	Produced by molten salt electrolysis. Refined electrolytically using molten salts, or by gas injection into liquid Al.
$Mg^{2+} + 2\bar{e} \rightarrow Mg$	-2.36	Produced by molten salt electrolysis or silicothermic reduction. Refined electrolytically using molten salts, or by distillation.

The relatively high reduction potentials of copper, nickel and zinc allows these metals to be processed hydrometallurgically with high current efficiency since the evolution of hydrogen, which decreases current efficiency, either does not occur or can be kept at a sufficiently low value. Copper electrowinning takes place within the electrochemical window of water. Nickel electrowinning solutions must be maintained at

a sufficiently high pH to minimize hydrogen evolution. The electrowinning of zinc at a high current efficiency is possible only because of the slow kinetics of hydrogen evolution on its surface.

Titanium, aluminium and magnesium cannot be deposited from aqueous solutions because most of the applied current would result in the evolution of hydrogen since a high cathodic polarization is required. Also, if exposed to air or water, these metals will form solid metal oxides, hydroxides or hydrides, further complicating the process. A true experimental equilibrium potential for the reduction of titanium is difficult to obtain because of the formation of both oxide and hydride films. The standard reduction potential of Ti listed in Table 1 was estimated based on corrosion potentials. Similar complications were encountered in determining the standard reduction potentials for aluminium and magnesium (Bard 1985). The Ti(II) oxidation state was found to be stable as $Ti(AlCl_4)_2$ in acidic $AlCl_3$-NaCl molten salts, the oxidation to Ti(III) and Ti(IV) was observed but the researchers were not able to reduce the titanium to its elemental form (Fung 1971).

Industrially, Al and Mg are produced by electrowinning at high temperatures in molten salt baths, from their oxide and chloride forms, respectively. Mg is also produced directly from its oxide at high temperatures by reduction using carbon and iron-silicon compounds. Ti is reduced at high temperature from its chloride by using Mg, requiring an in-line Mg electrowinning process.

The industrial production of reactive metals consumes vast amounts of energy, spurring the search for alternative, lower-energy processes. High temperature molten salt electrolysis of Al or Mg is more energy intensive than electrowinning Cu, Ni or Zn from aqueous solutions, both on a molar basis, and a per-electron basis. Some of the difference in power consumption between Cu, Ni and Zn compared with Al and Mg is due to the greater electrochemical potential required for the reduction of the latter pair. The remaining difference is due to solution resistances, because of the large anode-cathode spacing required in molten salt setups, and losses due to extra resistances in the hardware from being operated at high temperatures.

Table 2 Power consumption of industrial electrowinning operations

Metal	Average Industrial EW Power Consumption		
	kWh/kg	kWh/kmole	kWh/kmole-ē
Copper[a]	2	127	64
Nickel[b]	3.5	205	103
Zinc[a]	3.4	222	111
Aluminium[c]	15	405	135
Magnesium[c]	14	340	170

[a] Ettel, 1977
[b] Ji, 1994
[c] Creber, 2004

Hurley and Weir were some of the early investigators into the practical use of ILs. They successfully electrodeposited Al at room temperature from solutions of ethyl pyridinium bromide (EPB) with aluminium chloride and toluene or benzene (Hurley 1951). In these systems the pyridinium cation was easily reduced, thus consuming the bath solution and limiting the plating bath lifetime. To overcome this limitation, Wilkes *et al.* developed a class of ILs based on dialkyl-imidazolium salts in an effort to create a battery with an Al anode and a chlorine cathode (Wilkes 1982).

The imidazolium ILs have been shown to be suitable solvents for the electrowinning and electrorefining of aluminium with positive results in terms of energy consumption. Aluminium electrowinning in the $AlCl_3$–1-butyl-3-methyl imidazolium chloride (BMIC) system is reported to consume less than 10 kWh/kg-Al (Zhang 2003). This indicates the possibility of energy savings when compared with current industrial Al smelting practices. Zhang also ran Al electro-refining experiments and reported a power consumption of 2.5 kWh/kg-Al. This could signify a large energy savings when compared with the industrial 3-layer electrolytic process for refining Al that operates at 18 kWh/kg-Al.

Recently, a patent has been approved that details the production, refining and recycling of reactive metals with an example of Al electrodeposition of $AlCl_3$-BMIC (Wu 2005). A simplified flowsheet of primary metal production using ILs is shown in Figure 1. A dehydrated ore is chlorinated in a fluidized bed reactor, the metal chloride is condensed from the off-gas and combined with an ionic liquid. The metal of interest is electrowon as the solid metal is deposited at the cathode and chlorine gas is evolved at the anode. The electrowinning could be carried out at room temperature; however, for kinetic reasons the operating temperature would likely be ~375-450 K.

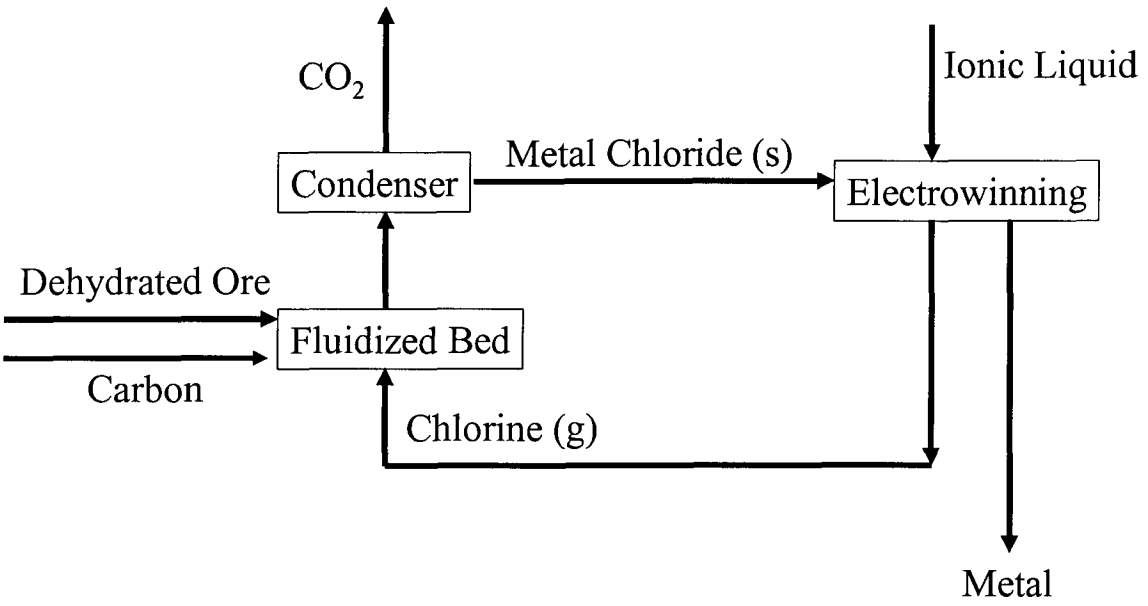

Figure 1 Simplified flowsheet of a primary metal production using ionic liquids.

As of this writing, the high costs of the imidazolium ILs limits their potential application. In contrast, phosphonium ILs are less expensive to produce than imidazolium and they are at least equivalent in terms of electrochemical and thermal stability (Hilgers 2003). It is believed that phosphonium-types are good alternatives to other ILs in many situations and thus deserve further research (Bradaric 2003). Since phosphonium ILs are understudied compared to pyridinium and imidazolium, this research was carried out using the phosphonium ILs with an emphasis on characterizing the basic properties of these novel solvents.

Research Objectives

Since the phosphonium ILs are understudied and information regarding their physical properties was not available, the first thesis objective was, to characterize their physical properties.

- Measure the density, viscosity and conductivity of nine phosphonium ILs
- Characterize metal salt-IL mixtures
- Model the data as a function of temperature for convenient reference

The second objective was, to characterize the electrochemical behaviour of the $AlCl_3$-$[P_{14,6,6,6}]Cl$ system. This system was selected since it exhibits stable conductivity behaviour over a wide range of temperatures and $AlCl_3$ concentrations. Also, similar aluminium chloride systems have been evaluated using other ILs providing a reference for this work.

- Determine the electrochemical window
- Determine the diffusion of the electroactive $Al_2Cl_7^-$
- Determine the anodic and cathodic reactions taking place and their limitations

The third thesis objective was, to electrodeposit aluminium from the phosphonium chloride ILs and thus perform the first reported electrodeposition of Al from these solutions.

- Electrodeposit Al in an electrowinning set-up (Cl_2(g) evolution at the anode) and in the electrorefining set-up (Al dissolution at the anode)
- Characterize the deposits in terms of morphology, occlusion of IL, current efficiency (C.E.) and power consumption

The final objective was, to evaluate opportunities with other reactive metal systems. Since it was determined from the conductivity measurements that $TiCl_4$ was soluble in $[P_{14,6,6,6}]Cl$, attempts were made to reduce the Ti(IV) and electrodeposit Ti from these system. Although no Ti deposit was obtained, some interesting observations were made.

Chapter 1 Literature Review

Ionic liquids are introduced in section 1.1 with an emphasis on the tetra-alkyl phosphonium ILs. The production, refining and recycling of aluminium, magnesium and titanium are then reviewed in sections 1.2, 1.3 and 1.4, respectively. Information is provided about the history of the processes as well as the mineralogy, mineral processing, alternative processes, and environmental considerations where relevant. The electrodeposition of Al, Mg and Ti from ILs, organic solvents and molten salts (not used industrially) are discussed in section 1.5 of this literature review.

1.1 Ionic Liquids

Ionic liquids are loosely defined as salts that are molten at temperatures below about 373 K (100 °C). This low melting temperature is often achieved by having a relatively large organic cation that lessens the cation-anion ionic interaction. The anion also has a strong effect on the melting point and other properties of the salt. Some of the common phosphonium cation and anions used to make ionic liquids are shown in Figure 2.

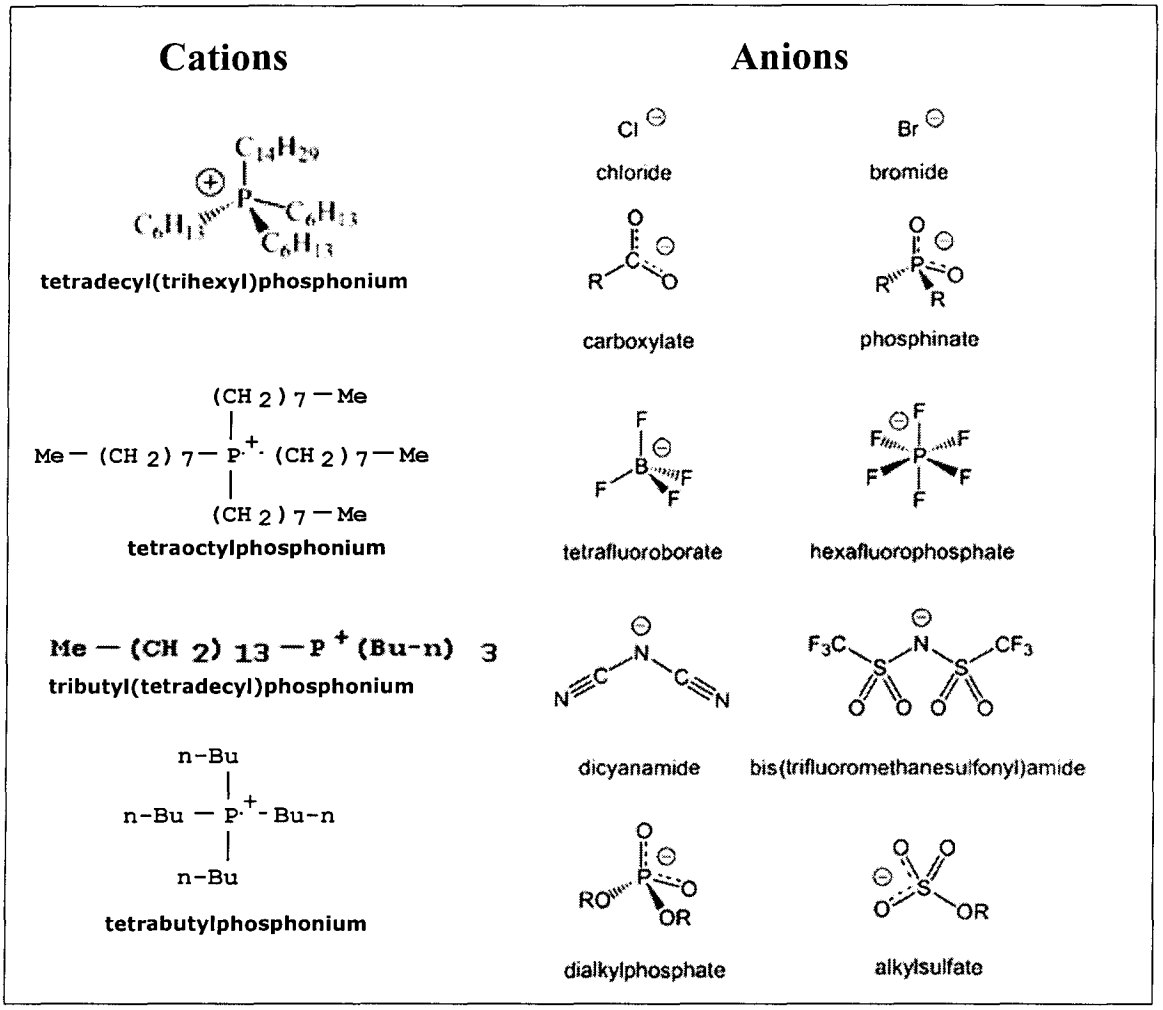

Figure 2 Examples of tetra-alkyl phosphonium cations and anions that have been used by Cytec Inc. to make ionic liquids (Cytec Inc., 2006).

In this thesis, two nomenclatures are used to represent the cations for tetra-alkyl ionic liquids. The first one, used in the case of a general reference to the cation, uses R and R' to represent alkyl groups of differing hydrocarbon chain length. For example $R_3PR'^+$ would be an asymmetric tetra-alkyl phosphonium cation with one chain differing from the three others. The second, more specific, nomenclature involves four numbers that correspond to the number of carbon atoms in each hydrocarbon chain, for example, $[P_{14,6,6,6}]^+$ is trihexyl(tetradecyl) phosphonium.

Imidazolium based ILs usually exhibit a higher conductivity than phosphonium based ILs due to their small cations whose charge is de-localized (Figure 3).

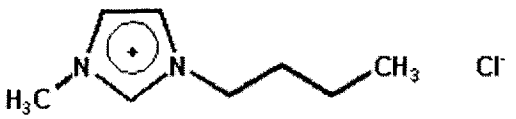

Figure 3 Structure of 1-butyl-3-methyl imidazolium chloride (BMIC).

Synthesis of phosphonium ILs

The tetra-alkyl phosphonium halides were prepared by Cytec Inc. by the nucleophilic addition of tertiary phosphines (PR_3) to haloalkanes [R'X (X = Cl, Br)], Equation 1 (Bradaric 2003 *Cited:* Johnson 1993 and Hartley 1994).

$$PR_3 + R'X \rightarrow [R'PR_3]X \quad [1]$$

Because of their larger radii and highly polarizable lone pair of electrons, the phosphonium salts are more nucleophilic than their ammonium counterparts, resulting in faster reaction kinetics. Another advantage phosphonium ILs have over ammonium ILs is that they tend to be more resistant to thermal decomposition (Bradaric 2003).

The phosphonium halides can then be converted to ILs with different anion types (A = $N(CN)_2^-$, $N(SO_2CF_3)_2^-$, PF_6^-, BF_4^-) by a metathesis reaction, Equation 2 (Bradaric 2003).

$$[R'PR_3]X + MA \rightarrow [R'PR_3]A + MX \quad [2]$$

Most of the recent electrodeposition work has been in the area of the chloride ILs, specifically the aluminium chloride-chloride salt systems. The primary equilibrium determining the anion species in chloro-aluminate systems is described by Equation 3. The equilibrium constant for this reaction in NaCl, BPC (butyl pyridinium chloride) and MEIC (1-ethyl-3-methyl-imidazolium chloride) are summarized in Table 3. The low value of the equilibrium constant (10^{-7} to 10^{-17}) indicates that aluminum tetrachloride is very stable, especially in the IL systems.

$$2AlCl_4^- = Al_2Cl_7^- + Cl^- \quad [3]$$

The concentration of metal salts in ILs is expressed in terms of the mole fraction of metal salt ($X_{metal\ salt}$). The mole fraction of the metal salt is defined in Equation 4.

$$X_{metal\ salt} = \text{moles of the metal salt/(moles of the metal salt + moles of IL)} \quad [4]$$

Table 3 The equilibrium constant for the primary dissociation of $AlCl_3$ in NaCl, BPC and MEIC.

System	Temperature K	Equilibrium Constant of Equation 3	Reference
$AlCl_3$-NaCl (X_{AlCl3} = 0.5-0.7)	448	$1.1 \cdot 10^{-7}$	Boxall 1973
	473	$2.2 \cdot 10^{-7}$	
	523	$8.6 \cdot 10^{-7}$	
	573	$2.4 \cdot 10^{-6}$	
	628	$5.8 \cdot 10^{-6}$	
$AlCl_3$-BPC (X_{AlCl3} = up to 0.67)	313	$1.2 \cdot 10^{-13}$	Schoebrechts 1981
	322	$4.5 \cdot 10^{-13}$	
	328	$7.5 \cdot 10^{-13}$	
$AlCl_3$-MEIC (X_{AlCl3} = 0.6)	313	$5 \cdot 10^{-17}$	Hussey 1986
	323	$8 \cdot 10^{-17}$	
	333	$3 \cdot 10^{-16}$	
$AlCl_3$-MEIC (X_{AlCl3} = 0.7-0.82)	473	$7.4 \cdot 10^{-15}$ *	Øye 1991

*Calculated from thermodynamic equilibrium parameters presented in Øye's model that included the data from Hussey (1986) and vapour pressure measurements at higher temperature and $AlCl_3$ concentration.

The chemistry of chloroaluminate-chloride ILs or other molten salt systems is characterized by the Lewis concept of acidity or basicity. The chloride ion acts as a Lewis base, being an electron donor. On the other hand, $AlCl_3$ is a Lewis acid as it has a large capacity to accept electrons. In this thesis, this Lewis acid-base concept is used to describe the systems. As an example, the $AlCl_3$-$[P_{14,6,6,6}]Cl$ system is considered basic at lower concentrations of $AlCl_3$ ($X_{AlCl3} < 0.5$) or when Cl^- is present in the melt. When the molar concentration of $AlCl_3$ is the same as $[P_{14,6,6,6}]Cl$ ($X_{AlCl3} = 0.5$), the melt is deemed neutral. Finally, at $X_{AlCl3} > 0.5$, the melt is considered to be acidic.

In highly acidic chloroaluminate solutions ($X_{AlCl3} > \sim 0.67$), $Al_3Cl_{10}^-$ has been shown to exist, resulting in a second equilibrium, Equation 5 (Abdul-Sada 1989):

$$2Al_2Cl_7^- = Al_3Cl_{10}^- + AlCl_4^- \quad [5]$$

At high temperatures and $AlCl_3$ concentrations, $Al_4Cl_{13}^-$ is also expected to exist (Øye 1991). Because of the high stability of $AlCl_4^-$, aluminium can only be deposited from acidic IL solutions; the deposition reaction proceeds as in Equation 6.

$$4Al_2Cl_7^- + 3e^- \rightarrow Al + 7AlCl_4^- \quad [6]$$

However, in inorganic melts such as $AlCl_3$-NaCl, it is possible to deposit aluminium from a basic system (Zhao 1997) (Equation 7).

$$AlCl_4^- + 3\bar{e} \rightarrow Al + 4Cl^- \quad [7]$$

Equation 8 describes the anodic reaction on an inert substrate, chlorine evolution, that would occur in an electrowinning (EW) setup from an acidic IL system.

$$6AlCl_4^- \rightarrow 3Al_2Cl_7^- + 3/2Cl_{2(g)} + 3e^- \quad [8]$$

The overall aluminium electrowinning reaction in chloroaluminate ILs is Equation 9 (Equation 6 + Equation 8).

$$Al_2Cl_7^- \rightarrow Al + AlCl_4^- + 3/2Cl_{2(g)} \quad [9]$$

1.2 Aluminium

Aluminium was first isolated in 1808 by H. Davy who produced a crude Al-Fe alloy. Compared with other reactive metals Al is a relatively new discovery as titanium was discovered in 1721 and magnesium in 1755. Later, in 1825, Hans Christian Oersted of Denmark created an Al amalgam by reacting aluminium chloride with a potassium amalgam. Pure aluminium was then obtained by boiling off the mercury under reduced pressure (Grjotheim 1977, p. 3).

The mechanical properties of the metal were not realized until 1845, when Friedrich Wöhler produced pin-head globules of Al by reacting aluminium chloride with potassium vapour (Chadwick 1958, p. 90).

A French chemist, Henri Étienne Sainte-Claire Deville, developed a method for commercial production in 1854. He first produced sodium by reacting sodium carbonate with charcoal. Aluminium chloride was then produced from bauxite ore (originally found at Les Baux, Provence, France). The ore (50-65% alumina) was crushed and reacted with caustic soda. Sodium aluminate leached into solution when water was added. The slurry was filtered and pure alumina was precipitated using carbon dioxide. The alumina was converted to aluminium chloride by heating it with charcoal and a stream of chlorine gas. Reduction of the aluminium chloride ensued from passing hydrogen gas to remove the chlorides as chlorine gas. The chlorine was removed from the gas by a reaction with a liquid sodium bath. This process produced 92% pure aluminium (with iron and silicon impurities) but purity was improved to 96% pure Al by using $NaAlCl_4$ instead of $AlCl_3$ since the former is less volatile and less hygroscopic (Grjotheim 1977).

The standard industrial method of reducing alumina was discovered in 1886 by two researchers working independently on different continents, Charles Martin Hall in America and Paul Louis Toussaint Héroult in France. This electrolytic process is known as the Hall-Héroult process. It became feasible with the availability of electric power (Chadwick 1958, p. 91). The following year (1887), Karl Josef Bayer of Austria patented an improved method to produce alumina from bauxite ore (German Patent 43,977 and U.S. Patent 382,505) that is the industrial standard today. Figure 4 describes the major operations involved in producing primary aluminium. The most energy intensive operation in the process is the reduction of alumina, followed by carbon anode production, alumina production and ingot casting (Choate 2003, p. 4).

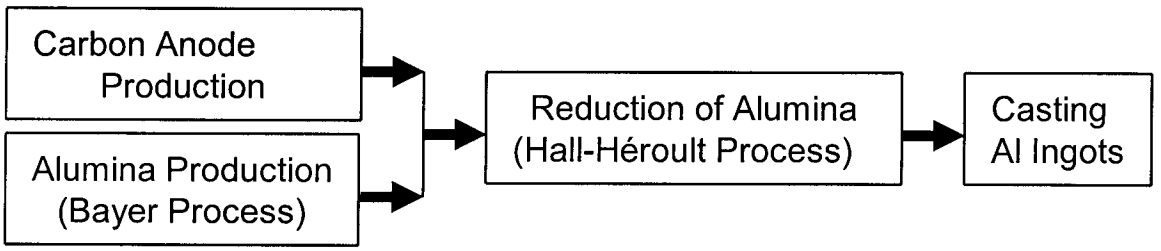

Figure 4 Major operations involved in the production of aluminium.

Ore types and alumina production

The most important aluminium ore is bauxite; "bauxite describes sedimentary rocks that contain economically recoverable quantities of the aluminum minerals gibbsite, boehmite and diaspore" (Frank 1997, p. 1068). Aluminum is rarely found in its native form, however; its existence has been reported in Russia, China and in lunar soil (Frank 1997, p. 1040). Bauxite deposits are usually in tropic or sub-tropic areas. In 2003, six countries accounted for 83% of the world's Bauxite production; Australia (38%), Guinea (11%), Jamaica (9%), Brazil (9%), China (8%), and India (6%) (Plunkert 2004, p. 31). Bauxite ore is usually surface mined and some of the clay is carried out by washing or screening and cycloning, and in some cases, hand sorting (IAI Website, 2004). There are over 1000 aluminium minerals in existence; the most commonly used form of aluminium for production purposes are its oxides. Table 4 summarizes the main aluminium oxides minerals.

Table 4 Aluminium oxide minerals (Frank 1997, Korbel 1999 and Websites: Webminerals and IAI).

Phase	Formula	Structure	Comments
Corundum	Al_2O_3	Trigonal	Formed at temperatures > 683 K
Diaspore	AlO(OH)	Orthorhombic	Higher leaching temperature than Böhmite
Böhmite	AlO(OH)	Orthorhombic	Less dense than Diaspore 3.0:3.4 g/cm^3
Bayerite	$Al(OH)_3$	Monoclinic	Natural Bayerite is rare
Gibbsite	$Al(OH)_3$	Monoclinic	Dominant form of alumina mined
Nordstrandite	$Al(OH)_3$	Triclinic	-

α for most densely packed structures (bayerite, diaspore and corundum)
γ for cubic packing (gibbsite and böhmite)
β for nordstrandite when the compound is an independent modification

A typical bauxite ore is composed of 30-60% Al_2O_3, mainly as gibbsite but can be up to 20% böhmite, 1-30% Fe_2O_3, 0.5-10% SiO_2, 0.5-10% TiO_2, and up to 2% CaO. Other minor constituents include: organic carbon, P_2O_5, V_2O_5, ZnO, Ga_2O_3, Cr_2O_3, S, F, and Hg (Authier-Martin 2001, p. 39).

The production of pure alumina (the Bayer Process), begins with bauxite ore being ground in ball mills and pre-treated with NaOH and CaO. Böhmite, gibbsite and diaspore are then selectively dissolved in heated sodium hydroxide solutions (125-255 g/L NaOH) at 373-533 K (Authier-Martin 2001, p. 36). The exact conditions required vary depending on the type of bauxite that is being processed. The leaching reaction takes place at elevated pressure and is described by Equation 10 (Frank 1997, p. 1072):

$$Al(OH)_3 + Na^+ + OH^- \rightarrow Na^+ + Al(OH)_4^- \quad [10]$$

The unwanted minerals (red mud) do not dissolve to a significant extent and are physically separated from the solution by decantation and filtration. Pure $Al(OH)_3$ is then precipitated upon cooling the solution. The $Al(OH)_3$ slurry is filtered and the solids are calcined at 1223-1373 K to produce smelter grade alumina (99.5% Al_2O_3) (Authier-Martin 2001, p. 36). Four or five tonnes of bauxite are required to produce two tonnes of alumina, which in turn only produces about one tonne of aluminium. The cost of alumina at U.S. smelting facilities ranged from 265-700 USD/tonne in 2006 (Plunkert 2007).

Carbon anodes

A large amount of the energy required to produce aluminium is spent on making carbon anodes. Carbon anodes are consumed during Al electrolysis at a rate of 0.4-0.5 kg-Anode/kg-Al produced (Frank 1997, p. 1045). In energy terms, this is 0.67 kWh/kg-

Al spent in anode production alone (Choate 2003, p.23). High purity anodes are required to prevent contamination of the aluminium. The production of the carbon anodes requires processing petroleum coke at 773 K followed by calcining at 1473 K. There are two main types of anodes that are used for aluminium electrolysis (1) pre-baked anodes, up to 20 / cell and (2) the Sàderberg type, that are baked *in-situ* using the waste heat of the furnace in the form of a large single anode / cell. For environmental reasons there has been a movement towards the pre-baked anodes (Sverdlin 2003, p. 22). The specific advantages of the pre-baked anodes are high electrical conductivity, high resistance against oxidation by the air above the cell, high mechanical strength, low porosity and high purity (Grjotheim 1977, p. 324).

Reduction of Al_2O_3

The Hall-Héroult process is the production of commercial purity (>99.0%) aluminium at high temperature (1223 – 1273 K) by reducing metallurgical alumina in a molten cryolite bath. This process step takes place in a steel shelled carbon lined cell (pot) where the alumina is fed from above and is reduced at the molten aluminium cathode that is submerged below the cryolite bath. Oxidation takes place at the consumable carbon anode and the aluminium is tapped from the cell by vacuum siphoning.

The overall Hall-Héroult cell reaction is described in Equation 11. The thermodynamic potential (E) of this reaction was calculated to be 1.19 V at 1233 K with alumina concentration saturated and unit activity (Frank 1997, 1053).

$$\tfrac{1}{2}\ \alpha\text{-}Al_2O_3(s) + \tfrac{3}{4}\ C(s) \rightarrow Al(l) + \tfrac{3}{4}CO_2(g) \qquad [11]$$

The power requirement of a state of the art aluminium plant is about 13 kWh/kg Al while the industrial average is 15 kWh/kg Al. The main reason is that the Söderberg facilities are less efficient than pre-baked facilities with point break feeders (90% vs. 94% average C.E.) (Creber 2007). The theoretical power requirement for the electrolysis of aluminium with carbon anodes at Hall-Héroult conditions was calculated to be 6 kWh/kg Al, considerably lower than a state of the art operation (Choates 2003, p. 25). Nolan Richards described the factors involved in potential requirements of a Hall-Héroult cell, Equation 12 (Richards 1994, p. 393):

$$V = E + |\eta_A| + |\eta_C| + I(R_A + 1/K \cdot d/A_B + R_C + R_{ex}) \quad [12]$$

Where,

E is the electrochemical decomposition potential of Al_2O_3 at the state of the cell (V)

η_A is the anode overpotential (V)

η_C is the cathode overpotential (V)

I is the line current (A)

R_A is the resistance of the anode stem (Ω)

K is the electrical conductivity of the bath (S/m)

d is the inter-electrode distance (m)

A_B is the cross sectional area of the bath (m^2)

R_C is the resistance of the cathode system out to the bus bar (Ω)

R_{ex} is the bus bar resistance (Ω)

The overpotentials (η_A and η_C) are considered to be the sum of four components: (i) charge across the double layer (ii) charge transfer between the bulk solution and the interface by diffusion (iii) chemical reactions in the solution or at the surface and (iv) crystallization reaction where atoms are added or removed from the lattice.

The energy parameters of aluminium electrowinning are tabulated in Table 5.

Table 5 Conditions for aluminium electrowinning by the Hall-Héroult process.

Processing rate / unit operation[a]	0.07	Tons/m^3/day
Current density	7000[a], 8000-8500[f]	A/m^2
Electrolyte conductivity[b]	250	S/m
Carbon consumption[c]	0.4-0.5	kg/kg-Al
Energy efficiency[b]	40-45	%
Current efficiency[b]	85-92 (up to 96[e])	%
Operating cell potential[b]	4.5 (as low as 4.0)[g]	V
Reversible cell potential[b] (E_{MF})	1.2	V
Anodic overvoltage[d] (n_a)	0.5-0.6	V
Cathodic overvoltage[d] (n_c)	0.1	V
Voltage drop in the electrolyte[a,b] (U_E)	1.8*	V
Voltage loss in the cell hardware (U_H)	0.85** (0.79[e])	V

[a] Evans 1995
[b] Ettel 1977
[c] Frank 1997
[d] Galasiu 1999
[e] Creber 2005
[f] Øye 1999
[g] Evans 2007
*Calculated (40% of 4.5 V)
**Calculated (4.5 V – EMF – η_A – η_C – U_E – U_H)

Using the information in Table 5 and considering the current inefficiency (C.I.) to be 5 %, the stray currents (S.C.) to be 1 % and the voltage loss in the hardware to be 0.85 V, an Ettel diagram describing the energy distribution of aluminium electrowinning using the Hall-Héroult method was produced (Figure 5). The surface area on the Ettel diagram represents the distribution of power utilization in a given process. The main reason for the increase in current efficiency since the 1970's are the lowering of the cell operating temperature to 1208 K and changes in the bath ratio of NaF to AlF_3 to about 1.1-1.15 (Evans, 2007). The largest portion of the power is required simply to overcome resistance in the electrolyte (U_E). The thermodynamic energy required to drive the electrochemical reaction (E_{MF}, Equation 11) also requires a large portion of the power. Smaller but not insignificant power losses are due to the resistances in the hardware (U_H) and the overpotential required for the anode reaction (η_a).

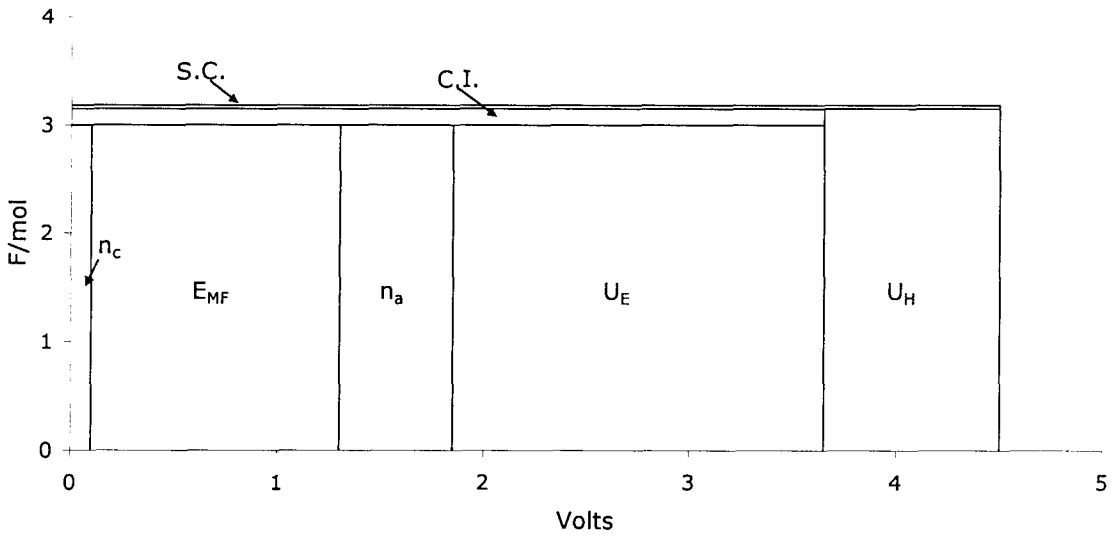

Figure 5 Hall-Héroult process Ettel diagram.

The high electrolyte resistance is due to a relatively large anode-cathode separation of at least 4 cm. Two of the main reasons for this large separation are: (1) The non-level aluminium-electrolyte interface, due to electromagnetic force induced by the electrowinning process, could cause short circuiting (Evans 1995, p. 200) and (2) The current efficiency drops as the electrodes approach each other. This occurs because the reduced aluminium becomes re-oxidized when in contact with dissolved CO_2 (Galasiu

1999, p. 512). Larger anode-cathode separations are avoided because of the ohmic losses. This allows the processing rate/unit cell area to be smaller, as larger cells would be required to do the same job with larger anode-cathode separation. An extra resistance in the process is due to coverage of the anode by gas bubbles, in the extreme case this results in an anode effect whereby the cell potential increases and cryolite is oxidized producing C-F gases.

The anode overpotential is significantly greater than the cathode overpotential, and thus, represents the highest research priority in reducing the cell voltage according to Richards (1994, p. 394). The primary anode half reaction is the evolution of carbon dioxide, Equation 13 (Frank 1997, p. 1049).

$$C + O_2 \rightarrow CO_2 + 4\bar{e} \qquad [13]$$

The evolution of CO_2 is due to kinetics factors as the formation of CO at these conditions is more thermodynamically stable. The oxygen in the electrolyte is actually present as $[Al_2O_2F_4]^{2-}$ and $[Al_2OF_6]^{2-}$ (Grjotheim, 1993, p. 41-43).

The largest component of the electrolyte is cryolite (Na_3AlF_6). Cryolite used to be found in substantial quantities in Greenland but is now usually synthesized, Equation 14 (Frank 1997, p. 1046).

$$6HF + 2NaOH + NaAlO_2 \rightarrow Na_3AlF_6 + 4H_2O \qquad [14]$$

Cryolite can also be recovered from spent pot linings used in aluminium reduction cells. The price of synthetic cryolite was 500-600 US$/t in 1983 (Frank 1997, p. 1046). A typical Hall-Héroult cell electrolyte composition is 75-90 % cryolite, 1-8 % alumina, 1-15% aluminum fluoride, 4-8 % calcium fluoride, 0-5% lithium fluoride and 0-5% magnesium fluoride (Sverdlin 2003, p. 22 and Frank 1997, p. 1045). The additives are used to increase the current efficiency, adjust the solubility of alumina or lower the operating temperature. The operating temperature must be maintained sufficiently low to allow some of the melt to freeze near the cell walls in order to protect them from corrosion.

Environmental considerations

Conventional aluminium reduction processes produce a variety of waste, mainly gases and solids. Table 6 summarizes the rate at which the waste is produced.

Table 6 Waste for smelting and ancillary processes in North America (Richards, 1994, p. 394-96).

Phase	Component	Rate (kg/kg-Al)	Comments
Solid	Spent Pot Liner	0.025	Disposal = 200$ / ton SPL
	Other	0.015	
Liquid	Total Effluents	$9 \cdot 10^{-6}$	
Gas (Emissions)	CO_2	1.4	GWP[b] = 1
	CO	0.15	
	CF_4[a] and C_2F_6	0.0016	GWP[b] = 5,700 and 11,900

[a] Gamble 2003, p. 215
[b] U.S. Department of Energy 2003, p. 21

Global Warming Potential (GWP) is the energy absorbing potential of a gas with respect to carbon dioxide. For example, one molecule of C_2F_6 emitted into the atmosphere will cause as much warming of the earth as 11,900 molecules of CO_2. This is a serious issue because if CO_2 from both anode combustion and the power source are considered, "the aluminum industry could be contributing up to 1.5% of the total CO_2 sourced from fossil fuels in the world" (Richards, 1994, p. 399). As for fluorocarbons, they are produced at a much higher rate when the Hall-Héroult cell experiences an anode effect. The anode effect occurs when the concentration of alumina in the melt drops below about 1% (Choate 2003, p. 34) and the melt no longer wets the surface of the anode causing the potential to increase dramatically. Measures have been taken to reduce the frequency and duration of anode effects, in 1948 there were 3-4 anode effects/pot/day whereas in 1999 this value was down to 0.05 anode effects/pot/day (Choate 2003, p. 26). At higher operating potentials that exist during an anode effect, C-F gases are readily produced. Since the C-F gases have very high GWP's the anode effect is undesirable both for the process and the environment. Other emissions produced during electrolysis include hydrogen fluoride, particulate fluorides, alumina particulates, volatile organics and sulfur dioxide (E.P.A. 1995, 12.1.2., p. 3). Modern fume treatment systems can help prevent a large portion of the gases produced from being released into the environment. Recent improvements in minimizing anode effects have the industrial C-F emissions down to 1.5 CO_2-eq/kg-Al produced and these C-F emissions are projected to drop to 0.3

kg CO_2-eq/kg-Al in the future according to David Creber of Alcan (Personal Communications, 2005). The development of inert anode technology would also significantly reduce the amount of CO_2 being generated (Evans 2007).

Alternative Processes

Although the Hall-Héroult process is presently the industry standard for aluminium production, many alternative processes have distinct advantages such as lower capital costs, lower energy costs, no carbon anode plant and less overall environmental impact. According to Welch (1999, p. 24) the aluminium industry's efforts to remain competitive are to "shift to high amperage technologies that are less energy efficient but more cost efficient".

Welch described some of the possible alternatives to conventional processing in his article. Table 6 is an overview of the main ideas. The minimum power consumption is based on the thermodynamic power requirement; it is not realistic that these power consumptions are attainable because of inherent power consumption due to electrolyte resistance, overpotentials, losses due to hardware, and etc. The drained cell and inert anode technologies would require a substantial change to the way the reduction step is operated today. The use of a wettable TiB_2 cathode would allow the anode cathode distance to be reduced since it is currently limited by waves and ripples on the surface of the molten Al cathode (Choate 2005). The oxygen evolution reaction on the inert anode would require a potential of 1 V more than the current CO_2 evolution using consumable carbon anodes. Advantages would be the elimination of the requirement to produce carbon anodes and an elimination of the large quantities of CO_2 produced. The chloride and sulfide would require an intermediate step to convert the alumina to aluminium chloride or sulfide. The chloride process can be carried out at lower temperatures using ionic liquid electrolytes (Zhang 2003). High temperature carbothermic reduction of Al_2O_3 may be used to produce Al with a 36% energy savings and 60% lower capital cost than a modern Hall-Héroult plant, a fully developed commercial process is believed to be only five years from being realized (Choate 2005).

Table 7 Alternative processes investigated for aluminium production (Welch 1999, p. 26).

Production Process	Features	Min. power consumption kWhr/kg-Al
Drained-Cell Technology	Cathode sloping and coating with aluminum-wettable TiB_2. The anode-cathode gap could then be reduced to ~2.5 cm, enabling substantial voltage lowering.	6.3
Inert Anode Cells (O_2 Evolution)	Eliminate consumable carbon anode by having an electrode material that evolves oxygen. Although the electrochemical potential would increase by 1 V (E° ~ 2.2 volts), the voltage increase would be (hopefully) less because of lower anode polarization. The superstructure of the existing cell could be refined, reducing capital costs. This could be combined with a Drained-Cell technology.	9.3
Chloride Process	Aluminous material converted to (anhydrous) $AlCl_3$ of adequate purity. $AlCl_3$ electrochemically decomposed in a multi-electrode cell at ~973 K, E° ~ 1.8 V. Electrochemically generated chlorine is recycled.	6.3
Ionic Liquid Chloride Process[a]	Aluminous material converted to (anhydrous) $AlCl_3$ of adequate purity. $AlCl_3$ electrochemically decomposed in a multi-electrode cell at ~373 K, E° ~ 1.8 V. Electrochemically generated chlorine is recycled.	< 9
Sulfide Process	Aluminous material converted to (anhydrous) Al_2S_3 of adequate purity. Aluminum sulfide electrochemically decomposed to recyclable S_2 and aluminum in a multipolar cell. E° ~ =1.0 V	5.2
Carbothermal Reduction	Convert aluminous material to an intermediate Al_4C_3 (or oxycarbide) chemically at T > 1973 K. React carbide with further oxide to evolve CO and produce aluminum (or alloy) at T > 2273 K. Refine the metal quality to a usable grade.	9.0

[a] Zhang 2003

Recently, the high cost of electricity in the U.S. has resulted in nearly 40% of the primary Al production capacity to be put on standby (Choate 2005). Choate speculates that the future will include carbothermic reduction, multi-polar cells or ionic liquid primary production processes that can operate economically on a scale that is an order of magnitude below that of current technology.

Many variations of the carbothermic process have been proposed, one that gained significant attention was the Toth process described by Grjotheim (1977, p. 11) whereby aluminium is chlorinated from unrefined Al_2O_3 at 1200 K (Equation 15).

$$Al_2O_3 \text{ (in clay)} + 3C + 3Cl_2 \rightarrow 2AlCl_3 + 3CO \qquad [15]$$

The chlorination step inevitably involves the chlorination of Fe and Ti that is present; Fe chlorides can be oxidized to recover the chlorine. Once the $AlCl_3$ is purified, manganese

is used to reduce the $AlCl_3$ to Al at 500 K. At 873 K in the presence of oxygen the $MnCl_2$ is converted to MnO and finally at 2000 K MnO is reduced back to Mn in the presence of carbon. The Toth process may be useful in the treatment of inexpensive minerals with low Al_2O_3 content (30-40%). The Al produced may contain some Mn (1%) so a refining step would be required to produce a high purity product. A different carbothermic reduction process is currently being developed by Alcoa and Elkem (Evans 2007).

Multipolar electrolytic cells greatly increase the productivity-per-unit-reactor volume, and were successfully demonstrated using $AlCl_3$ at commercial scale in the 1970's by ALCOA. The ALCOA chloride process was adopted by a plant in Palestine, Texas and is summarized here as described by Grjotheim (1977, p. 14). The process begins with the chlorination of pure alumina at 875-1075 K. The electrolysis of the $AlCl_3$ is done in a vertically stacked mulitpolar cell (20-30 cells spaced by 1 cm at about ~973 K). The electrolyte contained about 3-5 wt.% $AlCl_3$ with 53 wt. % NaCl, 40 wt.% LiCl and smaller amounts of $MgCl_2$, KCl and $CaCl_2$. Current densities of 8000-23000 A/m^2 were reported with an energy consumption of 9 kWhr/kg-Al (for the reduction step). The electrolysis produces liquid aluminium that falls to the bottom of the reactor and chlorine gas which is collected at the top. The energy distribution is summarized in by the following Ettel diagram (Figure 6) based on the information provided by Grjotheim for a single cell version of the ALCOA process (1977, p. 16). Stray currents and current inefficiencies were not considered. The thermodynamic reaction potential accounts for a much greater portion of the energy than in the Hall-Héroult process (Figure 5 vs. Figure 6). The thermodynamic energy is higher since chlorine is evolved instead of CO or CO_2 but this is made up for by the considerably lower losses due to electrolyte resistance and in the hardware. The anode overpotential is also slightly less in the chloride process.

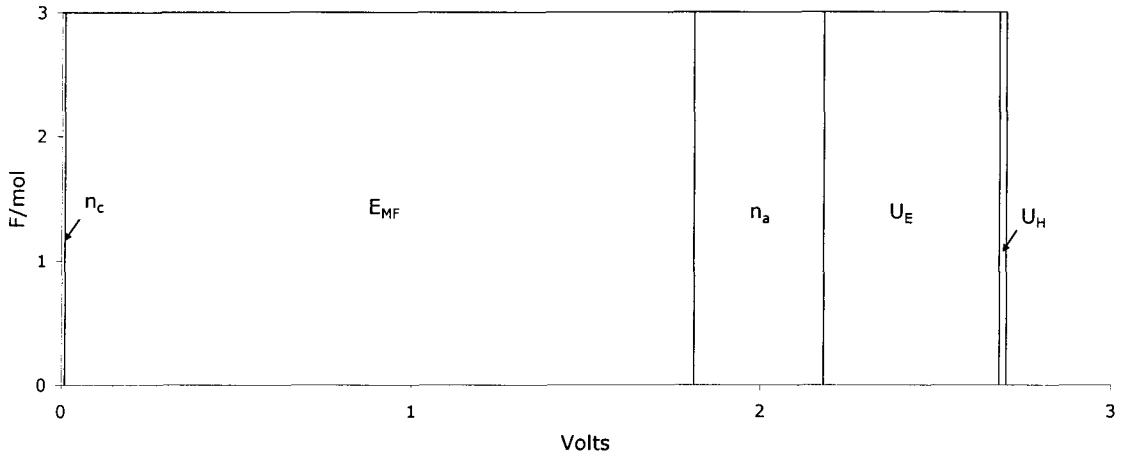

Figure 6 Simplified Ettel diagram for a single cell version of ALCOA aluminum chloride electrolysis process.

According to Choate (2005) new multipolar technologies that involve the reduction of alumina in lower temperature modified cryolyte baths are showing promise. An ionic liquid process would be similar to the multipolar cell setup except the operating temperature would be dramatically lower, possibly resulting in savings in both operating and capital costs. Choate stressed that the ionic liquid technology is "embryonic" and believes that commercialization is likely more than 20 years in the future. Evans stated that the development of primary Al production using IL technology has a higher benefit to cost and risk ratio than a novel carbothermic reduction process (2007).

One of the major issues in implementing a chloride based process is dealing with the off-gas that will consist of chlorine with alkali metal halides, alkaline earth halides and aluminium chloride. The chlorine must be purified for recycling and the halides should be separated and returned to the electrolyte. A process involving sequential condensation steps to achieve both of these goals was described in the patent of Jacobs (1975).

Since the world supply of bauxite is limited, new processes might be required in the future for the production of aluminium from aluminosilicates since they are considerably more abundant in nature (Grjotheim 1977, p. 7). Calcium aluminates are a low cost source of aluminium. However, the melting temperature of these salts is too high for direct electrolysis (1573-1773 K). Some technical challenges to processing this feed

are the low solubility of calcium aluminates in other molten salts and the density of the aluminium-alloy electrolysis product resulting in re-oxidation (Grjotheim 1977, p. 13).

Recycling and refining

Recycling (secondary production) of aluminium is economically and environmentally sound. Recycling aluminium requires 96% less energy than it does to produce aluminium from ore (Habashi 1997). Recycling also requires much less water than primary production (considerable water is required to produce alumina), approximately 11 billion liters of water were used to make aluminium cans that were not recycled in 2001 (Gitlitz, 2002 p. 15). The secondary aluminium industry is constrained by the supply and price of scrap Al. In 2003, 55% of scrap Al was new scrap produced during the manufacture of products while the other 45% was post-consumer scrap (Choate 2005).

Aluminium has been recycled ever since the metal was produced. It was not until the advent of used beverage container recycling, a standard feed, that large-scale producers began to incorporate this material into ingot production as used beverage containers account for a large portion of post consumer Al scrap. In 1995, 33% of the Reynolds Metal Company's Aluminium was from recycled feed (Øye 1999, p. 40). The recycling of used beverage containers begins with shredding of the metals. Metals such as iron are removed using a magnetic separator. Iron is recycled in a separate process. The fine particles and heavy metals are also separated using a vibrating screen. A delacquering (decoating) step to remove lacquer and ink is then carried out by blowing air at 773 K through the feed that is on a conveyer belt (website: Alcan UK, unfortunately the information no longer appears to be available online). This step can also be carried out at higher temperatures, for example the APROS delacquering process operates at 933 K (E.P.A. 12.8-2, p.10). The decoated aluminium is then melted at 973 K.

Although a significant amount of aluminium is being recycled, a tremendous amount is still ending up in the trash. An estimated 50.7 billion cans were not recycled in the U.S. in 2001. Had these cans been recycled, the equivalent energy savings would have been 16 million barrels of crude oil (Gitlitz 2002, p. 1). In the United States, 22% of all primary aluminium goes towards making aluminium cans (Gitlitz 2002, p. 8). Evans

(2007) noted that the mass of recycled beverage containers in the U.S. has been dropping since 1999 and the recycling rate of the containers is lower in Europe than in the U.S.

Hydrometallurgical cleaning is used to recover aluminium from dross, furnace skimming and slag. The general process begins with wet milling where water-soluble components are leached out. The remaining material is washed and screened to remove fines followed by magnetic separation to separate the iron (E.P.A. 1995, 12.8-2 p. 10).

Heavy media separation is used to concentrate aluminium from feeds such as shredded automobiles; concentrates of 80% aluminium from a 30% feed are typical (E.P.A. 1995, 12.8-2, p.10).

An important aspect of all aluminium recycling processes is to minimize the oxidation of aluminium during the melting process. An example of a method accomplish this is in a reverberatory-style melting furnace is vortex melting. A vortex is induced by a rotating disk. The vortex allows for quick melting of the light scrap because of swirling action and aids in submerging the scrap below the surface of the molten metal and salt flux (Øye 1999, p. 40). The molten aluminium is then purified by degassing and filtering on its way to the slow casting or further hot metal processing.

Demagging is a process that follows melting whereby the magnesium content of the aluminium is reduced from about 0.5% to 0.1%. Chlorine or fluorine is added to the melt as chlorine gas, anhydrous aluminium chloride, organic chloride, or aluminium fluoride. The chlorine or fluorine reacts with magnesium in the melt and the lower density magnesium compound reports to the slag layer or is released as a corrosive fume. The un-reacted chlorine from demagging is also released and accounts for a large portion of the hazardous gasses produced in secondary aluminium production (E.P.A. 1995, 12.8-10, p.10).

Metal matrix composites (MMC) are currently recycled by separating the aluminium from the composite by high exposure to high temperature molten salts to de-wet the ceramic particles from Al matrix. A recycling process using ionic liquids ($AlCl_3$-BMIC) was proposed by Kavaraman (2004) whereby the MMC is anodically polarized to dissolve the Al and the Al is then plated at the cathode. The current efficiencies reported are above 84% and the power consumption less than 6 kWhr/kg-Al at 376 K. The deposited Al contained about 1% Cu and lower concentrations of Mg, Ni, Zn and Fe.

For most applications, the purity of the aluminium produced from the Hall-Héroult process is sufficient (~99.7%). However, when higher purity Al is required, the Alcoa three layer electrolytic aluminium refining process can be used. The setup and operating temperatures and power consumption (17-18 kWh/kg-Al refined) is similar to the Hall-Héroult. The high energy requirements of this refining process are due to the small scale of the operation resulting in high heat loss (Wernick 1998, p. 485). The current efficiency of this type of process is nearly 100% (Davies 1976).

The Beck process for recycling and refining light metals purifies molten aluminium from alloys, and other non-metallic impurities by the addition of magnesium chloride combined with some metal oxides (Beck 1926). An example from the patent was the purification of a melt containing aluminium turnings and sheet metal waste with non-metallic impurities on the order of 1-3%. The procedure began by the adding of 3 kg of a mixture of 70% $MgCl_2$ and 30% MgO to the stirred melt. The melt was superheated by 100 degrees K and then cooled to the casting temperature. A slag formed that contained 96-99% of the impurities; the slag was separated upon pouring.

The Alcan sub-halide process was developed to refine Al alloy that might be produced by a carbothermic reduction. The process takes advantage of the fact that Al vaporizes at relatively low temperatures under vacuum in the presence of halides and at higher temperatures (1573 K) a sub-halide (AlCl(g)) can be formed (Grjotheim 1977, p.12). AlCl(g) is decomposed in a condenser to produce 2/3Al and 1/3$AlCl_3$. The presence of $FeCl_3$ or $MnCl_2$ may contaminate the product.

1.3 Magnesium

There seems to be some confusion as to exactly how magnesium was first isolated, however, it was probably first produced by H. Davy in 1808. Table 8 summarizes the major developments pertaining to the production of Mg, specifically the growth of the industry and the shift in the dominance of the two major production methods are compared (electrolysis vs. metallo-thermic reduction).

Table 8 Developments and history of magnesium production.

Date	Scientist	Development
[b]1755	J. Black	Recognized magnesium as an element
[a]1808	H. Davy	Mg was isolated by electrolysis of $MgCl_2$ using Hg cathode
[b]1808	H. Davy	Isolated Mg by electrolysis of a mixture of MgO and HgO
[d]1808	H. Davy	Produced an amalgam of Mg by electrolysis of moist $MgSO_4$ using Hg as a cathode
[g]1808	H. Davy	He found that magnesium oxide was the oxide of a previously unknown metal. He also was the first to isolate a small quantity of magnesium from magnesium oxide.
[a,c,f]1828	A.A. Bussy	Extracted Mg by reducing fused $MgCl_2$ with K and Na vapour
[a]1833	M. Faraday	Electrolyzed dehydrated $MgCl_2(l)$ to get Mg(l) and $Cl_2(g)$
[c]1852	R. Bunsen	Considerable quantity of Mg by electrolysis of $MgCl_2$
[a]1886		Industrial production of molten Carnallite, Germany
[d]1913		World production ~300 tons/year
[d]1914-1918		World production ~1,000 tons/year
[d]1938		World production ~25,000 tons/year -Almost exclusively by electrolysis
[a]1940	M. Pidgeon	First industrial metallo-thermic Mg extraction plant, Canada
1943		World production ~230,000 tons/year [c] World production 436,000 tons/year [g] U.S.: 73% electrolysis, 23% silico-thermic, 4% carbo-thermic [c]
[d]1969		World production ~158,300 tons/year (except USSR) 85-90% by electrolysis
2003		World production ~447,000 tonnes/year (except U.S.)[e] 80% by electrolysis[f] ~50% by electrolysis[e*]
[h] 2006		World production ~20% by electrolysis!

[a] Andreassen, 1997, p. 981
[b] Website (webelements.com)
[c] Strelets, 1977, p. ix
[d] Encyclopedia Britannica Website (http://www.britannica.com/)
[e] Kramer, 2004, p. 104
[e*] Estimated from the data in Kramer, 2004. Assuming Chinas production is non-electrolytic and the rest of the world is electrolytic.
[f] Website (http://www.magnesium.com/w3/data-bank/index.php?mgw=64)
[g] U.S. Bureau of Mines, 1963
[h] Harris, 2006

There are two established industrial processes for the production of magnesium; electrolysis of magnesium chloride melts (Figure 7) and metallo-thermic (silico-thermic) reduction of magnesium oxide (Figure 8). The literature review for this thesis will focus on the electrolytic reduction process only.

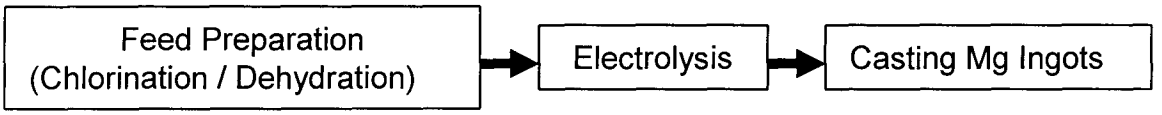

Figure 7 Major operations involved in the production of magnesium by electrolysis.

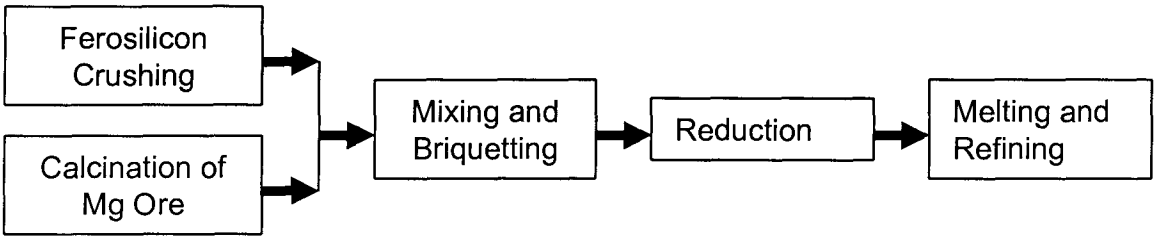

Figure 8 Major operations involved in the production of magnesium by metallo-thermic reduction.

The recent history of Mg production is very dynamic as far as processing route, the thermal production method dipped in popularity in the 1970's and 80's only to be brought back in recent years by China increasing their production drastically using the silicothermic reduction. China increased from 18% to 55% of the world's production between 1998 and 2002 (British Geological Survey, 2004, p. 2). This dramatic change by China's numerous labour intensive silico-thermic producers decreased the profitability of western magnesium producers limiting expansion and forcing several closures. One of the closures was Noranda's Magnola operation that used novel technology to recycle asbestos mine tailings in Quebec (Ficara 1998, p. 75). The only Canadian silicothermic operation is in Haley, Ontario. Timminco's Haley operation underwent "realignment to overcome intense labour utilization" (Froats 1980, p. 969) during the 1970's. This increase in the Mg output of China coupled with the demise of many North American electrolytic operations has resulted in the amount of Mg produced electrolytically to be as low as 20% (Harris 2006).

Presently, the main uses for Mg are as alloying agent for Al, desulfurization and nodularization in the iron and steel industry, for magnesium based alloys and in chemical

or metal production processes such as Ti, Zr, U, Be and Hf, and also as sacrificial anodes (Andreassen 1997, p. 1000).

Production

Ore types and production of magnesium chloride

In 1988, 42% of the magnesium produced was from dolomite ores, 36% from marine evaporates (brine deposits), 18% from seawater and 4% from magnesite (Andreassen 1997, p. 983). Out of over 1500 known minerals, more than 12% are magnesium compounds (Strelets 1977, p. 10). Some of the more common minerals are tabulated in Table 9.

Table 9 Magnesium-containing compounds (Andreassen 1997, p. 983).

Phase	Formula	Crystal System[a]	Comments
Dolomite	$CaMg(CO_3)_2$	Trigonal	
Magnesite	$MgCO_3$	Trigonal	
Brucite	$Mg(OH)_2$	Trigonal	
Serpentine[b]	$Mg_3Si_2O_5(OH)_4$	Monoclinic	Asbestos tailings
Carnallite	$KMgCl_3 \cdot 6H_2O$	Orthorhombic	Marine evaporites
Kieserite	$MgSO_4 \cdot H_2O$	Monoclinic	Marine evaporites
Bischofite	$MgCl_2 \cdot 6H_2O$	Monoclinic	Marine evaporites
Kainite	$MgSO_4 \cdot KCl \cdot 3H_2O$	Monoclinic	Marine evaporites
Langbeinite	$K_2Mg_2(SO_4)_3$	Isometric	Marine evaporites

[a] Webminerals Website 4
[b] Nagamori 1999, p. 103

Some typical compositions of dolomite and magnesite ores are shown in Table 10 with approximate concentration ranges.

Table 10 Typical magnesium ore compositions.

Type	Content, %			
	MgO	CaO	Al_2O_3	SiO_2
[a]Dolomite (Russian)	18.1-24.8	26.8-36.2	0.2-3.0	0.1-4.7
[a]Magnesite (Russian)	40.7-47.5	0.3-3.9	0.1-4.2	0.2-4.1

[a] Strelets, 1977, p. 11-12

When the HCl leaching of serpentine was compared magnesite, it was found that although they both produced similar concentrated salt solutions, the serpentine process yields about 25 times more wet filter cake and wash water than the magnesite process (Nagamori 1999, p. 103).

According to Strelets, "Pure natural magnesite is the best starting material for the manufacture of anhydrous $MgCl_2$ by chlorination" (1977, p. 19). Prior to chlorination, magnesium oxide is produced from natural magnesite by calcining in a rotary furnace or fluidized bed at 973-1073 K. Magnesium oxide is also prepared via $Mg(OH)_2$ from seawater or industrial wastes (e.g. potash industry) containing $MgCl_2$. Pure dolomite limestone is used as auxiliary material. The following reaction takes place at ~368 K with 2-5 g-$MgCl_2$/L in excess of the stoichiometry required, Equation 16 (Strelets 1977, p. 19).

$$MgCl_2 + Ca(OH)_2 \rightarrow Mg(OH)_2 + CaCl_2 \quad [16]$$

The moist $Mg(OH)_2$ precipitate is filtered out and calcined at 753 K.

Another method to prepare magnesium oxide is by way of basic magnesium carbonate. For example, magnesite is crushed to 15-25 mm in size and calcined in a rotary furnace. The calcined magnesite is ground to P_{90} of 0.0576 mm and hydrated with water, heated with steam and a dilute $Mg(OH)_2$ slurry is carbonated in a tower with CO_2(g) from the calcinations furnaces, Equation 17 (Strelets 1977, p. 20-25).

$$Mg(OH)_2 + 2CO_2 \rightarrow Mg(HCO_3)_2 \quad [17]$$

The combination of air sparging and centrifuging at 318-323 K allows for the precipitation of $MgCO_3.3H_2O$. The moist carbonate is then decomposed in a rotary furnace to produce pure MgO.

Chlorination

This description of the chlorination processes is limited to magnesia and dolomite feeds. Processes dealing with carnallite feeds are described in detail by Strelets (1977).

The chlorination of MgO in the presence of carbon is exothermic and thus does not require a great deal of supplied heat. Carbon is required as a reducing agent to limit the partial pressure of oxygen in the reactor. The IG Farben Process involves the formation of pellets (50% MgO) from $MgCl_2$ brine that are fed to the chlorinator while the MagCan process feed is crushed natural magnesite (Andreassen 1997, p. 985).

Industrial chlorination reactors are electric shaft furnaces that operate in the range of 1073-1473 K. Magnesium oxide is converted to magnesium chloride in the presence of carbon and chlorine gas (Strelets 1977, p. 28).

Another method for producing $MgCl_2$ from magnesite is the Australian Magnesium Process. In this process, magnesite is leached with HCl to produce $MgCl_2$ brine. Impurities are removed by precipitation and filtration. The solution is then dehydrated with glycol and crystallized with NH_3 as $MgCl_2.6NH_3$. The NH_3 is removed by heating in a fluidized bed (Ramakrishnan 2004, p. 173).

The production method of $MgCl_2$ from dolomite depends on the availability of hydrochloric acid or ammonia. The HCl process begins with crushed calcined dolomite being mixed with water at 368 – 373 K to 17% solids in solution (Strelets 1977, p. 61). The slurry is then diluted to 11% solids, cooled to 333 K and purged with CO_2 to precipitate the Ca as $CaCO_3$. Upon completion of the carbonation the slurry is neutralized to a pH of 7-8 with HCl converting the $Mg(OH)_2$ to $MgCl_2$. The slurry is then thickened and filtered into cake form. The ammonium chloride process begins with calcined dolomite being slaked as in the HCl process and the slurry is reacted with ammonium chloride (a waste product of the soda industry), Equation 18 (Strelets 1977, p. 63).

$$Mg(OH)_2 + Ca(OH)_2 + 4NH_4Cl \rightarrow MgCl_2 + CaCl_2 + 4NH_3 + 2H_2O \qquad [18]$$

Ammonia can be recycled to the soda industry. Calcium is precipitated by carbonation, similar to the HCl process.

Dehydration of $MgCl_2$

The presence of moisture during the electrolysis of magnesium chlorides is harmful to the process, hydrogen and oxygen evolution result is loss of current but more seriously moisture (or hydroxyl ions) will react with the magnesium to create MgO that can lead to passivation of the cathode. Magnesium chlorides obtained from aqueous solutions must then be dehydrated.

Reduction of $MgCl_2$

Mg electrolysis feed is of the form $MgCl_2$(s), $MgCl_2$(l), dehydrated carnallite ($MgCl_2$·KCl(s), Russia only) or $MgCl_2$·1.5H_2O(s). The feed contains 3-8% alkali chlorides as well as minor concentrations of C, SiO_2, MgO, SO_4^{-2}, B and heavy metal compounds (Andreassen 1997, p. 984). The products of electrolysis are chlorine gas and liquid Mg which are both less dense than the electrolyte. The separation of Cl_2(g) from Mg(l) is achieved either by cell partitions such as in the I.G. Farben cell or circulation of the electrolyte into a separation chamber as is used in the Norsk Hydro cell design (Evans 2007).

The properties of the melt vary with the melt composition, the precise conditions depends on the feed ($MgCl_2$ or carnallite). Generally lower viscosity is preferred as this facilitates separation of the Mg from the electrolyte. Surface tension is an important factor in that the cathode must be well wetted by Mg(l) to allow a high current yield. Density, fusibility, solubility, conductivity, vapour pressure, decomposition potential, dissolution of chlorine are other parameters that must be considered. Table 10 and Table 11 summarize the effects of major and minor melt components with respect to cell operating parameters such as the components concentration, melting point and decomposition potential (E).

Table 11 Electrolyte composition, major components (Strelets 1977, p. 148 and 207).

Component	Typical conc. wt.%	Melting point K	Decomposition E, V at 973 K	Effect
NaCl	50 – 60	1073	3.25	Increases current yield conductivity, decreases surface tension and liquidus temperature
$CaCl_2$	30 – 40	1047	3.28	Increases density, viscosity, surface tension and current yield, decreases liquidus temperature
$MgCl_2$	6-14	991	2.59	Current yield decreases if concentration < 8 wt% p. 227
KCl	0 – 6	1041	3.53	Decreases the activity of $MgCl_2$ Lower density than NaCl
$BaCl_2$	0 – 15	1232	3.62	Increases current yield Used to remove sulphates
LiCl	0 – 10	879	3.53	Increased conductivity, decreased density
Mg, Ca, Na Fluorides	1 – 2	-	-	Decreased surface tension of Mg Dissolves MgO passivation films

Table 12 Electrolyte composition, minor components (Strelets, 1977 p. 207 and p. 248).

Component	Max impurity content, %	Decomposition E, V at 973 K	Effect
$MnCl_2$	0.06 (Mn)	1.85	Sponge layer passivates the cathode
$FeCl_2$	-	1.16	Oxidizes at the anode Sponge layer passivates the cathode
$FeCl_3$	0.04	0.78	Reduces at the cathode Sponge layer passivates
$AlCl_3$		1.73	Can improve wettability of the cathode
$TiCl_3$	0.008 (Ti)	1.82	Sponge layer passivates the cathode
$TiCl_2$	0.008 (Ti)	1.83	Sponge layer passivates the cathode
Si	-	-	Contamination from electrolyser liner $Mg_2Si + 2H_2O \rightarrow SiH_4 + 2MgO$ $Mg_2Si + 4HCl \rightarrow SiH_4 + 2MgCl_2$
B_2O_3	0.002	-	Causes a strong cathode passivating film
MgO	0.5	-	Passivates the cathode Evolves at/and consumes the anode
MgS	-	3.4	-
SO_3	0.03	-	Forms MgS
H_2O	0.1	-	Forms MgO

Early Mg electrolysis cells had no diaphragms, however, in the 1930's, diaphragmed cells became commonplace. The diaphragms are actually partitions that are immersed 15 to 25 cm into the melt in order to separate the $Cl_2(g)$ from the Mg(l) (Strelets 1977, p. 250). Anodes are graphite and potash glass (p. 251). The cell is contained in a brick lined steel shell. Important parameters are the inter-electrode distance, electrode size, current density and temperature (current yield). Losses in efficiency are due to simultaneous discharge of other metal ions, reaction between the metal and gas liberated at the anode, reaction between the metal and the impurities contained in the electrolyte or with products of electrochemical side reactions, redox reactions involving polyvalent Mg ions, Mg droplets that dissolve from the cathode surface and circulate in the melt react with chlorine (p. 277-278).

The voltage balance for magnesium electrolysis is described by Equation 19 (Strelets 1977, p. 289), it is essentially the same as that of Al electrolysis.

$$U = E_{MF} + U_E + |\eta_a| + |\eta_c| + U_H \qquad [19]$$

Where,

U is the voltage applied to the electrolyser

E_{MF} is the decomposition voltage

U_E is the voltage drop in the electrolyte

η_a is the anodic overpotential

η_c is the cathodic overpotential

U_H is the voltage drop in the leads to the terminals

The IG cell was developed in 1930 while the Norsk Hydro Cell was introduced in 1978 and shortly thereafter the Alcan Multipolar Cell (1980). The industrial average power consumption for magnesium electrolysis is 15 kWh/kg-Mg (Creber 2005). The most energy efficient cell is the Alcan Multipolar cell that first operated in Osaka with power consumption of 9.5-10 kWh/kg-Mg including busbar loss (Sivilotti 1988, p. 817). During the electrolysis of Mg 150-200 kg of Cl_2(g)/tonne-Mg is collected (Strelets 1977, p. 306). Some of the operating parameters of the various Mg electrolysis technologies are summarized in Table 13.

Table 13 Operating parameters of industrial magnesium electrolysers (Andreassen 1997, 990-993)

Cells	Temp. K	Cl_2(g) Collected %	[a]E V	Pwr. kWh/ kg-Mg	C.E. %	Comments
IG	1023-1063	90-95	-	16-18	80-85	15-20 kg anode/tonne Mg graphite anode, steel cathode, >4.0 t/d[a]
Norsk Hydro	973-993	98	5.3	12-14	-	Solid or liquid feed
VAMI	973-1013	-	-	13.5	80	
Alcan	933-953	>97	-	9.5-10 [a]10.5	-	Multipolar cell Anhydrous $MgCl_2$ feed
Ishizuka	943	>96	-	-	76	Bipolar cell Anhydrous $MgCl_2$ feed
Dow	973	-	-	-	80	60-70 kg anode / tonne Mg Treats hydrous feed
[a]MagCorp	-	-	5.0	12.6	-	2.8 t/d
[a]AVISMA	-	-	4.7	13.5	-	0.7 t/d Bottom Entry
[a]UKTMP	-	-	4.8	13.2	-	1.8 t/d Top Entry

[a] Evans 2007

Alternative processes

The electrolysis of MgO in fused fluorides has been considered; the drawbacks to this process are low MgO solubility and metal collection problems (Andreassen 1997, p. 983, *Cited:* Lysenko 1987). Carbothermic reduction of MgO is not used industrially due to high reaction temperatures and rapid cooling suppresses MgO formation (Andreassen 1997, p. 983, *Cited:* Elkins 1967)

Recycling and refining

As is the case with aluminium, recycling magnesium requires much less energy than production of primary metal, 3 kWh/kg-Mg vs. 35 kWh/kg-Mg respectively (Riopelle 1996, p. 44 *Cited:* Hydro Magnesium 1995). Sources of secondary magnesium feed include automobile crank-cases, transmission housings, beverage cans, and scrap from product manufacture and sludge from magnesium melting operations. Recycling of this material is complicated by the presence of chemical or organic coatings and oil. Also iron is a problem as an iron/manganese ratio greater than 0.04 in magnesium alloys increases the metals general corrosion rate significantly (Riopelle 1996, p. 44). The conventional recycling technology involves scrap being charged into a steel crucible at 948 K, flux is added (chloride salts, potassium, barium, magnesium oxide, calcium fluoride). The melt is stirred with nitrogen or argon. Steel salts and oxides coagulate at the bottom of the furnace. The molten magnesium is then pumped, poured or ladled into a holding tank or cast into ingots. Emissions include: particles of magnesium oxides, nitrogen oxides, carbon monoxide and non-methane hydrocarbons (E.P.A. 1995, 12.12.3, p. 12).

To obtain chloride and fluoride-free products a fluxless method of recycling was developed similar to the conventional method except the melt is covered by a gas to prevent oxidation, either SO_2, HFCs, SF_6 or N_2 (Antrekowitsch 2002, p. 44). This process is only applicable to high quality scrap. The different classes of Mg scrap and recycling methods are described in Table 13.

Table 14 Secondary magnesium material and recycling scenarios (Antrekowitsch 2002, p. 46).

Scrap Class	Characterization	Problems	Recycling Methods
1A	High grade, clean, no impurities	-	Flux-free, recycling with flux
1B	Clean scrap with a high surface are to volume ratio	-	Recycling with flux
2	Clean scrap with aluminium or steel inserts (no Cu or brass)	Fe and Si content	Magnetic separation / ICF* if necessary
3	Clean, dry and uncontaminated turnings	High surface → melt loss, oxide content	Compacting, Increased flux quantity / cover gas
4	Flux free residues (dross, sludge)	Oxide and Fe content	Increased flux / ICF* if necessary
5	Painted or coated scrap (no Cu or brass)	Coating/painting → melt losses, Fe, Si, Ni content	Shot blasting, thermal decoating, ICF* if necessary
6	Oily and or wet turnings	Oil and moisture → melt losses, oxide content	Thermal treatment, chemical treatment, compacting, increased flux, cover gas
7	Unclean and contaminated, post consumer scrap	Oil and moisture, coating/painting → melt losses, oxide content, Fe, Si, Cu, Ni	Magnetic separation, shot blasting, thermal treatment, chemical treatment, ICF* distillation
8	Flux containing residues from Mg-recycling	High content of oxides, chlorides, fluorides (Mg< 30%), Fe-content	Expensive hydrometallurgical processing, at time not realized

*ICF is Intermetallic Compound Formation

Magnesium produced by electrolysis is considered crude Mg and is usually refined. Typical impurity levels are shown in Table 15. Impurities such as Fe, Si, Cu and Ni can be detrimental to the corrosion resistance mechanical properties and surface properties. Also, Mg used as a reductant for other metals must meet stringent purity requirements.

Table 15 Typical impurities in crude magnesium (Strelets, 1977, p. 308).

Impurity	Fe	Si	Ni	Cu	Mn	Al	Ca	Ti	Cl	N	O
ppm	300-500	20-60	10-20	1-20	30-60	10-50	30	50	150	20-200	200

Due to the strong interactions of Mg-Ni and Mg-Cu the removal of Cu and Ni by additives is practically impossible (Antrekowitsch, 2002, p. 48). Methods for refining magnesium are summarized in Table 16.

Table 16 Methods of refining magnesium (Strelets, 1977, p. 312-315 and Antrekowitsch, 2002, p. 47)

Refining Method	Impurities Removed
Flux refining	oxides, nitrides, and other non-metallic impurities, Zn, Cl, Ni
Addn. of Mn, Cr, Mo, Si, Be, Zr, B	Fe
Addition of Co or Zn chlorides	Si
Addition of Ti, Ti compounds, Ti sponge	non-metallic impurities, nitrogen, oxygen, hydrogen, (Fe>Si>Mn>Al>Zn)
Electrolysis	Cu, Mn, Fe, Cl, Ni
Sublimation/Condensation	Al, Fe, Si, Cu

Electrolytic refining is conducted at 973-993 K, the anodic current density is maintained at about 8000 A/m^2, the cathodic current density is 6000-10000 A/m^2. The inter-electrode distance is 7-12 cm. The high-energy expenditure of 9.5-10 kWh/kg-Mg and operating costs are the reasons that this technique has not been adopted by the industry. Sublimation has limited use due to high costs.

1.4 Titanium

A brief summary of the history of titanium is listed in Table 17. Both Gregor and Klaproth were aware of the chemistry involved in producing TiO_2 before 1800; however, it was not until 1918 that the product was commercially available in America. TiO_2 was produced by early researchers using an HCl leach to remove Fe from ilmenite. The remaining dried solid was fused with Na_2CO_3 and taken up in dilute HCl. The solution was then boiled, causing the precipitation of a hydrated TiO_2 (Barksdale 1966, p. 3).

Table 17 History of titanium production.

Year	Scientist	Development
[a]1791	Gregor	Isolated a metal oxide from the black magnetic iron containing sand (Ilmenite) at Manaccan in Cornwall named it Manaccanite
[a]1795	Klaproth	Investigated the red schorl rock in Boinik, Hungary, named the unknown metal Titanium and later showed it was the same as Manaccanite
[d]1887	Nilson and Petersson	94.7 % pure Ti obtained by reducing $TiCl_4$ with Na in an airtight steel cylinder
[a]1908	-	First preparation of pure titanium oxide
[a,b]1910	Hunter	Pure Ti (~99%) was prepared by reacting $TiCl_4$ with Na in a steel bomb at 973-1073 K
[a]1916		First full scale production, Norway
[e]1921	Headden	Proved TiO_2 was harmless to humans by eating (in a short time) 1 pound of TiO_2-$BaSO_4$ composite with glucose.
[b]1937	Kroll	Pure Ti was prepared by reacting $TiCl_4$ with Mg, a similar method is the industrial standard today
[c]2000	Chen, Fray, Farthing	Ti produced by electrodeoxidation of TiO_2 in molten $CaCl_2$

[a] Sibum 1997, p. 1130
[b] Kroll 1964, p. 363
[c] Chen 2000
[d] Barksdale 1966, p. 53
[e] Barksdale 1966, p. 134 *Cited:* Headdon, 1921

The production of metallic titanium is difficult because of its high melting point and affinity for nitrogen, carbon and oxygen (Barksdale 1966, p. 53). Most of the world's titanium is now produced by high temperature magnesio-thermic reduction (the Kroll process). The major operations involved in this process are shown in Figure 9.

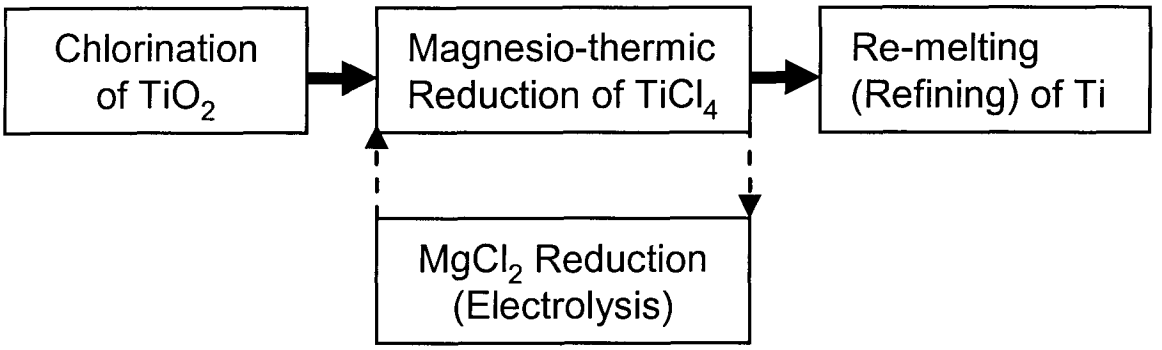

Figure 9 Major operations involved in the production of titanium.

Production

Ore types and production of titanium chloride

Titanium is found in the minerals rutile (TiO_2), ilmenite ($FeTiO_3$), and sphene ($CaTiSiO_5$), and is present in titanates and iron ores (Table 18).

Table 18 Common titanium-containing minerals (Sibum 1997, p. 1134-1137).

Phase	Formula	Crystal System	Comments
Rutile	TiO_2	Tetragonal	Anatase and Brookite (rhombic) are other modifications of TiO_2 TiO_2 is an important white pigment
Ilmenite	$FeTiO_3$	Trigonal	Economically important
Leucoxene	$Fe_2O_3TiO_2$		Weathering product of ilmenite Economically important
Perovskite	$CaTiO_3$	Orthorhombic	
Titanite	CaTi(SiO4)O	Monoclinic	Also known as sphene
Titanomagnetite	$Fe(Ti)Fe_2O_4$	Cubic / Rhomboedral	Largest Ti reserves in the world are of this form, not economical to process presently

Typical ore compositions are summarized in Table 18. Various combinations of flotation, gravity and magnetic separators are used to increase the grade (upgrade) the ilmenite ore (Barksdale 1966).

Table 19 Typical compositions of rutile, ilmenite and upgraded ilmenite (UGI) ores (Noda 1988, p. 760 and Sibum 1997, p. 1137).

%	TiO_2	Fe_2O_3	FeO	ZrO_2	SiO_2	Al_2O_3	V_2O_5	MnO
Rutile (Australia)	95.8	0.74	-	0.93	0.52	0.22	0.6	0.02
Rutile (South Africa)	95.4	0.7	-	0.46	1.75	0.65	0.65	-
Ilmenite (Norway)	43.8	14.0	34.4	-	2.2	0.6	0.3	0.3
Ilmenite (South Africa)	46.5	11.4	34.2	-	1.6	1.3	0.3	-
UGI (Japan)	95.4	1.64	-	0.19	0.56	0.67	0.24	0.07
UGI (Australia)	91.3	5.86	-	0.11	0.84	1.15	0.25	1.31

Chlorination

Once TiO_2 ore or concentrate is obtained, it is converted to $TiCl_4$ in a reducing atmosphere using calcined petroleum coke in a fluidized bed process as per Equation 20 (Sibum 1997, p. 1144 and 1160). $TiCl_4$ is a non-conducting colourless liquid with a room temperature density of about 1.73 kg/L and a boiling point of 406 K (Barksdale 1966, p. 93).

$$TiO_2 + 2Cl_2 + C \rightarrow TiCl_4 + CO_2 \qquad [20]$$

Oxygen is blown in to maintain the temperature between 1073 and 1473 K. Coke consumption ranges from 250-450 kg coke/tonne-TiO_2 chlorinated (Sibum 1997, p. 1144). The $TiCl_4$ obtained from chlorination usually contains free chlorine and some dissolved iron, silicon, vanadium or other elements from the charge (Barksdale 1966, p. 563). Crude $TiCl_4$ is purified to 99.9% (minimum) as follows (Sibum 1997, 1161):

- 4% solids are allowed to settle out
- Al is precipitated as aluminium oxide when its chloride reacts with water
- $SiCl_4$ and $SnCl_4$ are separated by distillation (< 406 K)
- $VOCl_3$ is reduced to $VOCl_2$ that precipitates by adding H_2S and Cu (363 K)
- $FeCl_3$ and $AlCl_3$ are separated by distillation (> 406 K)
- Unsaturated organic compounds aid in the separation of Cr and V oxy-chlorides
- Dissolved chlorine can be removed by heating with metal powders (Fe, Cu, Sn)
- Purification with H_2S at 413-573 K on a bed of Si or FeS to remove impurities

Reduction of $TiCl_4$

Almost all Ti metal is produced using the Kroll process save a few industrial plants in China that use the Hunter process (reduction using Na) (Sibum 1997, p. 1162). The magnesiothermic reduction of $TiCl_4$ is carried out in a mild steel vessel under a He or Ar atmosphere at 1023-1273 K (Barksdale 1966, p. 145). Higher temperatures can lead to iron contamination from the plain carbon steel reactor, while lower temperatures will increase reaction time (Sibum 1997, p. 1163). Solid Mg is charged into the batch reactor and heated until it melts. $TiCl_4$ is then fed into the reactor, since the reduction reaction (Equation 21) is very exothermic, external heating is no longer required (Nagesh 2004, 65).

$$TiCl_4(g) + 2Mg(l) \rightarrow MgCl_2(l) + Ti(s) \quad \Delta H^\circ_{1000K} = -412 \text{ kJ/mole} \qquad [21]$$

The crude Ti is generally purified of Mg and Ti chlorides using vacuum distillation (0.1 Pa, 1173-1273 K). Mg is regenerated by electrolysis as explained in Section 1.2. The energy consumption is 30 kWh/kg-Ti sponge. In this batch process the reduction stage requires 95 hours and distillation 85 hours (Sibum 1997, p. 1163).

Table 20 Progress in Ti Sponge production at Osaka Titanium Co. (Noda, 1988, 759-60)

Years	Ti Yield, %	kWh/kg-Ti	Major Improvements
1954-1977	91	37	-
1977-1980	95	23	Fluidized bed chlorination / Change in feed
1981	95	20	Combined Mg reduction and vacuum separation / Mg reduction up to 5 Ton batches
1982-1988	98	17	Multipolar cell for $MgCl_2$ electrolysis (110 kA) / Mg reduction up to 10 Ton batches

Alternative processes

Thermodynamic calculations suggest that alternative processes for direct reduction of titanium oxide to metal are less expensive than the Kroll process (Sibum, 2003 p. 394). However, some of the ideas have shortcomings as Sibum explains, for example, the reduction of TiO_2 with carbon is only possible at very high temperature (> 6300 K) and the reduction of TiO_2 with H_2 and inert gases leads to the formation of lower oxides. The reduction of TiO_2 with Ca occurs at a reasonable temperature range 873-1473 K.

Crude Ti (~90 % pure) can be produced by passing $TiCl_4$ through molten $MgCl_2$ on which a layer of Mg is maintained to reduce the $TiCl_4$ producing sponge that falls to the bottom of the reactor, Chisholm (1957). Similarly, a recent patent describes Ti being produced by supplying a mist of $TiCl_4$ to a bath of liquid Mg at temperatures of 1043-1223 K and collecting the fine particles at the bottom of the vessel before sintering to produce sponge (Nobuaki, 2005).

The FCC Cambridge process is an alternative production method to directly deoxidize titanium dioxide electrochemically in a bath of molten $CaCl_2$ at temperatures on the order of 1220 K (Chen, 2000). This technology is in the process of being piloted (Fray, 2004 p. 299). TiO_2 pellets are connected to a power source and polarized below their reduction potential. Ti^{4+} is reduced to elemental titanium through a series of non-stoichiometric phases, and O^{2-} is formed and migrates to the anodic site (a graphite rod or crucible) where it is mostly converted to oxygen gas. A patent was awarded for a similar deoxidation process for the production of Ti from TiO_2, the authors claim to have mitigated issues of diffusion bonding by controlling the TiO_2 particle size (Ward-Close, 2005). A recent patent indicates that de-oxidation of TiO_2 can also be carried out in ionic liquids (O'Grady 2007).

Recycling and refining

Multiple re-melting of titanium sponge results in the removal of volatile components. Depending on the application this may be all the refining that is required. To prepare premium quality titanium, re-melting is carried out in a vacuum arc melter. The titanium sponge is pre-densified in a hydraulic press; alloying agents are added before melting (Sibum 2003, p. 394). If high quality titanium scrap is available it can be recycled by melting processes such as cold hearth melting with electron beam or plasma heating in combination with a final vacuum arc-melting step. If the metal is not sufficiently high in quality it can still be used as an alloy addition or ferro-titanium (Sibum 2003, p. 398).

An electrorefining process was patented by Dean in 1959 in which an impure Ti anode (including oxygen and some carbide) was electrorefined in molten NaCl with a

small amount of $TiCl_2$ at 1123 K. Using a Ti cathode and passing a current of 3200 A/m^2; 99.9% pure Ti was obtained.

1.5 Electrodeposition of Reactive Metals

Aluminium

Solid aluminium has been electrodeposited from a variety of solutions including inorganic molten salts, organic molten salts (ILs) and other organic systems. Many of the aluminium electrodeposition research efforts have been for the purpose of producing aluminium coatings. The motivation for these coatings is that when exposed to air, aluminium forms an oxide layer that resists a variety of chemical attacks; the layer can be thickened by anodization, and displays good thermal and electrical conductivity. Furthermore, aluminium is easily polished and accepts varnish, it also exhibits a high reflectivity of light and heat which can be useful in the insulation of buildings and in optical devices (Zhao 1997). Alternatives to electrolytic plating of aluminium are thermal spray coating, hot dipping, roll binding and physical or chemical vapour deposition. Major factors such as cost and coating quality are often in favor of the electrolytic method (Zhao 1997).

Efforts have been made to deposit solid Al from molten salts. The $AlCl_3$-NaCl system has a eutectic point of 380 K at about 0.61 X_{AlCl3}. The temperature of an electrodeposition process would have to be kept above 428 K to prevent solid $NaAlCl_4$ from forming at the cathode. The temperature is also limited on the high end by the sublimation of $AlCl_3$ at temperatures as low as 453 K (Website: FACT). The deposition of Al from this system usually results in a dendritic deposit, the addition of lead or tin chlorides helped improve deposit quality but not to the point of making the process commercially viable (Berkowitz 1972, p. 55).

One issue with higher temperature solid deposition processes is that the deposits end up diffusing into the substrate material resulting in diffusion coatings (Berkowitz 1972, p. 53). For coating applications this diffusion process is a benefit as very strong bonding between the coating and underlying metal occurs. For production or refining of

metals, where a separation of the deposited metal from the substrate is required, diffusion bonding is a problem.

Aluminum was also deposited from $AlBr_3$-KBr melts (90:10% by weight), good thin deposits were obtained on W but thicker deposits became dendritic (Couch 1952). Couch and Brenner used this bath to evaluate a long list of metallic addition agents to improve the deposit quality. With additions in the range of 0.01-1 wt.% they found that chromic chloride, chromic oxide, lead chloride and lead oxide significantly improved the deposit quality while, cadmium chloride, silver chloride, sodium cyanide, sodium formate, sodium stannate, stannic phosphate, stannic chloride, stannic sulfate and zinc chloride resulted in slight levelling of the deposit.

One of the early successful Al deposits from ILs was from $AlCl_3$-ethyl pyridinium bromide (EPB) (Hurley 1951). The addition of benzene, toluene or xylene on the order of 20-50 volume % improved the deposit quality and allowed for the metal to be plated at room temperature. These organic molecules play the role of brighteners by adsorbing onto clusters of aluminium forcing the deposit to grow layer by layer (Endres 2003, p. 294). The researchers found that a concentration range of 50-59 wt. % $AlCl_3$ in EPB before the addition of toluene and benzene was optimal. Below 50 wt. % $AlCl_3$ a water soluble deposit was obtained which is believed to be diethyldihydrodipyridyl, the product of cation reduction. At $AlCl_3$ concentrations above 60 wt%, $AlCl_3$ was found to be included into the deposit. The brightness of the deposit generally increased with increasing current density up to a point above which the deposit became dark and non-adherent. Also, at higher current density, occlusion of pyridinium salts in the deposit has been reported (Zhao 1997). Safranek (1952) used essentially the same bath as Hurley and Weir but added methyl *t*-butyl ether at concentrations or 1 wt.% to improve the deposit quality, dimethylaniline was also reported to be effective. The addition of the methyl *t*-butyl ether increased the crystal plane orientation with (110) or (100) planes parallel to the basis metal. A superimposed alternating current was applied and was shown to improve the deposit quality.

Many researchers have investigated the $AlCl_3$-imidazolium chloride systems. High electrodeposition current efficiencies and current densities have been obtained. It was found, similar to the $AlCl_3$-EPB system in that the addition of benzene assisted in the

deposit quality. Benzene was found to encouraged the growth of the (220) Al crystal orientation (Liao 1997). Imidazolium ILs are more expensive to produce than other ILs and the addition of $AlCl_3$ is exothermic and can cause imidazolium to thermally decompose (Zhao 1997).

Aluminium was electrodeposited from acidic solutions of $AlCl_3$-BMIC at 373 K in both electrowinning and electrorefining setups (Lu, 2003). The current efficiency of the electrowinning experiments was highest for the shortest experiments and decreased with increasing time, the electrowinning power consumption was calculated to range from 12-16 kWhr/kg-Al produced. Lu suggested including a porous diaphragm separator or anion membrane cell design to limit the chlorine back reaction. The anode-cathode separation was 1 cm for both EW and ER set-ups. The electrorefining of aluminium in these solutions results in a dramatic reduction of the Si, Cu, Mg, Fe, Mn, Ni and Zn concentration in the refined metal (Al alloys 6111 and 383.1 were both tested). The electrorefining power consumption ranged from 2-3 kWhr/kg-Al. The formation of an anode slime during electrorefining limited the duration of the experiments. Dendritic growth of the Al was a significant problem during electrorefining.

Table 21 Electrodeposition of Al from molten salts and ILs.

Solvent	T. K	Deposit Substrate	CD A/m^2	C.E. %	Reference
$AlBr_3$-KBr	373-573	W	-	-	Couch 1952
$AlCl_3$-MCl (M is Alkali Metal)	< 423	-	100	-	Berkowitz 1972
$AlCl_3$-NaCl	448	GC, Pt, W	-	-	Rolland 1976
$AlCl_3$-MEIC with Benzene (X_{AlCl3}=0.6)	298	Cu	19-75	>98	Liao 1997
$AlCl_3$-MEIC	373	Cu, Pt	400-1700		Takahashi 1990
$AlCl_3$-BMIC (X_{AlCl3} = 0.6-0.67)	373-413	Cu	200-700	Up to 99	Zhang 2003
$AlCl_3$-BMIC (X_{AlCl3} = 0.6 or 0.67)	373	Al, impure Al and GC Anode, Cu Cathode	200-300	~100 (ER), 58-83 (EW)	Lu 2003
$AlCl_3$-HMIC	353-363	Extruded Carbon Anode, Cu WE	150-250	66-85	Zhang 2006
$AlCl_3$-BTMAC	298	Ni, Fe	0.5	-	Abbott 2001
Alkylaluminium and RX, and R_4NCl in aromatic solvents	363-373	-	100-150	-	Zhao, 1997
$AlCl_3$ and LiCl in $DMSO_2$	353-433	W	100	>90	Legrand 1994
$AlBr_3$ in Benzene and R_4NBr	298	-	200-1500	-	Zhao 1997 *Cited:* Simanavicius 1990
$AlCl_3$-EPB (X_{AlCl3}=0.67) with Benzene or Toluene	303	Cu, Fe, Pb, Ni, Sn Brass	50-200	81-92	Hurley 1951
$AlCl_3$-EPB (X_{AlCl3}=0.67) with toluene and methyl *t-butyl* ether (1wt.%)	303	Cu plated Cd-Ni Alloy	110-210	91-95	Safranek 1952

Fluorinated ILs such as $BMITf_2N$ (1-butyl-3-methylimidazolium bis(trifluoromethylsulfonyl) and $HMIPF_6$ (1-hexyl-3-methylimidazolium hexafluorophosphate) were considered as solvents for alumina in a direct reduction process (Zhang 2004). A process for the direct reduction from alumina would be advantageous as chlorination would not be necessary. The researchers have shown, using an EMF method, that alumina is soluble in C_6mimPF_6 to about 0.023 wt.% at 373 K.

Some of the most successful Al deposits are from organic plating baths. Despite this long list, many aprotic, polar chemicals such as acetonitrile, DMF, pyridine and

propylene carbonate have failed as solvents as Al^{3+} is reduced at a potential that is below the solvent decomposition potential (Peled 1976).

Williams claims to have deposited aluminium from solutions of 10 wt.% aluminium sulfate in anhydrous sulfuric acid with oleum in his patent (Williams 1920). A contradicting finding from the same year was that anhydrous aluminium sulfate is insoluble in pure sulfuric acid even in the presence of sodium sulfate (Davidson, 1925).

Early aluminium electroplating solutions involving $AlCl_3$ and $LiAlH_4$ in diethyl-ether baths known as Hydride, Brenner, or NBS (National Bureau of Standards) baths have been operated on a small scale since the late 1950's (Berkowitz 1972, p. 31). These baths were very unstable due to decomposition by oxygen, carbon dioxide, moisture laden air or by the anodic process (Berkowitz 1972, p. 35). They were also extremely flammable due to the ether (Graef 1985). Couch and Brenner (1952) evaluated a series of ethers as additives to the hydride baths. They found that anisole, diethyl ether, phenetole, ethyl *n*-butyl ether, Di *n*-propyl ether, THF and phenyl ether improved the deposit quality. Smooth deposits were also obtained by periodic current reversal. Improvements were made during the 1950's and between 1963 and 1969 the process was scaled up to a commercial size by two companies in a program sponsored by the NASA Langley research center (Berkowitz 1972). The General Electric company electroformed 80 cm diameter aluminium mirrors while Electro-Optical Systems Inc. produced aluminium hollow-core solar panels larger than 1 m^2. Berkowitz provided an example of the operating conditions of the General Electric bath; the important parameters are summarized in Table 22. The power consumption for this process (assuming 100% current efficiency) would be on the order of 35-55 kWhr/kg-Al.

Table 22 Operating parameters of an NBS bath (Berkowitz 1972, p. 38)

Bath Composition	3.4 M $AlCl_3$ and 0.4 M $LiAlH_4$ in diethyl ether
Volume	Up to 760 L
Temperature	293-303 K
Current Density	200 A/m^2
Cell Voltage	12-18 V
Electrode Spacing	6-12 cm
Anode	Al 1100 in Glass Cloth
Cathode	Ni or optical ground glass
Anode:Cathode Surface Area Ratio	1.1:1
Agitation	Magnetic Stirring or Rotating Cathodes

Later, in the 1970's more improvements were made to the baths were by the addition THF or a mixture of THF and benzene resulting in the bath being less flammable, toxic and increasing the bath lifetime. The improved baths were adopted industrially by the General Electric Company and Nisshin Steel Co. (Zhao, 1997) and it is known as the REAL process (room temperature electroplated aluminum) (Graef 1985).

The deposition of aluminium from these solutions was explained by Graef (1985) and Arora (1986). Firstly, aluminium hydride is formed when $AlCl_3$ is added (Equation 22).

$$4AlCl_3 + LiAlH_4 \rightarrow 4AlHCl_2 + LiAlCl_4 \quad [22]$$

A second compound, $AlCl_3(Et_2O.THF)_n$ is also formed in the presence of ether. $AlHCl_2$ is reduced to Al metal at the cathode and $AlCl_3.2THF$ reacts with the liberated H^- ion to regenerate aluminium hydride. $Li(C_2H_5)_2O^+$ is thought to be the principle current-carrying ion (Berkowitz 1972, p. 36).

Blue and Mathers (1936) deposited Al from $AlBr_3$ at current efficiencies above 75% from solutions of ethyl bromide and benzene. They found that 1 mL of ethyl bromide / g $AlBr_3$ was an optimum ratio to maximize current efficiency and deposit quality. They attempted to use $AlCl_3$ as the aluminium source but were not as successful; they believed that the bromide ion was required for anode dissolution. Toluene and xylene were added to brighten the deposits. An anode film formed with that limited the rate of the deposition process. The current efficiency dropped with operating time, for example, after 150 hours the C.E. went from above 80% to below 17%. The addition of ethyl bromide was used to increase the C.E. back above 80%.

Aluminium was also deposited from solutions of AlX_3 and aromatic hydrocarbon with MX (X = I, Br, Cl and F). Current efficiencies of 90% have been reported, inefficiencies were attributed to hydrogen evolution as well as reduction of the solvent. These baths did not last more than a few weeks (Peled, 1976). In general, $AlBr_3$ is used as its solubility in aromatic hydrocarbons is superior to $AlCl_3$ and the resulting bath is more conductive (Zhao 1997). In Peled's work, the effect of cation type was not substantial (M = Li, Na, K or NH_4) but the effect of anion was better with larger anions in terms of deposition quality and current efficiency, also the solubility of $MgBr_2$ was found to be much lower than the other alkali metal salts. The addition of quaternary ammonium

salts (ILs) were found to increase the deposit quality in terms of reduced dendrite formation but some of the ammonium ILs were incorporated into the deposit. Peled found that impurity metals such as copper and iron can be removed from the melt by pre-electrolysis onto a dummy cathode. The transference numbers were found to be 0.3 for K^+ and 0.7 for $Al_2Br_7^-$. This does is counter-intuitive since the smaller ion usually exhibits a higher transference number.

The cathodic behaviour of Al in $AlBr_3$ with ethylbenzene, toluene and HBr was studied by Capuano (1984). HBr was bubbled into the solution to modify the conductivity which was on the order of 0.1 to 0.8 S/m. The heat of activation of the deposition was determined to be on the order of 17 kJ/mole which suggests that the aluminum-alkylbenzene bond energy is lower than in the hydration energy of metal ions in aqueous solutions. The exchange current density (i_0) was determined to be 20 A/m^2 at 313 K. The electrodeposition of Al from these systems is believed to proceed as in Equation 23.

$$AlBr_2 \cdot n[(C_6H_4)(CH_3)_2]^+ + 3\bar{e} \rightarrow Al + n(C_6H_4)(CH_3)_2 + 2Br^- \quad [23]$$

The highest quality Al deposits (99.9999% pure Al) were obtained from the organoaluminium Sigal process which is currently licensed to AlumiPlate Inc. The main disadvantage of this process is the high cost of the organoaluminium compounds (Zhao 1997).

Table 23 Electrodeposition of aluminium from solutions other than molten salts or ILs.

Solvent	T. K	Deposit Substrate	CD A/m^2	C.E. %	Reference
$AlCl_3$ and LiCl in $DMSO_2$	353-433	W	100	>90	Legrand 1994
10% $AlCl_3$ in Acetonitrile with 1% KF or PF_3	273-373	-	200-300	-	Audrieth1931 *Cited:* Lablin 1917
Al from $Al_2(SO_4)_3$ in H_2SO_4 with oleum	>373	Al WE Carbon CE	(3 V)	-	Williams 1920
AlX_3 in EtBr and Benzene	293	-	155	>75	Blue 1936
Al in CH_3-I solution	-	Cu	200	40 V required!	Keyes 1933
$AlCl_3$ and $LiAlH_4$ in diethyl ether	298-313	Al, Ti and Cu Alloys	200-500	>90% is possible	Arora, 1986 Couch, 1952
$AlCl_3$ and $LiAlH_4$ in THF and benzene	-	Fe, Steel	1000	-	Zhao, 1997
$AlCl_3$ and $LiAlH_4$ in THF	-	Pt	600	-	Graef 1985
$AlBr_3$ in ethylbenzene and toluene with HBr	300-354	Cu, Steel	100	80	Capuano 1984 Zhao 1997
$AlBr_3$ in toluene or benzene and MX, M = Li, Na, K, NH_4 X = I, Br, Cl, F	298	Steel or Cu Cathode	5-400	90	Peled 1976
$AlBr_3$ in benzene, toluene, p-xylene and ethylbenzene	298-333	Pt	50-200	Up to 80	Shavkunov 2003

Magnesium

Magnesium and Mg-alloys were have been electrodeposited from organic ether solutions (Connor 1957). The solubility of $MgCl_2$ is very low in most organic solvents even at the boiling point. $MgBr_2$ was slightly more soluble than $MgCl_2$, yet neither was sufficiently soluble in benzene, phenyl ether, dioxane, phenetole, anisole, triethylamine, xylene and cyclohexylamine, even at elevated temperatures, for electrodeposition. Also, $MgBr_2$ reacted with THF, pyridine and N, N-diethylacetamide at room temperature to form precipitates. The highest purity magnesium obtained by Connor was from the $MgBr_2$:$LiBH_4$ (2:1 mole ratio) system in ether where white deposits up to 90% Mg (10% B) were obtained. $LiBH_4$ improved the conductivity of the bath. The use of magnesium anodes was problematic because they either did not dissolve or reacted with the bath.

Magnesium of purity greater than 99% was deposited at 313 K from solutions of toluene and CsF with organometallic Al and Mg (Mayer 1990). Mayer also cited other

research where high purity Mg was deposited from solutions of ether, Grignard reagents and boranes (Mayer 1990 *Cited:* Brenner 1971). Earlier investigations of the electrolysis of Mg from Grignard solutions included Evans (1930) and French (1930). The anodic and cathodic reactions were described by Evans (1941). The anodic reaction is believed to involve the formation of an alkyl radical (R·), that would then undergo coupling, disproportionation or some other reaction (Equation 24, X is a halide):

$$R_2MgX_2^- \rightarrow 2R\cdot + MgX_2 + 2\bar{e} \qquad [24]$$

The cathodic reaction is the reduction of Mg^{++}. Similar reactions were proposed if Mg^+ was present. The resistances of these solutions are very high; the potential required to deposit Mg at a current density of 23 A/m^2 from an ether solution of ethylmagnesium bromide was 110 V (Connor 1957 *Cited:* Overcash 1933).

More recently, the deposition pathway of Mg in the THF solution was studied using in situ Fourier Transform Infrared Spectroscopy (FTIR) (Aurback 2001). It was shown that the deposition of Mg involves the adsorption of RMg^+ or RMg· on the surface. In the case of $Mg(AlCl_{4-n}R_n)_2$ $Mg_xCl_y^+$ may be adsorbed. The solution species are believed to be stabilized by the THF molecules.

Table 24 Electrodeposition of solid magnesium.

Solvent	T. K	Deposit Substrate	CD A/m^2	Reference
$MgBr_2 \cdot 2EtO_2$ or C_2H_5MgBr in ether, THF and or $LiAlH_4$ and or $LiBH_4$	298	Cu	100	Connor 1957
Mg Grignard reagent in ether	-	-	-	Evans 1930 Evans 1941
Mg Grignard reagent in ether	-	Pt	2.4 (110 V)	French 1930
Mg Grignard reagent with ethyl bromide in ether	-	-	108	Berkowitz 1972, p. 49
$(C_2H_5)_2Mg$ in CsF-$(C_2H_5)_3Al$-$(C_4H_9)_3Al$ and toluene	313	-	100	Mayer 1990
RMgX, $Mg(BR_4)_2$, or $Mg(AlCl_{4-n}R_n)_2$ in THF R is alkyl or aryl and X is Cl or Br	-	-	-	Aurbach 2001

Titanium

Titanium in solution is reported to have been reduced to a metal or amalgam at a dropping mercury electrode (DME) from room temperature solutions of acetonitrile (AN) and tetraethyl ammonium ILs as supporting electrolytes (Kolthoff 1964). Titanium tetrachloride is believed to exist in AN with the following equilibrium (Equation 25). The dissociation constant is $7 \cdot 10^{-4}$ at 298 K.

$$2TiCl_4(CH_3CN)_2 = TiCl_3(CH_3CN)_3^+ + TiCl_5CH_3CN^- \quad [25]$$

The tetraethyl ammonium ILs used were $[N_{2,2,2,2}]ClO_4$, $[N_{2,2,2,2}]Cl$, $[N_{2,2,2,2}]Br$ and $[N_{2,2,2,2}]I$ and $[N_{2,2,2,2}]NCNS$. The bonding strength of titanium with the halides were found to decrease with increasing anion size (Ti-Cl > Ti-Br > Ti-I). Chlorotitanate IL melts have been prepared with MEIC, it was speculated that $TiCl_6^{-2}$ forms at X_{TiCl4} between 0 and 0.33 and $TiCl_5^-$ between 0.33 and 0.5 (Scheffler 1990).

Titanium was deposited onto a nickel cathode in LiCl-KCl melts at 673-773 K (Alpert, 1957). An alumina separator was used to isolate the anode and high current efficiencies were obtained. Current efficiency was also higher at higher current density, the main inefficiency being the reduction of $Ti^{3+} \rightarrow Ti^{2+}$ at the cathode. The Ti was reduced initially by a number of methods: (1) chemically reacting $TiCl_4$ with Li, (2) electrochemically reducing $TiCl_4$ at a graphite cathode, (3) Reducing $TiCl_4$ by exposure to Ti. The deposit obtained was generally dendritic and occlusion of the melt salt was occurring.

Titanium was also deposited on a ceramic from a molten LiCl-KCl solution (Kawase 2005). A Ti rod counter electrode was used and only a small amount of $TiCl_3$ was added to the melt (0.13 mole %). It was found that Ti(III) could be reduced to Ti(II) in solution by the addition of Al. It was also found that Ti(II) would reduce to a Ti-Al alloy (Ti_3Al) in the presence of Al. At current densities above 20 A/m^2, a dendritic deposit was obtained.

Many unsuccessful attempts were made to deposit titanium from non-aqueous solutions at the National Bureau of Standards in Washington D.C. according to Reid (1957). Classes of non-aqueous solvents tried include hydrocarbons, halogenated hydrocarbons, alcohols, ethers, ketones, acids, amines, amides, nitriles. Reid prepared

$TiCl_3$ by reacting $TiCl_4$ with hydrogen in an autoclave and also prepared many organometallic Ti compounds and borohydride compound but was also unable to produce any metallic deposit.

Ti-Al alloys of Ti content up to 19 atomic % were produced from acidic $AlCl_3$-EMIC melts at 353 K. Titanium used as the anode was found to oxidize to $TiCl_3$ that caused passivation at lower current density. At higher current density, $TiCl_4(g)$ was generated. The titanium was dissolved as $TiCl_2$ which was more soluble as the concentration of $AlCl_3$ in the melt increased (60 and 170 mmol/L at X_{AlCl3} = 0.60 and 0.667 respectively). The dissolution reaction was believed to proceed as described in Equation 26.

$$2Al_2Cl_7^- + TiCl_2(s) \rightarrow Ti(AlCl_4)_3^- + AlCl_4^- \quad [26]$$

The deposition of a Ti-Pt alloy was observed at a potential below -1.8 V vs. Ni/Ni(II) in a molten fluoride salt bath at 773 K. It is believed that titanium was reduced directly from Ti(III) (Clayton 1973). In a similar study of Ti(IV) in molten $NaBF_4$ at 693 K, no reduction to Ti(0) was observed (Clayton 1973b).

Table 25 Electrodeposition of solid titanium

Metal	Solvent	T. K	Deposit Substrate	CD A/m^2	C.E.%	Reference
Ti	AN with $[N_{2,2,2,2}]^+$ (ClO_4^-, Cl^-, Br^- or I^-)	298	Dropping Mercury Electrode	-	-	Kolthoff 1964
Ti	LiCl-KCl (58.5-41.5 mol %)	723-823	Si_3N_4	20-120	-	Kawase 2005
Ti	$TiCl_3$-$TiCl_2$-LiCl-KCl	673-773	Ni (Graphite CE)	10000	>80%	Alpert 1957
Ti-Al	$TiCl_2$ in $AlCl_3$-EMIC (X_{AlCl3}>0.5)	353	Cu	-	-	Tsuda 2003
Ti-Pt	K_2TiF_6 in LiF-NaF-KF	773	Pt	-	-	Clayton 1973

Chapter 2 Physical Properties of Ionic Liquids

A series of nine tetra-alkyl phosphonium ionic liquids were characterized in terms of their density, viscosity and conductivity over a range of temperatures (~298-420 K). The ILs were selected to evaluate the effects of cation size and symmetry, and the effects of different anions. The conductivity of metal-salt-IL mixtures was also studied. The conductivity of $AlCl_3$-EMIC was measured over a range of $AlCl_3$ concentrations for comparison purposes. The effects of anion and cation size, impurities (HCl and H_2O) and organic solvents (toluene) were also noted. The Vogel-Tamman-Fulcher Equation was used to model the viscosity and conductivity since ILs are known to be glass forming liquids, meaning they have the ability to be supercooled into a frozen structure or glass that has no long range ordering.

2.1 Experimental Aspects

Some basic information regarding the ILs tested is presented in Table 26. The upper limit of safe operation in an air environment was determined by Cytec Inc. using standard thermo-gravimetric analysis with scan rates of 5-10 K/min. The molecular mass of $[P_{14,6,6,6}]Cl$ and $[P_{14,4,4,4}]Cl$ were confirmed during this work using mass spectrometry.

Table 26 Molecular weight (MW), purity, melting point (T_{mp}) and upper limit of the safe operating temperature in an air environment of phosphonium ionic liquids (Cytec Inc.).

CYTEC IL #	IL	MW g/mol	Purity %	T_{mp} K	Upper limit K
101	$[P_{14,6,6,6}]Cl$	519.3	96-97	223	453
167	$[P_{14,4,4,4}]Cl$	435.2	95-99	318	453
164	$[P_{4,4,4,4}]Cl$	294.9	97	353	453
482	$[P_{8,8,8,8}]Br$	563.8	94-97	318	-
102	$[P_{14,6,6,6}]Br$	563.8	96-98	273	423
110	$[P_{14,6,6,6}]PF_6$	628.9	98	323	393
111	$[P_{14,6,6,6}]BF_4$	570.7	97	310	413
105	$[P_{14,6,6,6}]N(CN)_2$	549.9	97	< 293	448
109	$[P_{14,6,6,6}]N(SO_2CF_3)_2$	764.0	98	< 293	453

Information concerning the toxicity of ionic liquids is limited. They have an irritating effect on skin, eyes and mucous membranes but no information regarding injury or illness due to acute or chronic exposure is available.

The solubility of water in ILs is largely determined by the anion type (Seddon 2000). PF_6^- and $N(CF_3SO_2)_2^-$ anion types create ILs with the least water solubility (0.16 X_{H2O} in $[BMI]PF_6$), BF_4^- has moderate solubility in water and Cl^- and Br^- are more water soluble. Chloroaluminate ions such as $Al_2Cl_7^-$ and $AlCl_4^-$ will decompose in the presence of water. The cation type also has some influence on the solubility of water in ILs, increasing the alkyl chain length tends to decrease the solubility of water (Seddon, 2000). The long alkyl chains of $[P_{14,6,6,6}]Cl$ IL results in a limited solubility with water (~ 14% w/w H_2O/IL) despite having a Cl^- anion (Cytec Inc. 2006). Dry $[P_{14,6,6,6}]Cl$ exhibits high miscibility with organic solvents such as hexane, toluene, 2-hydroxypropane (IPA), diethyl ether, tetrahydrofuran and dichloromethane.

Sample preparation

All of the samples were stored and prepared in a Vacuum Atmosphere Co. Glove box (HE Series) under a dry nitrogen atmosphere (< 10 ppm O_2, H_2O). Anhydrous $AlCl_3$ (99.99% pure) from Alfa-Aesar and $AlBr_3$ (99.997 % pure) were used as received to prepare the binary mixtures unless indicated otherwise.

Impurities and Purification

To identify possible impurities, the samples were digested in a solution of H_2O_2 and H_2SO_4 at elevated temperature; the solution was then analyzed by ICP. This procedure was carried out at a commercial laboratory (International Plasma Laboratories in Richmond, B.C.). Table 27 lists the most prominent impurities in the samples. As seen below, sodium was present in higher concentrations in some of the samples. One significant source of Na contamination was during synthesis, as the ILs with anions other than chloride and bromide required an anion metathesis reaction. Despite washing, some sodium salts remained in the IL. The higher levels of aluminium in $[P_{14,6,6,6}]PF_6$ and $[P_{14,6,6,6}]BF_4$ may be due to dissolution of aluminium during production as both of these ILs contain fluorine compounds and possibly small amounts of hydrofluoric acid.

Table 27 Ionic liquid metal impurity content.

IL	Impurities (ppm)				
	Al	Ca	Cu	Fe	Na
$[P_{14,6,6,6}]Cl$	55	61	5	34	154
$[P_{14,6,6,6}]Br$	47	451	102	61	716

$[P_{14,6,6,6}]N(CN)_2$	42	222	62	34	445
$[P_{14,6,6,6}]N(SO_2CF_3)_2$	27	82	19	42	203
$[P_{14,6,6,6}]PF_6$	3665	339	40	164	9901
$[P_{14,6,6,6}]BF_4$	1629	490	14	101	4285
$[P_{4,4,4,4}]Cl$	74	89	8	71	448
$[P_{14,4,4,4}]Cl$	<0.2	31	12	<0.03	394
$[P_{8,8,8,8}]Br$	65	74	16	82	383

Other impurities that were identified by Cytec Inc. are summarized in Table 28. Cytec titrated with standardized $AgNO_3$ in a 75% aqueous 2-hydroxypropane solvent to determine the total chloride content. This result was combined with a corresponding NaOH titration to yield the $[PR_3H]Cl$ and HCl content. The volatile content (tetradecene isomers) was determined by Cytec using internal standard gas chromatography analysis of an octane extract.

Table 28 Known impurities (Cytec Inc., 2006).

IL	Impurities (wt. %)		
$[P_{14,6,6,6}]Cl$	0.1 - 0.4 tetradecene isomers	0.1-0.5 HCl	0.1-1.2 $[PR_3H]Cl$
$[P_{14,6,6,6}]Br$	0.1 - 0.4 tetradecene isomers	0.1-0.5 HBr	0.1-1.2 $[PR_3H]Br$
$[P_{14,6,6,6}]N(CN)_2$	0.5 Cl^-	0.3 H_2O	
$[P_{14,6,6,6}]N(SO_2CF_3)_2$	< 0.1 Cl^-	0.1 H_2O	
$[P_{14,6,6,6}]PF_6$	< 0.1 Cl^-		
$[P_{14,6,6,6}]BF_4$	< 0.1 Cl^-		
$[P_{4,4,4,4}]Cl$	0.1-0.6 HCl		0.1-1% $[PR_3H]Cl$
$[P_{14,4,4,4}]Cl$	0.2-0.5 tetradecene isomers	0.2-1.2 HCl 0.1-0.3 H_2O	0.1 to 1.5 $[PR_3H]Cl$

In the chloro-aluminate IL mixtures there are additional impurities caused by the reaction of aluminium chloride with water. Water is present in the ILs in some quantity despite precautions to remove it. The $[P_{14,6,6,6}]Cl$ used in this work was determined to contain 0.15 wt.% water by Karl Fisher titration (ASTM D4377) following a drying procedure of 10 hours at 453 K under vacuum. The samples were dried by Cytec Inc and the Karl Fisher titration was done by PowerTech Labs in Surrey, B.C. The water content of BMIC and HMIC that were used by other researchers in laboratory scale electrorefining of aluminium were determined to be 0.48 and 0.5 wt. % respectively (Kamavaram 2003, p. 39).

There remains some debate as to whether the reaction products of aluminium chlorides and water are in the form of oxychlorides, $AlOCl_2^-$ (Davis 2003), or hydroxy-chlorides, $AlOHCl_2$ (Sahami 1983). Either way, HCl will inevitably be produced by Equations 27 and or 28.

$$AlCl_4^- + H_2O \rightarrow AlOCl_2^- + 2HCl \quad [27]$$

$$AlCl_4^- + H_2O \rightarrow AlOHCl_2 + HCl + Cl^- \quad [28]$$

In acidic $AlCl_3$-BPC mixtures (higher molar concentration of $AlCl_3$ vs. BPC), the addition of water resulted in an exothermic reaction producing HCl gas and forming a white precipitate that eventually re-dissolved generating more gas (Sahami, 1983). Many different aluminium oxide and hydroxide chloride species have been detected in acidic melts using mass spectrometry, fast atom bombardment spectrometry and secondary ion mass spectrometry, they include: $AlCl_3OH^-$, $Al_2OCl_5^-$, $Al_2Cl_6OH^-$, $Al_3Cl_6O_2^-$, $Al_3Cl_7O_2H^-$, $Al_3Cl_8O^-$ and $Al_4Cl_9O_2^-$ (Mantz 1998). Similarly, $[TiOCl_4]^{-2}$ was identified when $TiCl_4$ reacted with water in and IL (Mantz *Cited:* Linga 1981).

Impurities can be identified and removed to a certain extent using methods described in Table 29. There are limits to the extent that halides and protons can be removed by washing with water and this method will introduce water into the IL. A stoichiometric amount of $EtAlCl_2$ must be added to the IL to remove protons or else it will remain in solution. The high vacuum method to remove protons is limited to chloroaluminate melts with $X_{AlCl3} < 0.56$ as the vapour pressure of $AlCl_3$ is high, leading to the removal of $AlCl_3$. Phosgene ($COCl_2$) will react with aluminium and titanium oxy and hydroxy chlorides to remove the oxygen and produce CO_2. Both phosgene and CO_2 can then be removed by vacuum. Carbon tetrachloride has also been used convert aluminum and tungsten oxides to chlorides in alkali haloaluminate melts (Chen 1993).

The introduction of halide impurities in non-halide ILs can be limited by the use of silver salts in the metathesis reaction (See Section 1.1) as opposed to sodium salts, due to the reaction proceeding closer to completion in the case of silver (Seddon 2000). The use of silver salts is a more expensive processing option. Ammonium salts are sometimes an option as an anion source for the metathesis reaction, if the IL is not soluble in acetone, the residual NH_4Cl can be precipitated from acetone, as an example, $EMIBH_4$ was produced from EMIC and NH_4BF_4 (Fuller 1997).

The oxide ion concentration in acidic $AlCl_3$-NaCl-KCl melts was determined by Karl Fischer titration and the results were shown to be in agreement with IR absorption bands (Kurayasu 1993). The Karl-Fischer titration method, usually used for determining H_2O concentration, is based on the reduction of iodine, Equation 29.

$$H_2O + I_2 + SO_2 + 3RN + CH_3OH \rightarrow 2RNHI + RNHSO_4CH_3 \quad [29]$$

The endpoint of the titration is detected using voltammetry and the concentration of iodine is related to the water or oxide concentration.

Table 29 Methods to identify and remove impurities (Hilgers 2003, p. 25-27).

Impurity	Likely Source	Test	Removal Method
Halides	Residuals from two step synthesis	Titrate with $AgNO_3$ Ion chromatography Electrochemical analysis Chloride-selective electrode[e]	Wash with water
Protons	Produced by exchange with strong acid Sensitive to hydrolysis	Add ionic liquid to water and measure the pH FTIR and NMR[g]	Wash with water High vacuum Treatment with $EtAlCl_2$[a]
Water	Uptake from air for hydrophilic ILs	IR spectroscopy Cyclovoltammetry Karl-Fischer titration	Dry at 333 K in vacuum Addition of Na(s) or BaO[g] Electrolysis [h] Drying using $MgSO_4$[i]
Oxides[b]	Water reacting with Al or Ti chloride species	IR spectroscopy Karl-Fischer titration[f]	Phosgene ($COCl_2$) under vacuum[c] CCl_4[d]

[a] Mantz 1998, Cited: Zawodzinski 1987
[b] Mantz 1998, Cited: Noël 1991
[c] Hussey 1988
[d] Chen 1993
[e] Seddon 2000
[f] Kurayasu 1993
[g] Bockris 1998
[h] Yuyama 2007
[i] Mehnert 2005

Purification of $AlCl_3$-$[P_{14,6,6,6}]Cl$ ($X_{AlCl3} = 0.67$)

Most of the $AlCl_3$-IL mixtures tested in this thesis were prepared by mixing $AlCl_3$ with the IL in the glove box with no further purification. Since it was found that impurities such as HCl resulted in a significant loss of current in many of the experiments, one batch of $AlCl_3$-$[P_{14,6,6,6}]Cl$ (X_{AlCl3} = 0.67) was prepared with extra precautions. In an electroplating operation, the deposit quality would be the most important parameter and a reduced current efficiency would be a lesser factor since usually only thin metal coatings are being plated. However, for an electrowinning or refining operation, a loss in current efficiency is a large expense as much more metal is being processed and the product is valued as a commodity.

The method used to remove HCl was exposure of the solution to a high purity Al foil (99.99 %). The concentration of HCl in the solution was indirectly monitored by the corrosion rate of the Al foil. Firstly, an attempt was made to remove HCl from neat IL (no $AlCl_3$). The Al foil (18 cm^2), was immersed in 50 g of $[P_{14,6,6,6}]Cl$. The neat IL was tested at two temperatures (373 and 393 K) in both cases after 24 hours of exposure no Al mass loss was measured. The IL was stable upon heating, no bubbles were formed and no changes in the clear liquid colour were observed. Perhaps the HCl in the neat IL is stabilized by the presence of water as H_3OCl, the concentration of water in the solution was 0.15 wt.% and the concentration of HCl was determined to be in the range of 0.1-0.5 wt.%, if the concentration of HCl was 0.3 wt.% this would correspond to a 1:1 mole ratio of H_2O to HCl. The stabilized H_3OCl may be less likely to remove from the solution by heating and vacuum and also may be less corrosive towards the aluminium solution that a dehydrated HCl.

Before mixing $AlCl_3$ to create the binary mixture, the aluminium chloride (Anhydrous, 99.99% pure, BP = 461 K) was sublimated as a precaution to remove any trace amounts of Al_2O_3 (BP ~= 3300 K), adsorbed water, HCl (BP = 358 K) or $FeCl_3$ (BP = 588 K) that may be have been present in the powder. A small amount of opaque (relative to $AlCl_3$) residue was observed after sublimating at temperatures in the range of 463-473 K. The sublimation apparatus is shown in Figure 10. The top portion containing the cold finger could be removed from the bottom portion and the vacuum line outlet valve allowed for the sublimation to be performed outside the glove box. The sublimation temperature was approximately 473 K and the cold finger cooling water temperature was approximately 260 K.

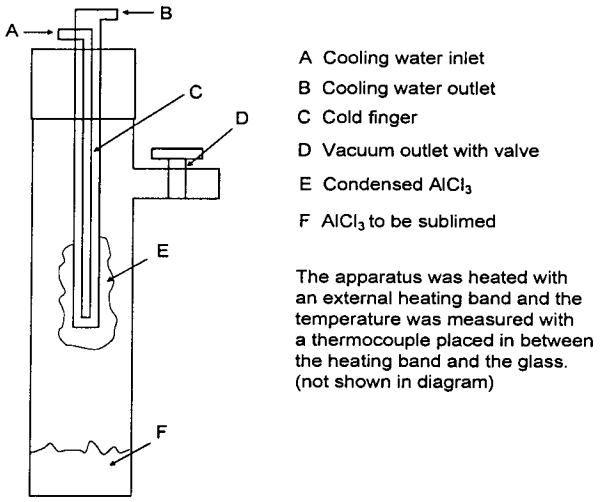

Figure 10 Glass sublimation apparatus used to prepare the $AlCl_3$ for the purified $AlCl_3$-IL mixture.

The $AlCl_3$-$[P_{14,6,6,6}]Cl$ (X_{AlCl3} = 0.67) was then prepared using the $AlCl_3$ that was sublimated and deposited and the IL that had been exposed to the pure aluminium foil. The dissolution of $AlCl_3$ in the IL was slightly exothermic but not nearly to the extent of similar mixtures using imidazolium chloride ILs (Lu, 2003). The mixing temperature ranged from 303-343 K. Some bubbling was observed throughout the mixing process, these bubbles are attributed to nitrogen that may have been trapped in the $AlCl_3$ and HCl that is forming upon the reaction of $AlCl_3$ with water in the IL (0.15 wt.%). HCl gas may be formed as the local temperature in the area near the dissolution reaction is higher than in the bulk solution. After most of the bubbling ceased, the solution was heated to 373 K and the Al foil was immersed in the liquid. After 23 hours of immersion, the corrosion sample was removed from the solution and the glove box and cleaned with acetone. Visual corrosion of the Al was then apparent as the surface was roughened, including above the solution immersion level, indicating the presence of HCl gas above the bath. A thin black film of an unknown substance was noticed. The rubber stopper was suspected as it may have been reacting with the HCl gas. The rubber stopper was removed after 94 hours resulting in a decreased amount of the black film; no film was apparent on the samples removed after 165 hours.

The corrosion rate was calculated from mass loss using Equation 30.

$$\text{Corrosion rate (mmpy)} = (8.76 \cdot 10^4 \cdot W)/(d \cdot A \cdot t) \qquad [30]$$

Where, W is the mass lost (g), d is the density of the material (g/cm^3), A is the initial exposed surface area of the metal (cm^2), t is the exposure time (hours), $8.76 \cdot 10^4$ is the conversion factor to change cm/hour to mm/year (mmpy).

The corrosion rate of the Al in the initial 23 hours was determined to be 1.25 mmpy (373 K). In a separate experiment at the same conditions using $AlCl_3$ that was not sublimed, the corrosion rate was found to be 1.28 mmpy indicating that the sublimation procedure was of little use in reducing the amount of corrosion-causing impurities. The corrosion rate of Cu and W in the first 24 hours same system (non-sublimed $AlCl_3$) but separated experiments were found to be 0.24 and 0.02 mmpy respectively. The effective sample surface area of the sample increased with corrosion due to surface roughening, this can be seen in the higher corrosion rate of the second measurement (Figure 11). The corrosion rate thereafter was lower than in the initial two measurements. There was some error in the later measurements as the sample was becoming fragile and some aluminium was being lost during the cleaning procedure. A fresh sample was introduced at about 190 hours; no mass loss was measured after the first 72 hours of immersion. The temperature was increased from 373 K to 388 K at 262 hours and the final corrosion measurement was 0.375 mmpy, significantly lower than the initial measurements for the first coupon.

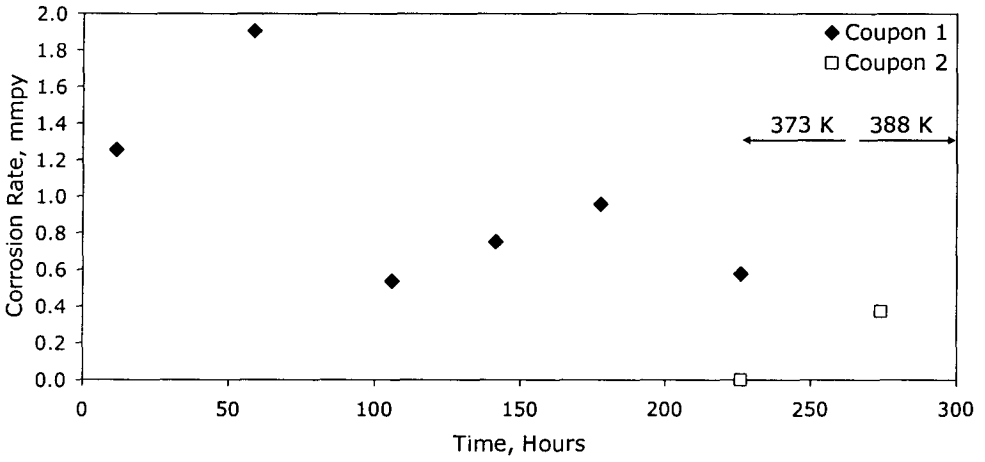

Figure 11 Corrosion rate of Al foil coupons (99.99% pure, 18 cm^2) in $AlCl_3$-$[P_{14,6,6,6}]$ (X_{AlCl3} = 0.67). The solution was stirred and heated to 373 or 388 K.

The total mass of Al corroded into the 75 g of $AlCl_3$-$[P_{14,6,6,6}]Cl$ (X_{AlCl3} = 0.67) was 0.169 g corresponding to 6.26 mmoles of Al or 18.8 mmoles of HCl based on the

stoichiometry of 3 HCl to corrode 1 Al. The HCl concentration removed from the solution was about 0.25 moles/kg. The maximum concentration of HCl impurities in the neat IL was calculated to be 0.12 moles/kg based on the R_3PHCl and HCl impurity values provided by Cytec Inc. An additional 0.11 moles/kg of HCl could be introduced when the $AlCl_3$-IL solution was prepared if all of the H_2O is converted to HCl. The resulting solution should contain a maximum of 0.23 moles/kg of HCl. Since all of the HCl was not removed, it is believed that some extra HCl was being introduced to the solution, probably from due to the small amounts of moisture contamination from the glove box or from moisture adsorbed onto the corrosion coupons during cleaning. This mixture will be referred to throughout the thesis as the purified $AlCl_3$-$[P_{14,6,6,6}]Cl$, $X_{AlCl3} = 0.67$.

2.2 Density

Ionic liquid density (ρ in kg/m^3) was measured over a range of temperatures. The density data was represented by a linear function of temperature. The density of the phosphonium ILs tested was low compared with most imidazolium or pyridinium ILs. A theoretical density was calculated for the ILs based on estimated anion volumes.

Experimental Aspects

Two experimental setups were used to measure the density. The first set-up used to measure the density of the neat ILs was a 25 mL glass pyncometer heated in a water bath. The samples were exposed to the atmosphere, however, the exposure was limited because of the very narrow tube and the outward flow of the IL as the solution was heated. The density of the chloro-aluminate mixtures could not be measured using the first setup because the aluminium chlorides were oxidized in the narrow tube causing blockage. To overcome this difficulty a 10 mL pyncometer with an open top was used. The temperature for this set-up was adjusted using an oil bath resulting in a wider temperature range. The atmosphere at the top of the pyncometer was purged continuously with dry nitrogen to minimize contact with oxygen or moisture. Solution was removed or added as required using an external syringe as seen in Figure 12. Some of the neat ILs were also tested using this setup and the results were comparable to the 25 mL setup. The density measurements of the neat ILs were generally only run one time since the experiments were found to be very reproducible. The density measurements of the chloroaluminate mixtures were carried out two or three times since the scatter in the data was noticeable, it should be noted that these experiments were not at equilibrium since some gas was being produced during the testing. The purified $X_{AlCl3} = 0.67$ mixture was more stable because it had been pre-heated for a long period of time to remove the HCl prior to the density measurement. Some examples of the experimental error are provided in the section as results of different experimental set-ups are compared.

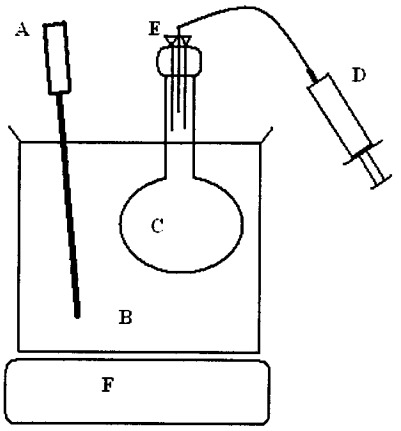

A Thermocouple

B Oil bath

C Pyncometer (10 mL)

D Syringe with extra solution

E Dry nitrogen inlet and gas outlet

Figure 12 Density measurement experimental set-up for the chloroaluminate ILs.

Results

Neat Ionic Liquids

The density of the neat ILs with various anions is presented as a function of temperature in Figure 13. In general, the larger anions resulted in a more dense solution with the notable exception of the $[P_{14,6,6,6}]Br$ that is more dense than would be expected based on the anion volume.

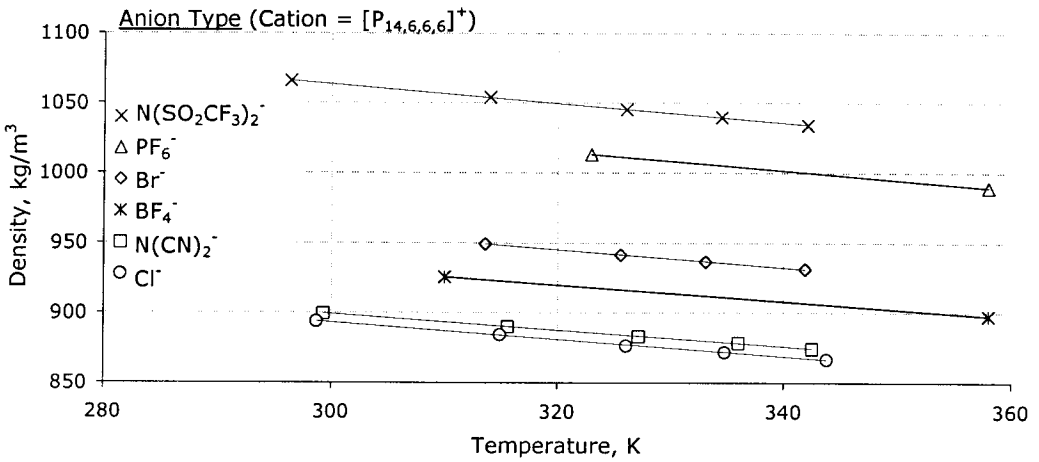

Figure 13 Effect of anion type on the density of trihexyl(tetradecyl) phosphonium ILs.

The smaller the cation, the denser the IL for the three phosphonium cations tested (Figure 14). The density measurement range for the smaller cation types ($[P_{4,4,4,4}]^+$ and

$[P_{14,4,4,4}]^+$) is limited to higher temperatures as the freezing point of the ILs is above room temperature.

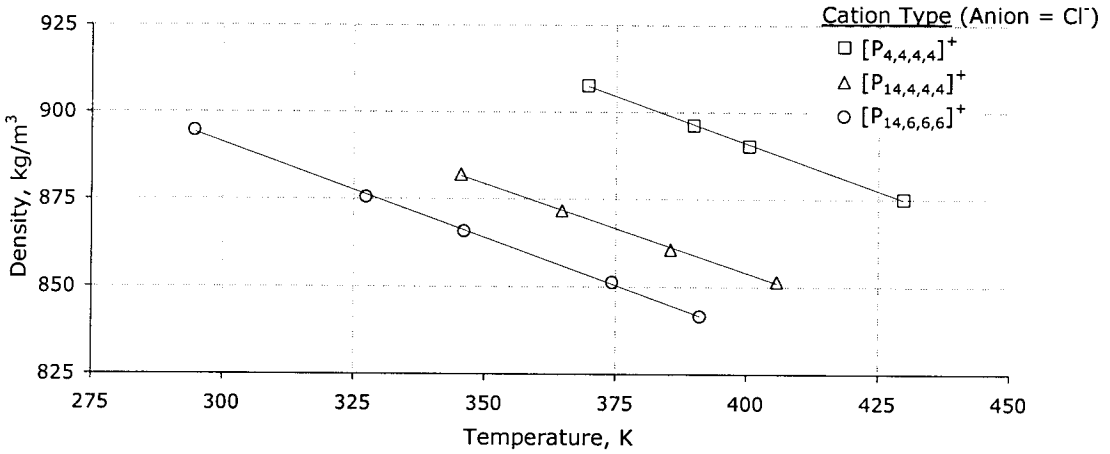

Figure 14 Effect of cation type on the density of phosphonium chloride ILs.

The effect of cation symmetry on density was small and is likely within the range of experimental error for these measurements (Figure 15).

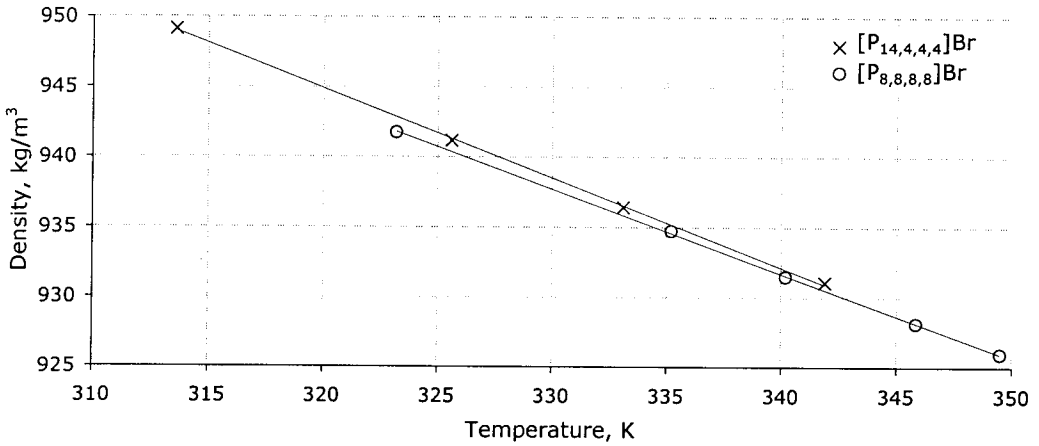

Figure 15 Effect of cation alkyl chain symmetry on the density of phosphonium bromide ILs.

Linear IL density functions are shown in Table 30. The 10 mL pyncometer was used for the measurement of $[P_{4,4,4,4}]Cl$ and $[P_{14,4,4,4}]Cl$ as the higher melting point of these liquids resulted in blockage of the narrow valve at the top of the 25 mL pyncometer. The density functions measured by Cytec were used for the fluorine containing ILs (BF_4^- and PF_6^-). Three density functions are provided for $[P_{14,6,6,6}]Cl$.

Table 30 Linear density functions for the neat ILs. 25 mL pyncometer used unless indicated otherwise.

Ionic Liquid	Linear Density Function ρ(T), kg/m^3 (T in Kelvin)	Temperature Range Tested K
$[P_{4,4,4,4}]Cl^t$	1106.7-0.5394T	370-430
$[P_{14,4,4,4}]Cl^t$	1057.4-0.5085T	345-406
$[P_{14,4,4,4}]Cl$	1063.4-0.5338T	323-350
$[P_{14,6,6,6}]Cl$	1054.6-0.5447T	295-391
$[P_{14,6,6,6}]Cl^t$	1076.2-0.6104T	299-344
$[P_{14,6,6,6}]Cl^*$	1073.8-0.5889T	273-363
$[P_{14,6,6,6}]Br$	1149.4-0.6390T	314-342
$[P_{14,6,6,6}]Br^*$	1148.9-0.654T	293-343
$[P_{8,8,8,8}]Br$	1136.8-0.6034T	323-350
$[P_{14,6,6,6}]PF_6^*$	1231.5-0.6764T	273-363
$[P_{14,6,6,6}]BF_4^*$	1105.9-0.5820T	273-363
$[P_{14,6,6,6}]N(CN)_2$	1072.8-0.5791T	299-343
$[P_{14,6,6,6}]N(SO_2CF_3)_2$	1271.3-0.6928T	296-342

* From Cytec Chemical Information Sheets
t 10 mL pyncometer used

The three density functions for $[P_{14,6,6,6}]Cl$ are plotted in Figure 16 to provide and indication of the range of experimental error using the different experimental setups. The average density at 325 K is 879.27 +/- 3.08 kg/L at a confidence level of 95% based on these three functions.

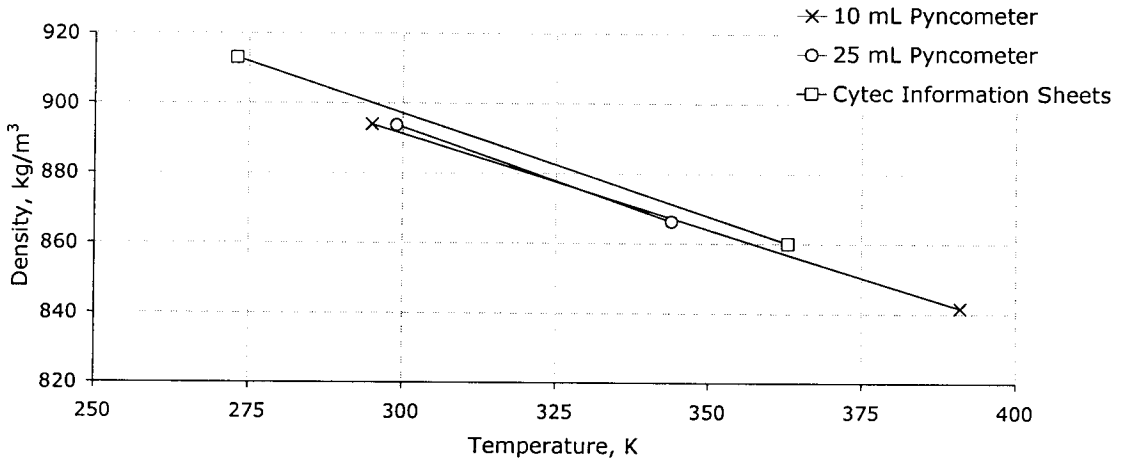

Figure 16 The density functions of $[P_{14,6,6,6}]Cl$ plotted to the range of temperatures tested.

Chloro-aluminate ILs

The density of the $AlCl_3$-IL mixtures were measured over a wide range of temperature and composition (Figure 17 and Figure 18). In the case of the acidic chloro-aluminate systems, there was a greater degree of scatter in the data. The scatter is the

result of a gas being produced in the IL at a temperature above about 333 K. As the temperature was increased the amount of gas produced was enough to decrease the volume of the solution. When the solution dropped below 10 mL, fresh solution was added to the pyncometer to compensate. A solution mass loss experiment was run (in triplicate) to determine the extent of the gas production, for 60 grams of the 0.67 mole fraction $AlCl_3$ solution, after 24 hours at 373 K, about 3% of the mass of the solution was lost to the gas phase. This mass loss mainly occurred within the first 15 hours, the rate then leveled off. The gas produced during these experiments was bubbled through 100 mL of deionized water causing the pH to drop from 4.3 to 1.8. It is thus suspected that some of the gas produced was HCl(g). Excess HCl could be produced by aluminium chloride ions reacting with water impurities in the IL. It is impossible that HCl would account for a 3 wt. % mass loss since it is only present in concentrations below 1 wt.%. Some $AlCl_3$ was also sublimed from the solution as the temperature is increased. The purified solution (X_{AlCl3} = 0.67) was already heated to temperatures above 373 K for a week, it was effectively pre-densified as is shown by the higher density at the room temperature condition, however, the density approaches that of the non-purified solution at higher temperatures.

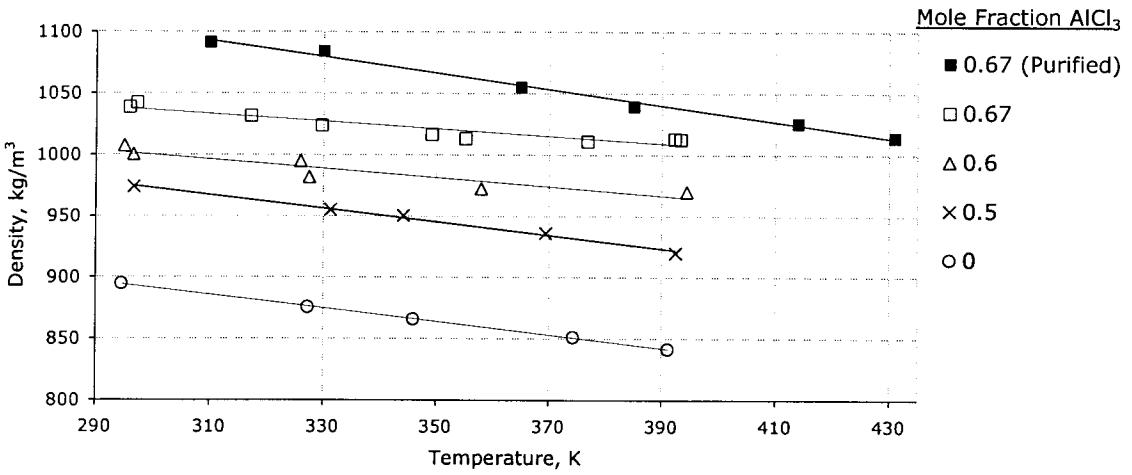

Figure 17 The density of $[P_{14,6,6,6}]Cl$-$AlCl_3$ as a function of $AlCl_3$ concentration and temperature.

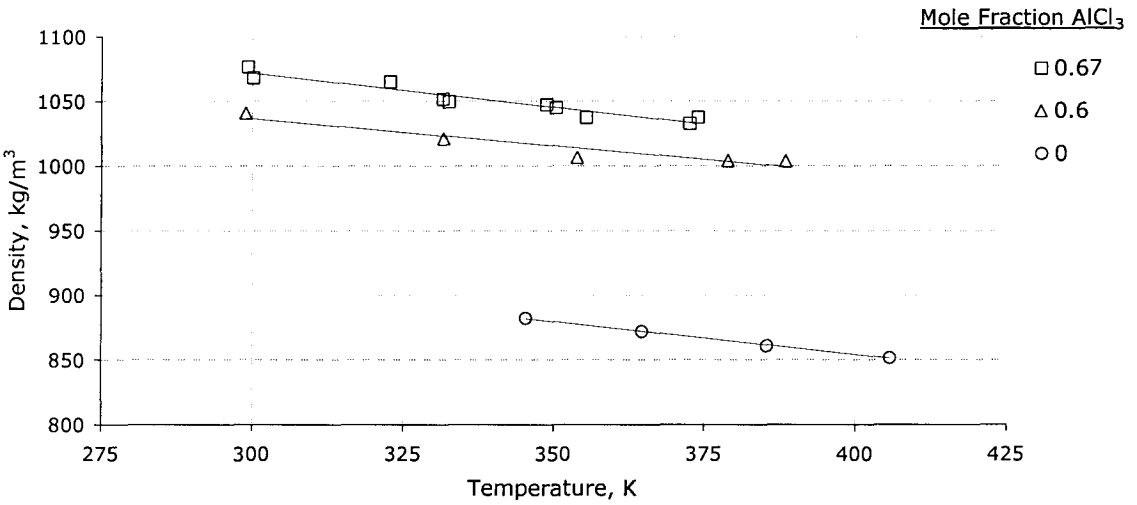

Figure 18 The density of $[P_{14,4,4,4}]Cl$-$AlCl_3$ as a function of $AlCl_3$ concentration and temperature.

The density functions of the chloroaluminate ILs are shown in Table 31.

Table 31 Linear density functions for the chloroaluminate ILs, 10 mL pyncometer used.

Ionic Liquid	X_{AlCl3}	Linear Density Function kg/m^3 (T in Kelvin)	Temperature Range Tested K
$AlCl_3$-$[P_{14,6,6,6}]Cl$	0.5	1138.6-0.5523T	297-392
	0.6	1112.1-0.3732T	295-394
	0.67	1126.3-0.3005T	296-393
	0.67 (Purified)	1298.1-0.6618T	310-431
$AlCl_3$-$[P_{14,4,4,4}]Cl$	0.6	1161.9-0.4189T	299-389
	0.67	1229.1-0.5256T	299-374

Calculated Density

The experimentally measured density at 298 K is compared with a calculated density based on the estimated molar volumes of the cations and anions by the generalized linear equation of Jenkins (1999). The generalized linear equation is an extension of the linear correlation of the lattice enthalpy against the inverse of the cubic root of the volume per molecule of for simple MX salts (Roobottom 1999 *Cited:* Mallouk 1984). The cation and anion volumes were taken from directly from the reference (Jenkins 1999) or calculated by Jenkins following a personal communication (2005). The ion volumes and estimated error are presented in Table 32.

Table 32 Ion volumes calculated by Jenkins (1999 and 2005)

Ion	Ion Volume, nm^3	Error, nm^3
$Al_2Cl_7^-$	0.265	0.019
$N(SO_2CF_3)_2^-$	0.2025	0.0229
$AlCl_4^-$	0.156	-
PF_6^-	0.109	0.008
BF_4^-	0.073	0.009
$N(CN)_2^-$	0.0631	0.0166
Br^-	0.056	0.014
Cl^-	0.047	0.013
$[P_{14,6,6,6}]^+$	0.8188	0.001
$[P_{14,4,4,4}]^+$	0.6746	0.0009
$[P_{4,4,4,4}]^+$	0.4343	0.0007
$C_6H_{11}N_2^+$ (EMI^+)	0.118	-

The density (kg/m^3) of the ILs were calculated from the ionic volumes using Equation 31.

$$MW/((V^+ + V^-)N_A) \qquad [31]$$

Where MW is the molecular weight (kg/mole). V^+ and V^- are the volumes of the cation and anion respectively (m^3) and N_A is Avogadro's number ($6.02 \cdot 10^{23}$ $mole^{-1}$).

Figure 19 compares the measured densities at 298 K with the calculated densities based on the ionic volumes. The two densities are clearly correlated for the series of $[P_{14,6,6,6}]^+$ salts, however, the calculated values overestimate the density by about 14%. According to Jenkins, the crystal packing calculations often overestimate the density and this is probably due to averaged ion volumes and the assumption made of sphericity.

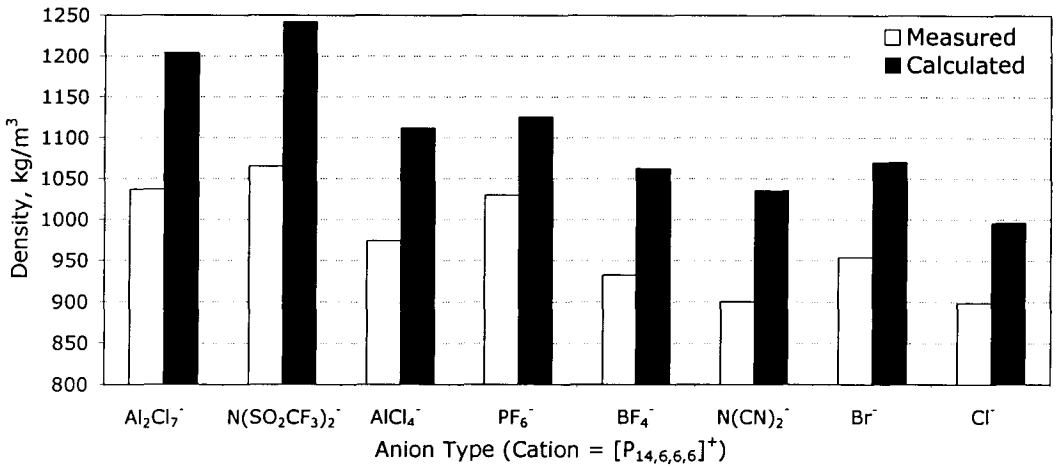

Figure 19 Comparison of the measured density (298 K) with the calculated density.

A theory was proposed to explain the larger volume obtained upon fusion of molten salts since even simple salts exhibit a 10-20% increase in volume upon melting (Bockris 1998, p. 632). The "Hole Model" is based on the formation of holes or vacancies similar to vacancies in a crystal lattice. The size and frequency of the holes are constantly fluctuating in the liquid. The distribution of the size of holes was established by Fürth where the distribution of holes in a liquid was established by relating work required for bubble formation and considering the surface tension of the liquid (Bockris 1998, p. 638 *Cited:* Fürth 1941). Using this model, it was shown that the mean hole radius is on the same order as the radius of ions comprising the liquid suggesting that the movement of ions involves waiting for these voids to appear and jumping into them.

2.3 Viscosity

Viscosity is the property of a fluid whereby motion is resisted internally. Although the viscosity of IL's are generally higher than most common solvents, they are usually treated as Newtonian fluids (Mantz 2003, p. 56). Newtonian fluids obey Newton's law of viscosity as described in Equation 32. The shear stress (F/A in Pa) is related to the velocity gradient (dv/dx in s^{-1}) by the dynamic or absolute viscosity (η in Pa·s).

$$F/A = \eta(dv/dx) \qquad [32]$$

Experimental Aspects

Viscosity measurements were performed outside the glove box using Cannon-Frenske type capillary viscometers (sizes 50, 150, 200 and 350 were employed). A schematic of the experimental set-up is provided in Figure 20. The temperature was controlled using an oil bath (G). The viscosity was calculated from the efflux time. The efflux time was the time required for the liquid to pass from Line A (I) to Line B (J) under the force of gravity.

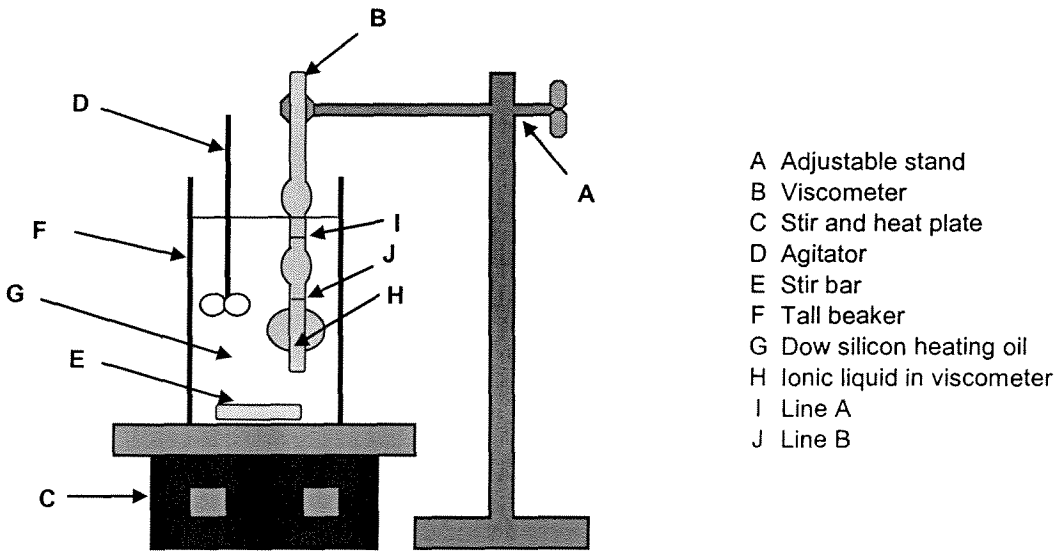

Figure 20 Viscosity measurement experimental set-up.

The experimental data was adjusted with respect to the temperature calibration of the viscometers; the viscometer was calibrated at 313 and 373 K. The samples were dried for 4 hours by heating to temperatures ranging from 393-428 K in a dry nitrogen environment prior to testing. Only the viscosities of the neat ILs were measured. The viscosity of the metal halide salt-IL mixtures were not measured since the chlorides would react quickly with oxygen and moisture in the air and it was not practical to run these experiments in the glove box because of the large amount of heat required. Generally, the experiments were only run once, when experiments were repeated it was found that the reproducibility was very high, an example of a repeated experiment is shown in Figure 21

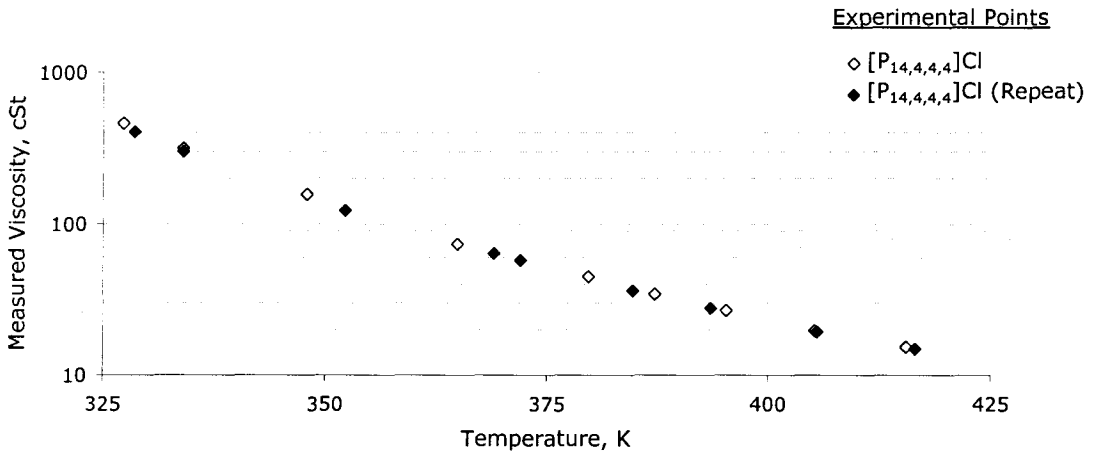

Figure 21 An example of repeated viscosity experiments for $[P_{14,4,4,4}]Cl$, measured (kinematic) viscosity vs. temperature.

Results

The measured kinematic viscosity (υ, cSt) data was converted to the dynamic or absolute viscosity (η, cP) using the density functions in Table 30 (ρ, kg/m^3) and Equation 33.

$$\eta = \upsilon\rho/1000 \qquad [33]$$

When multiple density functions were presented, the Cytec function was used if available, followed by measurements using the 25 mL pyncometer and finally the 10 mL pyncometer. The density functions were extrapolated to accommodate the temperature range of the viscosity experiments. The dynamic viscosity is presented in the form of an

Arrhenius plot in Figure 22. The smooth lines are nearly linear, however, there is a subtle curvature indicating slight non-Arrhenius viscosity behaviour, the deviation from linearity is most noticeable in the case of $[P_{4,4,4,4}]Cl$ which is has the highest melting point. The temperature-activation energy correlation may be increased as the liquids are supercooled since the size of cooperatively rearranging regions is determined by configuration restrictions according to the molecular-kinetic theory of Adam and Gibbs (1965). The non-linearity of the Arrhenius plot is more prominent in the $AlBr_3$-MEIB mixtures studied by Sanders (1986). Kamavaram and Reddy (2005) also reported non-Arrhenius viscosity behaviour in $AlCl_3$-BMIC and $AlCl_3$-HMIC systems. The viscosity of ILs is usually represented by the Vogel-Tamman-Fulcher equation (VTF).

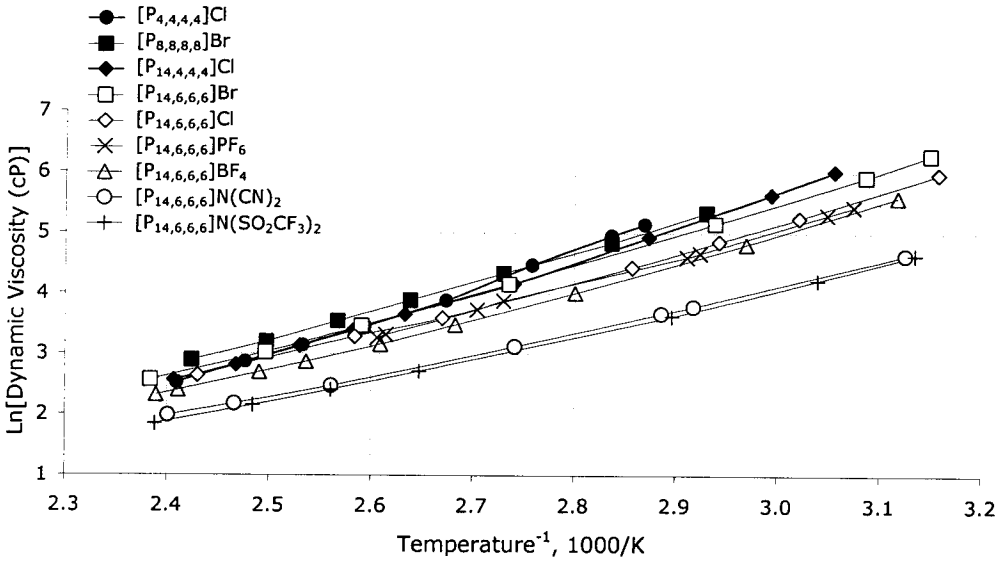

Figure 22 Dynamic viscosity of phosphonium ILs as a function of temperature.

The logarithmic form of the three parameter VTF equation was used to represent the change in absolute viscosity (η) of the ionic liquids as a function temperature (Sanders, 1986 *Cited:* Angell 1969) (Equation 34).

$$\ln(\eta) = B/(T-T_0) + 1/2\ln T + \ln(A) \qquad [34]$$

A and B are constants. T is the temperature and T_0 is the theoretical glass transition temperature (both in Kelvin). This calculated theoretical glass transition temperature is closely related to experimentally determined glass transition temperatures (T_g). In a study of fifteen differing materials, T_g/T_0 was found to be 1.30 +/ 8.4% (Adam

1965). A, B and T_0 were obtained by fitting the experimental data to the VTF model. Firstly, $\ln(\eta \cdot T^{-1/2})$ was plotted against $1/(T-T_0)$, the value of T_0 was then adjusted until the R^2 value of the Microsoft Excel® linear trend line was maximized (Figure 23). The R^2 value is the square of the product moment correlation coefficient, a higher value indicates that the variables are changing together. The R^2 value was higher than 0.99 for all of the fitted VTF data. T_0 was adjusted to a precision of one degree Kelvin. The slope of linear fit is B. After determining T_0 and B, the constant A was solved for by using it to minimize the difference between the experimental viscosity and the viscosity predicted by the VTF equation.

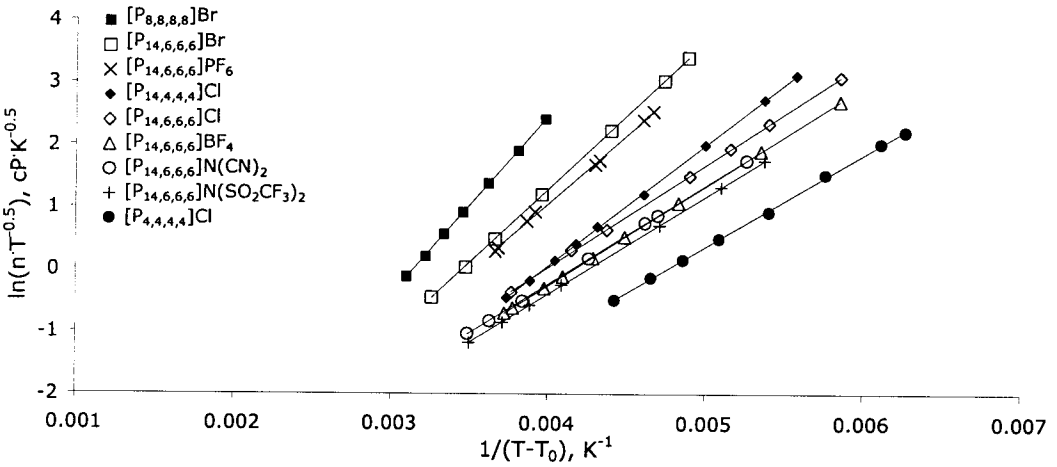

Figure 23 Linear fit of VTF parameters, T_0 adjusted to maximize linearity; B is the slope of the line.

In Figure 24, the dynamic viscosity is plotted with respect to absolute temperature. Experimental data points are compared with the VTF model values (indicated by a cross). The model reproduced the experimental values well at all temperatures for all the ILs. The viscosity generally decreased with increased anion size indicating that ion-interactions are a limiting factor in these systems.

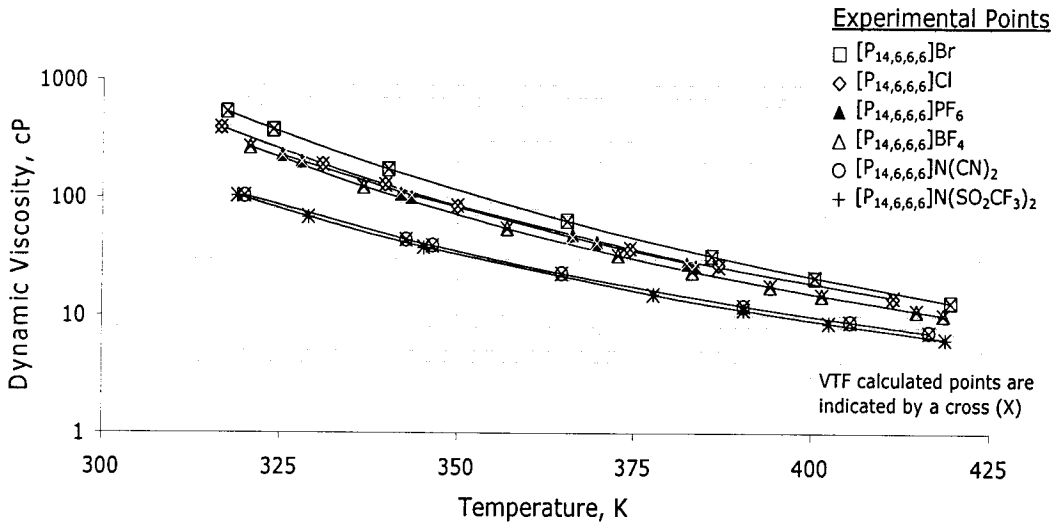

Figure 24 Effect of anion type on the dynamic viscosity of $[P_{14,6,6,6}]^+$ ILs as a function of absolute temperature.

The temperature dependent activation energy of viscous flow ($E_{a,\eta}$ in kJ/mol) was calculated from the differentiation of Equation 34, knowing that $E_{a,\eta} = RT^2(\partial \ln(\eta)/\partial T)$ (Sanders, 1986). The result is Equation 35.

$$E_{a,\eta} = -R(T^2/(T-T_0)^2 - RT/2) \qquad [35]$$

The activation energy of viscosity decreases with increasing temperature and was found to be lowest for the $N(CN)_2^-$ anion in the $[P_{14,6,6,6}]^+$ type ILs tested (Figure 25). Also, the values obtained for the Cl^- and BF_4^- anions are very close.

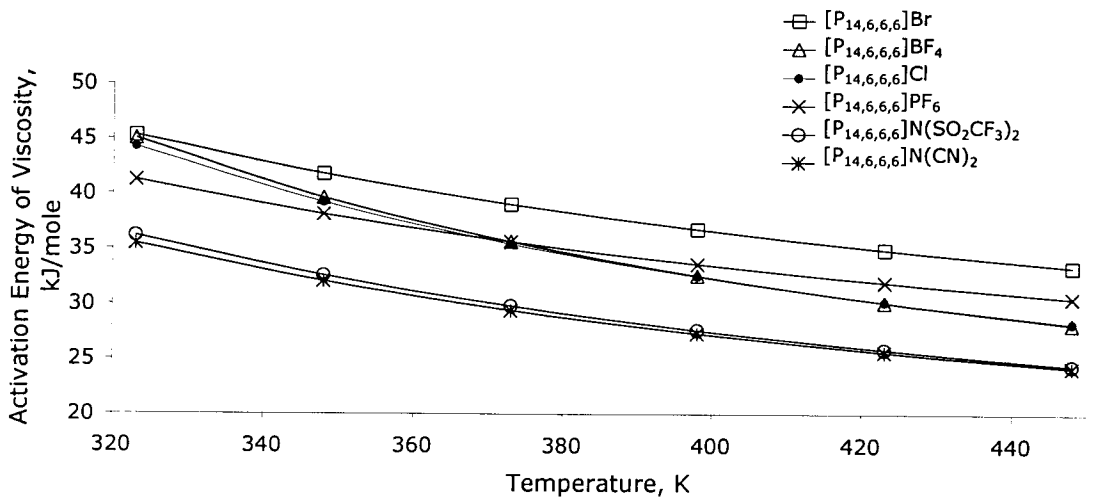

Figure 25 Effect of anion type on the activation energy of viscosity of $[P_{14,6,6,6}]^+$ ILs.

In Figure 26, the effect of cation size on viscosity is presented. At lower temperatures, the smaller cation results in a higher viscosity, however, as the temperature increases above 400 K, the viscosity of the three ILs tested becomes very close. The lower temperature viscosity measurements were very close to the melting point of $[P_{14,4,4,4}]Cl$ and $[P_{4,4,4,4}]Cl$.

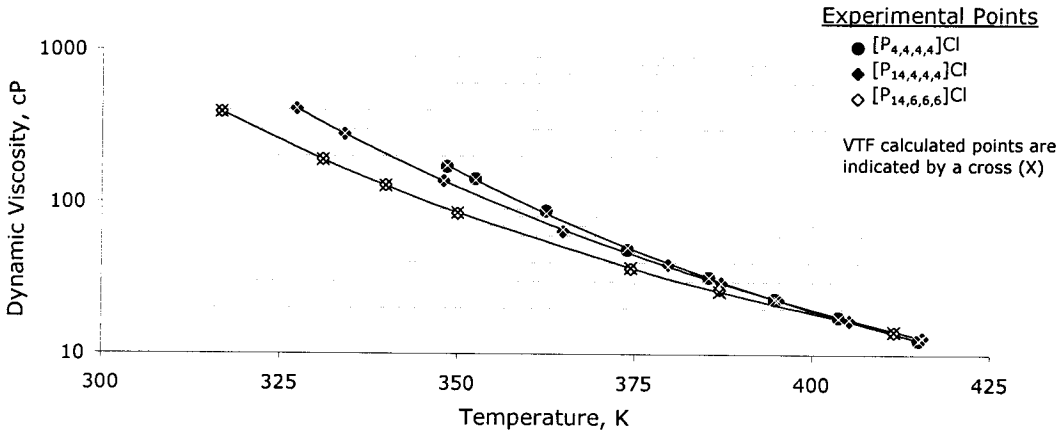

Figure 26 Effect of alkyl chain length on the dynamic viscosity of tetra-alkyl phosphonium chloride ILs as a function of absolute temperature.

From the activation energy plots (Figure 27), the much higher activation energy of viscosity of the shorter alkyl chain length ILs is noticeable, especially at lower temperatures. $[P_{4,4,4,4}]Cl$ is actually a super cooled liquid at temperatures below about 353 K.

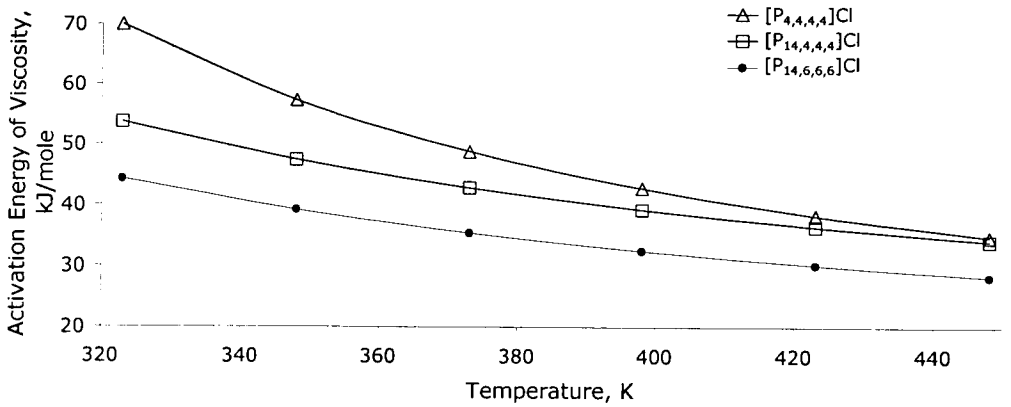

Figure 27 Effect of alkyl chain length on the activation energy of viscosity of phosphonium chloride ILs.

The viscosities of ILs with identical chemical composition but differing cation symmetry were compared in Figure 28. The symmetric $[P_{8,8,8,8}]Br$ is slightly more viscous than the asymmetric $[P_{14,6,6,6}]Br$.

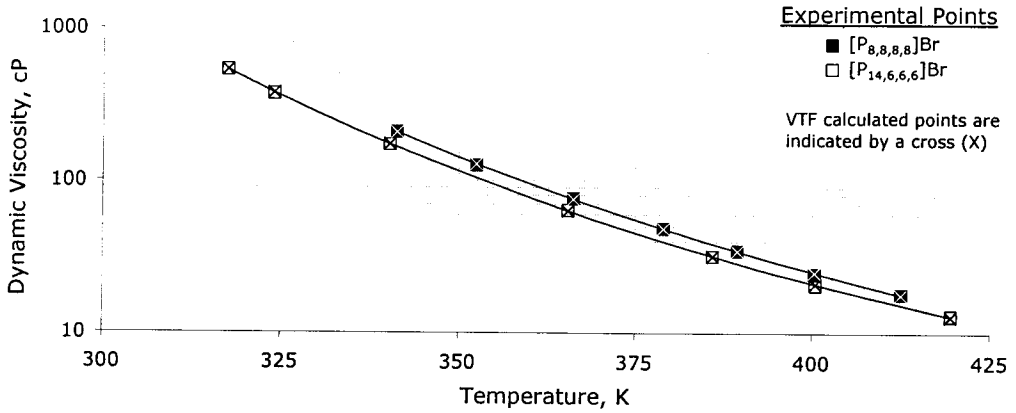

Figure 28 Effect of tetra-alkyl phosphonium bromide cation symmetry on the viscosity as a function of temperature.

The activation energy of viscosity is lower for the IL with the asymmetric cation, especially at higher temperatures (Figure 29).

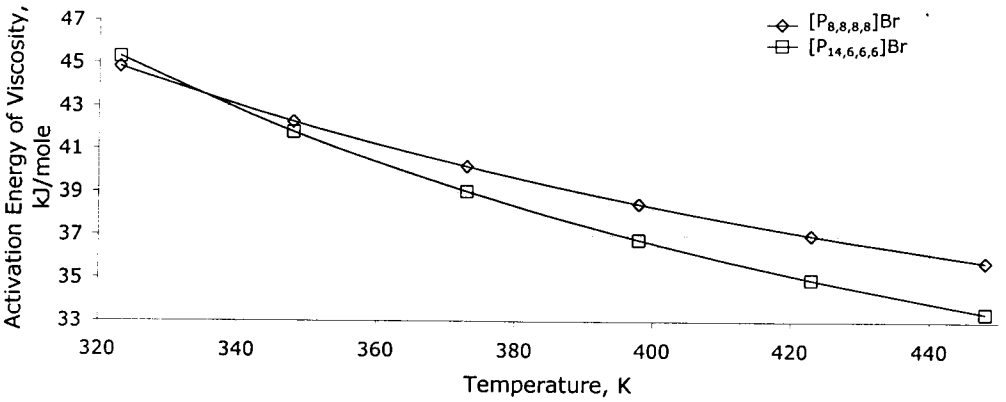

Figure 29 Effect of alkyl symmetry on the activation energy of viscosity of phosphonium bromide ILs.

Parameters for the calculation of the dynamic viscosity (cP) of tetra-alkyl phosphonium ILs using Equation 34 are presented in Table 33. The temperature range in which the experimental data was obtained is also provided.

Table 33 Summary of the VTF parameters used to fit the dynamic viscosity model of tetra-alkyl phosphonium ILs.

Ionic Liquid	A	B	T_0 K	Temperature Range, K
$[P_{4,4,4,4}]Cl$	$8.93 \cdot 10^{-4}$	1475.8	189	348-415
$[P_{14,4,4,4}]Cl$	$4.43 \cdot 10^{-4}$	1943.5	148	327-415
$[P_{14,6,6,6}]Cl$	$1.42 \cdot 10^{-3}$	1646.6	146	316-411
$[P_{14,6,6,6}]Br$	$2.75 \cdot 10^{-4}$	2371.2	113	317-419
$[P_{8,8,8,8}]Br$	$1.13 \cdot 10^{-4}$	2889.3	90	341-412
$[P_{14,6,6,6}]PF_6$	$4.25 \cdot 10^{-4}$	2206.0	111	325-383
$[P_{14,6,6,6}]BF_4$	$1.28 \cdot 10^{-3}$	1598.7	150	320-418
$[P_{14,6,6,6}]N(CN)_2$	$1.41 \cdot 10^{-3}$	1579.8	130	320-416
$[P_{14,6,6,6}]N(SO_2CF_3)_2$	$1.31 \cdot 10^{-3}$	1560.6	133	319-418

Aromatic hydrocarbons such as toluene and benzene have been used by researchers in the past to improve aluminium deposit quality (Hurley, 1952). The effect of toluene on the kinematic (measured) viscosity of $[P_{14,6,6,6}]Cl$ is shown in Figure 30. At concentrations of 1 wt.% toluene a very slight increase in the viscosity is noticed and at concentrations of 5 wt.% the increase became substantial. At temperatures above about 380 K the higher viscosity of the mixture appears to lessen slightly, it is likely that toluene is being lost above this temperature as its boiling point is 384 K. According to Seddon (2000), the presence of water and other co-solvents in ILs tends to reduce the viscosity however this effect was not observed in the case of toluene in $[P_{14,6,6,6}]Cl$.

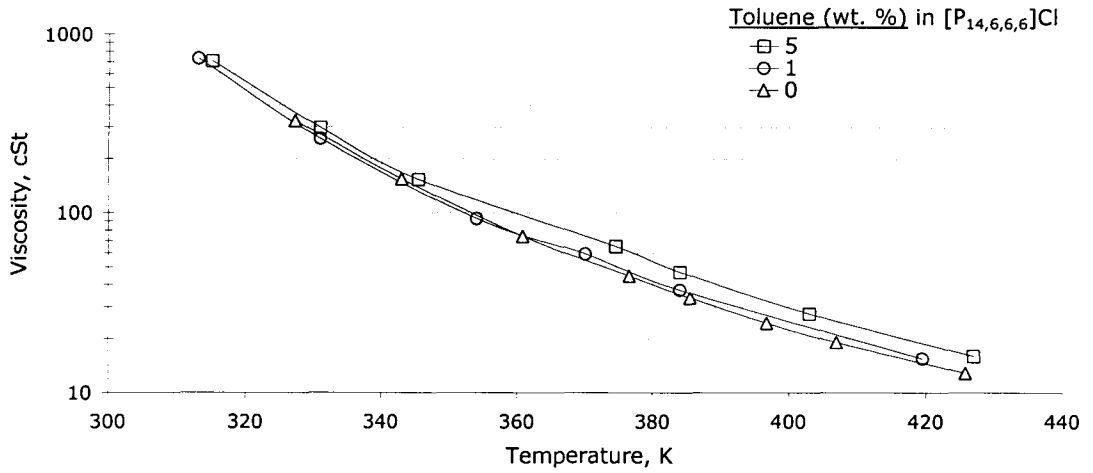

Figure 30 Effect of toluene on the viscosity of $[P_{14,6,6,6}]Cl$.

Phosphonium IL viscosity is somewhat higher than that of their ammonium counterparts (Bradaric 2003). Impurities are known to affect the viscosity of ionic

liquids; it has been shown that Cl^- contaminated [EMI]BF_4, [BMI]BF_4, [BMI]NO_3 and [OMI]NO_3 (0.5-2.2 mol/kg Cl^-) were 40-580% more viscous at 293 K ([BMI]NO_3 was tested at 318 K) compared with the same ILs with a Cl^- content < 0.02 mol/kg (Seddon 2000). Hydrogen bonding is thought to play a role in these systems thus the effects of Cl^- in the tetra-alkyl phosphonium ILs may not be as pronounced.

2.4 Conductivity

Solution conductivity is a critical parameter for any electrochemical process, especially in the case of primary metal production. In this section, the conductivity of ILs and metal-salt-IL mixtures is characterized. For the neat ILs and some of the chloro-aluminate melts both the measured specific conductivity (σ in S/m) and equivalent conductivity (Λ in $S \cdot m^2$/mol-eq) are presented. The specific conductivity is a more practical value as it can be directly compared with any solution and is the value of interest for design. The equivalent conductivity on the other hand, is more useful when evaluating the mechanism of conductivity and is also more appropriate for the modeling of the data using the Vogel-Tamman-Fulcher (VTF) equation. The conductivity values are compared with other IL systems as well as organic electroplating baths and industrial electrowinning and refining solutions.

Experimental Aspects

The specific conductivity (S/m) of the ILs was measured using a Jenway conductivity meter and "enterprise" probe (cell constant = 1 cm^{-1}). The experiments were carried out in a test-tube heated by an agitated oil bath (Figure 31). To maintain an oxygen and moisture free atmosphere in the test-tube, dry nitrogen (< 10 ppm O_2, H_2O) was purged continuously via two needles in the stopper.

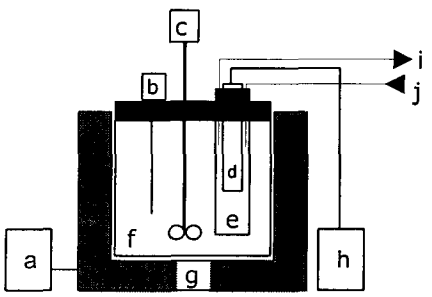

a Rheostat
b Thermocouple
c Agitator
d Conductivity/temperature probe
e Ionic liquid in test tube
f Fisherbrand heating oil
g Heating jacket
h Conductivity/temperature meter
i Nitrogen out
j Nitrogen in

Figure 31 Conductivity measurement experimental setup.

Temperature of the conductivity experiments was regulated using a heated and agitated oil bath. A time lapse of 55 minutes in between measurements was found to be adequate to ensure steady state conditions. The temperature measurements were made by the Jenway in-line thermocouple up to 378 K, for measurements above this value an

estimate was made based on the oil bath temperature. A second thermocouple (not depicted) was immersed in the test solution for some of the experiments to establish a relationship between the heating bath and the test solution at higher temperatures. The measured conductivity data presented are reported from statistical analysis and fitting between 6-10 steady state data points, usually with a third order polynomial. The equivalent conductivity was modeled using the VTF equation as was the dynamic viscosity.

The experimental error involved in the conductivity experiments was evaluated from six repeated conductivity experiments of $[P_{14,6,6,6}]Cl$ and $AlCl_3$-$[P_{14,6,6,6}]Cl$ (X_{AlCl3} = 0.6). The mean conductivity, 95% confidence interval, and standard error as a percentage of the mean are shown in Table 34. Generally, the 95% confidence interval was within 3% of the mean value. The standard error was higher for the neat $[P_{14,6,6,6}]Cl$ at lower temperatures, this was likely due to the fact that the sensitivity limit of the probe is approached since the conductivity is very low at these conditions.

Table 34 Experimental error in the conductance measurements, based on 6 repeat experiments.

Solution	T. K	Mean Conductivity S/m	95% Confidence Interval		Std. Error % of Mean
$[P_{14,6,6,6}]Cl$	298	0.00074	0.00067 -	0.00082	5.3
	323	0.00390	0.00321 -	0.00459	9.1
	348	0.01252	0.01186 -	0.01319	2.7
	373	0.02958	0.02839 -	0.03076	2.0
	398	0.05801	0.05616 -	0.05986	1.6
	423	0.10079	0.09762 -	0.10397	1.6
$AlCl_3$-$[P_{14,6,6,6}]Cl$ X_{AlCl3} = 0.6	298	0.00867	0.00804 -	0.00931	3.8
	323	0.04257	0.04051 -	0.04464	2.5
	348	0.09840	0.09269 -	0.10411	3.0
	373	0.18450	0.17408 -	0.19493	2.9
	398	0.30922	0.29397 -	0.32447	2.5
	423	0.48088	0.46109 -	0.50068	2.1

The neat IL samples were heated for 4 hours at 413 K under a constant dry nitrogen purge prior to testing to remove any excess water. This procedure only affected the conductivity of some of the ILs, the effect of the drying procedure is shown in Figure 32, the specific conductivity of $[P_{14,6,6,6}]Br$ decreased significantly while $[P_{14,6,6,6}]Cl$ was unaffected. $[P_{14,6,6,6}]Cl$ is produced by Cytec at a large scale and was dried at 453 K for

10 hours under vacuum. The bromide IL ($[P_{14,6,6,6}]Cl$) was produced at a smaller scale and was likely not subjected to the same drying procedure, Cytec was unable to confirm the drying procedure of this specific sample. The presence of water might increase the conductivity by hydrating the chloride ions insulating them from the strong cation-anion interactions that limit the mobility in these liquids. Ion interactions are discussed in more detail throughout this section of the thesis. The conductivity of $[P_{14,6,6,6}]Cl$, $[P_{14,4,4,4}]Cl$, $[P_{14,6,6,6}]PF_6$, $[P_{14,6,6,6}]BF_4$ did not change significantly by the drying procedure indicating that they were already dried thoroughly. The conductivity of $[P_{14,6,6,6}]N(CN)_2$ decreased while the conductivity of $[P_{4,4,4,4}]Cl$, $[P_{8,8,8,8}]Br$, $[P_{14,6,6,6}]N(SO_2CF_3)_2$ increased slightly following the drying. The slight increase in conductivity of some of the ILs upon drying remains unexplained.

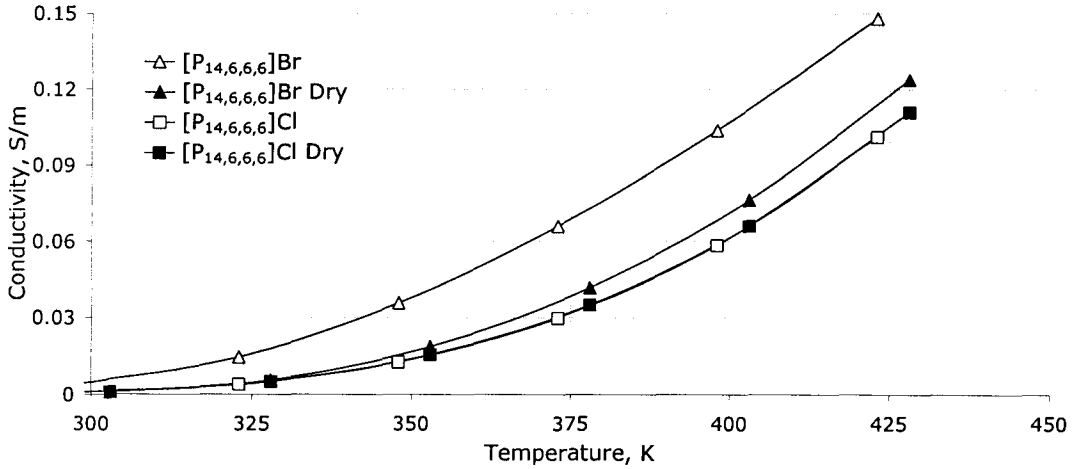

Figure 32 Effect of drying the ILs for 4 hours at 413 K on the conductivity of $[P_{14,6,6,6}]Br$ and $[P_{14,6,6,6}]Cl$.

Results

The phosphonium ILs tested were generally less conductive than pyridinium or imidazolium ILs due to their larger cations and possibly a more localized charge at the cation center resulting in increased cation-anion interaction. Cation-anion interaction may include the formation of cation-anion pairs, triple ions or even whole clusters of ions. Solutions with dielectric constants lower than 10 likely involve cluster formation (Bockris 1998, p. 315).

In order to obtain some insight into the mechanism of conductivity, the equivalent conductivity was calculated to adjust for the number of charge carriers in a given volume of solution using Equation 36.

$$\Lambda = \kappa \cdot MW/(\rho \cdot z) \quad [36]$$

Where, κ is the measured conductivity (S/m), MW is the molecular weight (kg/mol), ρ is the density (kg/m^3) from Table 30 and Table 31, z is the charge (1 for the ILs tested in this thesis). The molecular weight of the chloroaluminate systems were calculated by adding the equivalent molar mass of the $AlCl_3$ to the molar mass of the IL. For example, in the $AlCl_3$-$[P_{14,6,6,6}]Cl$ (X_{AlCl3} = 0.5), the molar mass would be 133.34 g/mol-$AlCl_3$ + 519.33 g/mole-$[P_{14,6,6,6}]Cl$ or 652.7 g/mol.

The molar conductivity is the same as the equivalent molar conductivity for the ILs tested since the cation and anion charges are one. The equivalent conductivities of charge carriers in most dilute aqueous electrolytes of 1:1 salts are 0.1 (+/- 25%) $S \cdot m^2$/mol-eq (Bockris 1998, p. 434).

Similar to the treatment of the kinematic viscosity data, the Vogel-Tamman-Fulcher (VTF) (Equation 37) was used to describe the conductivity of molten salts as a function of temperature as they are known to be glass forming liquids (Smedley 1980).

$$\Lambda = AT^{-1/2}\exp[B/(T-T_0)] \quad [37]$$

The equivalent conductivity (Λ in $S \cdot m^2$/mol-eq), A and B are constants, T is the temperature (Kelvin) and T_0 is the temperature at which the transport function approaches zero or the theoretical glass transition temperature.

Lu and Dreisinger estimated the T_0 of the $AlCl_3$-BMIC IL system at various $AlCl_3$ concentrations using the VTF equation (Lu, 2003). Sanders *et al.* showed that T_0 values estimated by fitting the conductivity data are comparable to both T_0 estimated by viscosity and experimental values of the glass transition temperature (T_g) for the $AlBr_3$-MEIB system (Sanders, 1986). Figure 33 and Figure 34 show the linear fit that relates $\ln(\Lambda \cdot T^{-0.5})$ to $1/(T-T_0)$ when the fit is maximized by varying T_0. B is the slope of the line. The standard error of T_0 with a 95% confidence interval was found to be +/- 9.4% of the mean based on six repeat experiments of $[P_{14,6,6,6}]Cl$.

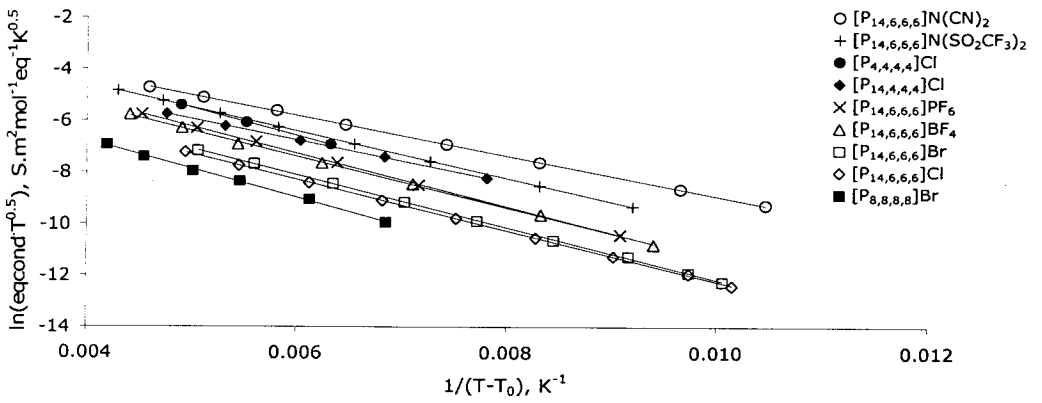

Figure 33 VTF equation parameters for the neat ILs; T_0 was the variable to optimize a linear fit.

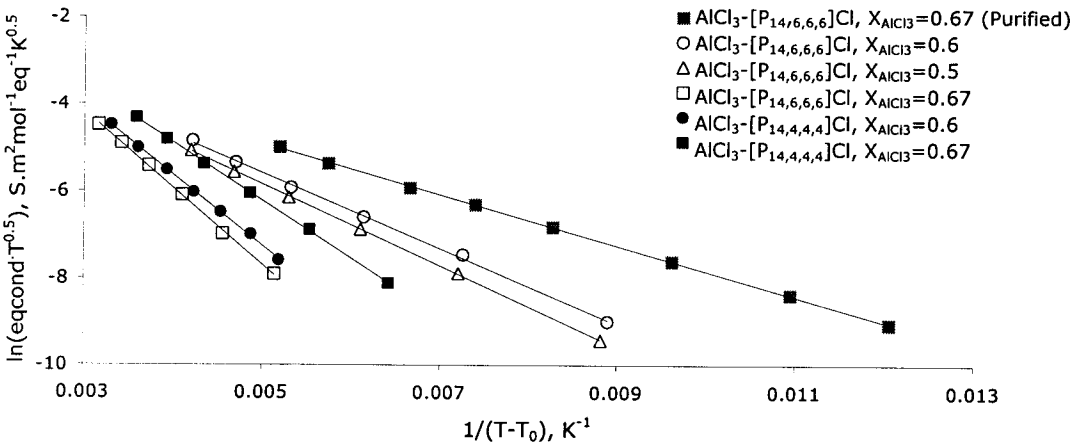

Figure 34 VTF equation parameters for the $AlCl_3$-IL mixtures; T_0 was the variable to optimize a linear fit.

In these systems the type of anion plays a role in determining the conductivity. In the series of $[P_{14,6,6,6}]^+$ ILs, it was found that a larger anion generally resulted in higher conductivity (Figure 35 and Figure 36). The only exception, $N(CN)_2^-$, was more conductive than would be expected based on its size. Larger anions tend to have a less localized charge, reducing cation-anion interaction that hinders migration. The conductivity of $HMIMBF_4$ was reported to be 0.85 S/m, this is much higher than $HMIMPF_6$ being only 0.28 S/m (Zhang, 2004). In the $[P_{14,6,6,6}]^+$ cation ILs, the effect of anion type is different, the PF_6^- anion system was found to be slightly more conductive than BF_4^-, at least at temperatures above 340 K. This difference between the two types is attributed to a stronger cation-anion interaction with a smaller anion in phosphonium IL, whereas in the more conductive imidazolium IL the frictional forces are limiting the

movement of the anion. NMR and IR studies confirmed ion-pairing interaction in $AlCl_3$-BPC systems (Lai, 1987 *Cited:* Taulelle 1983 and Tait 1984).

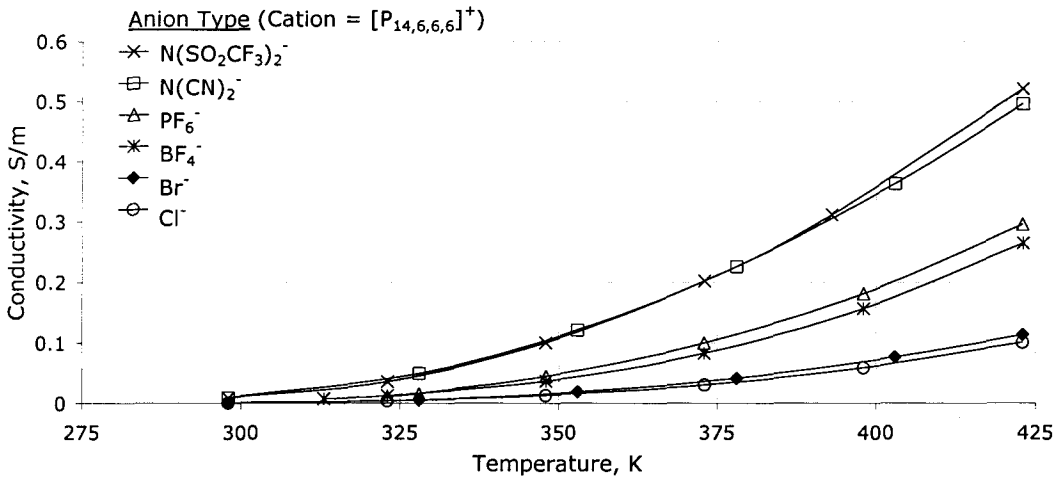

Figure 35 Effect of anion type on the measured conductivity of $[P_{14,6,6,6}]^+$ ILs.

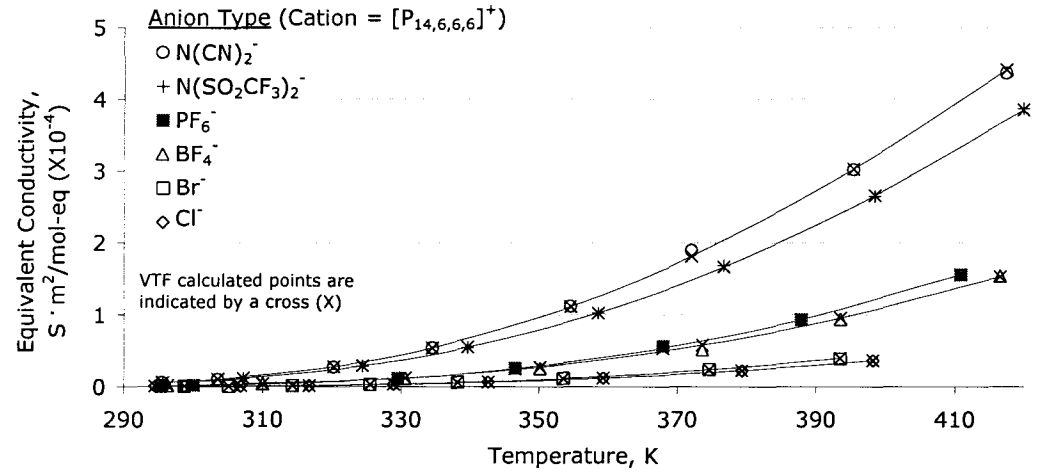

Figure 36 Effect of anion type on the equivalent conductivity of $[P_{14,6,6,6}]^+$ ILs.

Cation type also heavily influences the conductivity, and contrary to the anion effect, a smaller cation leads to increased conductivity. This is probably due to the fact that the cations in these systems are much larger than the anions and their movement is limited by frictional forces rather than cation-anion interaction. In Figure 37 and Figure 38, a strong effect of the cation volume is shown as the conductivity of $[P_{14,6,6,6}]Cl$, $[P_{14,4,4,4}]Cl$ and $[P_{4,4,4,4}]Cl$ are compared.

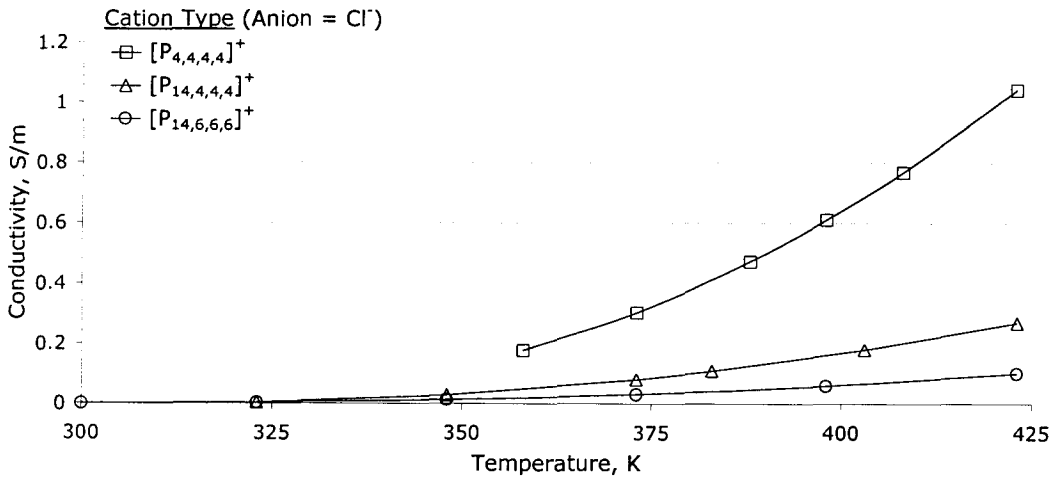

Figure 37 Effect of cation type on the measured conductivity of chloride phosphonium ILs.

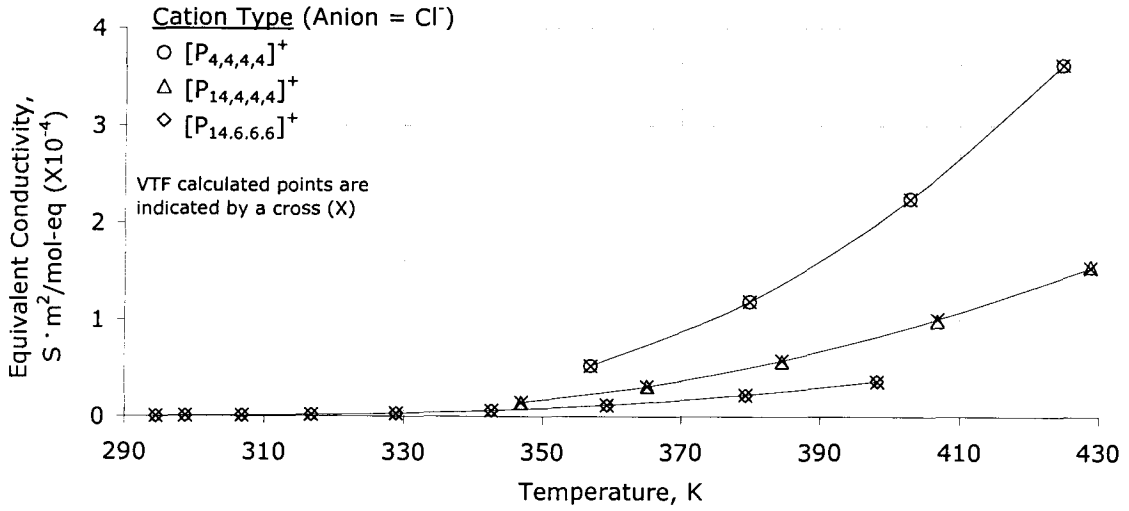

Figure 38 Effect of cation type on the equivalent conductivity of phosphonium chloride ILs.

Cation symmetry was found to have a modest effect on the conductivity as $[P_{14,6,6,6}]Br$ is compared with $[P_{8,8,8,8}]Br$ in Figure 39. The asymmetric bromide IL has a slightly higher conductivity than the symmetric IL at temperatures above about 360 K. The two ILs are of identical molecular weight and nearly identical measured densities. The asymmetry lowers the melting temperature from 316 to 273 K.

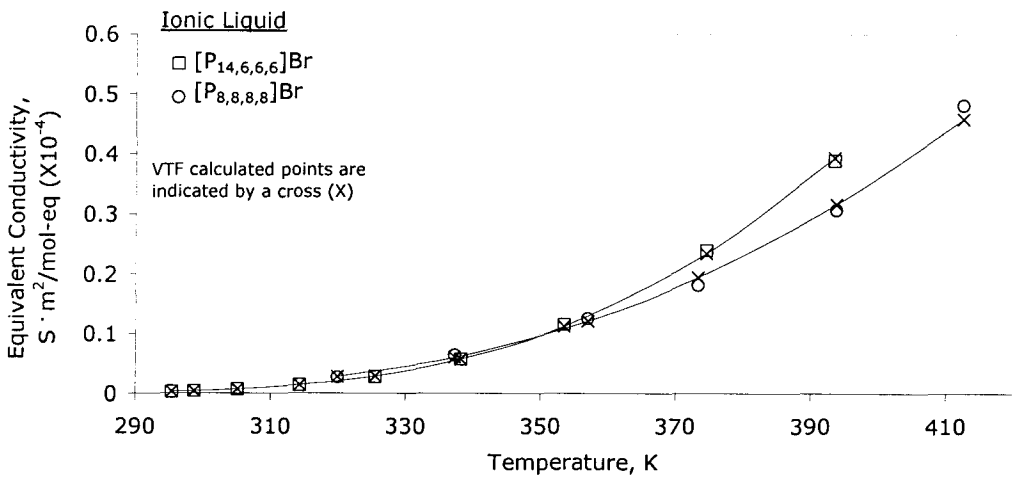

Figure 39 Effect of cation symmetry on the equivalent conductivity of tetra-alkyl phosphonium bromide ILs.

The equivalent conductivity ($S \cdot m^2/mol\text{-}eq$) of the neat phosphonium ILs can be calculated using Equation 37 and the parameters (A, B and T_0) presented in Table 35. The temperature range over which the experimental data was fitted is also provided in the table. The T_g of $[P_{14,6,6,6}]Cl$ was reported to be 217 K, which is about 11% higher than the value of T_0 reported here (196 K) (Cytec Inc. *Cited:* Del Sesto 2003).

Table 35 Summary of the VTF parameters used to fit the equivalent conductivity model of neat tetra-alkyl phosphonium ILs.

IL	A	B	T_o K	Temperature Range K
$[P_{4,4,4,4}]Cl$	$8.37 \cdot 10^{-1}$	-1065.5	199	357-425
$[P_{14,4,4,4}]Cl$	$1.50 \cdot 10^{-1}$	-808.7	219	347-429
$[P_{14,6,6,6}]Cl$	$9.70 \cdot 10^{-2}$	-989.9	196	295-398
$[P_{14,6,6,6}]Br$	$1.35 \cdot 10^{-1}$	-1017.7	196	295-394
$[P_{8,8,8,8}]Br$	$9.44 \cdot 10^{-2}$	-1102.2	174	320-413
$[P_{14,6,6,6}]PF_6$	$3.33 \cdot 10^{-1}$	-1028.6	190	300-411
$[P_{14,6,6,6}]BF_4$	$2.51 \cdot 10^{-1}$	-994.3	190	296-417
$[P_{14,6,6,6}]N(CN)_2$	$3.26 \cdot 10^{-1}$	-780.3	200	296-417
$[P_{14,6,6,6}]N(SO_2CF_3)_2$	$3.99 \cdot 10^{-1}$	-913.6	187	296-420

With the values of T_0 and B identified, the temperature dependent activation energy of conductivity ($E_{a,\Lambda}$ in J/mole) can be calculated. Equation 38 is derived by differentiating Equation 37 with respect to T ($\partial \ln\Lambda/\partial T$) knowing that $E_{a,\Lambda} = RT^2(\partial \ln\Lambda/\partial T)$ where R is the rate constant (8.31 J/mol·K) (Sanders 1986).

$$E_{a,\Lambda} = -RT/2 - RT^2B/(T-T_0)^2 \quad [38]$$

The activation energy of conductivity is presented as a function of temperature for the neat ILs in Figure 40, Figure 41 and Figure 42. Some of the data was extrapolated to higher temperatures than were actually measured. For the various anion types, the activation energy tends to decrease with increasing IL conductivity however; this is not the case with respect to cation size and symmetry.

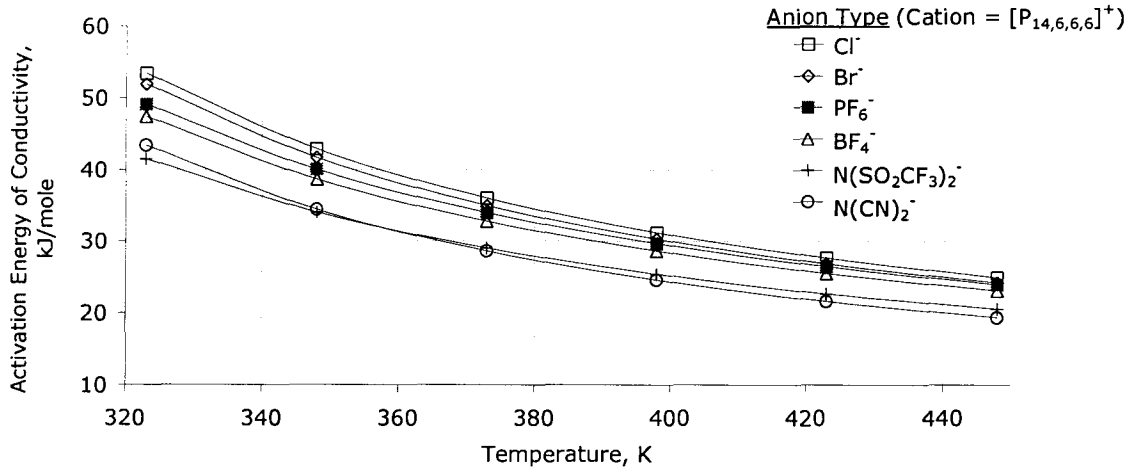

Figure 40 Effect of anion type on the activation energy of conductivity in $[P_{14,6,6,6}]^+$ ILs.

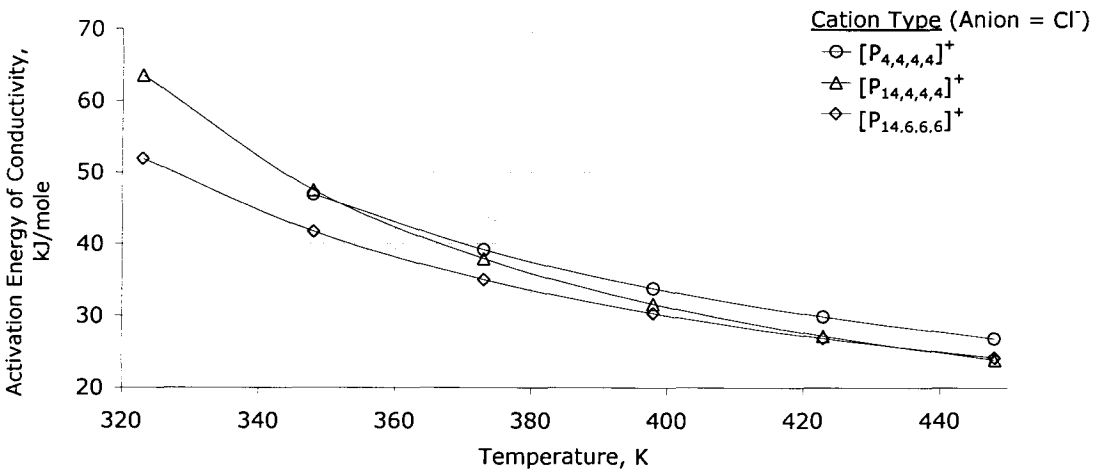

Figure 41 Effect of cation type on the activation energy of conductivity in phosphonium chloride ILs.

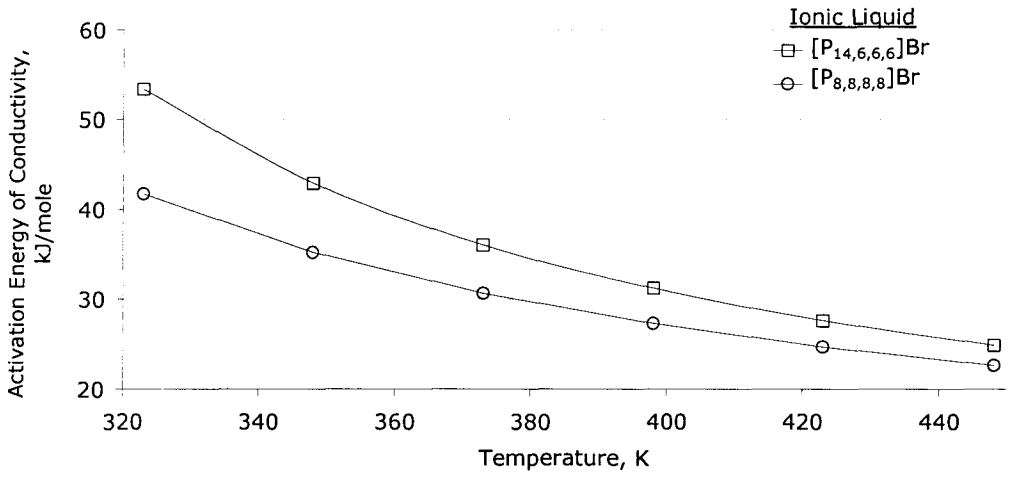

Figure 42 Effect of cation symmetry on the activation energy of conductivity in phosphonium bromide ILs.

Conductivity of binary halo-aluminate-IL mixtures

The formation of $Al_2Cl_7^-$ at $X_{AlCl3} > 0.5$ lowers the conductivity of EMIC-$AlCl_3$ and BMIC-$AlCl_3$ and results in a slight increase in conductivity of BBIC-$AlCl_3$. In the case of the phosphonium systems, a significant increase in the conductivity is noticed when $Al_2Cl_7^-$ is formed. $[P_{4,4,4,4}]$Cl-$AlCl_3$ forms an intermediate solid phase at compositions near X_{AlCl3}=0.5. Since the solid phase had a high melting point the conductivity at temperatures below about 420 K was not determined.

The conductivity of chloro and bromo-aluminate IL systems were also investigated as a function of temperature and concentration of AlX_3 (X = Cl or Br). The increased conductivity of halo-aluminate ILs with AlX_3 concentration is the result of the formation of AlX_4^- and $Al_2X_7^-$ complexes which are more mobile compared with X^- due to less cation-anion interaction. This enhanced mobility of larger anions is counter intuitive if considering only the size, but can be rationalized by the decreased effect of cation-anion pairing or bonding due to the lower charge density (Fannin 1984). The colour of the IL began as clear and remained clear with smaller additions of AlX_3 ($< X_{AlX3} = \sim 0.3$). Upon further addition of AlX_3 the colour changed to a dark red tone that became darker as the concentration of AlX_3 increased. There was some undissolved AlX_3 in the experiments at 0.7 mole fraction AlX_3, dissolution did occur occurred upon heating to elevated temperatures.

In the case of the $AlCl_3$-$[P_{14,6,6,6}]Cl$ system, the conductivity increased with increasing concentration of $AlCl_3$ suggesting that ionic interaction is limiting the conductivity at all concentrations tested (Figure 43).

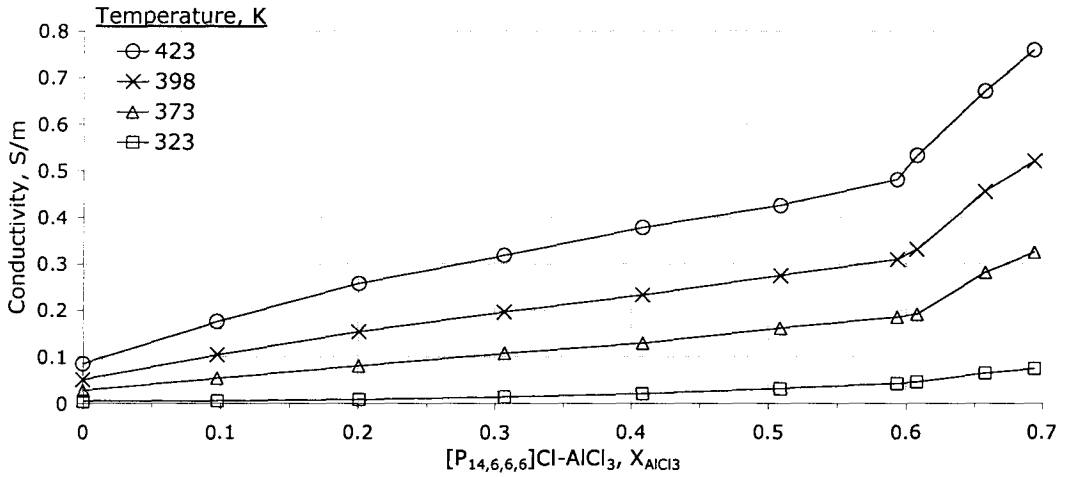

Figure 43 Measured conductivity of the $AlCl_3$-$[P_{14,6,6,6}]Cl$ system.

The conductivity of purified $AlCl_3$-$[P_{14,6,6,6}]Cl$ (X_{AlCl3} = 0.67) was found to be slightly lower that that of the solution that was prepared with the $AlCl_3$ and $[P_{14,6,6,6}]Cl$ with no efforts to remove HCl (Figure 44). Since the purified IL should have a slightly higher concentration of $AlCl_3$ due to corrosion of the pure Al foil and this would normally increase the conductivity, it was determined that the presence of HCl results in increased conductivity of this system.

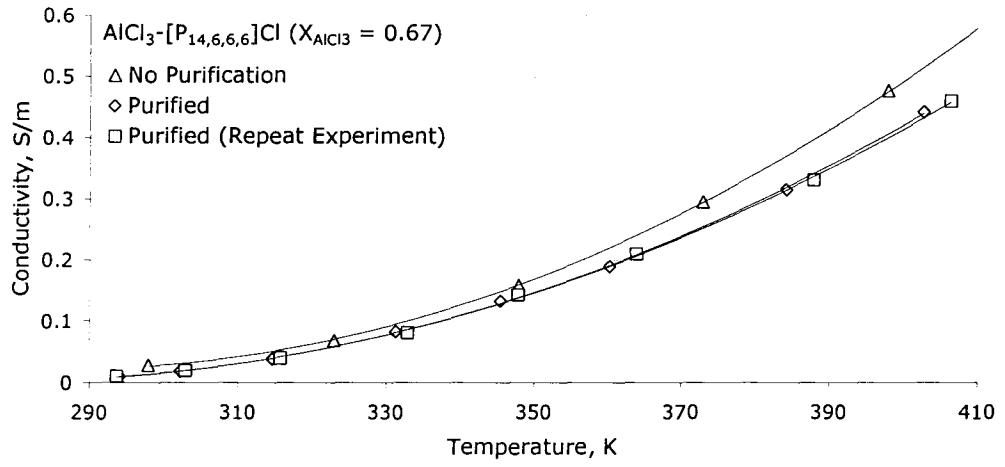

Figure 44 The effect of purification of $AlCl_3$-$[P_{14,6,6,6}]Cl$ (X_{AlCl3} = 0.67) on the solution conductivity. The $AlCl_3$ was sublimed and the solution was heated and exposed to high purity Al to remove H^+.

The equivalent conductivity of the $AlCl_3$-$[P_{14,6,6,6}]Cl$ mixtures is presented in Figure 45, the data was also modeled with the VTF equation.

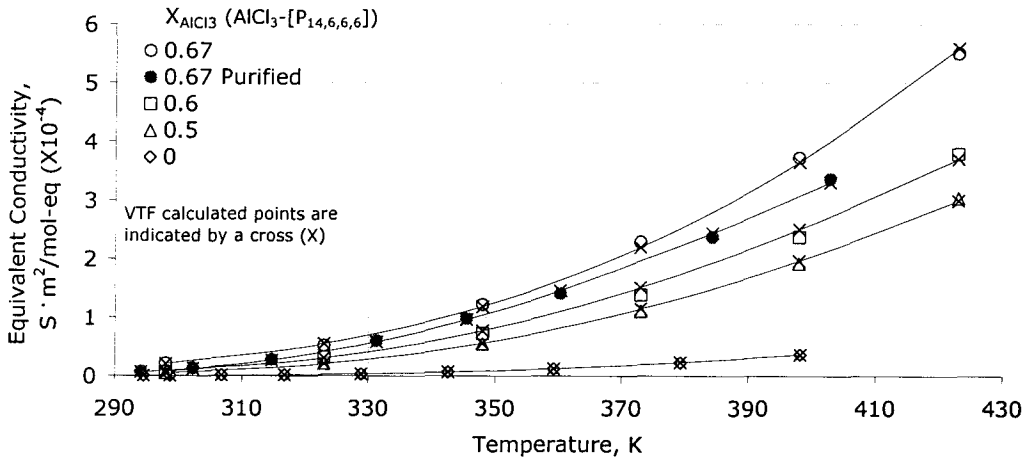

Figure 45 Equivalent conductivity of the $AlCl_3$-$[P_{14,6,6,6}]Cl$ system.

The activation energy of conductivity of the $AlCl_3$-$[P_{14,6,6,6}]Cl$ mixtures is seen in Figure 46. It appears that the purification strongly affects the activation energy, especially at lower concentrations. The 0.67 X_{AlCl3} melt contains the most HCl while the purified version contains the least. The HCl seems to allow for lower activation energy at lower temperature but the activation energy is not lessened with temperature as dramatically as the purified mixture.

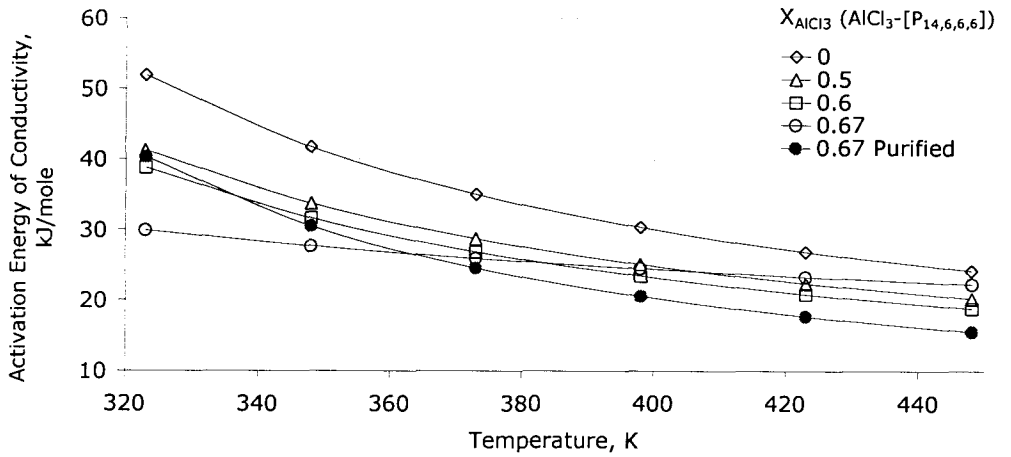

Figure 46 Effect of $AlCl_3$ and purification on the activation energy of conductivity in $AlCl_3$-$[P_{14,6,6,6}]Cl$ ILs.

The analogous bromide system exhibited slightly higher conductivity at lower concentration of $AlBr_3$, however, the conductivity is lower at higher temperatures (> 323

K) at X_{AlBr3} between 0.35 and 0.45 and at concentrations above 0.6. This is attributed to the presence of water impurities as the $[P_{14,6,6,6}]Br$ was not dried prior to these experiments. Water in certain ILs may lead to the formation of liquid crystal phases. These smectic phases (long-range order in the arrangement of molecules in layers to form a regular two-dimensional lattice) have been known to form at elevated temperatures in quaternary phosphonium chloride and bromide salts in the presence of moisture (Abdallah 2000, Chen 2003, and Gowda 2004). The molecular ordering results in conductivities that are lower than in similar isotropic ILs (Chen 2002). It was observed that the drying procedure lowered the conductivity of the neat $[P_{14,6,6,6}]Br$ (Figure 37 (dry) vs. Figure 47 $X_{AlBr3} = 0$ (not dry)), the $[P_{14,6,6,6}]Br$ used to prepare all of the $AlBr_3$-$[P_{14,6,6,6}]Br$ binary mixtures was used as received from Cytec. When preparing the solution with the highest concentration ($X_{AlBr3} = 0.7$) a vigorous reaction took place and the resulting solution was appeared to be considerably more viscous than at lower $AlBr_3$ concentration.

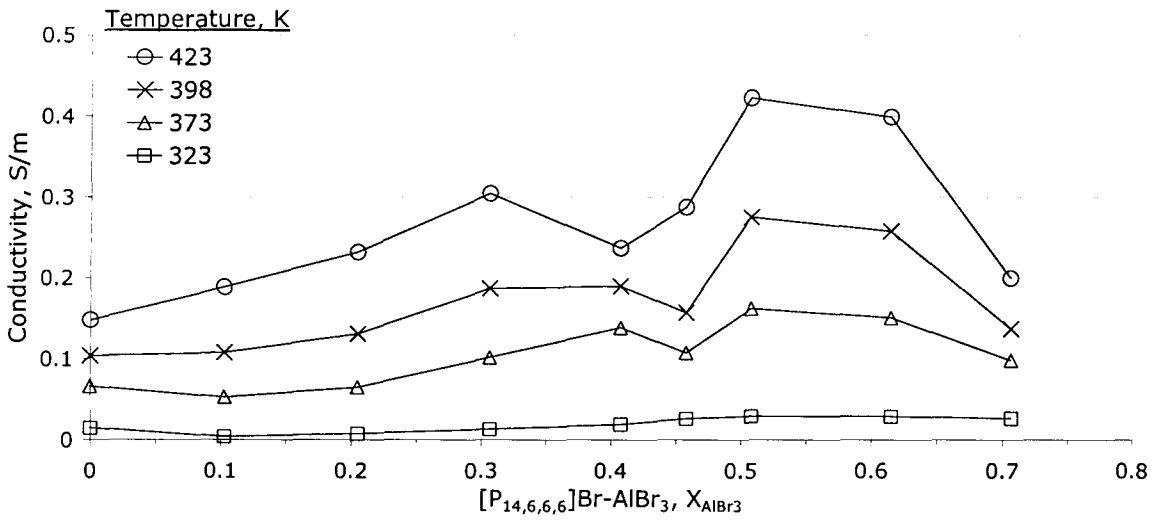

Figure 47 Measured conductivity of the $AlBr_3$-$[P_{14,6,6,6}]Br$ system.

The tributyl system was similar to the trihexyl, in that the conductivity generally increased with increasing additions of $AlCl_3$ (Figure 48). The conductivity seemed to level out a bit at $AlCl_3$ mole fractions from ca. 0.4-0.6. This leveling out of the conductivity in the region of the neutral melt could be due to the buffering effect a hydroxychloride aluminium species (Mantz 1998). A significant increase in the

conductivity at elevated temperatures and $AlCl_3$ concentrations greater than ca. 0.67 mole fraction was also noticed.

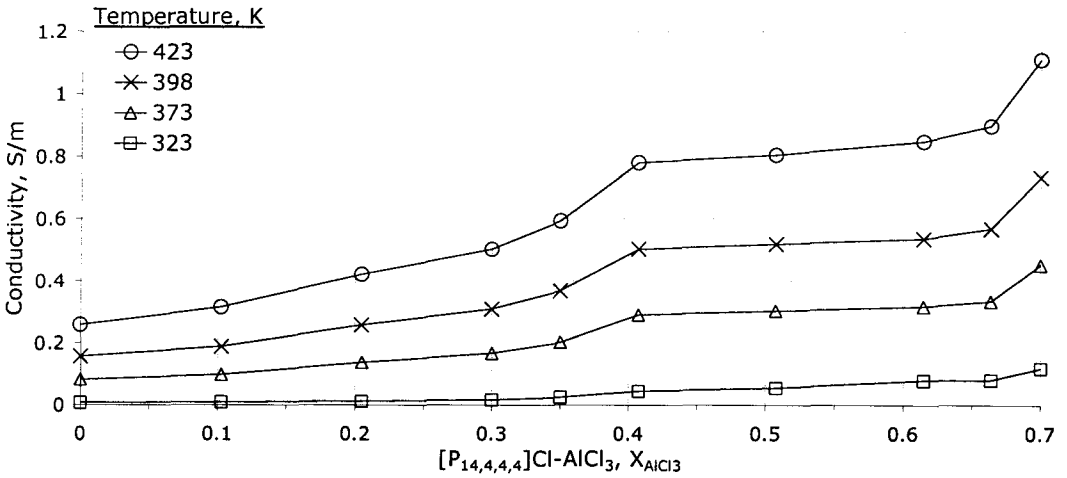

Figure 48 Measured conductivity of the $AlCl_3$-$[P_{14,4,4,4}]$ system.

The same trend of increasing conductivity with addition of $AlCl_3$ was observed when considering the density and molar mass of the solutions (Figure 49). Without the addition of $AlCl_3$, $[P_{14,4,4,4}]Cl$ is solid at room temperature.

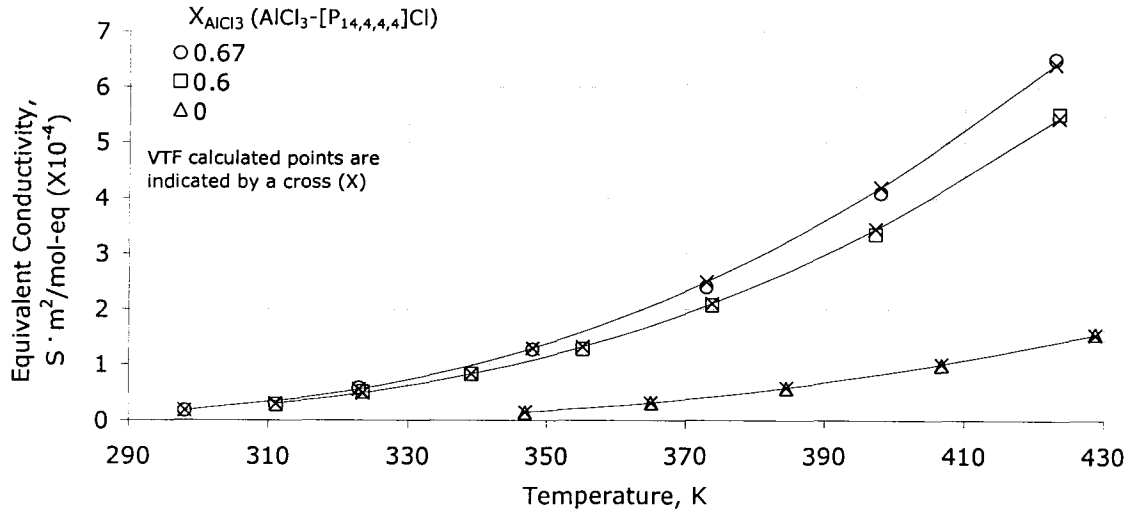

Figure 49 Equivalent conductivity of the $AlCl_3$-$[P_{14,4,4,4}]$ system.

The activation energy of conductivity is lowered considerably by the addition of $AlCl_3$, especially at lower temperatures as seen in Figure 50.

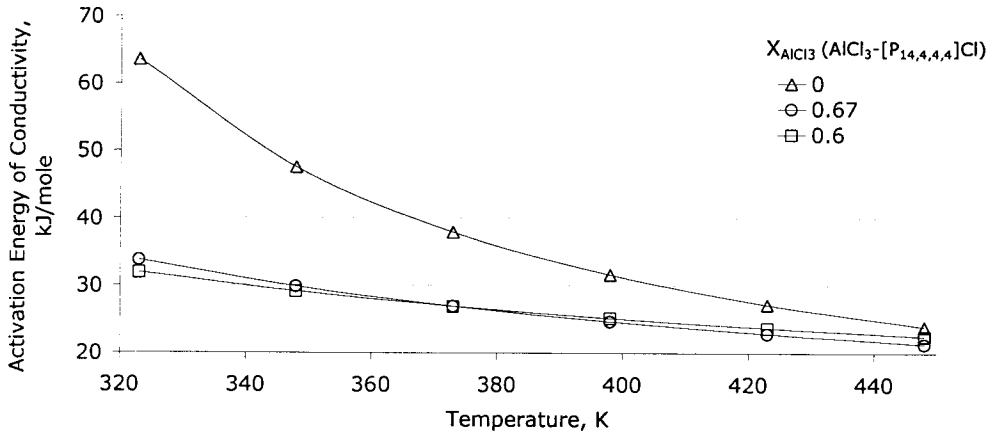

Figure 50 Effect of $AlCl_3$ on the activation energy of conductivity of $AlCl_3$-$[P_{14,4,4,4}]Cl$ ILs.

The $AlCl_3$-$[P_{4,4,4,4}]Cl$ system exhibited the highest conductivity of all the phosphonium ILs tested during this study (Figure 51). Similar to $AlCl_3$-$[P_{14,6,6,6}]Cl$, the conductivity generally increased with increasing $AlCl_3$ concentration. The relatively small tetra-butyl cation of $[P_{4,4,4,4}]Cl$ allows high conductivity throughout most of the concentration range. An exception was the formation of an intermediate phase (possibly a smectic phase where the molecules are ordered in layers) at the neutral melt composition (0.5 mole fraction $AlCl_3$) where a solid was present at temperatures below about 403 K. An increase in conductivity at the nearby compositions of 0.45 and 0.55 mole fraction $AlCl_3$ was observed at elevated temperatures. The melting point of $AlCl_3$-BPC and $AlCl_3$-EMIC are known to reach a maximum value at X_{AlCl3} = 0.5, 280 and 305 K respectively (Takahashi 1999). The conductivity at X_{AlCl3} = 0 (323 and 373 K) was measured using a supercooled liquid.

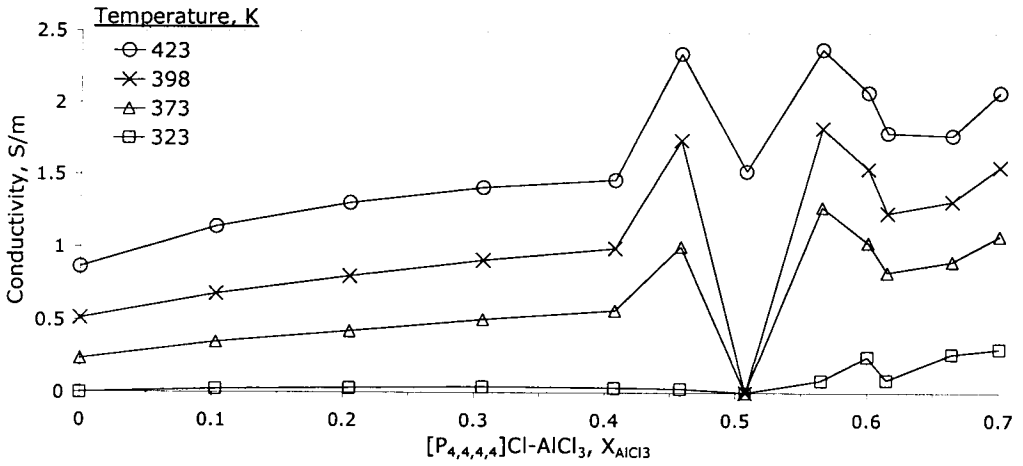

Figure 51 Measured conductivity of the $AlCl_3$-$[P_{4,4,4,4}]Cl$ system.

The VTF parameters used to model the equivalent conductivity of the chloroaluminate IL systems are shown in Table 36. Purifying the IL by exposure to high purity aluminium increased the theoretical glass transition temperature by 106 K. This indicates that the presence of HCl has the ability to lower the solution glass transition temperature.

Table 36 Summary of the VTF parameters used to model the equivalent conductivity $AlCl_3$-tetra-alkyl phosphonium chloride ILs.

Ionic Liquid	A	B	T_0 K	Temperature Range K
$AlCl_3$-$[P_{14,6,6,6}]Cl$ $X_{AlCl3} = 0.5$	0.277	-894.4	188	298-423
$AlCl_3$-$[P_{14,6,6,6}]Cl$ $X_{AlCl3} = 0.6$	0.266	-830.7	189	298-423
$AlCl_3$-$[P_{14,6,6,6}]Cl$ $X_{AlCl3} = 0.67$	2.34	-1679.1	107	298-423
$AlCl_3$-$[P_{14,6,6,6}]Cl$ $X_{AlCl3} = 0.67$ (Purified)	0.136	-570.0	214	294-402
$AlCl_3$-$[P_{14,4,4,4}]Cl$ $X_{AlCl3} = 0.6$	1.91	-1549.6	122	311-424
$AlCl_3$-$[P_{14,4,4,4}]Cl$ $X_{AlCl3} = 0.67$	1.28	-1267.5	146	293-423

In an effort to increase the conductivity of the phosphonium ILs, NaCl was added to the solution to introduce a smaller cation (Na^+) to the system. The solubility of NaCl was found to be low; less than 1 wt.% NaCl dissolved in both acidic and basic chloroaluminate IL mixtures. The low solubility and likely small dissociation of the dissolved NaCl resulted in no significant change in the conductivity of $[P_{14,6,6,6}]Cl$ or $AlCl_3$-$[P_{4,4,4,4}]Cl$ (X_{AlCl3} = 0.6) (Figure 52). The solubility of NaCl in $[BMI]BF_4$ was found to be < 0.28 wt.% at 298 K, the IL contained less than 200 ppm H_2O (Seddon, 2000). In acidic chloroaluminate systems the solubility of alkali halide salt should increase as these salts will react with $Al_2Cl_7^-$ and buffer the melt at the neutral point in terms of Lewis acidity (Koronaios 2001).

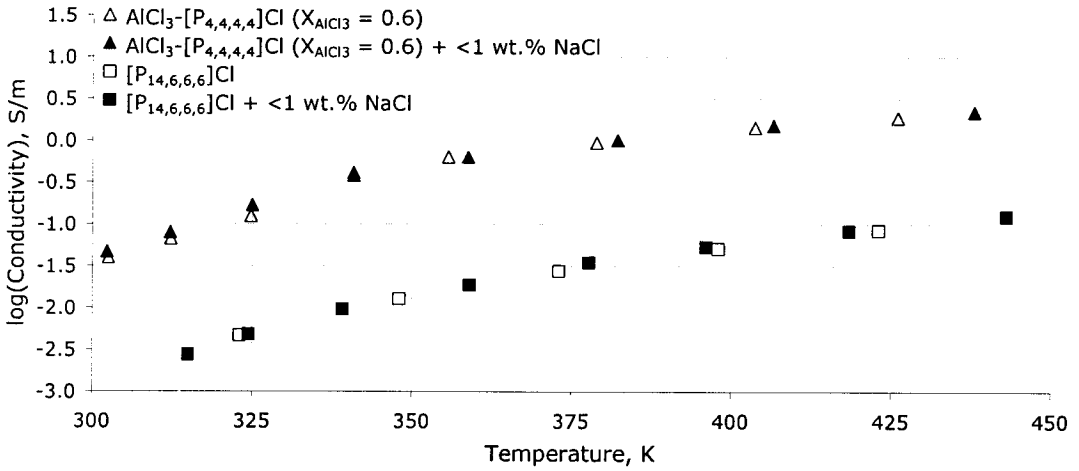

Figure 52 Effect of the addition of 1 wt. % NaCl to acidic and basic chloroaluminate melts. Note: The solubility of NaCl was low in both systems.

The conductivity of the $AlCl_3$-EMIC system was also measured (Figure 53). The magnitude of the conductivity is much higher than with the phosphonium ILs. In this case, the conductivity reaches a maximum at near-neutral compositions. The conductivity of this system has been explained in terms of ion association (Lipsztajn 1985). A similar plot of the $AlCl_3$-MEIC system at 373 K by other researchers revealed similar values however, in the maximum conductivity is clearly obtained at $X_{AlCl3} = 0.5$ (Fannin, 1984). This suggests that more $AlCl_3$ was added than is required to reach the neutral composition, this may be due to the fact that the IL was used as received, some $AlCl_3$ may have reacted with impurities in the IL causing the peak conductivity to be shifted to the right on this plot. The conductivity of $AlCl_3$-imidazolium chloride ILs generally decreased with increasing cation volume, for example, the conductivity decreased as the cation changed from $[MMI]^+ > [MEI]^+ > [MPI]^+ > [MBI]^+ > [BBI]^+$ over a wide range of $AlCl_3$ concentration (Fannin 1984).

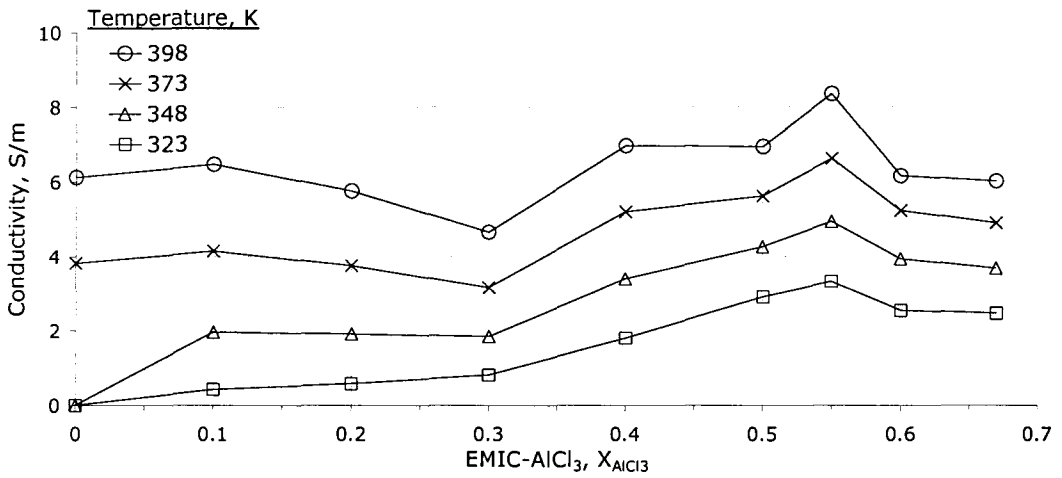

Figure 53 Measured conductivity of the $AlCl_3$-MEIC system.

The effects of anion and cation volume on the conductivity are summarized in Figure 54, Figure 55 and Figure 56. The anions were considered to be solely $Al_2Cl_7^-$ and $AlCl_4^-$ at 0.67 and 0.5 X_{AlCl3} respectively however, in reality there is a range of species present at these concentrations. The ion volumes presented were taken from a consistent set of data or calculated using the generalized linear equation as described by Jenkins (1999). The cation volume of EMI^+ was taken from McEwen (1999). The phosphonium IL conductivity generally increased with increasing anion volume. The only exception was $N(CN)_2^-$ which appears to exhibit an unusually high conductivity given this trend. $N(CN)_2^-$ also behaves unusually in terms of the melting point of MEI^+ ILs with different anions. The larger anions tend to cause a decrease in the melting point with the exception of $N(CN)_2^-$ which exhibits a lower melting point than expected. The melting point of the MEI^+ ILs for different anion types are as follows 360, 364, 252, 279, 333, 280, 270 for Cl^-, Br^-, $N(CN)_2^-$, BF_4^-, PF_6^-, $AlCl_4^-$, $N(SO_2CF_3)_2^-$ respectively (Holbrey 2003). The anion volume of $N(CN)_2^-$ was recently estimated to be 0.086 nm^3 (Ye 2007), which is higher than the 0.063 nm^3 estimate of Jenkins and partially explains the unusual behaviour. $N(CN)_2^-$ is a V-shaped anion, thus its representation as a spherical anion in the anion volume calculations may account for some of the discrepancy, however, a full explanation cannot be offered based on the experiments that were conducted during this research. PF_6^- also has a higher melting point than would be expected based on the anion volume.

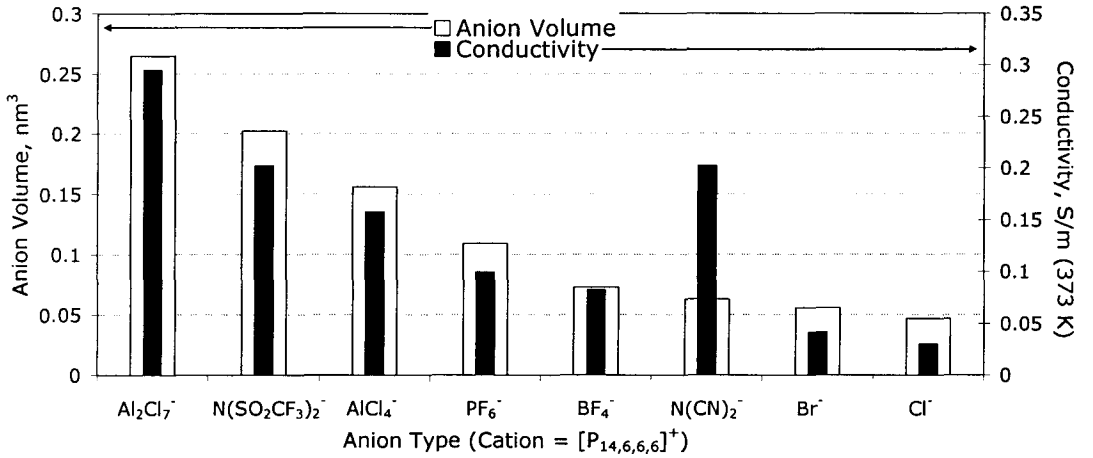

Figure 54 The relationship between anion volume and the measured conductivity of $[P_{14,6,6,6}]^+$ ILs.

The anomaly of the high conductivity of the $N(CN)_2^-$ anion appears even more striking when considering the equivalent conductivity of the solution (Figure 55).

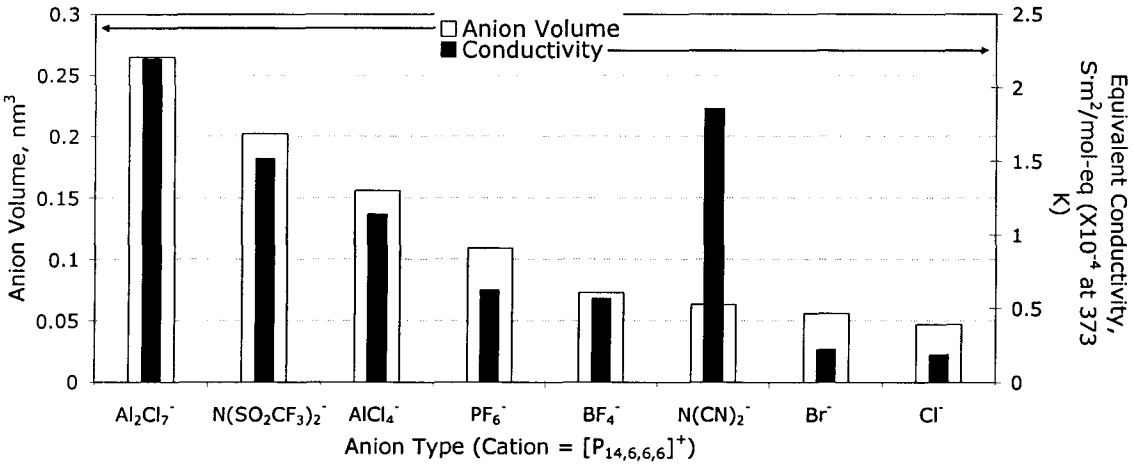

Figure 55 The relationship between anion volume and the equivalent conductivity of $[P_{14,6,6,6}]^+$ ILs.

The IL conductivity is strongly influenced by the size of the cation as seen in Figure 56. The smaller cation is more mobile as the frictional forces are decreased.

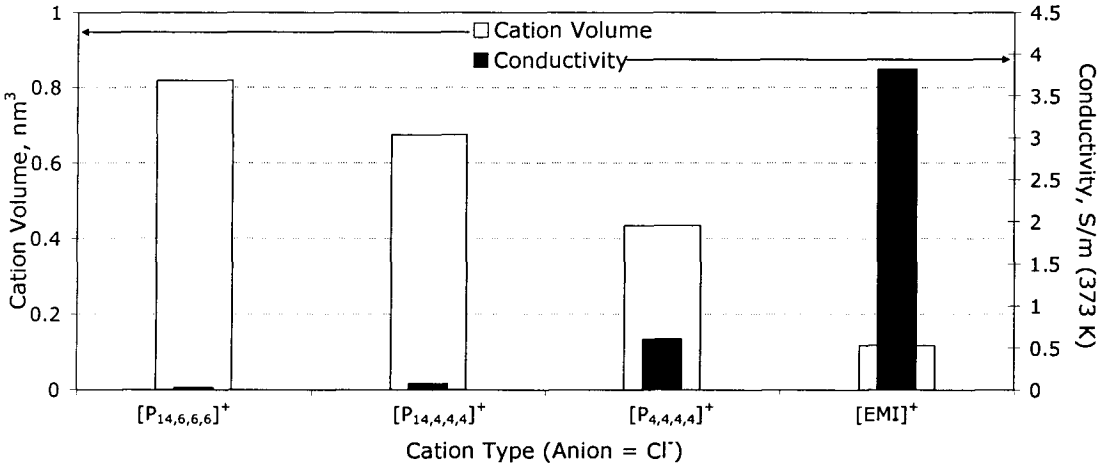

Figure 56 The relationship between cation volume and the measured conductivity of phosphonium chloride ILs.

The effect of the increased mobility on the measured conductivity is slightly exaggerated as another effect is the increased number of charge carriers when the cation is smaller (and the IL is denser), this effect is eliminated by considering the equivalent conductivity (Figure 57).

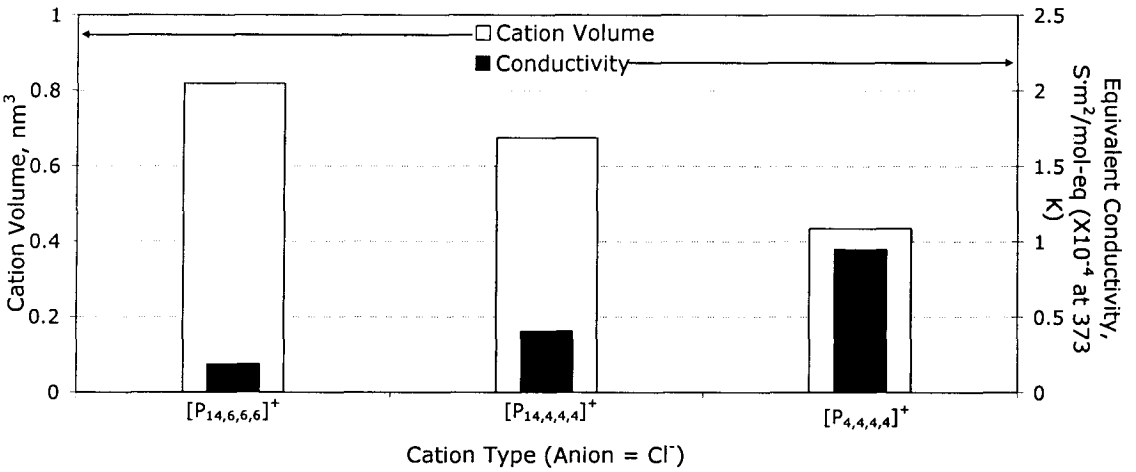

Figure 57 The relationship between cation volume and the equivalent conductivity of phosphonium chloride ILs.

Table 37 summarizes the conductivities of some chloroaluminate IL systems at room temperature. The tetra-alkyl phosphonium ILs tested were found to be at the low end of the conductivity spectrum due to their relatively large cations. It is interesting to see that the conductivity of the tri-methyl-phenyl ammonium chloride (TMPAC) is on the same order as the pyridinium and imidazolium ILs. TMPAC is the ammonium

equivalent of the phosphonium ILs with one alkyl chain substituted by a phenyl ring, its electrochemical stability was found to be the same as MEIC (Jones, 1989).

Table 37 The conductivity and density of halo-aluminate ILs at 298 K.

IL System	κ S/m	Λ $S \cdot m^2/mol\text{-}eq$ ($X10^{-4}$)	ρ kg/L	Reference
$AlCl_3$-MPC ($X_{AlCl3} = 0.67$)	0.81	2.2	1.441	Mantz, 2003
$AlCl_3$-EPC ($X_{AlCl3} = 0.67$)	1.0	2.9	1.408	Mantz, 2003
$AlCl_3$-PPC ($X_{AlCl3} = 0.67$)	0.8	2.5	1.375	Mantz, 2003
$AlCl_3$-BPC ($X_{AlCl3} = 0.67$)	0.67	2.2	1.346	Mantz, 2003
$AlCl_3$-MMIC ($X_{AlCl3} = 0.66$)	1.5	4.3	1.404	Wilkes, 1982
$AlCl_3$-EMIC ($X_{AlCl3} = 0.66$)	1.5	4.5	1.389	Wilkes, 1982
$AlCl_3$-EMIC ($X_{AlCl3} = 0.66$)	1.4	-	-	this work
$AlCl_3$-BMIC ($X_{AlCl3} = 0.66$)	0.92	3.0	1.334	Wilkes, 1982
$AlCl_3$-BBIC ($X_{AlCl3} = 0.66$)	0.6	2.3	1.252	Wilkes, 1982
$AlCl_3$-TMPAC ($X_{AlCl3} = 0.67$)	0.34	-	-	Jones, 1989
$AlCl_3$-BTMAC ($X_{AlCl3} = 0.67$)	0.19 (308 K)	-	-	Abbott, 2001
$AlCl_3$-$[P_{14,6,6,6}]Cl$ ($X_{AlCl3} = 0.67$)	0.028	0.206	1.037	this work
$AlCl_3$-$[P_{14,4,4,4}]Cl$ ($X_{AlCl3} = 0.67$)	0.027	0.177	1.072	this work
$AlCl_3$-$[P_{4,4,4,4}]Cl$ ($X_{AlCl3} = 0.67$)	0.051	0.24	1.18	this work
50.0-50.0 mol% EMIC / $AlCl_3$	2.3	5.0	1.294	Wilkes, 1982
50.0-50.0 mol% BMIC / $AlCl_3$	1.0	2.5	1.238	Wilkes, 1982
$AlCl_3$-BBIC ($X_{AlCl3} = 0.5$)	0.5	1.5	1.164	Wilkes, 1982
$AlCl_3$-$[P_{14,6,6,6}]Cl$ ($X_{AlCl3} = 0.5$)	0.007	0.047	0.974	this work
$AlCl_3$-$[P_{14,4,4,4}]Cl$ ($X_{AlCl3} = 0.5$)	0.007	0.04	1.00	this work

The conductivity of organic aluminium electroplating solutions are on the same order as that of ILs at room temperature (Table 38). These solutions are limited to operation at lower temperature due to their low vapour pressure and flammability. The phosphonium ILs require heating to temperatures above 373 K to exhibit similar conductivities as these room temperature organic electroplating solutions.

Table 38 Conductivity of Al electroplating solutions near room temperature (Liao 1997).

Electrolyte	Temp. K	κ S/m
1.31 M Al_2Br_6 + 1.05 M KBr in toluene	299	0.63
1.25 M Al_2Br_6 + 1.00 M LiBr in toluene	299	0.45
0.7 M $AlCl_3$ + 0.7 M $LiAlH_4$ in 58% THF-42% benzene (v/v)	293	0.40
0.06 M $LiAlH_4$ + 1.03 M $AlCl_3$ + 0.42 M $LiAlCl_4$ in THF	298	0.95
0.26 M $LiAlH_4$ + 1.24 M $AlCl_3$ + 0.07 M $LiAlCl_4$ in THF	298	0.71

The solution conductivity is a critical operating parameter for industrial electrowinning and refining processes as the potential loss (U_E in Volts) due to the

solution resistance are proportional to the anode-cathode spacing (d in m), the current density (j in A/m^2) and inversely proportional to the conductivity (κ in S/m), Equation 39.

$$U_E = (1/\kappa)\cdot d\cdot j \qquad [39]$$

As the cost of energy increases it is expected that many of the hydrometallurgical refining and winning operations will increase the electrolyte conductivity by increasing temperature and chloride concentration to minimize the potential losses due to solution resistance (Ettel, 1977). Similarly, the trend in the industry has been to minimize the electrode gap for the same reason; a small spacing is limited by irregular plating and the risk of short circuiting. Typical hydrometallurgical electrowinning and refining solutions are much more conductive than the organic Al plating solutions as seen in Table 39 (compared to Table 38). Also, the high temperature molten salt for Al electrowinning is considerably more conductive than the hydrometallurgical solutions.

Table 39 Conductivity of industrial electrowinning and refining solutions (Ettel, 1977).

Electrolyte	T. K	κ S/m
Nickel EW (catholyte)	333	12
Nickel ER	333	20
Zinc EW	313	50
Copper ER	333	65
Al EW	1273	250

Conductivity of other metal salts

The conductivity of various metal salts were tested in $[P_{14,6,6,6}]Cl$ (Figure 58). The conductivity of the solution is increased upon addition of $AlCl_3$ and $FeCl_3$, and $TiCl_4$ while the addition of $MgCl_2$ lowered the conductivity slightly. Both $AlCl_3$ and $FeCl_3$ likely react with Cl^- to form charged tetrahedral complexes ($AlCl_4^-$ and $FeCl_4^-$). It has been speculated that anhydrous $TiCl_4$ will react with Cl^- to form $TiCl_6^{2-}$ and $TiCl_5^-$ at higher concentrations when added to EMIC (Scheffler 1990). The dissolution reaction of $TiCl_4$ in $[P_{14,6,6,6}]Cl$ was slightly exothermic. The $AlCl_3$ mixture was a dark red colour while the $FeCl_3$ solution was black. $TiCl_4$ dissolved completely; the resulting colour was pale yellow. $MgCl_2$ was only slightly soluble despite heating to 373 K and stirring overnight.

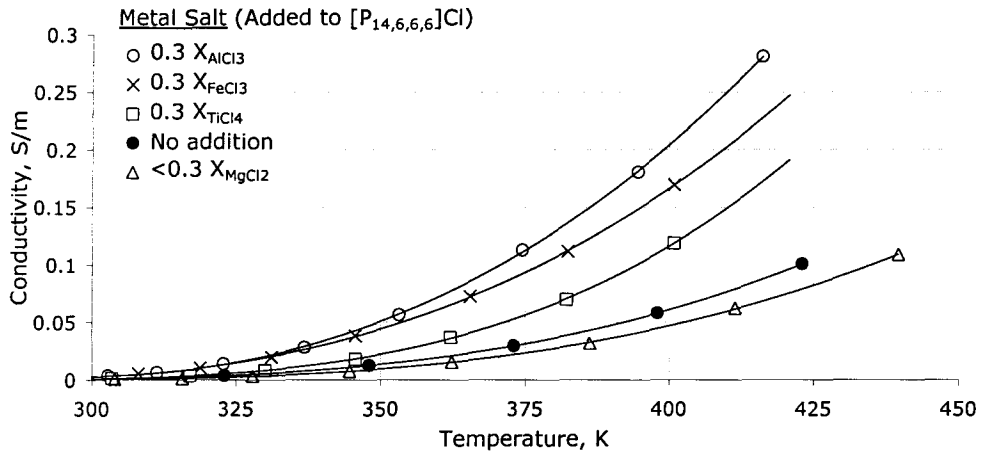

Figure 58 Measured conductivity of metal salt-$[P_{14,6,6,6}]Cl$. Note: $MgCl_2$ was only slightly soluble.

The addition of $FeCl_3$ increased the conductivity of $[P_{14,6,6,6}]Cl$ at the two concentrations tested (Figure 59).

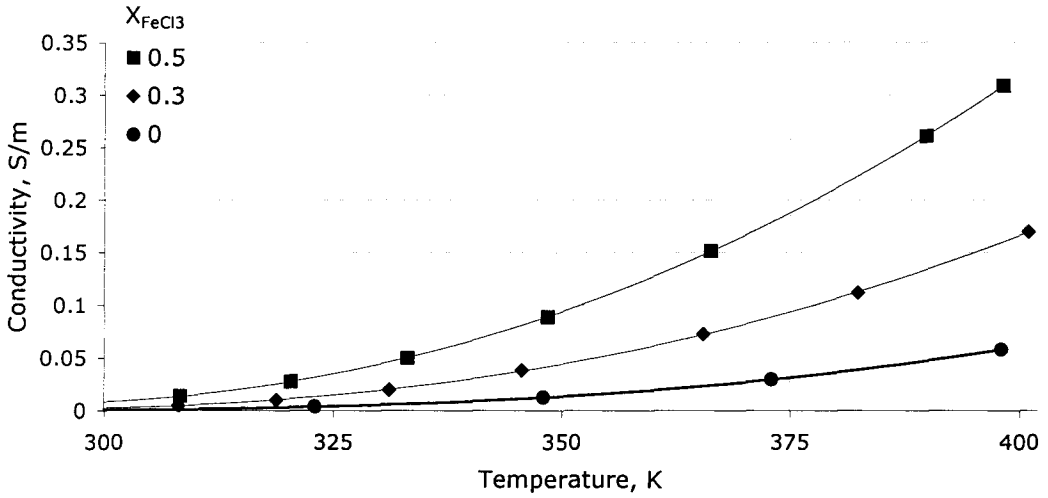

Figure 59 Measured conductivity of the $FeCl_3$-$[P_{14,6,6,6}]Cl$ system.

The conductivity of $TiCl_4$-$[P_{14,6,6,6}]Cl$ also increased with increasing concentration of $TiCl_4$, however at higher concentration (X_{TiCl4} = 0.42) and higher temperatures, the conductivity appears to be approaching that of (X_{TiCl4} = 0.3). This is an indication that some $TiCl_4$ is being removed from the solution as a gas. A small amount of bubbling was observed at temperatures above about 373 K in the 0.42 mole fraction solution only.

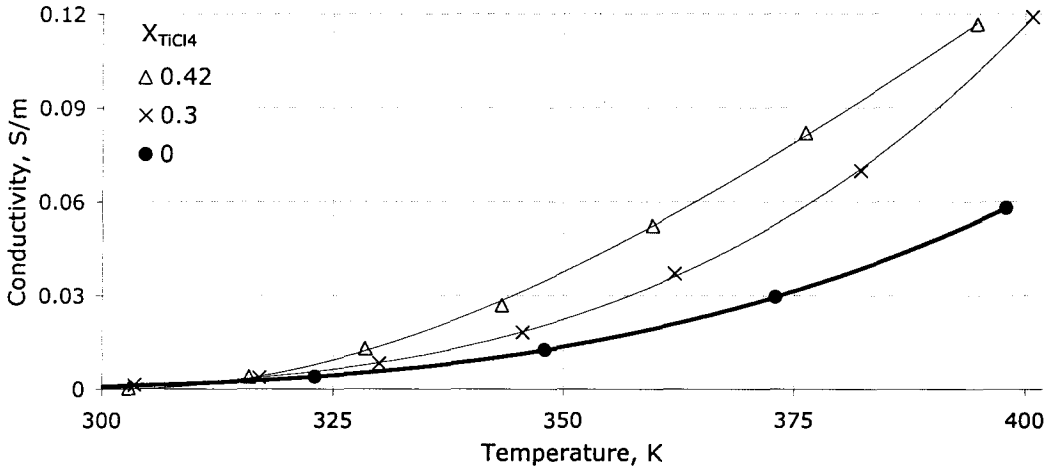

Figure 60 Measured conductivity of the $TiCl_4$-$[P_{14,6,6,6}]Cl$ system.

There are many possible combinations of metal salts and ILs, although they were not all thoroughly investigated during this work some scoping experiments were carried out to obtain an idea of the solubility and changes in conductivity of the ILs when mixed with metal salts. Table 40 summarizes some IL-metal salt systems in terms of the solution colour (when noted), change in conductivity and solubility limit if undissolved salts were noticed. The changes in the measured conductivity (κ) were indicated by the following symbols: = (no significant change), ↑ (increase) or ↓ (decrease).

Table 40 Solubility of metal salts $[P_{14,6,6,6}]^+$ ILs, colour indicated when noted.

Ionic Liquid	$AlCl_3$	$MgCl_2$	$FeCl_3$	$TiCl_4$	$AlBr_3$
$[P_{14,6,6,6}]Cl$ Clear	<0.7 X_{AlCl3} κ ↑ Dark Red	<0.3 X_{MgCl2} κ ↓ White	<0.7 X_{FeCl3} κ ↑ Black	0.42 X_{TiCl4} κ ↑ Yellow	-
$[P_{14,6,6,6}]Br$ Clear	-	-	-	-	< 0.7 X_{AlBr3} κ ↑
$[P_{14,6,6,6}]PF_6$ Clear	κ ↓	κ =	κ = Black	-	-
$[P_{14,6,6,6}]BF_4$ Clear	<0.3 X_{AlCl3} κ ↑ (slightly)	0.3 κ = Blue	0.3 κ ↑ (slightly) Black	-	-
$[P_{14,6,6,6}]N(CN)_2$ Light Orange	κ ↓ Yellow	<0.3 X_{MgCl2} κ = White	0.3 X_{FeCl3} κ = Black	-	-
$[P_{14,6,6,6}]N(SO_2CF_3)_2$ Clear	0.3 X_{AlCl3} κ =	Low Solubility κ = Clear	0.3 X_{FeCl3} κ = Black	-	-

2.5 Summary

Linear density-temperature functions were established for nine tetra-alkyl phosphonium ILs and six $AlCl_3$-IL mixtures. The kinematic viscosity of the ILs was measured and the dynamic viscosity calculated using the density functions was presented. Similarly, the conductivity of the nine tetra-alkyl phosphonium ILs and a number of different metals salt-IL mixtures were measured. The measured and molar equivalent conductivities were presented (for the mixtures where the density was known). The dynamic viscosity and the molar equivalent conductivity as a function of temperature were modeled using the VTF equation.

The ILs tested consisted of a bulky tetra-alkyl phosphonium cation and a relatively small anion. A smaller cation resulted in increased conductivity due to a lessening of the frictional forces limiting mobility. On the other hand, ILs with larger anions tended to exhibit an increase in the conductivity; this is attributed to a lessening on the cation-anion interactions. The $[P_{14,6,6,6}]N(CN)_2$ IL exhibited an unusually high conductivity, the reason for this was not determined, however, it is speculated that the V-shape of the anion may be a factor. Another possibility is that since $N(CN)_2^-$ exhibits a resonance structure, this could lead to a de-localized charge lessening the anion-cation interaction. Asymmetry in the cation resulted in a slight decrease in viscosity and an increase in conductivity at elevated temperatures as $[P_{14,6,6,6}]^+$ was compared with $[P_{8,8,8,8}]^+$ using a bromide anion.

As for the halo-aluminate IL systems, an increase in $AlCl_3$ generally increased the solution conductivity due to the formation of larger anions ($AlCl_4^-$ and $Al_2Cl_7^-$) that reduced cation-anion interaction. This is different from $AlCl_3$-imdazolium IL systems as imidazolium ILs exhibit a conductivity maximum near $X_{AlCl3} = 0.5$. The $AlBr_3$-$[P_{14,6,6,6}]Br$ system appeared to form liquid crystal phases at higher temperatures and concentrations of 0.3-0.5 and >0.6 X_{AlBr3} due to the presence of water. A drying procedure may help prevent this since it was determined (after the fact) that the $[P_{14,6,6,6}]Br$ tested contained a significant amount of water. An intermediate solid phase with a relatively high melting point (>398 K) was identified in the $[P_{4,4,4,4}]Cl$-$AlCl_3$ system near 0.5 X_{AlCl3}. $AlCl_3$-$[P_{4,4,4,4}]Cl$ was the most conductive phosphonium system

tested, the high melting point phase restricts the operating temperature of an electrodeposition process to high values since cathodic polarization will result in a local solution concentration close to X_{AlCl3}=0.5.

The phosphonium ILs tested exhibit low conductivity compared with other types of ILs. The conductivity of ILs are comparable to organic aluminium electroplating baths despite having the advantage of a much greater operating temperature range. The conductivity of ILs are lower than hydrometallurgical electrowinning and electrorefining solutions and much lower than high temperature molten salt baths such as molten cryolite at 1273 K.

Other metal salts such as $FeCl_3$ and $TiCl_4$ were found to be soluble in $[P_{14,6,6,6}]Cl$ and result in an increase in the solution conductivity. It is speculated that species such as $FeCl_4^-$, $TiCl_6^{-2}$ and $TiCl_5^-$ are formed. The solubility of $MgCl_2$ in the chloride ILs was low, however, $MgCl_2$ appeared to be at least moderately soluble in $[P_{14,6,6,6}]BF_4$ and $[P_{14,6,6,6}]PF_6$, the dissolution of $MgCl_2$ did not increase the solution conductivity.

The theoretical glass transition temperatures of the ILs were estimated by fitting the Vogel-Tamman-Fulcher equation to the measured dynamic viscosity and equivalent conductivity. T_0 calculated from the viscosity data is lower than the T_0 from the conductivity measurements (Table 41). The average of the two T_0 values was found to be between 50 and 180 K lower than the melting point of the ILs. The accuracy of the T_0 values obtained from fitting the data is not very high based on the large discrepancy between those calculated from the viscosity and conductivity data.

Table 41 Summary of calculated glass transition temperatures (T_0).

Ionic Liquid	T_0 (From η) K	T_0 (From Λ) K	T_0 Average K	T_{mp} K (Table 26)
$[P_{4,4,4,4}]Cl$	189	199	194	353
$[P_{14,4,4,4}]Cl$	148	219	184	318
$[P_{14,6,6,6}]Cl$	146	196	171	223
$[P_{14,6,6,6}]Br$	113	196	155	273
$[P_{8,8,8,8}]Br$	90	174	132	318
$[P_{14,6,6,6}]PF_6$	111	190	151	323
$[P_{14,6,6,6}]BF_4$	150	190	170	310
$[P_{14,6,6,6}]N(CN)_2$	130	200	165	<293
$[P_{14,6,6,6}]N(SO_2CF_3)_2$	133	187	160	<293

Calculated "theoretical" glass transition temperatures (T_0) were compared with experimental values for the $AlCl_3$-MEIC system (Fannin 1984). The experimentally determined glass transition values (T_g) were on the order of 10-70 K higher than the calculated values. The glass transition temperatures were distinguished from the freezing of the IL by an increase in viscosity followed by a sudden fracturing of the melt near the T_g. The glass transition was only observed in their experiments at X_{AlCl3} in the range of 0.3-0.42 and 0.6-0.7 (Fannin 1984). The same researchers also calculated the activation energies of conductivity over a range of temperatures (298-373 K) and imidazolium chloride cation types (MMI^+, MEI^+, MPI^+, MBI^+, BBI^+). They observed that $E_{a,\Lambda}$, decreased with increased temperature and attributed this to a decrease in ion association. They also found that the activation energy increased with increasing cation size with the exception of the smallest cation that seemed to be anomalously high, the reason for this was not explained. When comparing the three different sized phosphonium chloride cation it was observed that the larger cation generally has smaller activation energy of conductivity except at temperatures above ~398 K where the $E_{a,\Lambda}$ of $[P_{14,4,4,4}]Cl$ becomes lower than $[P_{14,6,6,6}]Cl$. This can be explained by considering the cation volume. In the case of the imidazolium chloride ILs the conductivity is limited by the cation-anion interactions, as both the cation and anion are relatively small, the increased temperature will lessen this effect most when there are stronger cation-anion interactions (the smaller cation). In the phosphonium chloride systems, while ion interactions are still present, the limiting factor to increased conductivity are the frictional forces associated with the bulky cation, so an increase in temperature of these ILs resulted in a larger increase in conductivity in the IL with the bulkier cation ($[P_{14,6,6,6}]^+$). The activation energy of conductivity decreased with increasing temperatures for all of the ILs, this is consistent with results from the $AlBr_3$-MEIB system (Sanders 1986). The magnitude of the activation energy of viscosity and conductivity of the phosphonium ionic liquids are higher than for high temperature molten salts (>20 KJ/mole compared with < 20 KJ/mole respectively) (High temperature molten salt values from Abbott 2004).

Cohen and Turnbull provided a mathematical treatment of molten salts that were supercooled suggesting that the volume of free space (or holes) increases linearly with temperature, at the glass transition temperature the free volume 0 (Bockris 1998 *Cited:*

Cohen 1959). The idea of free volume approaching 0 at T_0 seems to be reasonable for phosphonium ILs tested. The density of the ILs at T_0 is within 8 % of the theoretically calculated densities. Abbott (2004) showed that the activation energy of viscosity is related to the size of ions and size of voids present in ionic liquids which lends credence to the hole theory.

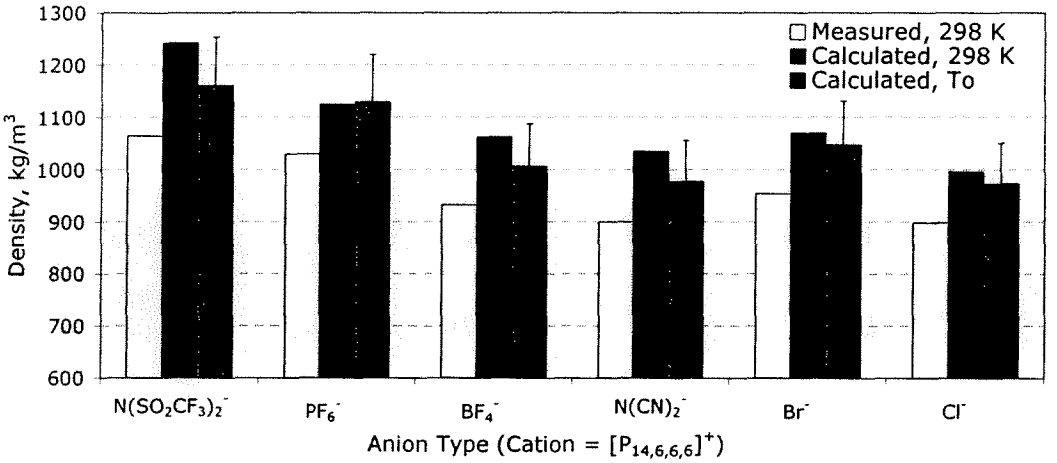

Figure 61 Comparison of the densities of $[P_{14,6,6,6}]^+$ ILs with different anions. The measured density is at 298 K, the calculated density is based on the anion and cation volume calculations of Jenkins (1999) and the density at T_0 was estimated using extrapolating the density functions back to T_0. The average T_0 values from Table 41 were used.

The ratio of the activation energy of viscosity to conductivity is compared for the ILs tested over a range of temperatures in Figure 62. The values are lower at lower temperatures and increase with temperature indicating that the conductivity increases faster than the relative decrease in temperature. The ratio is the highest with the asymmetric cation types at low temperatures, the ratio for $[P_{4,4,4,4}]Cl$ remains relatively constant over the range of temperatures. The higher values at higher temperatures for most of the ILs may be indicative of some alternate mechanism of conductivity such as a cluster hopping mechanism that only takes place under an electric field and thus does not affect the viscosity.

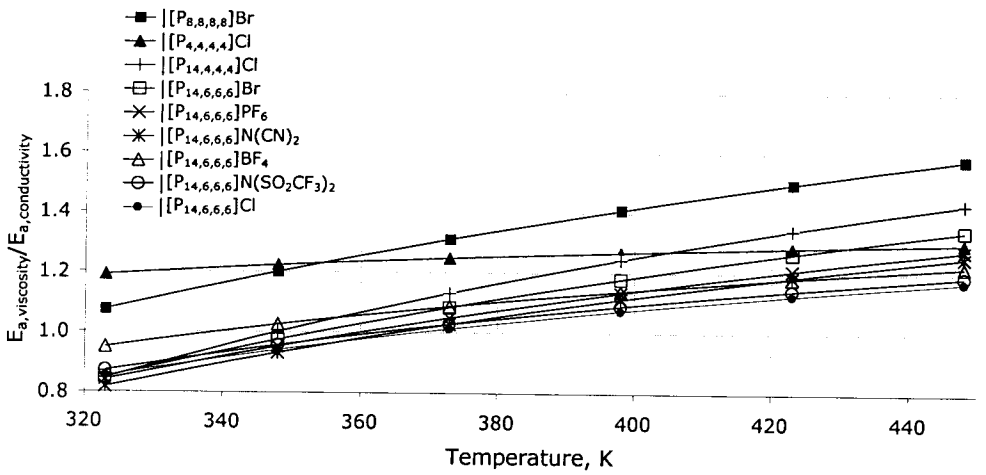

Figure 62 The ratio of activation energy of viscosity to conductivity ($E_{a,\eta}/E_{a,\Lambda}$).

Chapter 3 Electrochemistry

Electrochemical experiments were performed to study the features of the $[P_{14,6,6,6}]Cl$ IL and the $AlCl_3$-$[P_{14,6,6,6}]Cl$ system. The chloride system was selected for test-work because aluminium has been deposited from chloroaluminate-IL systems in the past and the chemistry is established. The $[P_{14,6,6,6}]Cl$ IL was specifically chosen since it is a liquid at room temperature making it easier to handle, it is also the IL that Cytec produces at the tonne scale for other purposes and they were able to supply a large amount. If a higher conductivity solution is required, $[P_{14,4,4,4}]Cl$ should be used. The $AlCl_3$-$[P_{4,4,4,4}]Cl$ is more difficult to work with because of the high temperature melting phase that forms at $X_{AlCl3} = 0.5$. Cyclic voltammetry was used to determine the electrochemical window of the ILs and to calculated the diffusion of $Al_2Cl_7^-$ in the $X_{AlCl3} = 0.67$ solution. Cathodic and anodic polarization was employed to study the reaction kinetics over a wide range of overpotentials and temperatures. This chapter is concluded with a discussion of the double layer at the cathode.

3.1 Experimental Aspects

All of the samples were prepared in a Vacuum Atmosphere Co. Glove box (HE Series) under a dry nitrogen atmosphere (< 10 ppm O_2, H_2O). The anhydrous $AlCl_3$ used was 99.99% pure.

The reference electrode (RE) used was an aluminium wire (99.999% pure) immersed directly in the solution positioned 1 mm from the working electrode (WE). Attempts were made to isolate the reference electrode in a separate compartment with a glass frit junction, however, the high viscosity of the IL and small pores of the glass frit did not allow for sufficient contact between the bulk solution and the reference solution. It is possible to devise a separated reference electrode system, with a more porous separator and a less viscous (and more conductive) reference solution such as $AlCl_3$-EMIC ($X_{AlCl3} = 0.6$) where the experimental solution will be in contact with the reference solution. For these experiments, a separated reference system was not deemed essential as no reactions were taking place that were altering the surface of the Al RE, the Al wire was not contaminating the experimental solution since the concentration of Al was

already very high and the concentration of species in the bulk solution was not changed significantly during the course of any of the electrochemical experiments so the reference potential was stable. As for the working and counter electrodes, they were made from 99.99% pure Al, 99.99% pure Pt or 99.9% pure Cu.

The electrochemical experiments were conducted in a 50 mL test tube; the setup is shown in Figure 63. Prior to using the aluminium wire as a reference electrode the wire was cyclically polarized quickly (0.2 V/s) through a potential range of about 2 V to remove any oxide from the aluminium surface, the reference electrode surface was deemed to be ready for use when subsequent cyclic voltammograms were superimposed. Usually about 6 cycles was sufficient to ensure stable potential measurement. The open circuit potential of a copper wire is roughly 0.6 V vs. the Al wire in the acidic chloro-aluminate / phosphonium IL systems at 373 K. The thermocouple used was a Traceable® Extra-Long-Stem-Thermometer which was calibrated to within +/- 1 degree at 297 K. The thermocouple was compared with an alcohol based thermometer and appeared to be within 2 degrees of each other for temperatures up to 400 K. The thermocouple was isolated from the IL by a glass sheath filled with silicone heating oil.

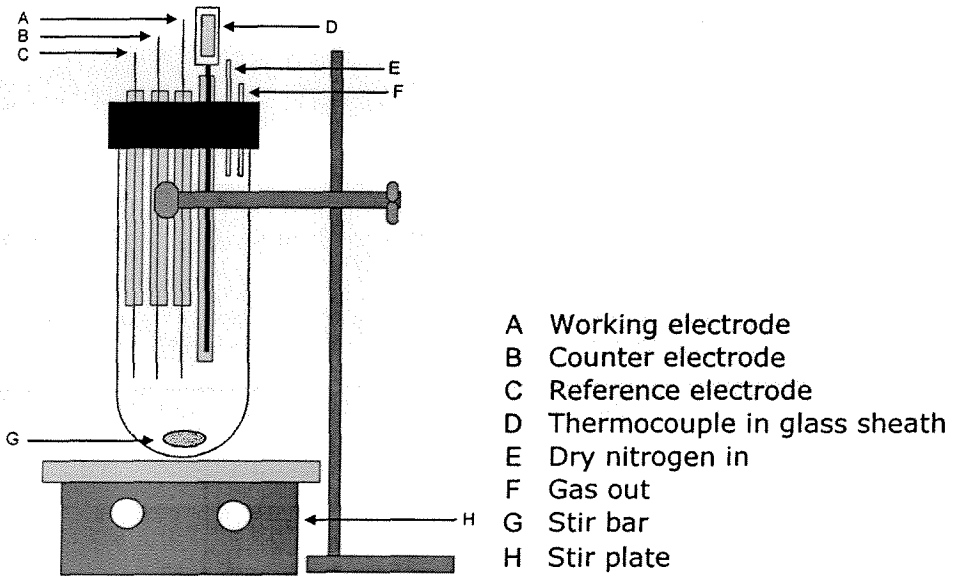

Figure 63 Electrochemical experiment setup.

During the potential controlled experiments, the ohmic drop was compensated for by current interrupt feedback, this is a software feature that makes very short current interruptions and estimates the resistance due to the electrolyte based on the immediate

drop in potential. Heating was provided by an oil bath or an external heating band. The electrochemical experiments were performed either under a continuous dry nitrogen purge or inside the glove box (N_2 environment). The solution was stirred for the cyclic voltammograms to determine the electrochemical window but was unstirred for the determination of the diffusion of $Al_2Cl_7^-$ and for the anodic and cathodic polarization experiments.

3.2 Cyclic Voltammograms

Cyclic voltammograms (CV) were performed to investigate the electrochemical features in the $AlCl_3$-$[P_{14,6,6,6}]$ system over a wide concentration range (X_{AlCl3} = 0, 0.3, 0.5, 0.6 and 0.67) at a temperature of 373 K (Figure 64). The electrodes used were a Pt wire WE and Pt Foil CE and Al wire RE. The Pt WE was used in the case of the determination of the electrochemical window as it is noble metal. Pt also exhibits superior corrosion resistance and it is catalytic to many reactions, minimizing the reaction overpotentials. The Al wire RE was employed since it provided a stable potential being pinned at its corrosion potential and since the Al system was being investigated so there was no risk of contaminating the solution with a different metal. It should be noted that the reference potential shifts slightly with the addition of $AlCl_3$, it seems to be a cathodic shift relative to the current associated with hydrogen evolution. The scan rate was 5 mV/s and it began at the open circuit potential (OCP) (about 0.6-0.9 V vs. Al wire), the OCP seemed to be higher when the $AlCl_3$ concentration was lower. The scan proceeded anodically (positive) to 2 V vs. Al wire and was then reversed until it reached -2.5 V and reversed again to return to the OCP or to 2 V in the case of the acidic solutions (X_{AlCl3} = 0.6 and 0.67). The five scans are presented at the same scale in Figure 64. The explanation of the features of the scans relies on information that is available in the literature as well as insight gained during the electrodeposition experiment in the later chapters of this thesis. The scans have been complicated to some extent by the presence of impurities in the IL. Some of the descriptions of the CV features are speculative and are not backed up with proof (such as analysis of the electrodes post-experiment or analysis of the off-gas etc.).

The first scan at the top of Figure 64 represents the neat IL $[P_{14,6,6,6}]Cl$ (X_{AlCl3} = 0). The first increase in current noticed was the anodic (positive) current at 1.7 V; this is attributed to the evolution of chlorine gas. The next current is cathodic current that begins at 0.35 V, this is due to the evolution of hydrogen from the presence of HCl and tri-alkyl phosphonium salt. The magnitude of the hydrogen evolution current appeared to reach a steady state at about 7 A/m^2. This current is expected to be lower on substrates other than platinum, for example in a separate experiment, the steady state current density of a copper substrate polarized at -1 V vs. Al/Al(III) at the same temperature was found to be 2.2 A/m^2. The HCl concentration in the neat IL is approximately 0.1-0.5 wt. % (Cytec Inc. 2006). The cathodic current beginning at about -1.9 V is due to the reduction of the cation. Not counting the current due to the impurities, the electrochemical window of the neat IL, $[P_{14,6,6,6}]Cl$ (X_{AlCl3} = 0) is 3.6 V, this is considerably higher than basic EMIC which was found to be on the order of 2.6-2.8 V (Table 42) indicating that $[P_{14,6,6,6}]^+$ is about 0.8-1 V more electrochemically stable than EMI^+. The reduction of the cation likely involves electron transfer to an alkyl radical, Equation 40 (Hudson, 1968).

$$R'R_3P^+ + \bar{e} \rightarrow PR_3 + \cdot R' \qquad [40]$$

Similarly, the electrochemical reduction of BP^+ was explained by the formation of a pyridinyl radical species that rapidly dimerized (Lai 1987, *Cited*: Gale, 1980).

The second cyclic scan performed at X_{AlCl3} = 0.3 is similar to X_{AlCl3} = 0, the current due to the initial cathodic scan is higher than the reverse cyclic scan resulting in a hysterysis. The reason for the higher cathodic current upon the addition of $AlCl_3$ in these experiments is because excess HCl is generated due to a reaction of $AlCl_3$ with the water impurities (0.15 wt.%). The Pt surface may be a preferential site for this HCl production reaction leading to a locally higher concentration. This would explain the hysterysis as the local excess of HCl would be consumed on the forward cathodic scan.

The scan at X_{AlCl3} = 0.5 is similar to the scan at 0.3 and the hysterysis is growing with increased addition of $AlCl_3$. There is even a small hysterysis appearing at the anodic end of the scan, this hysterysis is also likely due to the higher concentration HCl. $AlCl_4^-$ is known to be more electrochemically stable than Cl^- thus the oxidation of $Cl_2(g)$ should be occurring at a higher potential at this concentration of $AlCl_3$.

The acidic melt (X_{AlCl3} = 0.6) includes some new features. During the initial forward scan, there is a small peak at about 1.5 V, this is most likely due to the dissolution of Al from an Al-Pt surface alloy that was formed during the prior experiment that was conducted in an acidic chloroaluminate system. The electrode cleaning procedure included a polarization to (+1 V) remove Al from the Pt but this potential was not high enough to dissolve these types of surface alloys. The charge contained in this feature was determined to be about $2.4 \cdot 10^{-4}$ C (the feature is also seen in the scan at X_{AlCl3} = 0.67), while the charge associated with the dissolution of one monolayer of Al should be about $4.3 \cdot 10^{-4}$ C, this relatively close agreement between the two values supports the idea of an Al-Pt surface alloy dissolving. Under potential deposition (UPD) of Al on Au was identified using Scanning Tunneling Microscopy (STM) from an acidic solution of $AlCl_3$-[BMIM]Cl (Endres 2003). Two UPD peaks show up at 0.9 and 0.4 V vs. Al/Al^{3+} corresponding to two dimensional Al-Au alloys and small Al islands respectively. UPD of Al on Cu was found using XRD in a study of the $AlCl_3$-MeEtimCl system (Stafford, 2000). The UPD is attributed to Cu-Al alloying that begins at potentials below about 0.25 anodic of Al/Al^{3+}. The alloy was tentatively identified as Cu_3Al. UPD of Al on Pt was also observed at about 0.1 V anodic to the Al rest potential in a study of the deposition of Al from $AlCl_3$-NaCl systems on various substrates (GC, W and Pt) (Rolland 1976). In the same study, it was found that the deposition of Al on the GC substrate required 0.05 V of overpotential. The remaining anodic current on the initial forward anodic scan is due to Cl_2(g) evolution due to HCl, the scan was not high enough to see the Cl_2(g) evolution due to $Al_2Cl_7^-$. On the reverse scan cathodic current is apparent beginning at potentials below about 0.8 V similar to the X_{AlCl3} = 0.5 system. This is again attributed to HCl now in the form of hydrogen evolution as well as some contribution due to an Al-Pt surface alloy forming. At potentials below about -0.1 V the usually smooth curve becomes rough, this is due to the nucleation of Al and Al deposition begins to occur, along with hydrogen evolution. On the reverse cathodic scan, the hysterysis is still present but not as prominent as in the X_{AlCl3} = 0.5 and the current density is higher. As the potential increases above -0.1 V the stripping of aluminium becomes the dominant reaction. The stripping reaction reaches a maximum current at about 0.1 V due to the use of the available $AlCl_4^-$ that was generated during the cathodic

polarization. This local concentration effect was more evident and is explained further in the following paragraph concerning the $X_{AlCl3} = 0.67$ scan.

The final CV was performed in $AlCl_3$-$[P_{14,6,6,6}]Cl$ ($X_{AlCl3} = 0.67$). The small anodic peak attributed to the dissolution of an Al-Pt alloy appears at 1.2 V which is about 0.3 V below where it was noticed in the $X_{AlCl3} = 0.6$ solution, this might be due to the shift in the reference potential as the reference electrode is changing along with the changes in the solution potential. Increasing X_{AlCl3} from 0.6 to 0.67 requires about 34% more $AlCl_3$. The chlorine evolution reaction appears to begin at a similar potential as in the neat ionic liquid, the line is noticeably curved suggesting the presence of more than one reaction ($HCl \rightarrow Cl_2(g)$, $AlCl_4^- \rightarrow Cl_2(g)$, and $Al_2Cl_7^- \rightarrow Cl_2(g)$). On the cathodic side, the cathodic current begins at potentials below 0.4 V this concurs with a shift in the reference potential as the cathodic current began below 0.8 V in $X_{AlCl3} = 0.6$. The cathodic current increased significantly at potentials below about -0.25 V vs. Al/Al(III) due to the deposition of aluminium. As for the anodic scan following the deposition of aluminium, two peaks are noticed; the first peak corresponds to the stripping of Al, the reverse of Equation 13 since there will be a locally high concentration of $AlCl_4^-$ resulting from the deposition of Al. The second peak is also due to the stripping of Al however the reaction likely proceeds as described in Equation 41 since the concentration of $AlCl_4^-$ in this solution is generally low.

$$10Al_2Cl_7^- + Al \rightarrow 7Al_3Cl_{10}^- + 3\bar{e} \qquad [41]$$

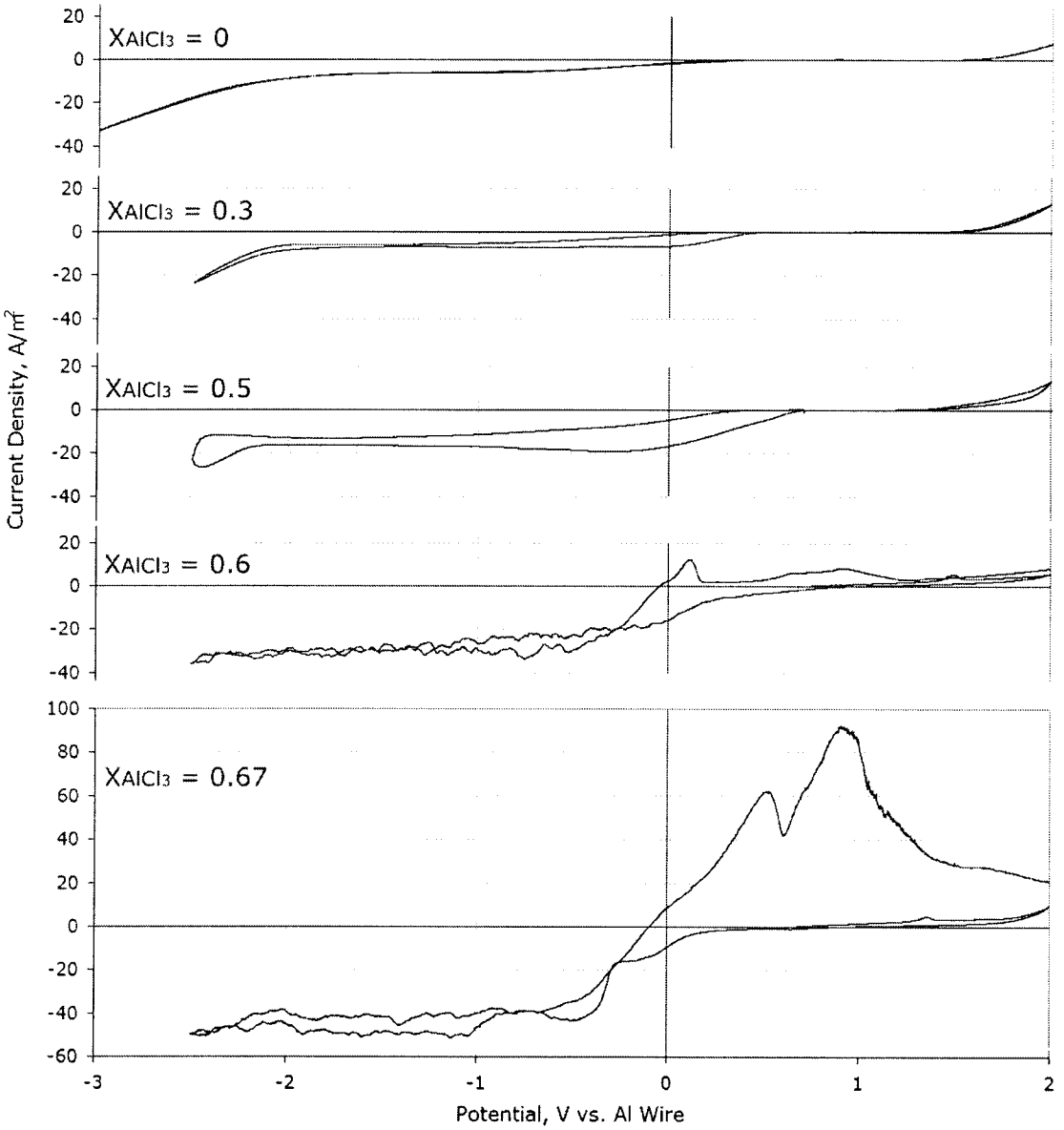

Figure 64 Cyclic voltammograms of the $AlCl_3$-$[P_{14,6,6,6}]Cl$ with various concentrations of $AlCl_3$ at 373 K. Pt wire WE (0.096 cm^2), Pt foil CE (2 cm^2), Al wire RE, the WE-CE and WE-RE spacing was 1 mm. Scanning from OC (~ 0.7 V vs. Al wire) to +2 V to -3 V to +2 V). SR = 5 mV/s. The solutions were stirred using a magnetic stir-bar.

The deposition and stripping of aluminium on a copper wire are shown using cyclic voltammetry (Figure 65). Most of the electrodeposition experiments were carried out on a Cu substrate. Pt is not a practical substrate because of its high cost. Attempts to deposit Al on an Al or W substrates resulted in powdery deposits which were undesirable as IL tended to be occluded. The current density of the deposition and stripping were

higher at higher concentrations of $AlCl_3$, (also observed in Figure 64). The conductivity of the mixture also increases with $AlCl_3$ concentrations, 0.18 to 0.28 S/m from 0.60 to 0.66 mole fraction $AlCl_3$ respectively at 373 K. At $X_{AlCl3} = 0.6$ and potentials above ~0.7 V, the current is believed to be due to the oxidation of Cu.

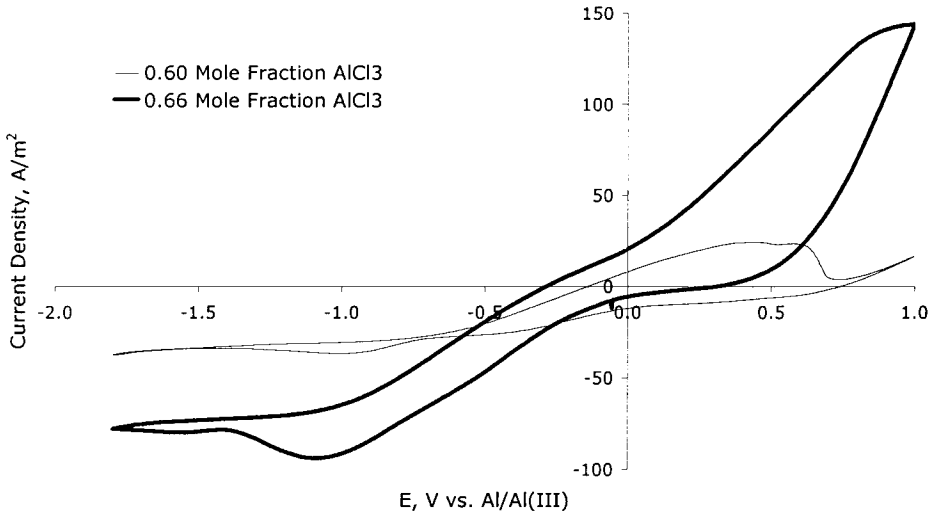

Figure 65 Cyclic voltammogram (2nd cycle) depicting the stripping and deposition of aluminium on a copper wire substrate from $AlCl_3$-$[P_{14,6,6,6}]Cl$, 373 K, 25 mV/s scan rate.

In summary, the electrochemical window of $[P_{14,6,6,6}]Cl$ being 3.5 V is high compared with other basic Cl^- based ILs such as imidazolium and pyridinium. ILs such as $[BMIM]PF_6$, Neutral $AlCl_3$-BPC, and Neutral $AlCl_3$-EMIC exhibit larger electrochemical windows because of the increased stability of their anions (Table 42).

Table 42 The electrochemical window of ILs.

Ionic Liquid	WE / RE	Cathodic Limit	Anodic Limit	E Window V	Reference
$[BMIM]PF_6$	Au / Pt	-2 V Reduction of $BMIM^+$	2 V Oxidation of Au	4	Endres 2003
$[P_{14,6,6,6}]Cl$	Pt / Al	Reduction of $[P_{14,6,6,6}]^+$	Oxidation of Cl^-	3.5	This work
Basic $AlCl_3^-$ EMIC	W / Al	Reduction of Im^+	Oxidation of Cl^-	2.6 2.8	Lipsztajn 1983 Zhang 2003
Acidic $AlCl_3^-$ EMIC	W / Al	Deposition of Al	Oxidation of $Al_2Cl_7^-$	2.9	Lipsztajn 1983
Neutral $AlCl_3^-$ EMIC	W / Al	Reduction of Im^+	Oxidation of $AlCl_4^-$	4.4	Lipsztajn 1983
Neutral $AlCl_3^-$ BPC	W / Al	Reduction of $BuPy^+$	Oxidation of $AlCl_4^-$	3.6	Lipsztajn 1983

By comparing the electrochemical window of the neutral $AlCl_3$-IL systems (X_{AlCl3} = 0.5) we can see that EMI^+ is considerably more stable than BP^+, the electrochemical windows being 4.4 and 3.6 V respectively. In a separate electrochemical study of $[N_{1,4,4,4}]N(SO_2CF_3)_2$ and $BMIPF_6$ it was found that $[N_{1,4,4,4}]^+$ was more stable than BMI^+, possibly up to 2 V (Quinn 2001). Since tetra-alkyl ammonium ILs also exhibit large electrochemical windows, the increased stability is likely due to the insulating effect of the four hydrocarbon chains.

3.3 Diffusion

The diffusion coefficient of the electroactive $Al_2Cl_7^-$ (D_{Al2Cl7}) was estimated to be 0.3, 1.1, 1.6, 2.4 and 4.7 ($\cdot 10^{-13}$ m^2/s) at 347, 366, 380, 389 and 399 K respectively from the peak current of cathodic potentiodynamic scans at various scan rates on Al using the Berzins and Delahay formula (Figure 66).

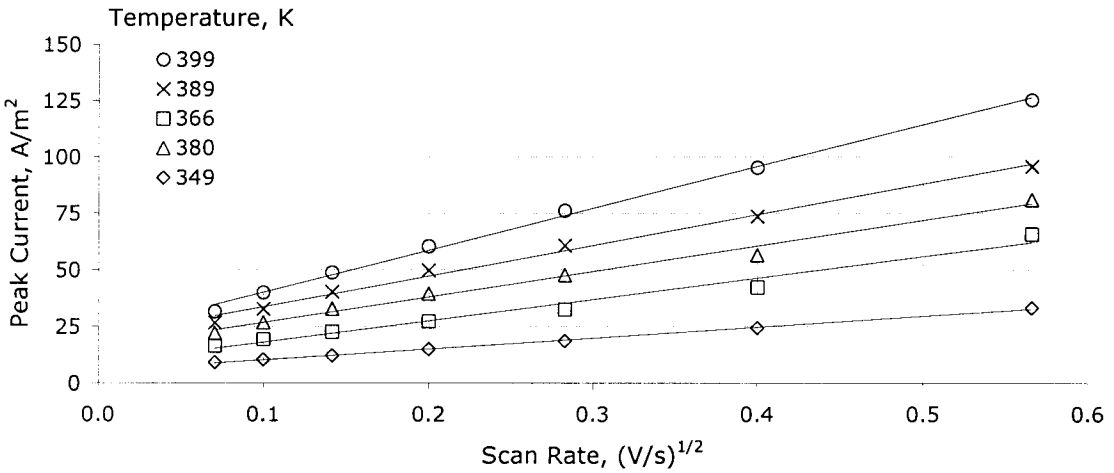

Figure 66 Peak cathodic current as a function of temperature and scan rate. 0.67 X_{AlCl3} in $AlCl_3$-$[P_{14,6,6,6}]Cl$. The electrodes were: Al plate WE (0.72 cm^2), Al wire RE, and two Al plate CEs (6 cm^2). WE-CE spacing was 2 mm. WE-RE spacing was 1 mm. No stirring.

The experiments were also carried out using a copper substrate (Figure 67).

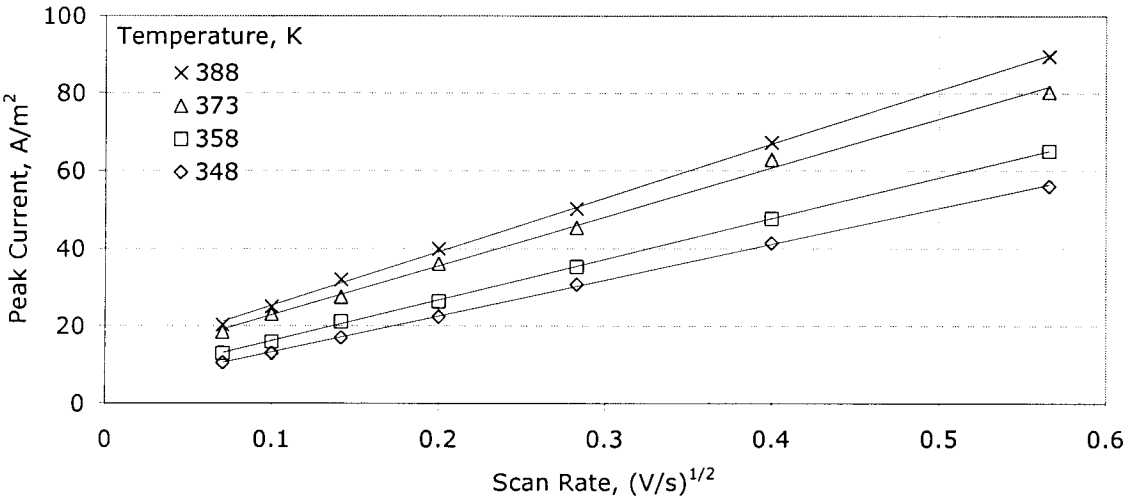

Figure 67 Peak cathodic current as a function of temperature and scan rate. 0.67 X_{AlCl3} in $AlCl_3$-$[P_{14,6,6,6}]Cl$. The electrodes were: Cu plate WE (0.4 cm^2), Al wire RE, and two Al plate CEs (6 cm^2). WE-CE spacing was 2 mm. WE-RE spacing was 1 mm. No stirring.

The diffusion constant for the reversible deposition of Al on a solid planar Al or Cu electrode was calculated using Equation 42 (Berzins 1952). This equation was derived for the specific situation when the reduced species is a solid. The equation was adjusted from its original form to include temperature as a variable. This is a solution to Fick's second law of diffusion where the concentration of electro active species in the diffusion zone is changing with time. The concentration of electroactive species was solved for by Berzins and Delahay as a function of time and distance from the cathode. The boundary condition was defined by the Nernst equation and the relationship between potential as a function of scan rate. The initial condition is that the concentration of $Al_2Cl_7^-$ at the cathode surface is equal to the bulk concentration. The complete calculation details are found in the paper (Berzins 1952).

$$D_{Al2Cl7} = (11728427 \cdot T^{-1/2} \cdot n^{3/2} \cdot C \cdot i_p^{-1} \cdot \nu^{1/2})^{-2} \quad [42]$$

The constant 11728427 in Equation 42 includes Faradays constant (F) and the Universal Gas constant (R), the units are $(C/mol\text{-}\bar{e})^{3/2} \cdot (mol\text{-}Al_2Cl_7 \cdot K/J)^{1/2}$. T is the temperature in Kelvin. The number of electrons (n) involved in the reduction of $Al_2Cl_7^-$ (3/4 based on Equation 6). The linear relationship of $i_p/\nu^{1/2}$ $(A/m^2 \cdot (s/V)^{1/2})$ was determined from the slopes of the lines in Figure 66. C is the molar concentration of $Al_2Cl_7^-$ $(mole/m^3)$ calculated from the density function of the purified 0.67 X_{AlCl3} in $[P_{14,6,6,6}]Cl$ (Table 31). D is the diffusion constant of $Al_2Cl_7^-$ (m^2/s). It was assumed for these calculations that the solution was pure and that the aluminium was present solely as $Al_2Cl_7^-$.

The diffusion of $Al_2Cl_7^-$ was also calculated using the Randles-Sevcik equation for comparison purposes (Zanello 2003, p. 54). This equation was derived for reactions where both the product and reactant are soluble but has been used to evaluate reactions where the reduced species is solid. Treating the peak current data with this equation results in diffusion constants for $Al_2Cl_7^-$ that are higher than with the Berzins and Delahay formula (Figure 68). Lu and Dreisinger (2003) used the Randles-Sevcik equation to calculate the diffusion of $Al_2Cl_7^-$ in acidic $AlCl_3$-BMIC ILs, they found the diffusion values to be slightly higher than those obtained from potentiostatic studies.

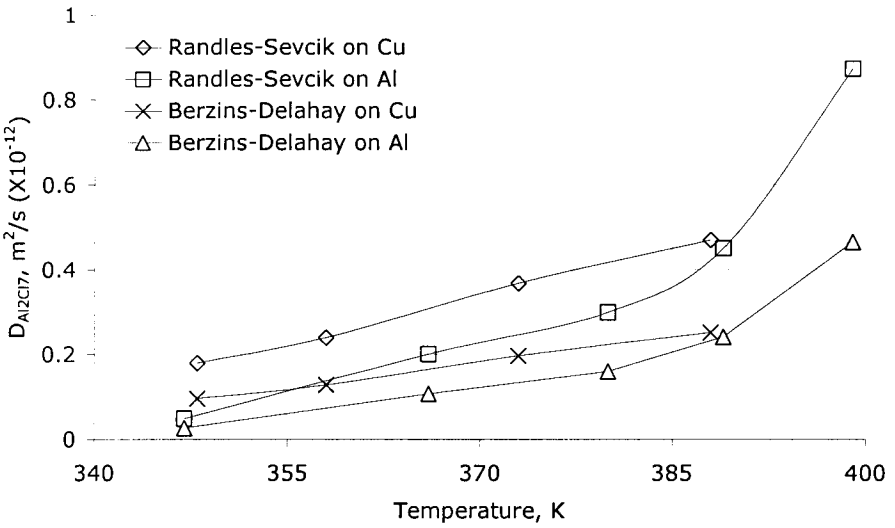

Figure 68 Calculated diffusion constants for $Al_2Cl_7^-$ in purified $AlCl_3$-$[P_{14,6,6,6}]$ (X_{AlCl3} = 0.67).

The calculated diffusion constants for $Al_2Cl_7^-$ in various solutions and temperatures are summarized in Table 43. The mobility in the phosphonium IL is by far the lowest of any of these systems. The diffusion of Ti(II) (added as $TiCl_2$) in acidic $AlCl_3$-MEIC melts was found to decrease with increasing Ti(II) concentration, the range tested was 0.013-0.17 mol/L (Tsuda 2003).

Table 43 The diffusion coefficient of $Al_2Cl_7^-$.

System	Temp. K	Cathode	D_{Al2Cl7} m^2/s	Reference
$AlCl_3$-$[P_{14,6,6,6}]Cl$ (X_{AlCl3} = 0.67)	347 366 380 389 399	Al	$0.3\cdot10^{-13}$ $1.1\cdot10^{-13}$ $1.6\cdot10^{-13}$ $2.4\cdot10^{-13}$ $4.7\cdot10^{-13}$	This Work (Berzins-Delahay)
$AlCl_3$-$[P_{14,6,6,6}]Cl$ (X_{AlCl3} = 0.67)	348 358 373 388	Cu	$0.9\cdot10^{-13}$ $1.3\cdot10^{-13}$ $2.0\cdot10^{-13}$ $2.5\cdot10^{-13}$	This Work (Berzins-Delahay)
$AlCl_3$-BMIC (X_{AlCl3} = 0.6)	303 333 353 373	Cu	$3.4\cdot10^{-11}$ $7.7\cdot10^{-11}$ $1.4\cdot10^{-10}$ $2.0\cdot10^{-10}$	Lu, 2003
$AlCl_3$-BMIC (X_{AlCl3} = 0.6)	303 383	Cu	$5.2\cdot10^{-12}$ $1.0\cdot10^{-11}$	Kamavaram, 2004 Kamavaram, 2002
$AlCl_3$-NaCl (X_{AlCl3}= 0.508)	443	W GC Pt	$4.1\cdot10^{-10}$ $5.5\cdot10^{-10}$ $3.2\cdot10^{-10}$	Rolland 1976
$AlCl_3$-BPC	333	W GC Pt	$5.1\cdot10^{-11}$ $8.0\cdot10^{-11}$ $8.0\cdot10^{-11}$	Robinson, 1980
$AlCl_3$-EMIC	298	W	$9.1\cdot10^{-11}$	Takahashi 1999 *Cited:* Bolkan, 1987
Ti(II) in $AlCl_3$-EMIC (X_{AlCl3}>0.5)	353	Cu	$5.5\text{-}20\cdot10^{-11}$ ($D_{Ti(II)}$)	Tsuda 2003
$TiBr_6^{2-}$ $AlBr_3$-MEIB X_{AlBr3} = 0.4	333	GC	$3.07\cdot10^{-11}$ (D_{TiBr6})	Sun 1989

Once the diffusion $Al_2Cl_7^-$ was determined, the diffusion of $[P_{14,6,6,6}]^+$ was calculated using the Nernst-Einstein Equation (Equation 43) that relates the equivalent conductivity (Λ) to the diffusion of the ions (Bockris 1998, p. 457). This equation was derived for the condition of infinitely dilute solutions so its application in this situation is far from ideal.

$$\Lambda = (zF^2/RT)(D_+ + D_-) \qquad [43]$$

Where z is the valence of the electrolyte (1 for $AlCl_3$-$[P_{14,6,6,6}]Cl$ (X_{AlCl3} = 0.67)), F is Faraday's number, R is the Universal Gas Constant, T is the temperature in Kelvin and D_+ and D_- are the diffusion constants for the cation and anion respectively.

Having measured the equivalent conductivity and estimated the diffusion of D_{Al2Cl7}, the diffusion of the cation ($D_{[P14,6,6,6]}$) was calculated using Equation 43 and presented in Table 44. From these calculations, it appears that the cation is responsible for over 99% of the conductivity which does not seem to be realistic. This method of calculating the diffusion coefficient is flawed since the Nernst-Einstein relationship requires that the species that are involved in diffusion must also be responsible for conduction, however, ion-pairs do not respond to an electric field. According to Bockris, in systems where ion-pairs are formed, the Nernst-Einstein relationship exhibits discrepancies up to 25% when the conductivity is related to diffusion coefficients (Bockris 1998, p. 457). Another related issue is that in ILs there is no solvent in which a concentration gradient can be established, since $Al_2Cl_7^-$ is being consumed at the cathode there is a concentration gradient established based on the anion species present (Cl^-, $AlCl_4^-$ $Al_2Cl_7^-$ and $Al_3Cl_{10}^-$). This is clearly different from the aqueous systems from which the diffusion equations and the Nernst-Einstein relationship were established. Also, because $Al_2Cl_7^-$ is an anion, the electrostatic repulsion by a cathodically charged surface may have contributed to its low diffusion value.

Table 44 The diffusion of $[P_{14,6,6,6}]^+$ calculated using Equation 43.

Ionic Liquid	Temperature K	Λ S·m²/mol-eq (Table 36)	D_{Al2Cl7} m²/s (Table 43)	$D_{[P14,6,6,6]}$ m²/s
$AlCl_3$-$[P_{14,6,6,6}]Cl$ X_{AlCl3}=0.67 Purified	347	$1.0\cdot10^{-4}$	$2.6\cdot10^{-14}$	$3.2\cdot10^{-11}$
	366	$1.7\cdot10^{-4}$	$1.1\cdot10^{-13}$	$5.6\cdot10^{-11}$
	380	$2.3\cdot10^{-4}$	$1.7\cdot10^{-13}$	$7.8\cdot10^{-11}$
	389	$2.7\cdot10^{-4}$	$2.4\cdot10^{-13}$	$9.4\cdot10^{-11}$
	399	$3.2\cdot10^{-4}$	$4.7\cdot10^{-13}$	$1.1\cdot10^{-10}$

Further experimental work could be performed to confirm whether these calculated diffusion coefficients are representative of the system. Specifically, the Hittorf method could be employed to experimentally determine the transport numbers to identify the contributions of the cations and anions to the overall conductivity (Bockris 1998, p. 489). For example, cation transport numbers were determined to be 0.71 and 0.76 for MEI^+ in the $AlCl_3$-MEIC and $AlBr_3$-MEIB systems respectively (Hussey, 1985 and 1987). The chloride system was studied in the basic region (0.3-0.5 X_{AlCl3}) while the bromide system was studied over a larger concentration range (0.3-0.71 X_{AlBr3}). The higher anion transport in the chloride system could be due to their smaller size. The

transport number for MEI^+ in $AlCl_3$-MEIC was found to 0.8 in acidic systems and 0.7 in basic and neutral melts (Dymek 1984). It is likely that the bulkier anion in the acidic system slows down its movement. This rational of relative size and frictional forces also explains why MEI^+ carries more of the charge than $Al_2Cl_7^-$ (See Table 32 for ion volumes). However, the calculation of a large diffusion coefficient for the bulky phosphonium cation in Table 44 remains unexplained.

3.4 Potentiodynamic Polarization

Cathodic and anodic potentiodynamic scans were conducted in order to characterize the electrode kinetics (Figure 69). At the lowest temperatures tested, 353 and 375 K, the anodic current appears to be limited at potentials above about 0.4 V. This is likely due to the formation of $AlCl_3$ on the surface leading to passivation. Similar passivation phenomena were observed during the anodic polarization of Al in $AlCl_3$-KCl-NaCl melts between 373 and 433 K (Holleck 1972). It has been observed that the maximum current density for the stripping of aluminium in $AlCl_3$-BPC and $AlCl_3$-MEIC systems (X_{AlCl3} = 0.67) over a range of temperatures (293-373 K) is about 1/3 of the maximum deposition current density indicating that an electrorefining process will probably be limited by the dissolution of the anode (Takahashi, 1990). Increasing the temperature above 375 K was found to lessen the anodic passivation in this phosphonium IL system. The cathodic current density is limited by mass transport of $Al_2Cl_7^-$.

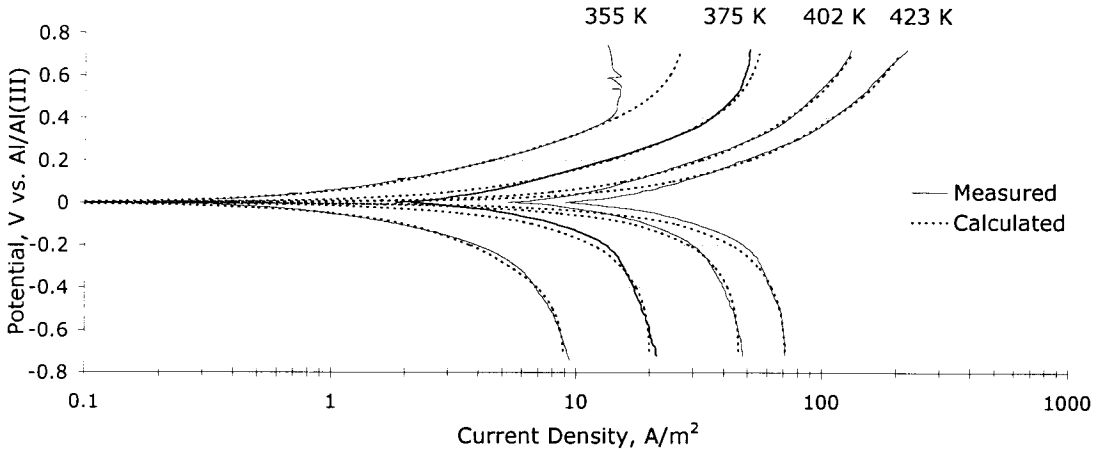

Figure 69 Potentiodynamic polarization curves of Al deposition (cathodic) and stripping (anodic) as a function of solution temperature. The solution was 0.67 X_{AlCl3} in $[P_{14,6,6,6}]Cl$. The electrodes were: Al plate working (1 cm^2) and counter (6 cm^2) electrode, Al wire reference electrode. SR = 1 mV/s. Current interrupt IR compensation was employed. No stirring.

The kinetic current (i_k) was modeled using the Butler-Volmer equation, Equation 44 where η is the over-potential in V, n is the number of moles of reactant per electron and depends on the reaction stoichiometry (Zanello, 2003 p. 34).

$$i_k = i_o \left[e^{-(\alpha n F\eta/(RT))} - e^{((1-\alpha) n F\eta/(RT))}\right] \quad [44]$$

The diffusion limited current (i_d) was calculated as Equation 45, where K is a mass transfer factor that represents the ratio of the diffusion coefficient of the limiting species to the boundary layer thickness and C_o is the bulk concentration of the limiting species (mol/L).

$$i_d = nFKC_o \quad [45]$$

The three reactions considered are summarized in Table 45. Reaction 1 is the deposition and stripping of aluminium, its equilibrium potential is lower than the reference potential, for the model it was assumed to be -70 mV vs. Al wire reference (Al/Al(III)). The potential value of Reaction 1 was estimated during the fitting of the model to the data, the negative value is due to the corrosion of the Al quasi-reference electrode by the HCl impurities. Reaction 2 is hydrogen evolution, also due to the HCl impurities, the equilibrium potential for this reaction was considered to be 350 mV based on the cyclic voltammogram of the IL on Pt (Figure 64). Reaction 3 is the stripping of

aluminium at higher potentials (Equation 41), this reaction was considered to begin at potentials above 375 mV, also based on Figure 64 and was only included in the model at the higher temperature (402 and 423 K). The α coefficients in Equation 25 were 0.4, 0.5 and 0.5 for Reaction 1, 2 and 3 respectively. The α coefficient for the deposition of Al (Reaction number 1) was determined to be 0.4 in acidic solutions of $AlCl_3$-BMIC at 303 K (Kamavaram, 2004). The n term was taken to represent the ratio of moles of electrons in the reduction reaction to the moles of reducible species.

Table 45 The reactions considered in the modeling of the polarization curves.

Number	Reaction	Equilibrium Potential mV vs. Al/Al(III)	n	α
1	$4Al_2Cl_7^- + 3\bar{e} \leftrightarrow Al + 7AlCl_4^-$	-70	3/4, 3/7	0.4
2	$2HCl + 2\bar{e} \rightarrow H_2(g)$	< 350	1	0.5
3	$10Al_2Cl_7^- + Al \rightarrow 7Al_3Cl_{10}^- + 3\bar{e}$	> 375	3/10	0.5

The cathodic current (i_c) is described by Equation 46.

$$i_c = (1/i_{k1} + 1/i_{d1})^{-1} + (1/i_{k2} + 1/i_{d2})^{-1} \quad [46]$$

The anodic current (i_a) is described by Equation 47.

$$i_a = -(1/i_{k1} + 1/i_{d1})^{-1} - (1/i_{k2} + 1/i_{d2})^{-1} + i_{k3} \quad [47]$$

The model was fitted to the measured data by adjusting the exchange current densities (i_o) as well as the kinetic parameters (K). The concentration of $Al_2Cl_7^-$ was first calculated assuming that all Al in solution was in this form, a provision of 10% was made for the aluminium that might be in the form of $AlCl_4^-$ and $Al_3Cl_{10}^-$, this value is a rough approximation as speciation data for this system is presently not available. The concentration of H^+ in the solution was estimated from the concentration of the HCl in the ionic liquid (0.5 wt. %). HCl will be produced if water is associated with the $AlCl_3$ when the solutions are being prepared and some HCl will be lost to the vapour phase upon heating, neither of these considerations was included in the model.

Table 46 Model parameters for Figure 69.

Temperature, K	355	375	402	423
i_{o1}, A/m^2	0.57	2.13	6.49	11.53
i_{o2}, A/m^2	0.003	0.016	0.067	0.163
i_{o3}, A/m^2	-	-	8.2	16
K_1 Cathodic, m/s	$7.5\cdot10^{-8}$	$1.3\cdot10^{-7}$	$3.0\cdot10^{-7}$	$5.1\cdot10^{-7}$
K_1 Anodic, m/s	$1.0\cdot10^{-5}$	$2.1\cdot10^{-5}$	$3.8\cdot10^{-5}$	$5.8\cdot10^{-5}$
K_2, m/s	$2.5\cdot10^{-7}$	$8.6\cdot10^{-7}$	$2.1\cdot10^{-6}$	$2.9\cdot10^{-6}$
$Al_2Cl_7^-$, mol/L	1.23	1.22	1.21	1.21
$AlCl_4^-$, mol/L	0.068	0.068	0.067	0.067
H^+, mol/L	0.1	0.1	0.1	0.1

This model is helpful in demonstrating the contributions of the various reactions resulting in the overall measured current. Figure 70 depicts the contribution of hydrogen evolution current and aluminium deposition and stripping current at 355 K. The reference potential is actually a mixed potential consisting of hydrogen evolution and aluminium dissolution. In terms of deposition of aluminium, a significant fraction of the current will be lost to hydrogen evolution and the current efficiency may be increased by increasing the cell potential. Zhang and Reddy noticed an increase in current efficiency on the order of 10-15% when they increased the cell potential from 3 to 3.5 V during the electrowinning of aluminium from HMIC-$AlCl_3$ at 353 K (Zhang, 2006).

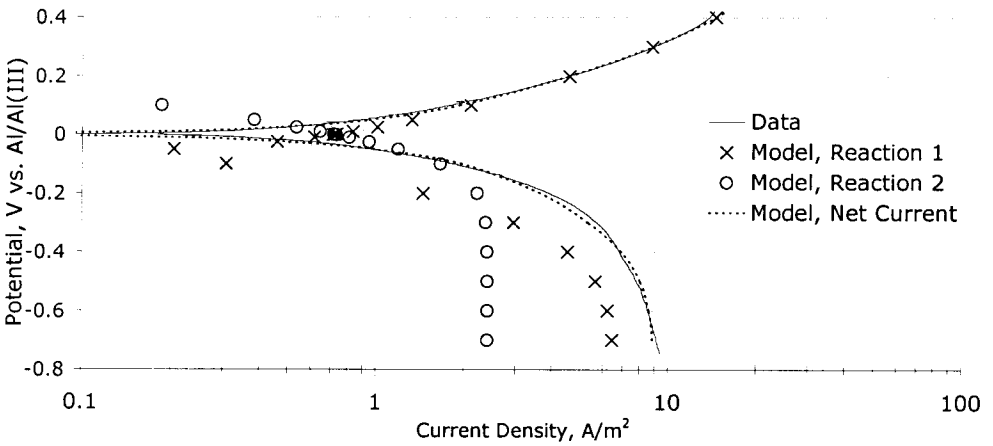

Figure 70 Current contributions of hydrogen evolution and aluminium deposition/stripping to the model of the potentiodynamic polarization of Al in 0.67 X_{AlCl3} $AlCl_3$-$[P_{14,6,6,6}]Cl$ at 355 K. The electrodes were: Al plate working (1 cm^2) and counter (6 cm^2) electrode, Al wire reference electrode. SR = 1 mV/s. Current interrupt IR compensation was employed. No stirring.

Similar potentiodynamic polarization experiments were performed in the same solution that was treated to remove the HCl by corrosion of pure Al foil (Figure 71).

Some of the features now become more evident. Evidence of a small amount of hydrogen evolution can still be seen near at low cathodic overpotentials and temperatures (347 and 366 K). Upon further cathodic polarization a peak current is evident, this is likely due to the nature of the deposited Al, it was observed that deposition on an Al substrate tends to occlude the IL and generates a passive film, the passivity appears to be lessened with increasing temperatures. This passivation of the Al cathode was not noticed in the unpurified solution. The presence of HCl may limit the amount of IL that is occluded in the deposit. It is possible that the evolution of $H_2(g)$ provided some slolution mixing in the vicinity of the cathode. As for the anodic scan, there are clearly two dissolution reactions, one faster reaction that occurs at low overpotentials and one slower reaction that occurs as the potential increases. In between the two reactions and at higher potentials anodic current minimum is diminished, this appears to be passivation behaviour. At higher temperatures, the passivation is diminished as the second dissolution reaction becomes more significant. At temperatures below about 385 K, the anodic reaction is slower than the cathodic reaction but above this temperature the peak anodic current is higher than the diffusion limited current. The peaks may not have been resolved in Figure 69 as more of the Al was present as $AlCl_4^-$ in the unpurified solution. During purification, Al was added to the solution by corroding the Al coupon increasing X_{AlCl3} slightly ($AlCl_4^- + AlCl_3 \rightarrow Al_2Cl_7^-$).

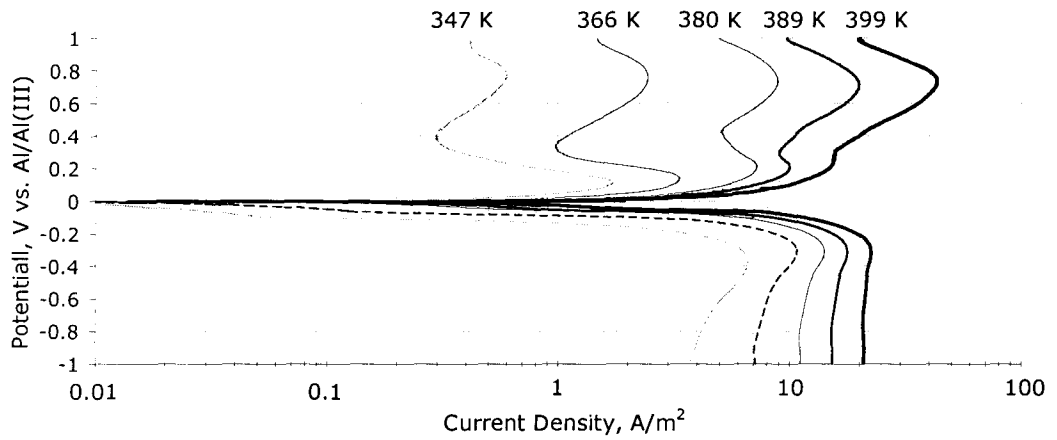

Figure 71 Potentiodynamic polarization curves of Al deposition (cathodic) and stripping (anodic) as a function of solution temperature. The solution was 0.67 X_{AlCl3} in $AlCl_3$-$[P_{14,6,6,6}]Cl$. The solution was purified by removal of HCl by exposure to high purity Al and sublimation of the $AlCl_3$. The electrodes were: Al plate working (0.72 cm^2) and counter (6 cm^2) electrode, Al wire reference electrode. SR = 1 mV/s. Current interrupt IR compensation was employed. No stirring.

The cathodic scan was repeated at 399 K at a very slow scan rate (0.05 mV/s) in Figure 69. The increased current may be caused by an increase in cathode surface area as the Al is deposited. Also at higher potentials the current appears to drop, this is due to the passivation of the cathode that occurs when too much IL is occluded in the deposit.

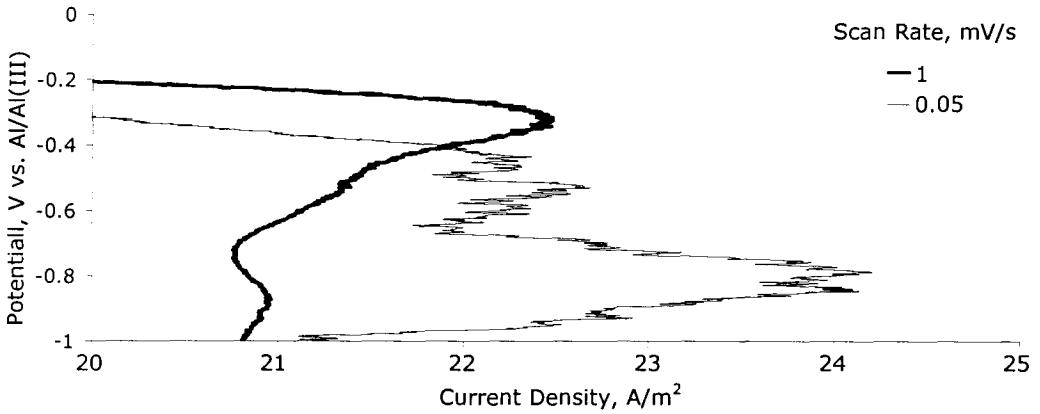

Figure 72 The effect of scan rate on the current density during the cathodic polarization of Al at 399 K. The solution was 0.67 X_{AlCl3} in $AlCl_3$-$[P_{14,6,6,6}]Cl$. The solution was purified by removal of HCl by exposure to high purity Al and sublimation of the $AlCl_3$. The electrodes were: Al plate working (0.72 cm^2) and counter (6 cm^2) electrode, Al wire reference electrode. Current interrupt IR compensation was employed. No stirring.

The diffusion limited current density is inversely proportional to the diffusion layer boundary layer thickness (δ), Equation 48 (Popov 2002).

$$i_d = nFDC_o/\delta \quad [48]$$

The diffusion limited cathodic current density was obtained from the model of the cathodic current for the deposition of Al at -0.7 V (Example: Figure 70, Reaction 1) in the case of the unpurified IL system. For the purified IL the maximum cathodic current was used (Figure 71). The values obtained over a range of temperatures are presented in Figure 73; the trend line is a second order polynomial. The limited current density of Al deposition obtained from the two different methods is in fairly close agreement for the temperature range of about 350-400 K.

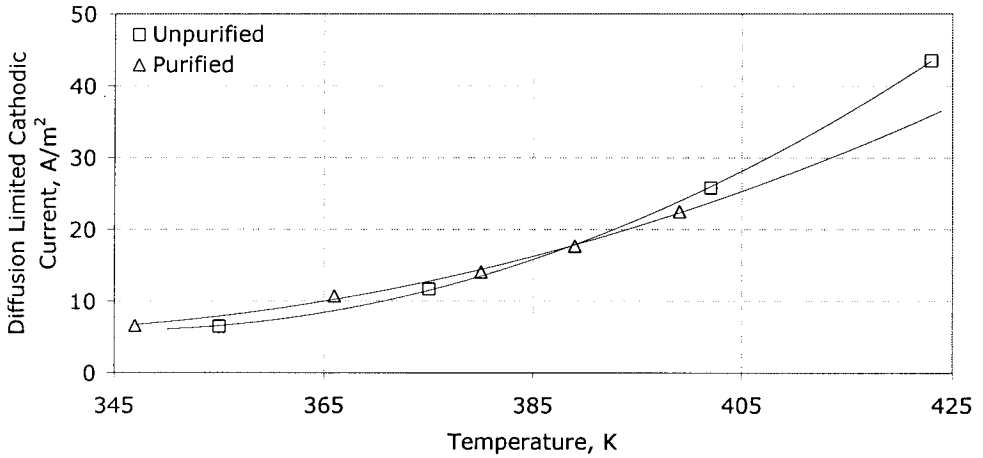

Figure 73 Diffusion limited cathodic current due to deposition of Al from cathodic potentiodynamic scans. $AlCl_3$-$[P_{14,6,6,6}]Cl$, $X_{AlCl3} = 0.67$.

Knowing the diffusion limited current density and the diffusion of $Al_2Cl_7^-$ as a function of temperature, the diffusion boundary layer thickness (δ in m) was calculated using Equation 48. Where n is 3, D_{Al2Cl7} was estimated from Figure 68 and C_o was calculated from the average of the density functions for the purified and unpurified $AlCl_3$-$[P_{14,6,6,6}]Cl$, $X_{AlCl3} = 0.67$ (Table 31). The boundary layer thickness increases with temperature.

Table 47 Diffusion boundary layer thickness as a function of temperature and parameters used in the calculations.

Temperature K	Average i_d A/m^2	D_{Al2Cl7} m^2/s	C_o of $Al_2Cl_7^-$ moles/m^3	δ m
350	6.6	$4.0 \cdot 10^{-14}$	1315	$2.3 \cdot 10^{-6}$
360	8.1	$8.5 \cdot 10^{-14}$	1309	$4.0 \cdot 10^{-6}$
370	10.6	$1.3 \cdot 10^{-13}$	1302	$4.5 \cdot 10^{-6}$
380	14.0	$1.7 \cdot 10^{-13}$	1296	$4.5 \cdot 10^{-6}$
390	18.4	$2.7 \cdot 10^{-13}$	1289	$5.6 \cdot 10^{-6}$
400	23.7	$5.4 \cdot 10^{-13}$	1283	$8.4 \cdot 10^{-6}$

One problem with these diffusion layer thickness calculations is that this is a pure electrolyte system, the lack of supporting electrolyte may change the mechanism by which the diffusion is happening. Since $Al_2Cl_7^-$ is being consumed at the cathode, the only concentration gradient possible would be an excess of $AlCl_4^-$ at the cathode and $Al_2Cl_7^-$ being transported from the bulk.

3.5 Electric Double Layer

From the results of the electrochemical experiments, we can imagine the electric double layer that forms in the vicinity of the cathode in an acidic solution of $AlCl_3$-$[P_{14,6,6,6}]Cl$ (Figure 74). The applied potential supplies electrons to the cathode surface. Anions are can be chemically adsorbed to the metal surface; $Al_2Cl_7^-$ will also be oriented to some extent due to its dipole. It is possible that some chloride ions are shed from the $Al_2Cl_7^-$ as it approaches the cathode. The supply of $Al_2Cl_7^-$ is under diffusion limited control and the anion is quickly consumed once reaching the cathode surface. $AlCl_4^-$ is produced when $Al_2Cl_7^-$ is reduced. $AlCl_4^-$ is electrochemically stable and will move away from the cathode by the forces of diffusion and migration. The $[P_{14,6,6,6}]^+$ cation is physically adsorbed to the cathode due to its positive charge but the ion is sufficiently electrochemically stable as to not be reduced unless the cathode is highly polarized. The adsorbed anions and cations result in inner and outer planes with thicknesses on the order of 5 Å based on the radius of the ions. The diffuse boundary extends out on the order of 5 μm based on the boundary layer thickness calculations at temperatures of 350-400 K.

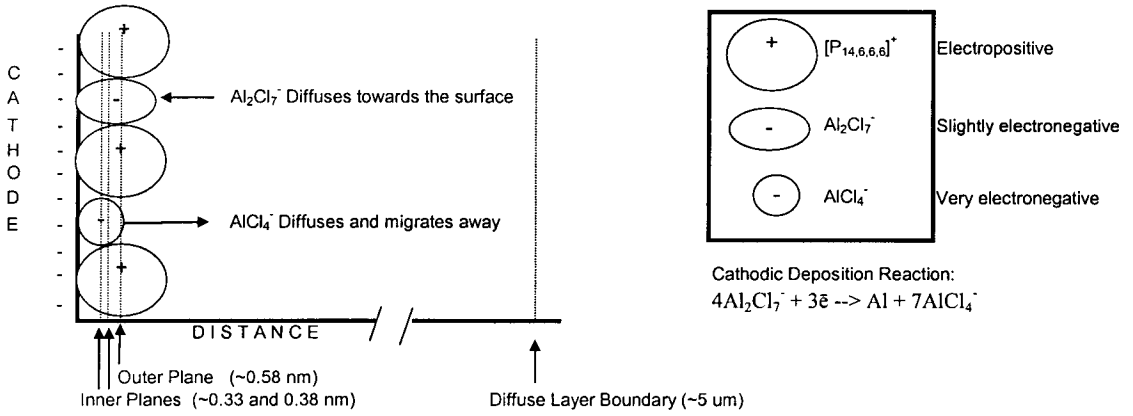

Figure 74 Schematic of the cathode double layer during deposition of Al in Lewis acidic $AlCl_3$-$[P_{14,6,6,6}]Cl$. Note: the ions are not drawn to scale.

The corresponding potential profile in the double layer is described in Figure 75. The negative potential at the cathode is decreased further within the inner planes due to the presence of adsorbed anions (this is assuming there is anion adsorption). The outer plane is more positively charged and the potential increases due to adsorption of the

cation. The potential then gradually increases until the outer edge of the diffuse boundary layer is reached. It is difficult to determine whether this potential profile actually exemplifies this IL system since there is limited information in the literature regarding this topic. It is possible that the double layer behaviour is completely different, for example, a layered structure might form where the layers alternate by positive and negative charges and the Al^{+3} in solution may access the cathode by tunneling through the cations that are adsorbed (effectively covering the cathode). Russian scientists described the molten salt double layer as an electrical multi-layer after using a binary distribution function to interpret XRD measurements (Aurbach 1999, p. 494 *Cited:* Esin 1956, p. 3 and Dogonadze 1964, p. 778). More recently, ionic liquid double layer work was critiqued by Kronyshev (2007), he admitted that this effort brought about more questions than answers.

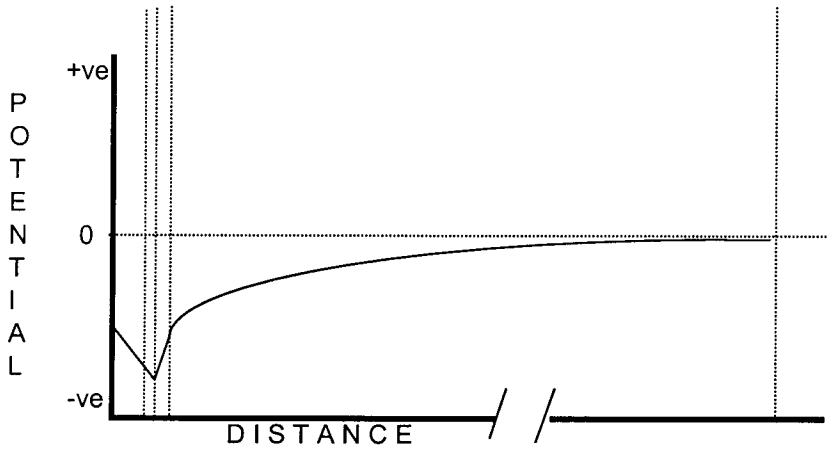

Figure 75 Schematic of the potential profile of the cathodic double layer during deposition of Al in an acidic $AlCl_3$-$[P_{14,6,6,6}]$ melt. The changes in potential and distances are not to scale.

Chapter 4 Deposition of Aluminium

Although aluminium was electrodeposited during some of the experiments in the third chapter, the deposit morphology has not yet been characterized. In this chapter, aluminium electrodeposition from phosphonium chloroaluminate ILs is investigated.

Electrodeposition of metal from solution requires that an energy barrier be overcome since the metal is in a low energy state when in solution, often complexed with anions (Al^{3+} is surrounded by Cl^- in this case). Deposition takes place at the metal-solution interphase. The metal is composed of positive ions distributed in a lattice surrounded by what is described as a free electron gas. At the metal surface, these electrons extend outside the lattice to form a surface dipole layer. The electric field at an aqueous solution-metal interphase can be as high as 10^6-10^7 V/cm (Paunovic 1998, p. 39). When this electric field is sufficiently high, the energy barrier that keeps ions in solution can be overcome and the metal ions in solution will proceed to join the lattice as a solid.

In the first section of this chapter, Al was deposited at a constant potential with a glassy carbon counter electrode or a pure Al counter electrode. The deposit substrate used for most of the experiments was Cu. W and Al substrates were tested as cathodes but seemed to promote a powdery Al deposit that occluded much of the IL, resulting in a soft deposit that became a resistance barrier over time. A wide range of Al deposit morphologies were observed on the Cu substrate. They ranged from smooth to spherical to dendritic depending on the experimental conditions. The highest current efficiency observed in the first series of experiments (Section 4.2) was 66% due to the presence of HCl in the melt. In Section 4.3, the galvanostatic technique was employed to deposit the Al; the anode-cathode spacing was reduced to 2 mm, improving the power consumption. It was also shown that the current efficiency could be increased by a pre-reduction of the HCl. In Section 4.4 a mini-pilot plant was setup using purified $AlCl_3$-$[P_{14,6,6,6}]$ (X_{AlCl3} = 0.67). The solution was purified by exposing it to high purity Al foil at an elevated temperature. This procedure reduced the HCl impurities by about 90%. The same purified solution was used for all of the experiments in Section 4.4, demonstrating that the bath is of high quality and is not quickly degraded.

4.1 Experimental Aspects

The experimental setup used was the same as that for the electrochemical experiments (Chapter 3). The first series of electrodeposition experiments were potential controlled with respect to a reference electrode (Section 4.2). Later, in Sections 4.3 and 4.4 the reference used was the counter electrode, allowing the calculation of power consumption.

The theoretical mass deposited during an electrochemical experiment where a measured current (I in A) is passed for a time (t in s) is calculated considering the molecular weight (MW) of the metal being deposited (26.98 g/mole for Al), (3 $\bar{e}$ for Al) and F is 96485 C/mol (Equation 49).

$$\text{Theoretical mass deposited} = (I \cdot t \cdot MW/(n \cdot F)) \quad [49]$$

The electrodeposition current efficiency (C.E. in %) is calculated as the ratio of mass of metal deposited to the theoretical mass deposited based on the current passed during a deposition experiment (Equation 50).

$$\text{C.E.} = (\text{Mass deposited/Theoretical Mass deposited}) \cdot 100\% \quad [50]$$

The power consumption (kWhr/kg-metal) was calculated using Equation 51.

$$\text{Power consumption} = E_{avrg} \cdot I_{avrg} \cdot t/(\text{Mass} \cdot 3600) \quad [51]$$

Where Mass is the measured mass of the electrodeposit, except if the electro-deposited mass exceeded the theoretical mass deposited in which case the theoretical mass deposited was used.

SEM provided high–resolution micrographs of the samples as well as information regarding elements present using BEI and Energy Dispersive Spectroscopy (EDS). The SEM used was a Hitachi S–3000N with an EDS system and Quartz analysis software. The working distance for the EDS measurements was 15 mm.

An indication of the amount of IL occluded in the deposit was obtained by the Al/Cl ratio measured using EDS (Sections 4.3 and 4.4). A high Al/Cl ratio indicates little occlusion of IL. An Al/Cl value of 0.22 would indicate no deposit (IL only). Since the measurement is taken from the surface only this does not provide information about the bulk deposit. The examination of sample cross sections indicated that the bulk deposit

can be relatively free of occluded IL and yet near the surface there is some trapped solution. This is, to some extent, an indication of insufficient rinsing of the sample, because when the deposit structure was dendritic and fragile it was difficult to remove the IL without losing some of the deposit, and so, the samples were gently rinsed.

4.2 Potentiostatic Deposition

The potentiostatic technique was used for initial deposition experiments in order to avoid reducing the cation. Based on the cyclic voltammograms, a potential of –1.1 V vs. Al/Al(III) was selected as the potential for constant potential aluminium electrowinning experiments. This potential allows for a relatively high deposition current and ensures that the organic cation is not being reduced. Figure 76 depicts the current density of the constant potential deposition experiments. The solutions of higher concentration of $AlCl_3$ provided a higher deposition current, on the order of 70 A/m^2. The concentration of Al in $AlCl_3$-[$P_{14,6,6,6}$] (X_{AlCl3} 0.67) is about 7 wt.%. Lu and Dreisinger obtained electrowinning current densities of 300 A/m^2 from $AlCl_3$ -BMIC melts (X_{AlCl3} = 0.56) at 373 K (Lu 2003). The deposition from X_{AlCl3} = 0.66 was repeated to obtain a higher mass of deposit in order to calculate the current efficiency. Unfortunately, the mass of the deposits was not significant since working electrode surface area was only about 0.3 cm^2. The current efficiency was estimated to be 75 and 60 % for the 2 and 5 hour tests, respectively, based on the deposit thickness. A possible source of inefficiency is the reaction of the freshly deposited aluminium with dissolved chlorine gas (Equation 52).

$$2Al + 3Cl_2(g) \rightarrow 2AlCl_3 \qquad [52]$$

The power consumption was not calculated for these deposition experiments because the applied potential was not measured.

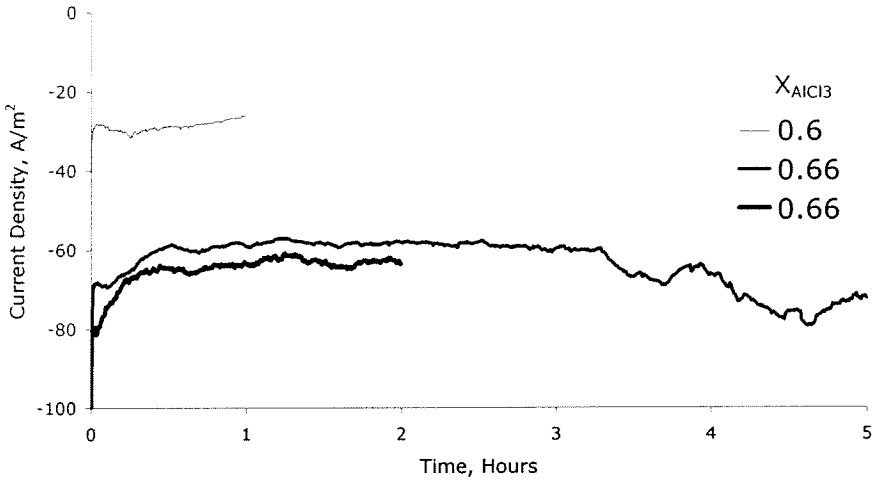

Figure 76 Potentiostatic aluminium deposition from $AlCl_3$-$[P_{14,6,6,6}]Cl$, E = –1.1 V vs. Al/Al(III), 373 K, Cu wire WE (~0.3 cm^2), Al wire RE, GC CE (0.5 cm^2).

Secondary electron micrographs of the 2 hour deposit at 0.66 mole fraction $AlCl_3$ are seen in Figure 77. The EDS analysis of the spot in Figure 77 (left) revealed that the metal was aluminium with only small amounts of oxygen and chlorine, due the oxide, and possibly some residual IL on the surface. At higher magnification (Figure 77 (right)) what is believed to be the structure of the oxide film becomes visible.

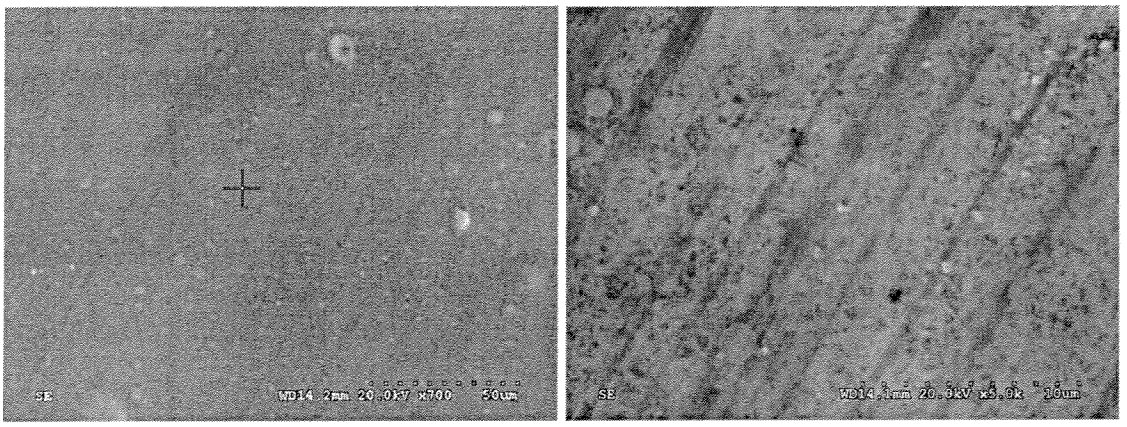

Figure 77 Secondary electron micrographs of Al electrowinning deposit, 2 hours at 373 K, -1.1 V vs. Al/Al(III), 0.66 X_{AlCl3} in $AlCl_3$-$[P_{14,6,6,6}]Cl$, EDS analysis spot is the cross (left) Higher magnification (right).

Backscattered electron micrographs of the deposit cross sections from 0.66 mole fraction $AlCl_3$ are shown in Figure 78. The higher molecular weight of the copper wire

appears bright compared with the surrounding aluminium. The deposits were smooth and dense. This is an important finding as Lu and Dreisinger were only able to produce dendritic deposits from the BMIC-$AlCl_3$ solutions.

The electrodeposited Al adhered well to the Cu substrate except for a small section highlighted in Figure 78 (left) that cracked and separated from the copper wire due to the stresses of grinding. The ability of the Al to be separated from the underlying metal can be useful in electrowinning and refining processes. The resulting deposit from the 5 hour experiment Figure 78 (right) is shown to be extremely smooth and dense.

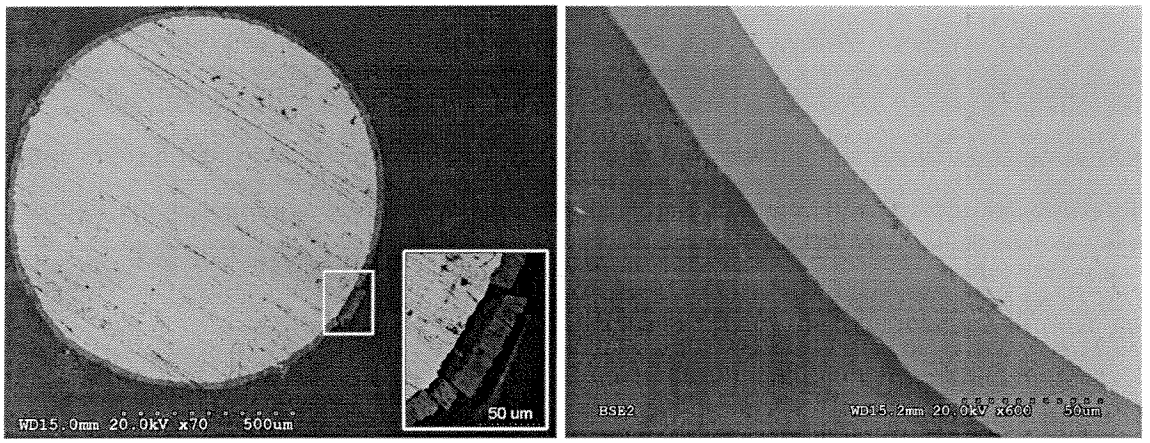

Figure 78 Cross sectioned Backscattered Electron Images of Al deposited on Cu wire, -1.1 V vs. Al/Al(III), in $AlCl_3$-$[P_{14,6,6,6}]Cl$ (X_{AlCl3} = 0.66) at 373 K, (left) 2 hours (right) 5 hours.

Aluminium was then deposited on a slightly larger scale from similar melts using a copper plate as the cathode and pure aluminium metal as the counter electrode. In this refining-like setup the counter reaction is the dissolution of aluminium instead of chlorine evolution. The duration of the experiments was 22-24 hours and the potential of the working electrode was set with respect to the counter electrode. Figure 79 shows the current density with time. A potential of -1.0 V vs. the Al CE resulted in an increase in current density compared with -0.75 V. The increased current density at 388 K is indicative of a dendritic growth structure.

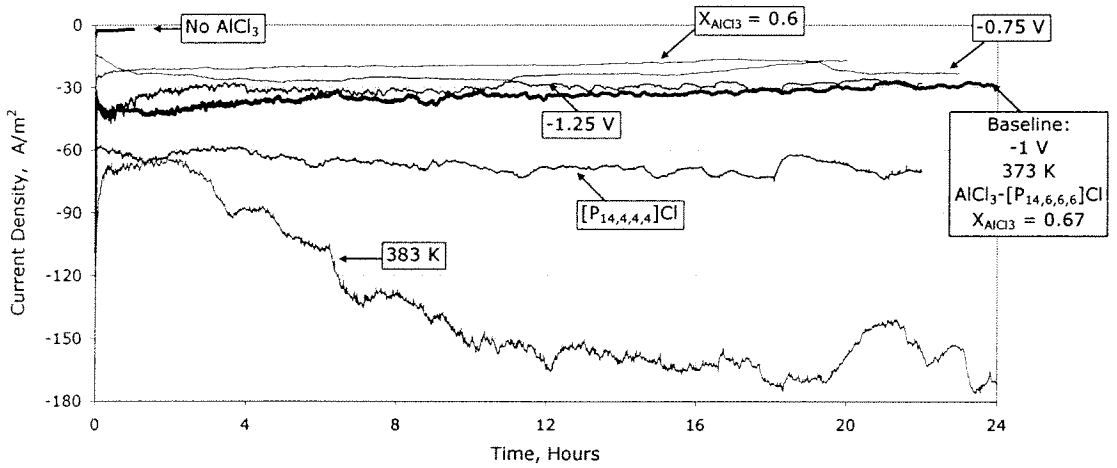

Figure 79 Potentiostatic deposition of Al from $AlCl_3$-$[P_{14,6,6,6}]Cl$ (X_{AlCl3} = 0.67) cathode potential set with respect to the Al CE, Anode-Cathode spacing was 3 or 4 mm, single Al plate anode (~4 cm^2), Cu plate cathode (0.5 cm^2).

The SEM micrographs comparing the structures of the yielded deposits show that the deposit morphology is significantly affected by small changes in the operating conditions. At 373 K the aluminium deposits in a fairly dense spherical configuration, the spheres ranged from about 5–25 μm diameter. At higher overpotentials (-1.25 V, Figure 80 right) the deposit surface appears roughened. With the temperature increased to 388 K a dendritic structure with higher surface area is dominant, as seen in Figure 82. When the concentration of $AlCl_3$ was lowered to X_{AlCl3}=0.6 (Figure 83 (left)) the resulting microstructure appears to be more like a corrosion sample than a deposit. The deposit from a solution prepared using the smaller cation type IL $[P_{14,4,4,4}]$ yielded spheres that were composed of platelets (Figure 83 (right)).

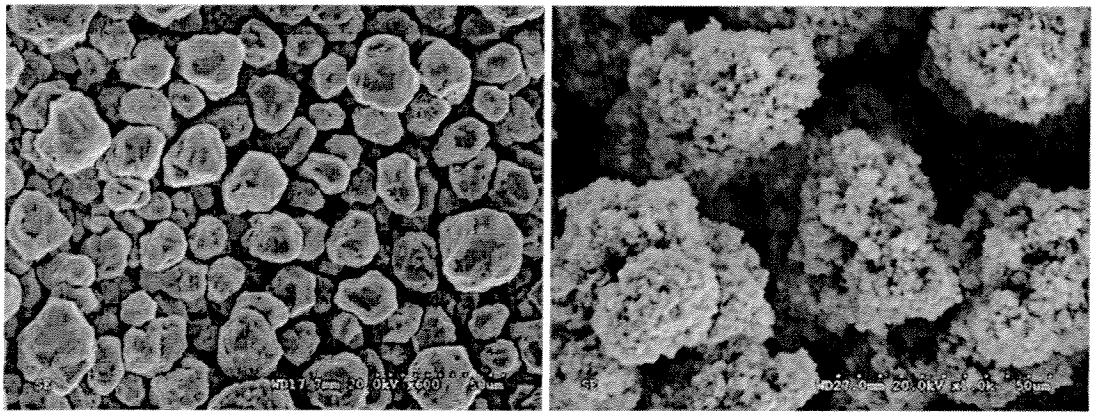

Figure 80 SEM micrograph of aluminium electrorefining deposit from $AlCl_3$-$[P_{14,6,6,6}]Cl$ (X_{AlCl3} = 0.67) at 373 K. 23 hours at -0.75 V, 600X (left) 22 hours at -1.25 V, 1000X (right).

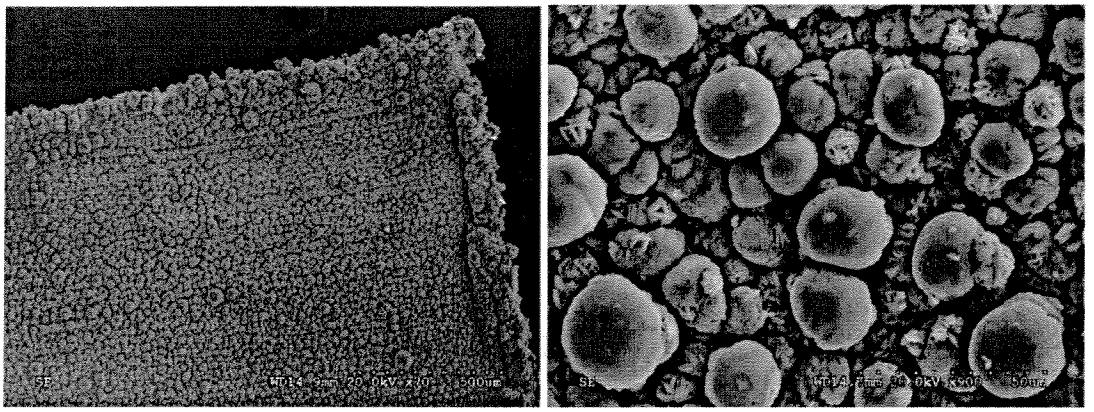

Figure 81 SEM micrograph of aluminium electrorefining deposit after 24 hours at -1.0 V vs. Al CE in $AlCl_3$-$[P_{14,6,6,6}]Cl$ (X_{AlCl3} = 0.67) at 373 K, 70X (left) 900X (right).

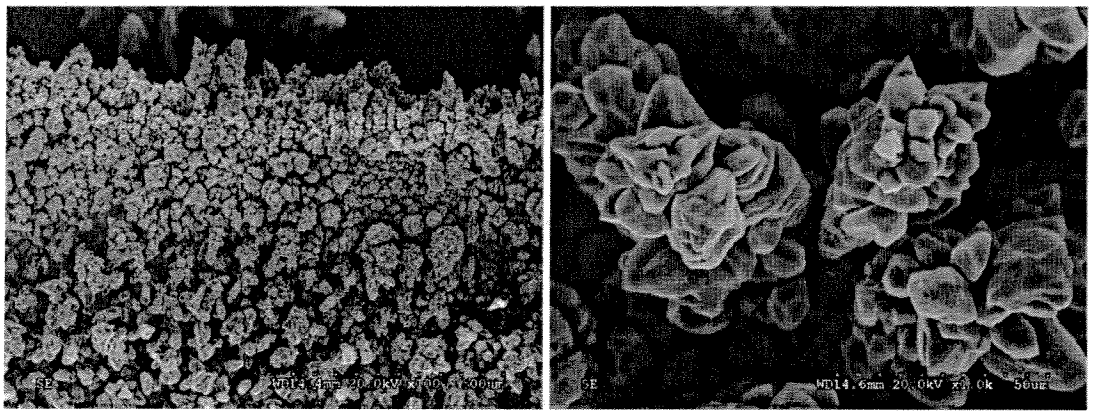

Figure 82 SEM micrographs of aluminium electrorefining deposit after 24 hours at -1.0 V vs. Al CE in $AlCl_3$-$[P_{14,6,6,6}]Cl$ (X_{AlCl3} = 0.67) at 388 K, 100X (left) 1000X (right).

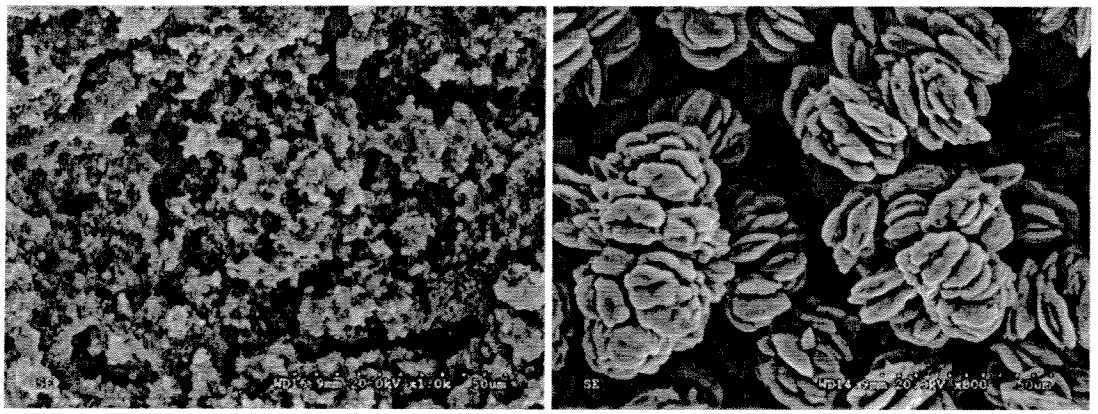

especially in the case of the dendritic deposit. A micrograph of the deposit from $AlCl_3$-$[P_{4,4,4,4}]Cl$ was not shown as it was a large, soft metal/ionic liquid mixture that expanded quickly and short circuited the experiment. Based on the conductivity measurements for this system, when the aluminium is depositing from $AlCl_3$-$[P_{4,4,4,4}]Cl$, the solution local to the cathode becomes depleted in $Al_2Cl_7^-$ and freezes.

Table 48 Summary potentiostatic electrodeposition of Al on Cu plate (0.5 cm^2), pure Al plate CE.

Bath Composition	A-C mm	T. K	Applied Potential V	Avg. CD A/m^2	C.E. %	Power Consumption kWhr/kg-Al
$AlCl_3$-$[P_{14,6,6,6}]Cl$ (X_{AlCl3} = 0.67)	3	373	0.75	24	54	4.2
	3	373	1.0	34	42	7.2
	4	373	1.25	30	55	6.8
	3	388	1.0	135	14*	21.7
$AlCl_3$-$[P_{14,6,6,6}]Cl$ (X_{AlCl3} = 0.60)	4	373	1.0	19	31	9.6
$AlCl_3$-$[P_{14,4,4,4}]Cl$ (X_{AlCl3} = 0.67)	3	373	1.0	67	66	4.5
$AlCl_3$-$[P_{4,4,4,4}]Cl$ (X_{AlCl3} = 0.67)	3	373	1.0	181	-	-

*Low current efficiencies can sometimes be partially explained by the deposit being lost in the solution or during cleaning, especially when a fragile dendritic structure was formed.

The EDS spot analysis indicated that the electrodeposited Al was of high purity as only Al and small amounts of O were revealed in the spectrum. It is possible that there is some AlH_3 in the deposit since HCl was present in the solution. The EDS technique is not effective at detecting hydrides.

4.3 Galvanostatic Deposition

The galvanostatic technique was employed to study the deposition of aluminium at various temperatures and current densities from unstirred $[P_{14,6,6,6}]Cl\text{-}AlCl_3$ (X_{AlCl3} = 0.67). The electrochemical setup was a copper cathode plate (~4 cm^2) sandwiched between two aluminium plate anodes (~11 cm^2 each). The cathode-anode separation was 2 mm. An electrochemical pretreatment was carried our prior to the experiments to clean the cathode surface in a consistent manner. The cathode was cycled four times at 0.1 V/s over a range of 2 V. The deposition time ranged from four to twenty hours.

The solutions used were freshly prepared in all cases except for deposition number 6. The solution for number 6 was pre-treated to remove H^+ by cyclically polarizing pure aluminium rods over a potential of -1 V to + 1 V vs. Al wire for five days at a temperature of 343 K. A significant increase in the current efficiency was then observed. The deposit also appeared brighter, both in the SEM micrograph and at a macroscopic scale.

Table 49 Deposition of aluminium from $[P_{14,6,6,6}]Cl\text{-}AlCl_3$ (X_{AlCl3} = 0.67), two anode setup, copper cathode, anode-cathode spacing was 2 mm.

Experiment	Deposition Time Hours	Temperature K	Current Density A/m^2	Average Potential V	Current Efficiency %	Power Consumption kWhr/kg Al	Deposit Purity Al/Cl ratio	Morphology
1	20	386	23	0.9	80	3.3	17.7	bubbles
2	20	400	25	0.8	58	4.2	68.6	platelets
3	4	427	45	0.5	59	2.5	No Cl	platelets/spheres
4	4	429	40	0.8	63	3.7	135.7	spheres
5	4	429	48	0.6	65	2.7	No Cl	spheres
6*	5.6	383	33	0.7	92	2.3	No Cl	spheres

*HCl was removed from solution by pre-electrolysis

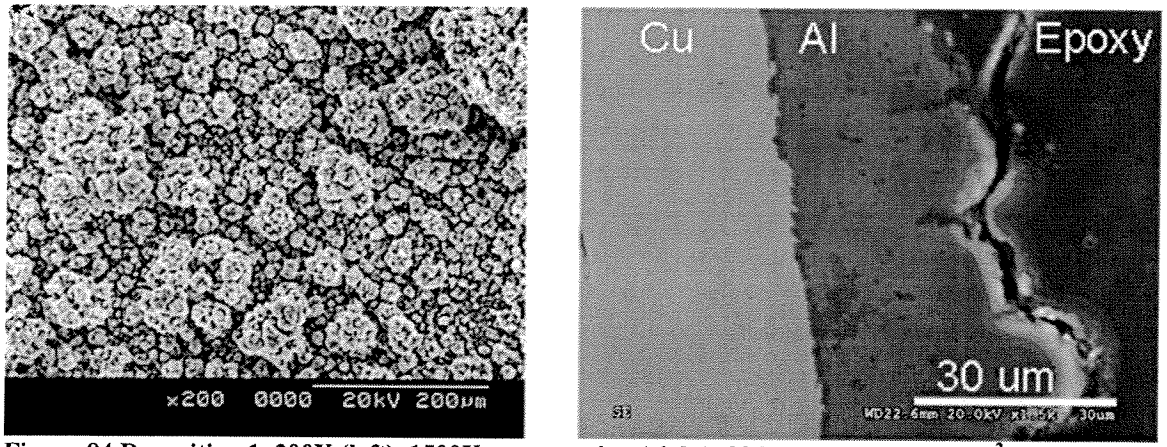

Figure 84 Deposition 1, 200X (left), 1500X cross-section (right), 20 hours, 386 K 23 A/m^2.

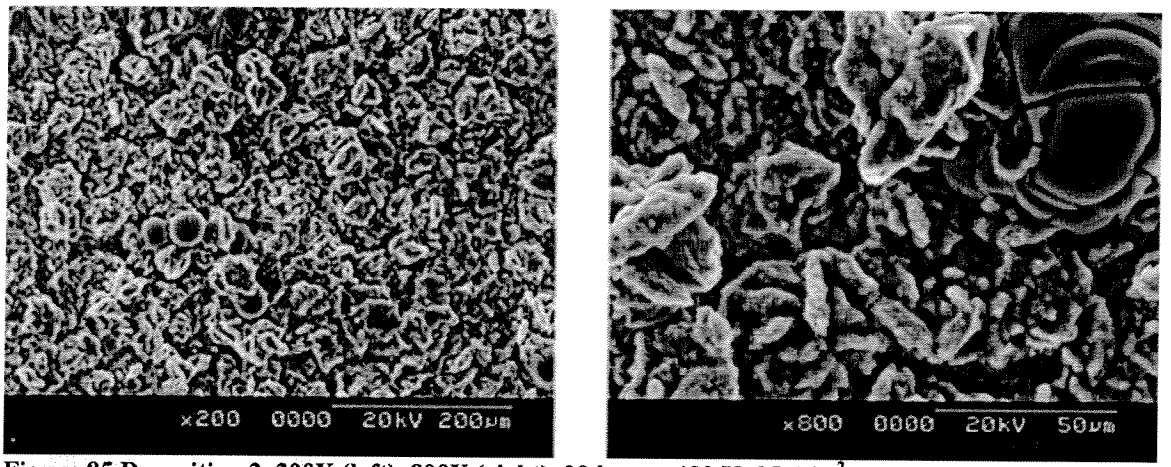

Figure 85 Deposition 2, 200X (left), 800X (right), 20 hours, 400 K, 25 A/m^2.

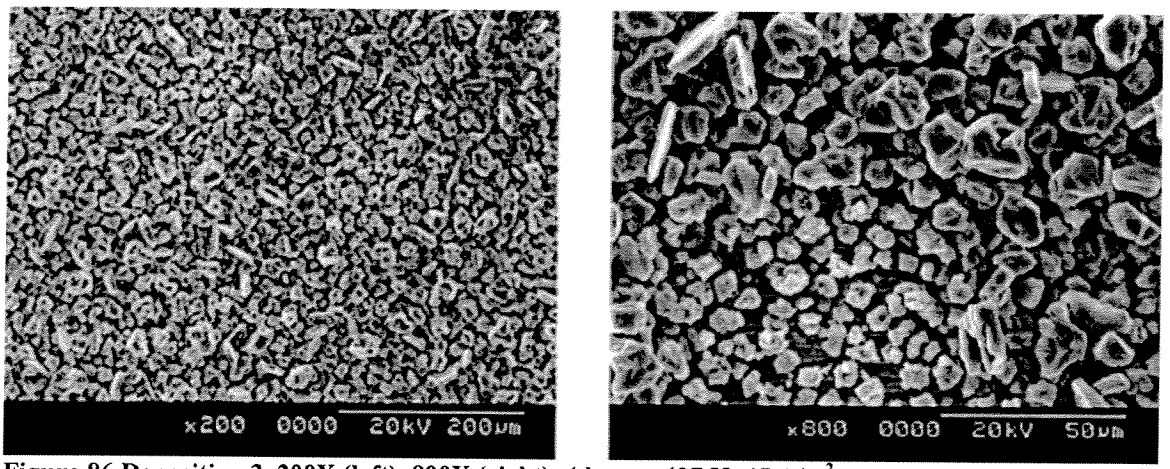

Figure 86 Deposition 3, 200X (left), 800X (right), 4 hours, 427 K, 45 A/m^2.

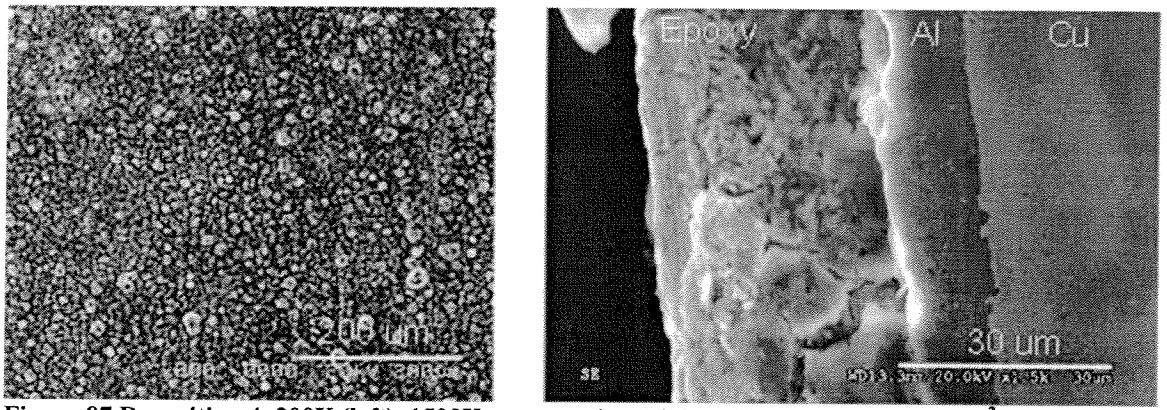

Figure 87 Deposition 4, 200X (left), 1500X cross-section (right), 4 hours, 429 K, 40 A/m^2.

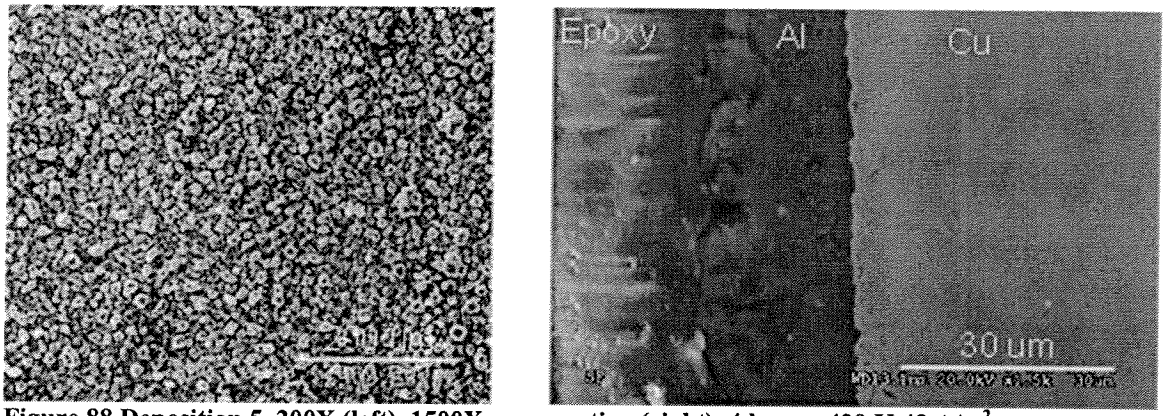

Figure 88 Deposition 5, 200X (left), 1500X cross-section (right), 4 hours, 429 K 48 A/m^2.

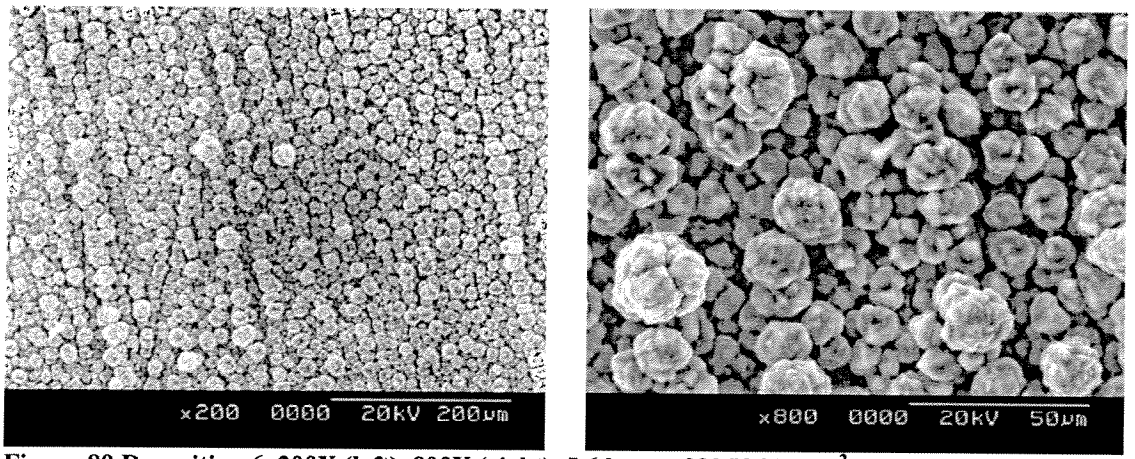

Figure 89 Deposition 6, 200X (left), 800X (right), 5.6 hours, 383 K 33 A/m^2.

Zhang and Reddy produced Al deposits with morphologies similar to depositions from BMIC-$AlCl_3$ at 353 K from an electrowinning set-up (Zhang 2006). They initially observed the small spherical structure (after 1 hour). The morphology changed to that of a deposit that has occluded some IL with higher IL circulation flow rates (5 and 20 ml/min) (after 2 hours).

4.4 Mini Pilot Plant

The purpose of the mini-pilot plant was to evaluate the re-usability of the bath as this will be critical to the feasibility of any industrial application. The apparatus is the same as described in Figure 63; a slightly larger test-tube was used. Kamavaram (2004) investigated the re-usability of a bath set-up to recycle aluminium metal matrix composites; it was found that the current density slowly decreased with each additional experiment, the decrease was about 5% after four two-hour experiments. The decrease was attributed to a declining electrolyte concentration, this was not explained further but presumably this meant that there was some contamination of oxygen or water and the aluminium chloride species were slowly being oxidized.

Potential controlled experiments were employed to study the deposition characteristics of Al from the purified solution. A temperature of 395 K was used. This temperature was chosen to maximize the reaction kinetics while minimizing possible losses of $AlCl_3$ as its vapour pressure at this temperature is approximately 0.012 atm. (Knovel 2005). Figure 90 is a plot of the change in current density with time during the deposition experiments. An increase in current density is an indication of the formation of a dendritic deposit as the surface area is increasing and the current density calculation is based on the original surface area only. The experiments at higher potentials (0.75 and 0.5 V) exhibited the highest current density and also the fastest growing dendrites that ended the experiments prematurely by short circuiting after 5.2 and 12.4 hours respectively. The experiments at 0.3 and 0.4 V also exhibited some dendritic growth; however, it was to a much lesser extent than that at 0.75 and 0.5 V. The dendrites grew preferentially at the corners and edges in all cases. The stirring of the solution using a magnetic stir bar increased the current density at 0.4 V slightly.

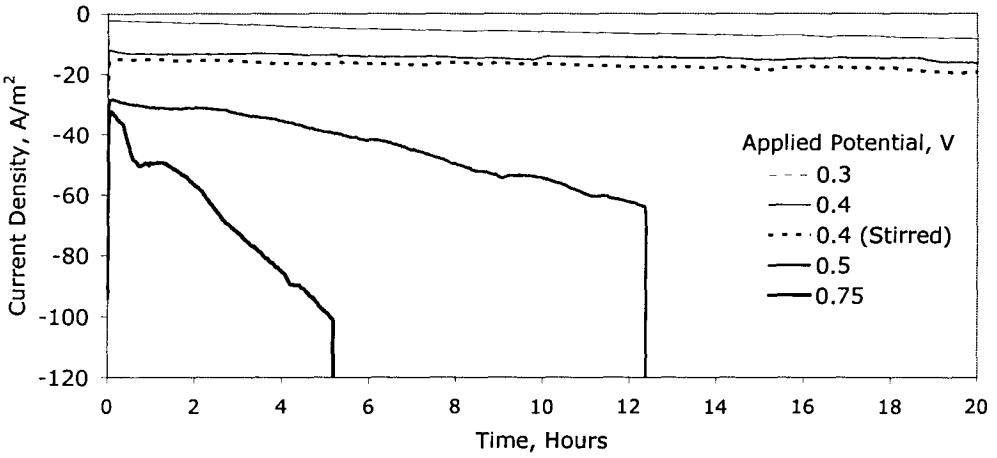

Figure 90 Potentiostatic deposition of Al from $AlCl_3$-$[P_{14,6,6,6}]Cl$ (X_{AlCl3} = 0.67) cathode potential set with respect to the Al CE. All of the experiments were carried out using the same solution. Solution was purified by removal of HCl by corrosion of pure Al and the $AlCl_3$ was sublimated. The temperature was 395 K +/- 2 K.

The deposits are characterized in terms of current efficiency, power consumption and deposit purity in Table 50. The current efficiency ranged from 84-108%. Experimental error in the measurement of the final cathode mass was due to loss of mass due to dendrites breaking off while rinsing with acetone. In some of the deposits the IL is also believed to be trapped in the deposit structure to a certain extent or was not removed completely during the rinsing process. There is also some current inefficiency due to hydrogen evolution; this was minimized by the purification procedure but was not eliminated completely. The deposit purity is an indication of the amount of IL that was entrained in the deposit near the surface, the Al/Cl ratio (wt./wt.) was obtained by an EDS area scan of the area shown in the bulk deposit micrographs (Figure 91-Figure 96 left). The deposit at 0.75 V was of the lowest purity as the fast dendritic growth trapped a considerable amount of the solution. Al was deposited in the electrowinning setup in the final experiment (number 7). Dimensionally stable anodes (DSA) were employed that were provided by PERMASCAND (DSA sample # PSC 101). The current efficiency was very low since $Cl_2(g)$ was likely re-oxidizing the deposit; however, a very thin and smooth deposit was visible. Under these conditions, there was no anode film formed on the DSA. There was no obvious degradation of the electroplating bath over the course of the campaign based on the experimental results. It was noticed that the solution became slightly darker and more viscous. This is attributed to an increase in the aluminium

oxides and oxychlorides due to slow contamination of moisture in the glove box and adsorbed on the electrode surfaces.

Table 50 Potentiostatic deposition of Al from $[P_{14,6,6,6}]Cl\text{-}AlCl_3$ (X_{AlCl3} = 0.67), Al or DSA anodes (~6 cm^2 total), copper cathode (~1 cm^2), anode-cathode spacing = 2 mm, temperature = 395 +/- 2 K, solution purified by corrosion of pure Al.

Experiment (In testing order)	Deposition Time Hours	Current Density A/m^2	Potential V	Current Efficiency %	Power Consumption kWhr/kg-Al	Deposit Purity (Al/Cl ratio)	Comments
1	5.2	67.5	0.75	-	-	1.3	Short Circuit
2	12.4	44.0	0.5	-	-	12.4	Short Circuit
3	20	5.8	0.3	84	1.06	35.9	-
4	20	14.3	0.4	97	1.23	6.1	-
5	20	17.0	0.4	90	1.32	13.2	Stirred
6	22	6.7	0.2	108	0.59	7.8	Galvanostatic
7	4	25	4.2	23	55	-	Galvanostatic DSA Anodes T = 417 K

It should be noted that the deposit morphology may be strongly influenced by the cell design and the cell design in for these experiments was not optimized. The first deposit that grew dendritically and quickly short circuited also appeared to occlude a significant amount of the ionic liquid based on the Al/Cl ratio. The low Al/Cl ratio is also due to the fact that the IL was not totally removed during rinsing since the structure was fragile and efforts were made to minimize sample loss. In Figure 91 (left) the bulk deposit is seen, it appears as if there are some spherically structured deposits with a layer of IL residue on the surface. The corner of this electrodeposit is where a large dendrite formed and extended out to the counter electrode Figure 91 (right).

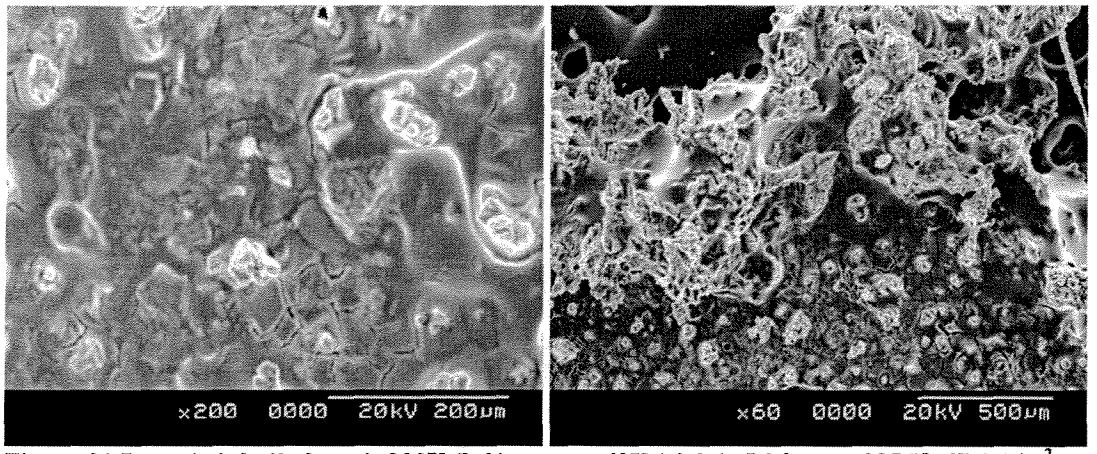

Figure 91 Deposit 1, bulk deposit 200X (left), corner 60X (right), 5.2 hours, 395 K, 67.5 A/m^2.

Dendritic growth always occurred preferentially at the edges, particularly the bottom edge of the deposit. The edge effects are mainly due to the concentration of the electric field. Another factor in this setup is the solution flow due to convection. The less dense solution from which Al was deposited flowed upwards resulting in a higher concentration of Al in solution near the bottom of the cathode. The dendrites in the unstirred solutions, deposits 2, 3 and 4 (Figure 92 Figure 93 Figure 94 (right)) were more pronounced than when the solution was stirred, deposit 5 (Figure 95 (right)).

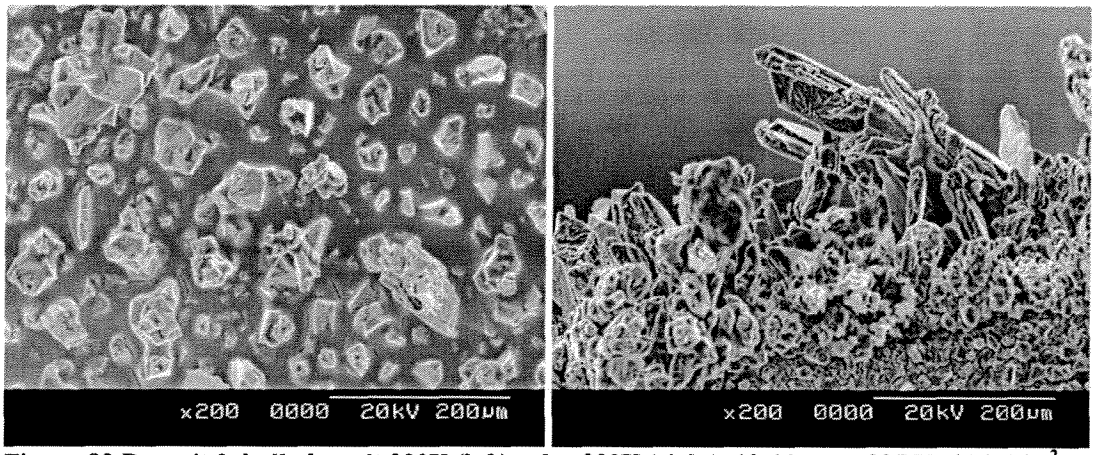

Figure 92 Deposit 2, bulk deposit 200X (left), edge 200X (right), 12.4 hours, 395 K, 44.0 A/m^2.

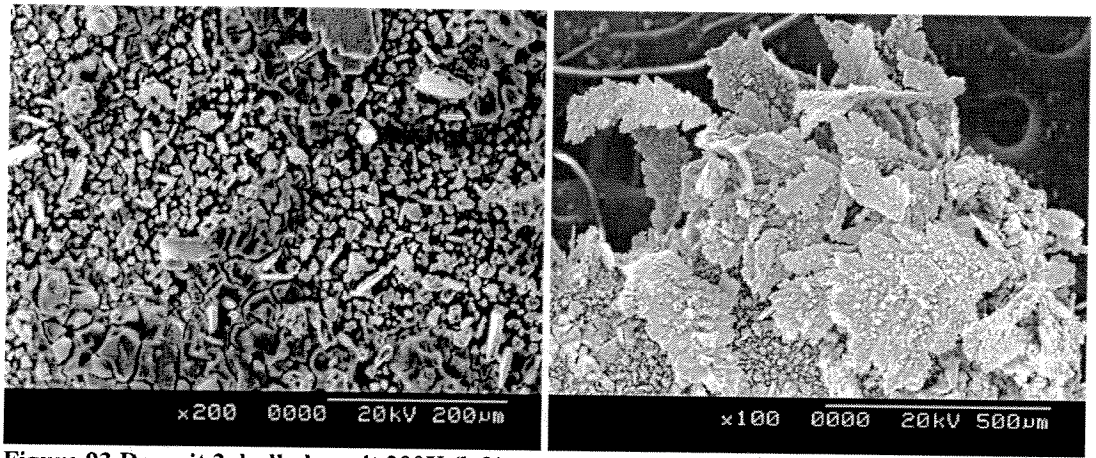

Figure 93 Deposit 3, bulk deposit 200X (left), corner 100X (right), 20 hours, 395 K, 5.8 A/m^2.

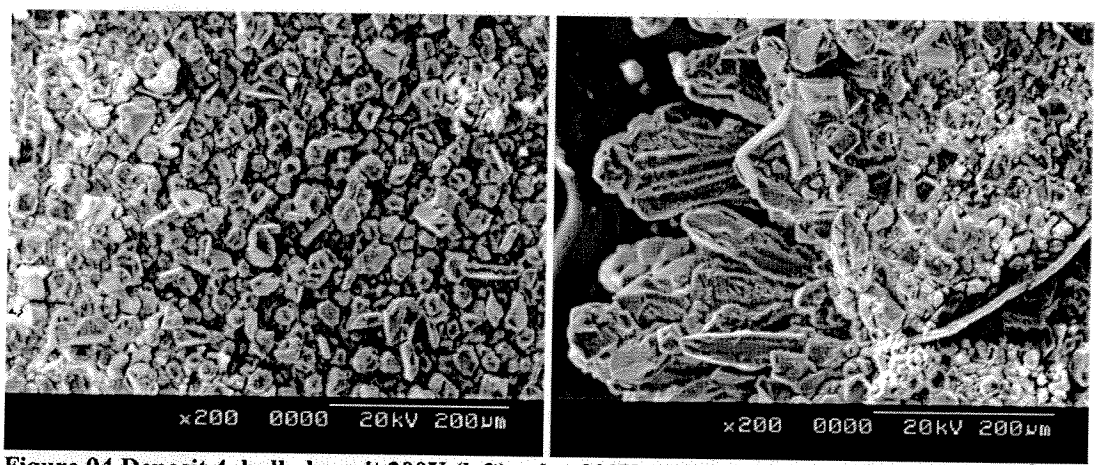

Figure 94 Deposit 4, bulk deposit 200X (left), edge 200X (right), 20 hours, 395 K, 14.3 A/m^2.

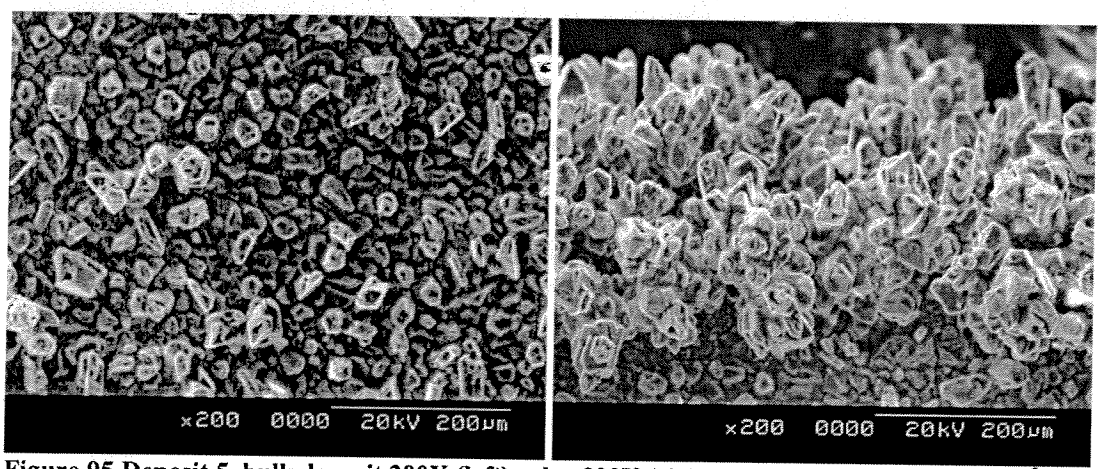

Figure 95 Deposit 5, bulk deposit 200X (left), edge 200X (right), 20 hours, 395 K, 17.0 A/m^2.

The galvanostatic deposit at 6.7 A/m^2 consisted of very small spheres and dendritic growth was less prevalent (Figure 96). The galvanostatic technique minimizes the dendritic growth because if the surface area is increased due to dendritic growth, the

applied potential will drop to maintain the set current; thus, the growth does not accelerate as in the case of the potentiostatic deposits at higher potentials (0.5 and 0.75).

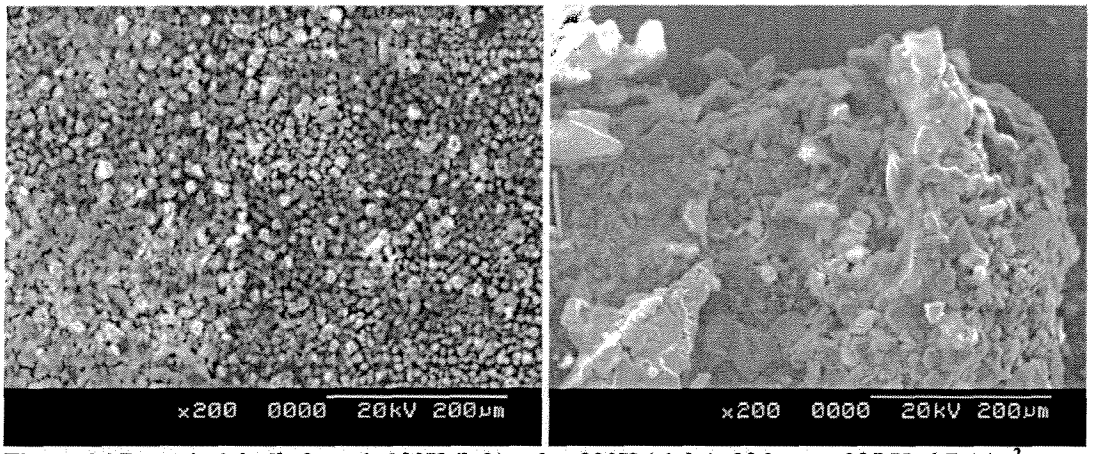

Figure 96 Deposit 6, bulk deposit 200X (left), edge 200X (right), 22 hours, 395 K, 6.7 A/m^2.

Deposits 2, 3 and 4 were cross sectioned and polished with 1 µm alumina powder (Figure 97 Figure 98). The aluminium deposit close to the copper substrate is generally smooth and dense (Figure 97).

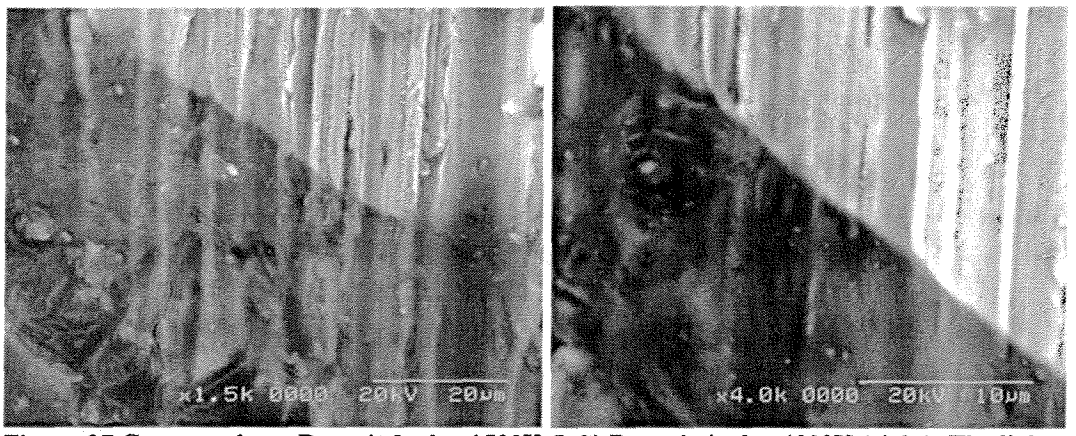

Figure 97 Cross sections: Deposit 2 edge 1500X (left) Deposit 4 edge 4000X (right), The lighter colour is the copper plate.

Figure 98 (left) is deposit 3, the current passed during this experiment was quite low, thus the deposit is quite thin. In Figure 98 (right) there appears to be some cracking of the deposit. The roughness is due to the dendritic structure and some cracking may have been introduced during grinding and polishing of the sample.

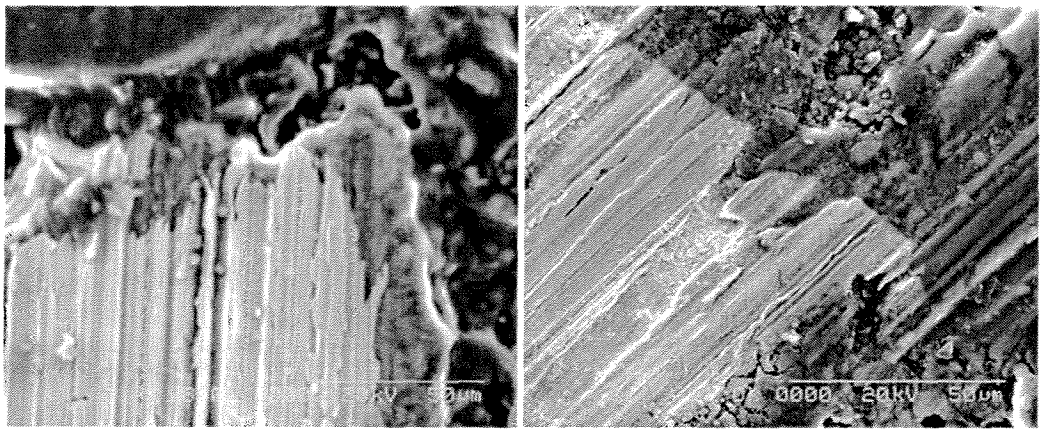

Figure 98 Cross sections: Deposit 3 corner 800X (left) Deposit 4 corner 1000X (right), The lighter colour is the copper plate.

4.5 Summary

Aluminium was electrodeposited from $AlCl_3$-$[P_{14,4,4,4}]Cl$ and $AlCl_3$-$[P_{14,4,4,4}]Cl$ (X_{AlCl3} = 0.6 and 0.67) at temperatures ranging from 373 to 429 K. Current efficiencies obtained were as high as 80% in the unpurified solution and above 95% in the purified solutions. Power consumptions as low as 0.6 kWh/kg-Al were observed (in the purified solution at low current density). In the electrowinning set-up, the current efficiency is compromised by the reoxidation of Al by $Cl_2(g)$.

The low power consumption of the experimental electrodeposition experiments is strongly dependent on the small anode-cathode spacing of 2 mm since the conductivity of the melt is low. If the anode-cathode spacing were to be increased the power requirement will increase greatly. This is shown in the following three Ettel diagrams (Figure 99, Figure 100 and Figure 101). Only the cathode overpotential (n_c), the potential loss due to resistance in the electrolyte (U_E) and the anode overpotential (n_a) were considered in these diagrams. The thermodynamic potential (EMF) for this Al electrodeposition experiment does not exist since the anode reaction is aluminium dissolution. The current efficiency should be near 100% if the melt is sufficiently free of protons (it was 90% for the experiment that Figure 99 is based on); it was not included in the diagrams. The loss of power due to resistance in the hardware (U_H) should be low since this process occurs at low temperatures. The process conditions are that of the potentiostatic electrodeposition experiment number 5 in Table 50 (395 K, 17 A/m^2). The anode overpotential was estimated to be triple that of the cathode overpotential based on the polarization curves in Figure 71, this varies with temperature. The electrolyte resistance was calculated using Equation 39 knowing that conductivity of the melt is 0.375 S/m from Figure 44. In the first Ettel diagram it was known that the overall potential was 0.4 V from the experiment. The following two diagrams were calculated by changing the anode-cathode spacing to 1 cm and 10 cm respectively. These are modest anode-cathode spacings for industrial standards; however, this causes high power requirements that hinder the economic viability of electrowinning or electrorefining processes that require $[P_{14,6,6,6}]Cl$ as the solvent.

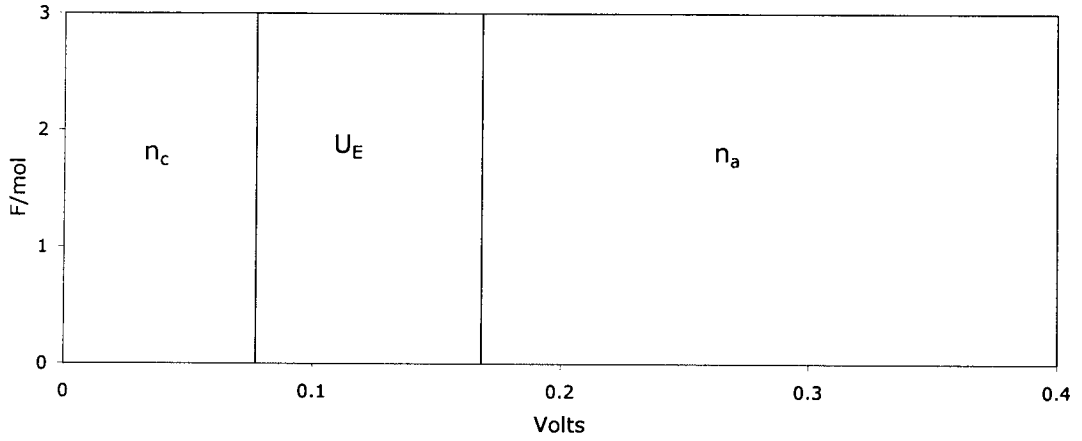

Figure 99 Ettel diagram for the electrodeposition of Al with an Al anode. The electrode spacing is 2 mm. The solution was $AlCl_3$-$[P_{14,6,6,6}]Cl$ (X_{AlCl3} = 0.67) at 395 K with a current density of 17 A/m^2.

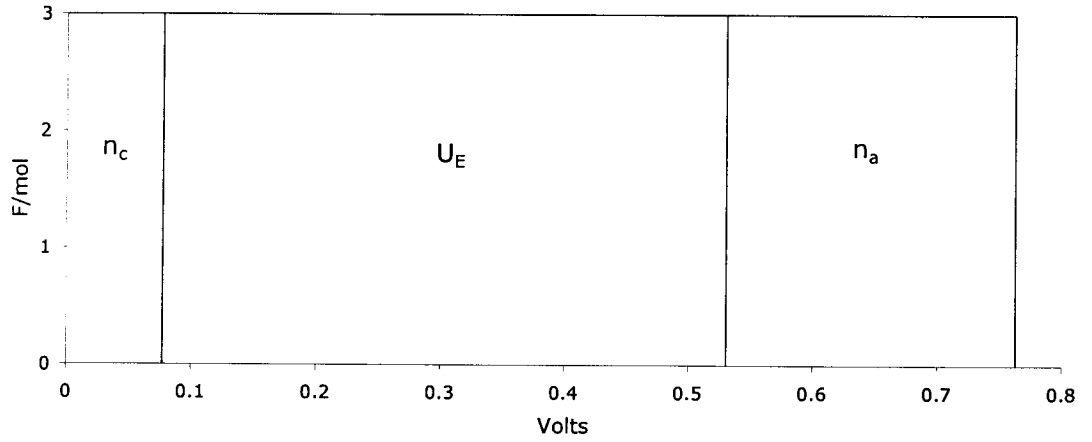

Figure 100 Ettel diagram for the electrodeposition of Al with an Al anode. The electrode spacing is 1 cm. The solution was $AlCl_3$-$[P_{14,6,6,6}]Cl$ (X_{AlCl3} = 0.67) at 395 K with a current density of 17 A/m^2.

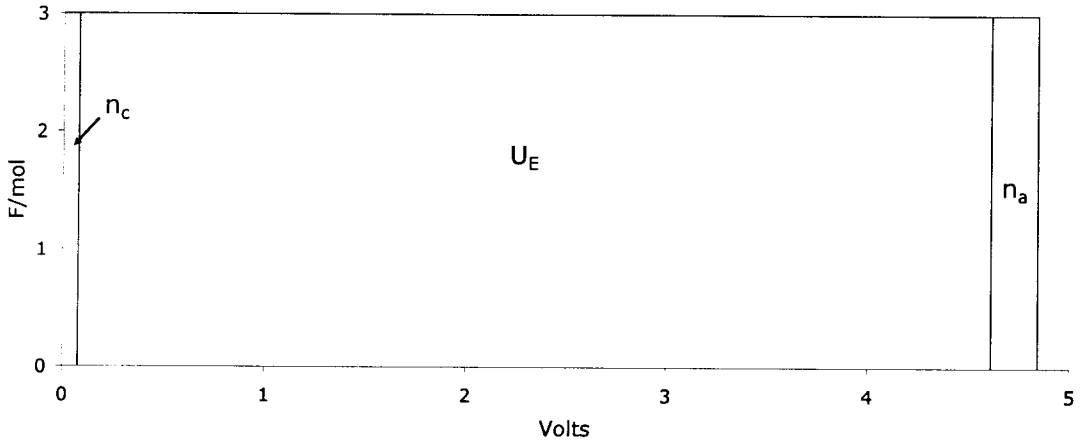

Figure 101 Ettel diagram for the electrodeposition of Al with an Al anode. The electrode spacing is 10 cm. The solution was $AlCl_3$-$[P_{14,6,6,6}]Cl$ (X_{AlCl3} = 0.67) at 395 K with a current density of 17 A/m^2.

Summary

The Al deposit morphology ranged from spherical deposits of varying size to dendritic growth. In many cases the dendrites grew preferentially on the edges. The purity of metal deposited was very high, EDS spot analyses often revealed only Al and a small amount of oxygen. However, in many of the deposits the IL was occluded, this was characterized by the ratio of Al to Cl of an area EDS measurement. Solution agitation may help reduce occlusion of the IL.

In Winand's theory of electrocrystallization (1992) the electrodeposit morphology is related to two parameters. The first is the ratio of the current density to the concentration of the metal containing ion that is to be reduced and the second is the deposit inhibition. Inhibition can be affected by the presence of ions different from that containing the metal to be deposited that hinder the cathodic process. The ions $[P_{14,6,6,6}]^+$, $[P_{14,4,4,4}]^+$, $AlCl_4^-$, H^+ may act as inhibitors in these systems. During the deposition of Cu from H_2SO_4-$CuSO_4$ solutions, $[N_{2,2,2,2}]Cl$ is considered a weak inhibitor as it blocks the development of spiral growth (Winand 1992, p. 573). Based on Winand's diagram of polycrystalline electrodeposits, the deposition of Al appears to be operating at low to medium inhibition intensity and high to very high current density to concentration ratio. By increasing the inhibition intensity, the dendritic growth could be minimized. Muresan and Varvara explain that compact smooth, adherent and bright deposits are obtained when the charge transfer overpotential is moderate and the electrocrystallization overpotential is large (Muresan 2005). These parameters can be modified to some extent with temperature, stirring and current density however; the most common practice is the addition of some type of additive known as a leveler or brightener.

Levelling by the addition of a leveling agent occurs when the leveling agent is adsorbed at the surface of a protrusion slowing the growth at this high point. The roughness of Al deposits from $AlCl_3$-MEIC (X_{AlCl3} = 0.67) solutions was improved by the addition of small amounts of 1,10-phenanthroline (Takahashi, 1999). Oleic ($C_{18}H_{34}O_2$) and linoleic acid ($C_{18}H_{32}O_2$) were used to increase the quality of aluminium electrodeposited on copper from a room temperature solution of $AlCl_3$ and $LiAlH_4$ in ether (Schickner 1960). Aluminum deposit quality was improved in $AlBr_3$-EBP (0.67 X_{AlBr3}) systems with toluene by the addition of about 1% methyl tert-butyl ether ($C_5H_{12}O$) (Safranek, 1954). Safranek's patent also claims that ethyl ether ($C_2H_5OC_2H_5$),

diphenyl oxide ($C_{12}H_{10}O$), dimethyl aniline ($C_8H_{11}N$), di-o-tolyl-urea ($C_{15}H_{15}ON_2$), di-o-tolyl-thiourea ($C_{15}H_{16}N_2S$) and dichloroethylene ($C_2H_2Cl_2$) aid in giving the desired bath properties.

An Al electrowinning process will likely require some type of a separator to isolate the catholyte or anolyte to reduce the re-oxidation of deposited Al by $Cl_2(g)$. Celgard® 4510 microporous polypropylene film was used in a concentration cell with 0.33 X_{AlCl3} as the anolyte and 0.6 X_{AlCl3} as the catholyte in MEIC (Dymek, 1984). Nafion was used as the separator in a rechargeable Cd-Br battery (Dymek, 1987).

The electroplating baths can probably be re-used indefinitely since the cation is not being reduced. Problems will arise from the slow contamination by moisture and oxygen that result in the formation of aluminium chlorides and oxychlorides. They do not pose any immediate problems but over time will likely interfere with the process due to increased solution viscosity and loss of $AlCl_3$. Methods to chlorinate the oxychlorides such as with phosgene gas should be investigated. If the bath is operated at high temperature and high concentration of $AlCl_3$, there will be some loss of $AlCl_3$ to the gas phase. Operation under pressure would help reduce this and possibly extend the allowable operating temperature range higher which would increase reaction kinetics.

Chapter 5 Reduction of Titanium

Two solutions of $TiCl_4$-$[P_{14,6,6,6}]Cl$ were prepared at different $TiCl_4$ concentrations (X_{TiCl4} = 0.333 and 0.5). The clear and colourless liquid $TiCl_4$ was added to a clear and colourless liquid $[P_{14,6,6,6}]Cl$ at room temperature. The more dense $TiCl_4$ turned yellow upon contact with the $[P_{14,6,6,6}]Cl$ and fell to the bottom of the test-tube. A 99.7% pure titanium sheet was immersed in the solution (in contact with both layers) in an attempt to reduce the Ti(IV) to Ti(III) or Ti(II) by oxidizing the metallic titanium. The corrosion of the titanium metal was very low. After one week (no mixing) there remained two distinct layers, a clear and colorless upper layer (mainly $[P_{14,6,6,6}]Cl$)) and a coloured lower layer (mainly $TiCl_4$). The lower layer colour was yellow and green for X_{TiCl4} = 0.33 and 0.5 respectively. Upon mixing, a homogenous solution was obtained. The mixing reaction was exothermic with the formation of some bubbles, probably mainly HCl from the reaction of $TiCl_4$ with the 0.15 wt.% water impurities in the $[P_{14,6,6,6}]Cl$. Asides from the titanium oxychlorides formed, titanium is believed to exist mainly as $TiCl_6^{-2}$ in the X_{TiCl4} =0.333 mixture and $TiCl_5^-$ in the X_{TiCl4} =0.5 mixture. Ti(IV) is known to be complexed as $TiBr_6^{-2}$ in basic $AlBr_3$-MEIB ILs (Sun 1989) and the reduction to of Ti(IV) to Ti(III) is described by Equation 53.

$$TiBr_6^{2-} + \bar{e} = TiBr_6^{3-} \qquad [53]$$

The reference electrode and counter electrodes were Ti plates. The RE was exposed to the solution 1 mm from the WE, it was isolated from the solution elsewhere using a thick layer of Teflon tape. The open circuit potential of the copper plate was negative with respect to the Ti metal indicating that the Ti was in a passive state and that the reference potential was stabilized by the Ti(IV)/Ti(III) couple. Since the concentration of Ti(III) was very low, this potential is shifted upwards. The copper on the other hand may be stabilized set by the corrosion of Cu.

The cathodic polarization of Cu was studied in the two mixtures over a range of temperatures (Figure 102 and Figure 103). At the lower concentration of $TiCl_4$ (X_{TiCl4} = 0.33) the reduction curve is fairly smooth, the majority of the current is probably due to the reduction of Ti(IV) to Ti(III), there may be some contribution from the reduction of H^+.

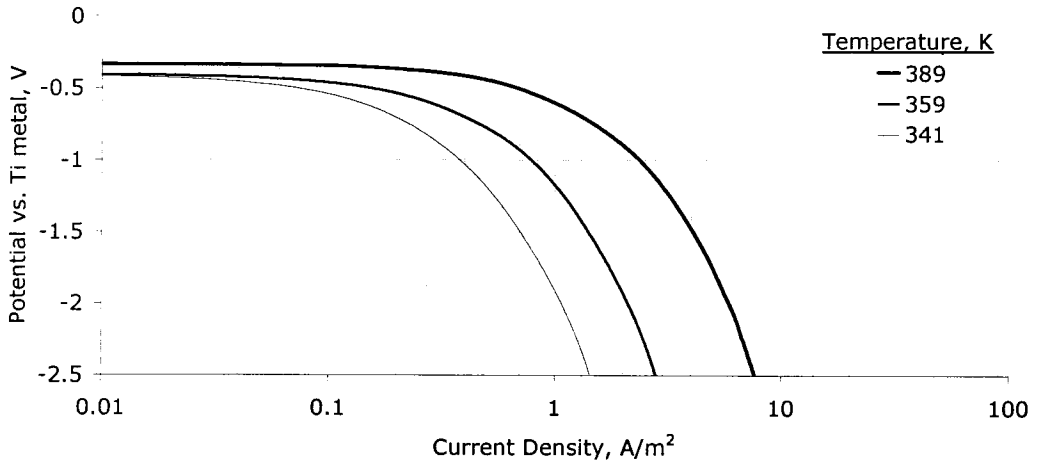

Figure 102 Cathodic polarization of Cu in $TiCl_4$-[$P_{14,6,6,6}$] (X_{TiCl4} = 0.33), solution stirred. Cu WE (0.5 cm^2), Ti CE (16 cm^2), Ti RE. WE-CE spacing = 2 mm. WE-RE spacing = 1 mm. Scan rate = 5 mV/s.

At higher concentrations of $TiCl_4$ (X_{TiCl4} = 0.5), the cathodic current is roughly increased by an order of magnitude (Figure 103). At potentials of about -1.2 V vs. Ti metal, a second reduction current is observed, this is attributed to the reduction of Ti(IV) and Ti(III) to Ti(II).

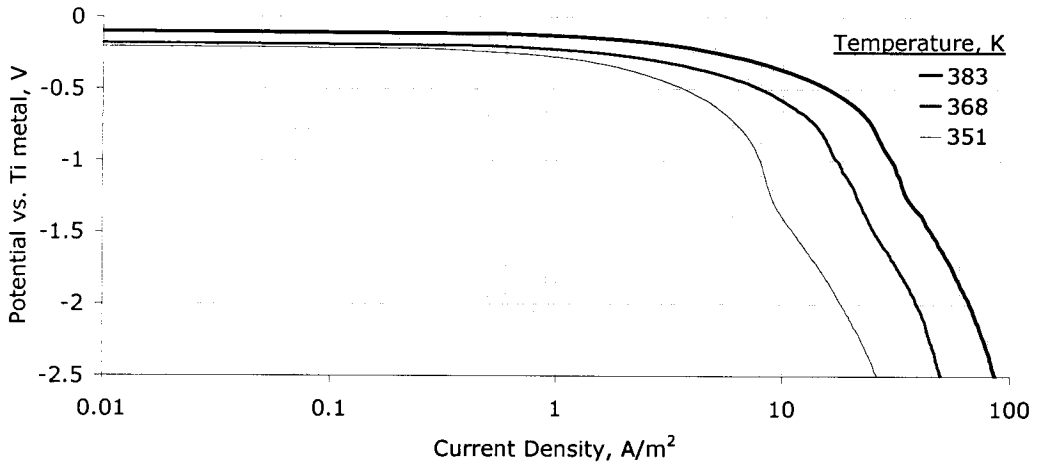

Figure 103 Cathodic polarization of Cu in $TiCl_4$-[$P_{14,6,6,6}$] (X_{TiCl4} = 0.5), solution stirred. Cu WE (0.7 cm^2), Ti CE (16 cm^2), Ti RE. WE-CE spacing = 2 mm. WE-RE spacing = 1 mm. Scan rate = 5 mV/s.

Magnesium powder (99.8% Pure, Density = 1.74 g/cm^3, Max particle size = 50 μm from Goodfellow, England) was added to both titanium solutions at a ratio of 1 mole Mg : 1 mole of $TiCl_4$ in an attempt to reduce the Ti(IV) to Ti(III) or Ti(II). No extensive reaction was observed at room temperature and the temperature of the solution remained

relatively unchanged. However, the solution colour in the 0.33 X_{TiCl4} system changed from an orange to a slightly green colour indicating the formation of Ti(III).

The 0.33 X_{TiCl4} solution was heated to 373 K and stirred for six hours. Following the heating and mixing, cathodic scans were performed over a range of temperatures (Figure 104). The observed currents are higher than those in the solutions before Mg was added.

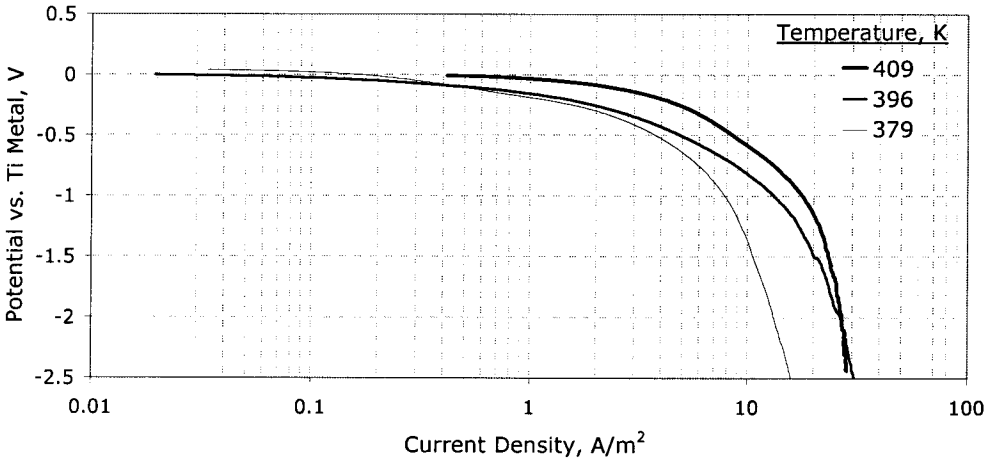

Figure 104 Cathodic polarization of Cu in $TiCl_4$-$[P_{14,6,6,6}]$ (X_{TiCl4} = 0.33) after adding Mg powder. Cu WE (0.5 cm^2), Ti CE (16 cm^2), Ti RE. WE-CE spacing = 2 mm. WE-RE spacing = 1 mm. Scan rate = 5 mV/s, solution stirred.

Prior to cathodically polarizing the X_{TiCl4} = 0.5 solution with Mg added, titanium plates were cyclically polarized overnight to attempt to remove HCl. It was observed that the current density was quite low initially but it increased with the number of cycles (Figure 105). This was not expected, if anything, the current density should decrease slightly as the HCl impurities were consumed. The initial current is limited due to the oxidation of Ti(III) to Ti(IV). The increase in current was determined to be due to the corrosion of the titanium plates Ti to Ti(III) or Ti(IV). The total mass of Ti lost was 0.0314 g with 20 cm^2 exposed after being cyclically polarized for 24 hours.

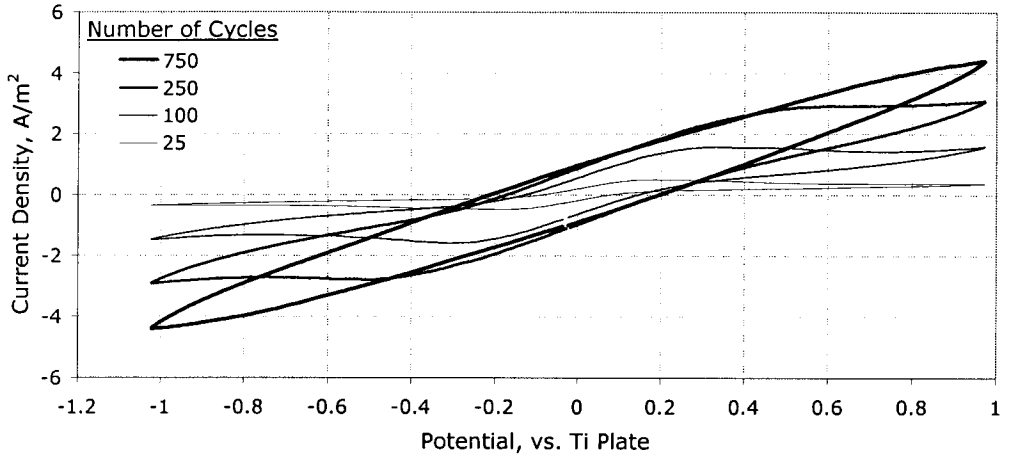

Figure 105 Cyclic polarization of Ti plates (10 cm^2 each), Ti plate RE $TiCl_4$-$[P_{14,6,6,6}]$ (X_{TiCl4} = 0.5) after adding Mg powder, solution stirred. Scan rate = 50 mV/s, temperature = 373 K.

Following the cyclic polarization, the copper cathode setup was introduced into the solution and the copper was cathodically polarized to -2.5 V vs. a Ti metal reference (Figure 106). Notice that the open circuit potential of the copper is very close to 0 at all temperatures indicating that the potential of both metals (Cu WE and Ti RE) are being held constant by the Ti(III)/Ti(IV) couple. Upon polarization, the initial current is attributed to the reduction of Ti(IV) to Ti(III). There is also a second current that becomes apparent at potentials below about -2.1V at 377 K and below about -1 V at 399 and 413 K. This second current could be due to the reduction of the $[P_{14,6,6,6}]^+$ cation, or also the reduction of Ti(IV) and Ti(III) to Ti(II) is a possibility.

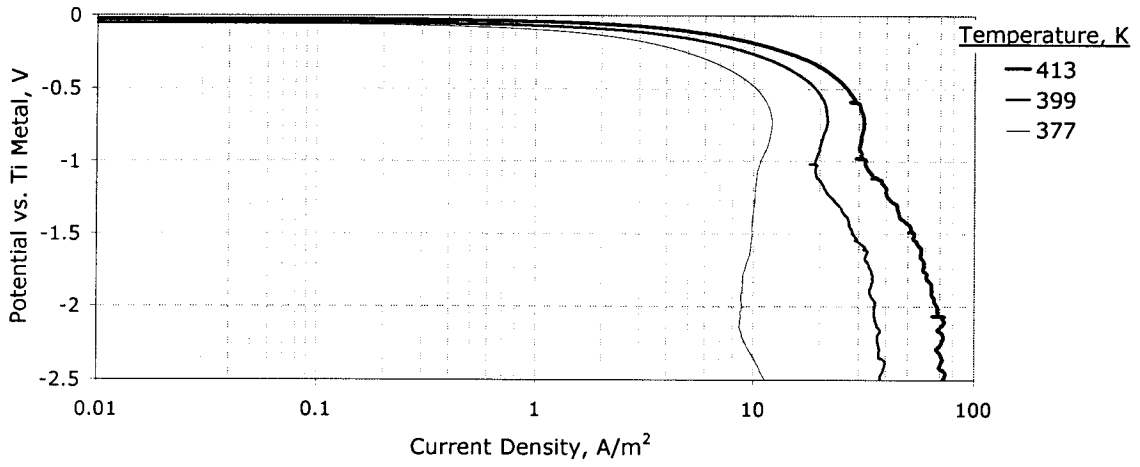

Figure 106 Cathodic polarization of Cu in $TiCl_4$-$[P_{14,6,6,6}]$ (X_{TiCl4} = 0.5) after adding Mg powder, solution stirred. Cu WE (0.5 cm^2), Ti CE (16 cm^2), Ti RE. WE-CE spacing = 2 mm. WE-RE spacing = 1 mm. Scan rate = 5 mV/s, solution stirred.

The potentiostatic deposition of Ti was attempted in the $TiCl_4$-$[P_{14,6,6,6}]$ mixtures by cathodic polarization at -2.5 V for approximately 2 hours. The $X_{TiCl4} = 0.5$ solution exhibited a higher current density than $X_{TiCl4} = 0.33$ however, in both cases there was no Ti deposited. The Mg powder was collecting on the $X_{TiCl4} = 0.5$ electrode set-up probably causing the roughness observed and eventually leading to a short circuit.

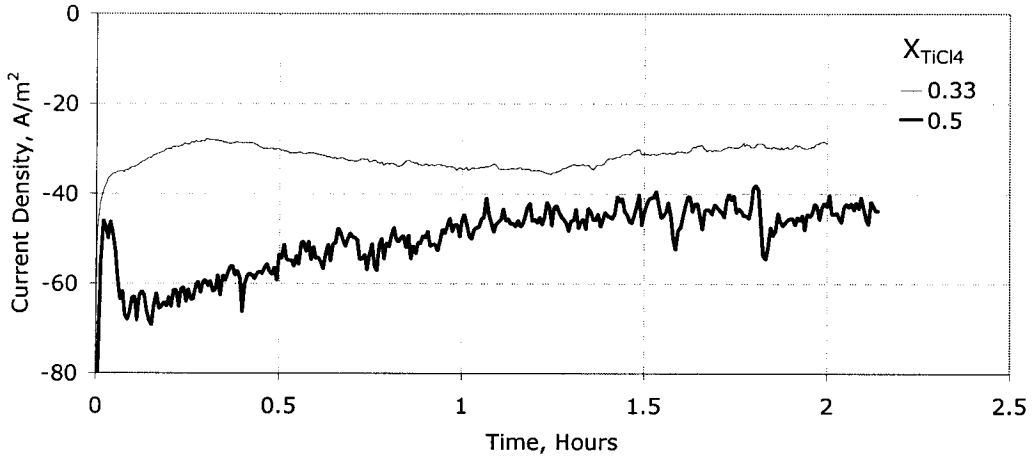

Figure 107 Potentiostatic polarization of Cu (0.5 cm^2) at -2.5 V vs. Ti metal, in $TiCl_4$-$[P_{14,6,6,6}]$ (after adding Mg powder, Ti plate CE's (16 cm^2 total) at 413 K, solution stirred.

Although these experiments did not yield a Ti deposit, it is not concluded that it is impossible to deposit Ti from these solutions. It is important to pre-reduce the Ti(IV) and isolate the anodic reaction from the cathode to eliminate the possibility of Ti(IV) being converted to Ti(III) at the cathode. Corrosion of titanium was attempted but failed because the passive layer protected the metal sufficiently, however, it was shown that with cyclic polarization of the Ti, dissolution of the metal is possible in these solutions (at least at $X_{TiCl4} = 0.5$). Also, using Mg powder to reduce Ti(IV) was attempted, it appears that some reduction did take place but the reaction did not proceed quickly or to completion despite the heating and stirring.

Chapter 6 Conclusions and Recommendations

The density, viscosity and conductivity of tetra-alkyl phosphonium ILs were evaluated over large temperature range. Linear density temperature functions were determined. The viscosity and conductivity temperature functions were modeled with the VTF equation. The conductivity of the phosphonium ILs tested was found to be lower than for other common ILs, this is mainly attributed to the relatively large cation size. Since electrolyte conductivity is an important parameter for electrowinning and refining, the low conductivity of the phosphonium ILs may limit their commercial application. Some more conductive phosphonium ILs might be produced by selecting different alkyl chains. The small cation size is desirable in terms of conductivity but too small of a cation will result in ILs with high melting temperature. Since asymmetry in the cation lowers the melting point of the liquids it is recommended to develop tetra alkyl phosphonium ILs cations based on triethyl, trimethyl or tripropyl phosphine combined with a longer halo-alkane or possibly a phenyl group similar to TMPAC.

Many binary metal chloride-IL mixtures were prepared and characterized in terms of their conductivity. Aluminium, iron and titanium chloride were soluble in the chloride ILs and resulted in increased solution conductivity. Some efforts should be made to characterize the titanium chloride-IL system using NMR or Raman spectroscopy since no literature information was found on the subject. The solubility of magnesium chloride in the chloride ILs was much lower and no increase in conductivity was observed. The solubility of magnesium chloride was higher in $[P_{14,6,6,6}]BF_4$ and $[P_{14,6,6,6}]N(CN)_2$, thus, the chemistry of these systems should be studied. Also, the anodic reactions of the non-chloride or bromide ILs should be studied since these ILs generally exhibited higher conductivity and this information is not readily available in the literature.

The $AlCl_3$-$[P_{14,6,6,6}]Cl$ system was studied using electrochemical polarization techniques. The electrochemical window of $[P_{14,6,6,6}]Cl$ was determined to be considerably larger than EMIC (~0.8 V). This is an important finding as the phosphonium ILs may be a more suitable choice of IL where a high cathodic polarization is required. The diffusion of $Al_2Cl_7^-$ was determined from the peak current during

cathodic polarization and calculated using the Berzins-Delahay formula. The verification of these values using experimental techniques is proposed for future work.

Electrodeposition of aluminium from the chloride system was studied over a range of temperatures, solution chemistries and anode-cathode configuration. The deposition current densities obtained are low compared with previously tested imidazolium systems. This is due to the large cation / low solution conductivity. At high cathodic polarization, the current density is limited by diffusion of the electroactive species ($Al_2Cl_7^-$). The anode reaction is limited by passivation at lower temperatures. The current efficiency was compromised by the presence of HCl and $Cl_2(g)$. The current efficiency was improved from 70-80% to above 90%. This was done by removing HCl by corroding of cyclically polarizing pure Al. With careful removal of HCl in the refining set-up current efficiencies approaching 100% should be obtainable. As for the electrowinning setup, the presence of $Cl_2(g)$ can also compromise the current efficiency, this gas must be separated from the cathode. Future work should be done to determine best way to separate the $Cl_2(g)$. With a high current efficiency and lower current density, the specific power consumption was found to be quite low (as low as 0.6 kWhr/kg-Al in the refining setup).

The deposit morphology is another important parameter. A range of different deposits were observed during this study. The presence of HCl and $Cl_2(g)$ can have a leveling effect by preferentially dissolving any protrusions from the deposit. With higher current densities, dendritic structures tended to be formed. Research should be undertaken to identify possible leveling agents that are effective and have a minimal impact on the current efficiency and overall power consumption. Cell design should also be more carefully considered in future work as the current distribution will affect the deposit morphology as well as other operational parameters.

A high resistance solid film was found to form on the glassy carbon anode during prolonged electrodeposition experiments at high temperature, future work should be done to ensure that there is no detrimental interaction between chlorine gas that is produced and the ionic liquid. Also, in some situations, the aluminium electrodeposit morphology was such that ionic liquid was occluded causing a resistance barrier at the cathode, this

usually happened when a deposit was attempted on material other than Cu. The presence of an oxide film on the cathode is suspected to promote this undesirable deposit. The oxide probably limits the mobility of the adsorbed aluminium species resulting in the formation of a powdery deposit. Methods should be devised to remove these oxides so that these processes can be flexible as to which substrate is used.

For the commercial application of these solutions it is important that they can be re-used for long periods of time. The main problem with the aluminium chloride system is the inevitable buildup of aluminium oxychlorides and aluminium oxide. Although they seem to be relatively inert, eventually they will cause problems by increasing the solution viscosity. Methods must be developed to either remove these contaminants or possibly re-chlorinate then in-situ.

The operating temperature of a process that involves the deposition of Al from $AlCl_3$-phosphonium IL, should be as high as possible to minimize energy consumption and maximize kinetics. It would make sense to carry out these reactions in a pressurized vessel. This would help in maintaining the inert atmosphere, allow higher temperatures and help maintain the $AlCl_3$ in the solution since its vapour pressure is not insignificant. Phosphonium ILs will withstand higher temperatures than imidazolium ILs.

As for the deposition of Ti, it was shown that the titanium tetrachloride can be electrochemically reduced; however, no metal deposits were observed at the conditions tested. Since Ti has multiple oxidation states (Ti(IV), Ti(III) and possibly Ti(II)) it will be necessary to pre-reduce most of the titanium first before electrodeposition will occur. This pre-reduction was attempted by corroding Ti and by adding Mg powder but in both cases reaction did not proceed to completion. Passivation of the Ti and Mg are likely interfering with the reactions and further work should be undertaken to tackle this issue. Also, this reduction could be carried out electrochemically but will require that the anolyte and catholyte are separated.

References

ABBOTT, A.P., D. Boothby, G. Capper, D.L. Davies, R.K. Rasheed, 2004. Deep Eutectic Solvents Formed between Choline Chloride and Carboxylic Acids: Versatile Alternatives to Ionic Liquids. *J. Am. Chem. Soc.* 126(29), 9142-9147.

ABBOTT, A.P., C.A. Eardley, N.R.S. Farley, G.A. Griffith, A. Pratt, 2001. Electrodeposition of aluminium and aluminium/platinum alloys from $AlCl_3$ / benzyltrimethylammonium chloride room temperature ionic liquids. *Journal of Applied Electrochemistry,* 31 p. 1345-1350.

ABDALLAH, D.J., A.J. Robertson, H. Hsu, R.G. Weiss, 2000. Smectic Liquid-Crystalline Phases of Quaternary Group VA (Especially Phosphonium) Salts with Three Equivalent Long n-Alkyl Chains. How Do Layered Assemblies Form in Liquid-Crystalline and Crystalline Phases? *J. Am. Chem. Soc.* 122, p. 3053-3062.

ABDUL-SADA, A.K., A.M. Greenway, K.R. Seddon, T. Welton, 1989. Upon the existence of $[Al_3Cl_{10}]^-$ in room temperature chloroaluminate ionic liquids. *Organic Mass Spectrometry*, 24 p. 917-918.

ADAM, G. and J.H. Gibbs, 1965. On the Temperature Dependence of Cooperative Relaxation Properties in Glass-Forming Liquids. *Journal of Chemical Physics*, Vol. 43 (1), p. 139-146.

ALPERT, M.B., F.J. Schultz and W.F. Sullivan, 1957. Electrolytic Preparation of Titanium from Fused Salts I. Preliminary Electrolytic Studies with Diaphragmed Cells. *Journal of The Electrochemical Society,*. Vol. 104 (9), p. 555-559.

ANDREASSEN, K., Aune, T. K., Haugerød T., *et al.*, 1997. 20 Magnesium. *In:* F. Habashi, *ed. Volume II - Handbook of Extractive Metallurgy*, Wiley-VCH, Toronto, 981-1038.

ANGELL, C.A. and C.T. Moynihan, 1969. *In: Molten Salts Characterization and Analysis*. G. Mamantov Ed. Marcel-Dekker, New York, p. 315-375.

ANTREKOWITSCH, H., G. Hanko, P. Ebner, 2002. Recycling of Different Types of Magnesium Scrap, *In:* H.I. Kaplan, *ed. Magnesium Technology 2002*, TMS, 43-48.

ARORA, S.M., 1986. Aluminium Coatings for Corrosion Control. *Proceedings of Electrodeposition and Electroforming,* R.P. Damba and J. Balachandra Eds., Feb 20-22, Bangalore India.

AUDRIETH, L.F. and H.W. Nelson, 1931. Electrodeposition of Metals from Non-Aqueous Solvents. *Chem. Rev.*, Vol. 8, No. 2, April, p. 335-352.

AURBACH, D., 1999. *Nonaqueous Electrochemistry*. New York: Marcel Dekker Inc.

AURBACH, D., A. Schechter, M. Moshkovich, Y. Cohen, 2001. On the Mechanisms of Reversible Magnesium Deposition Processes. *Journal of The Electrochemical Society*, Vol. 148 (9), p. A1004-A1014.

AUTHIER-MARTIN, M., Forte G., Ostap S., See J., 2001. The mineralogy of bauxite for producing smelter-grade alumina, *JOM*, 53(12), 36-40.

BARD, A. J., R. Parsons, J. Jordan, eds. 1985. *Standard Potentials in Aqueous Solution.* New York: Marcel Dekker Inc.

BARKSDALE, J., 1966. *Titanium Its Occurrence, Chemistry and Technology*. 2nd Edition, The Ronald Press Company, New York.

BECK, T.R., 1926. Method of Recovering Light Metals form Scrap and the Like. US Patent 1,576,080.

BERKOWITZ, J. B. and N.H. Emerson, 1972. *Plating Methods*. NASA SP-5114, Arthur D. Little Inc. Washington, D.C.

BERZINS, T., and P. Delahay, 1952. Oscillographic Polarographic Waves for the Reversible Deposition of Metals on Solid Electrodes. *J. Am. Chem. Soc.* Vol. 75, p. 555-559.

BLUE, R.D. and F.C. Mathers, 1936. Aluminum plating from organic baths. *Transactions of the Electrochemical Society*, p. 519-527.

BOCKRIS, J.O.M., and A.K.N. Reddy, 1998. *Modern Electrochemistry 1 Ionics 2nd Edition*. Plenum Press, New York.

BOLKAN, S.A., J.T. Yoke, *Inorg. Chem.* 134, p. 1698.

BOXALL, L.G., H.L. Jones, R.A. Osteryoung, 1973. Solvent Equilibria of $AlCl_3$-NaCl Melts. *J. Electrochem. Soc.* February, p. 223-231.

BRADARIC, C., A. Downard, C. Kennedy, A. J. Robertson and Y. Zhou, 2003. in *Ionic Liquids as Green Solvents Progress and Prospects*, R. Rogers and K. Seddon, Editors, American Chemical Society, p. 41.

BRENNER, A. and J. L. Sligh, 1971 *Trans. Inst. Met. Finish, 49.*

BRITISH GEOLOGICAL SURVEY, 2002. *World Mineral Statistics 1998–2002,* Minerals Programme Publication No. 16

BRITISH GEOLOGICAL SURVEY, 2004. Magnesium commodity profile. Available from: http://www.mineralsuk.com/britmin/magnesium_23Apr04.pdf
[Accessed 10 December 2004]

CALLISTER, W.D., 1997. *Materials Science and Engineering an Introduction*, 4th ed. Toronto: John Wiley & Sons, Inc.

CAPUANO, G.A., W.G. Davenport, 1984. Cathodic Polarization of Aluminum in Alkylbenzene Electrolytes, *J. Electrochem. Soc.*, November, 2595-2600.

CARLIN, R.T., and R.A. Osteryoung, 1989. Aluminum Anodization in a Basic Ambient Temperature Molten Salt. J. Electrochem. Soc. Vol. 136, No. 5, May, 1409-1415.

CHADWICK, R., *et al.*, 1958. 4 New Extraction Processes for Metals *In:* C. Singer, E.J. Holmyard, A.R. Hall, T.I. Williams, eds., *A History of Technology Volume V - The Late Nineteenth Century*, London: Oxford University Press, 72-101.

CHISHOLM, D.S., Method of Producing Crude Metal. U.S. Patent 3,102,807 1963.

CHEN, G.S., I.W. Sun, K.D. Sienerth, A.G. Edwards, G. Mamantov, 1993. Removal of Oxide Impurities from Alkali Haloaluminate Melts Using Carbon Tetrachloride. *J. Electrochem. Soc.,* Vol. 140, No. 6, p.1523.

CHEN, G.Z., D.J. Fray and T.W. Farthing, 2000. Direct Electrochemical Reduction of Titanium Dioxide to Titanium in Molten Calcium Chloride, *Nature*, 407, 361.

CHEN, H., D.C. Kwait, Z.S. Gönen, B.T. Weslowski, D.J. Abdallah,| R.G. Weiss, 2002 Phase Characterization and Properties of Completely Saturated Quaternary Phosphonium Salts. Ordered, Room-Temperature Ionic Liquids. *Chem. Mater.* 14, p. 4063-4072.

CHOATE, W.T., A. Aziz, R. Friedman, 2005. New Technologies Will Sustain the U.S. Primary Aluminum Industry. *Light Metals 2005*, Halvor Kvande Ed., TMS, p. 495-500.

CHOATE, W.T., and J.A.S. Green, 2003. U.S. Energy Requirements for Aluminum Production: Historical Perspective, Theoretical Limits and New Opportunities, U.S. Department of Energy and Renewable Energy, Washington, D.C., U.S.A.

CLAYTON, F.R., G. Mamantov, D.L. Manning, 1973a. Electrochemical Studies of Titanium in Molten Fluorides. *J. Electrochem. Soc.*, September, p. 1193.

CLAYTON, F.R., G. Mamantov, D.L. Manning, 1973b. Electrochemical Studies of Titanium in Molten Sodium Tetrafluoroborate. *J. Electrochem. Soc.*, September, p. 1199.

COHEN, M.H. and D. Turnbull, 1959. Molecular Transport in Liquids and Glasses. *J. Chem. Phys.* 31: 1164.

CONNOR, J.H., W.E. Reid Jr., G.B. Wood, 1957. Electrodeposition of Metals from Organic Solutions V. Electrodeposition of Magnesium and Magnesium Alloys. Journal of the Electrochemical Society, January, Vol. 104, p. 38-41.

COUCH, D.F. and A. Brenner, 1952. A Hydride Bath for the Electrodeposition of Aluminum. *J. Electrochem. Soc.* (99) p. 234-244.

CYTEC INC., Phosphonium Salt Information Sheets. Available from: www.cytec.com
[Accessed 1 December 2006]

CREBER, D., 2004-2006. Personal Communications, David is a senior engineer with Alcan Inc. and works in the area of electrolytic processes.

DAVIDSON, A.W., 1925. Solutions of Salts in 100% Sulfuric Acid. Solvolysis and Double Decomposition Reactions. *J. Am. Chem. Soc.*47, p. 968.

DAVIES, C.W. and A.M. James, 1976. *A Dictionary of Electrochemistry*. The Macmillan Press Ltd. London.

DAVIS, J., C. Gordon, C. Hilgers, P. Wasserscheid, 2003. in Ionic Liquids in Synthesis, P. Wasserscheid and T. Welton, Editors, Wiley-VCH, Germany, p. 17.

DEAN, R.S., 1959. Method of Reducing Titanium Oxide. U.S. Patent 2,904,428.

DEL SESTO, R.E., F. Ghebremichael, N. E. Heimer, 2003. Nonlinear Optical Ionic Liquids, C. Low and J. S. Wilkes, Eds. A.C.S. 226th National Meeting, New York, September 7-11.

DIAW, M., A. Chagnes, B. Carré, P. Willmann and D. Lemordant, 2005. *J.Power Sources,* 146, p. 682.

DOGONADZE, R.R., Chizmadzhev, Y.A., 1964. *Proc. Acad. Sci., SSSR, Phys. Chem. Sect.* (Engl), 157, 778.

DYMEK, C.J. Jr., J.L. Williams, D.J. Groeger, 1984. An Aluminum Acid-Base Concentration Cell Using Room Temperature Chloroaluminate Ionic Liquids. *J. Electrochem. Soc.,* Vol. 131, No. 12. p. 2887-2892.

DYMEK, C.J. Jr., G.F. Reynolds, J.S. Wilkes, 1987. A Rechargeable Cadmium-Bromine Battery Using Room Temperature Chloroaluminate Molten Salts. *J. Electrochem. Soc.,* Vol. 134, No. 7, p. 1658-1663.

ELKINS, D.A. et al. 1967. An Economic and Technical Evaluation of Magnesium Production Methods, Part 2; Carbothermic, US Bureau of Mines RI 6946.

ENDRES, F., 2003. in *Ionic Liquids in Synthesis*, P. Wasserscheid and T. Welton, Editors, Wiley-VCH, Germany, p. 294-318.

ESIN, O.A., 1956. *Zh. Fiz. Khim.*, 30, 3.

ETTEL, V.A., 1977. Energy Requirements in Electrolytic Winning and Refining of Metals. CIM Bulletin, July, p. 179.

EVANS, J.W., 1995. Electricity in the Production of Metals: From Aluminum to Zinc. *Metallurgical and Materials Transactions B,*Vol 26B, April, 189-208.

EVANS, J.W., 2007. The Evolution of Technology for Light Metals over the Last 50 Years: Al, Mg, and Li. *JOM*, February, p. 30-38.

EVANS, W.V. R. Pearson, D. Braithwaite, 1941. Electrolysis of arylmagnesium bromides in ethyl ether: the behavior of short-lived aryl-free radicals. *J. Am. Chem. Soc.* 63, p. 2574-6.

FANNIN, A.A. Jr., D.A. Floreani, L.A. King, J.S. Landers, B.J. Piersma, D.J. Stech, R.L. Vaughan, J.S. Wilkes, J.L. Williams, 1984. *J. Phys. Chem.*, 88, p. 2614.

FAURE, C. and J. Marchal, 1964. Magnesium by the Magnetherm Process. *Journal of Metals*, Sept, 721-723.

FICARA, P., E. Chin, T. Walker *et al.*, 1998. Magnola: A novel commercial process for the primary production of magnesium. *CIM Bulletin.* Vol. 91, No 101, 75-101.

FORTÉ, G. and Girard R., 2004. Alcan Bayer Process Experimental Centre, M.J. Collins and V.G. Papangelakis, eds. *Pressure Hydrometallurgy 2004, 34th Annual Hydrometallurgy Meeting*, Oct 23-27, Banff, Alberta, Canada, 43-54.

FRANK, W.B., Haupin W.E., Dawless R.K., *et al.*, 1997. 21 Aluminum *In:* F. Habashi, ed., *Volume II - Handbook of Extractive Metallurgy*, Toronto: Wiley-VCH, 1039-1127.

FRAY, D.J. and G. Z. Chen, 2004. Reduction of titanium and other metal oxides using electrodeoxidation. *Materials Science and Technology*, Vol. 20, p. 295.

FRENCH, H.E. and M. Drane, 1930. Electrolysis of Grignard Solutions. *J. Am. Chem. Soc.* 52, p. 4904.

FROATS, A., 1980. Pidgeon Silicothermic Process in the 70's. *In:* C. J. McMihn ed. *Light Metals*, 969-979.

FULLER, J., R.T. Carlin, R.A. Osteryoung, 1997. The Room Temperature Ionic Liquid 1-Ethyl-3-methylimidazolium Tetrafluoroborate: Electrochemical Couples and Physical Properties. *J. Electrochem. Soc.*, Vol. 144, No. 11, p. 3881-3886.

FUNG, K.W. and G. Mamantov, 1972. Electrochemistry of Titanium(II) in $AlCl_3$+NaCl Melts. *J. Electroanal. Chem.*, 35 p. 27-34.

FÜRTH, R., 1941a. On the Theory of the Liquid State, I. The Statistical Treatment of the Thermodynamics of Liquids by the Theory of Holes. *Proc. Cambridge Phil, Soc.* 37: 252.

FÜRTH, R., 1941b. On the Theory of the Liquid State, II. The Hole Theory of the Viscous Flow of Liquids. *Proc. Cambridge Phil, Soc.* 37: 281.

GALASIU, I., R. Galasiu, J. Thonstad, 1999. Chapter 9 Electrochemistry of Molten Salts, *In:* D. Aurbach *ed.*, *Nonaqueous Electrochemistry*, Marcel Dekker, Inc. New York, 461-591.

GALE, J. and R.A. Osteryoung, 1979. Inorg. Chem. 18, p 1603.

GALE, R.J. and R.A. Osteryoung, 1980. J. Electrochem. Soc., 127, p. 2167.

GAMBLE, H.A., et al., 2003. A streamlined, portable mid-IR TDL based system for on-site monitoring of PFC's from potroom exhaust ducts. Light Metals Warrendale, PA, United States, 215-219.

GITLITZ, J. 2002. Trashed Cans the Global Environmental Impacts of Aluminum Can Wasting in America, Container Recycling Institute, Arlington, Virginia, U.S.

GRAEF, M.W.M, 1985. The Mechanism of Aluminum Electrodeposition from Solutions of $AlCl_3$ and $LiAlH_4$ in THF. *J. Electrochem. Soc.* Vol. 132. No. 5, p. 1038-1046.

GRJOTHEIM, K., C. Krohn, M. Malinovký, K, Matiašovský, J. Thonstad, 1977. Aluminium Electrolysis The Chemistry of the Hall-Héroult Process. Aluminium-Verlag GmbH·Düsseldorf.

GRJOTHEIM, H. and Kvande H., eds. 1993. Introduction to Aluminium Electrolysis. Understanding the Hall-Heroult Process, 2nd edition, Aluminium Verlag.

GOWDA, G.A.N, H. Chen, C.L. Khetrapal, R.G. Weiss, 2004. Amphotropic Ionic Liquid Crystals with Low Order Parameters. *Chem. Mater.* 16, p. 2101-2106.

HABASHI, F., 1997. 1 The Metal Industry *In:* F. Habashi, ed. *Volume I - Handbook of Extractive Metallurgy*, Toronto: Wiley-VCH, 1-23.

HARRIS, R., S. Kashani-Nejad and K.W. Ng , 2006. Current Magnesium Production Technologies - Where should they head?. Presented at the Conference of Metallurgists, Montreal, Magnesium Technology in the Global Age Symposium, October 2.

HARTLEY, F.R., Ed. 1994. The Chemistry of Organophosphorus Compounds Vol. 3: Phosphonium Salts, *Ylids and Phophoranes*, John Wiley and Sons Inc., New York, USA.

HEADDEN, W.P, 1921. *Colorado Agr. Exp. Sta. Bull.* 267.

HILGERS, C., 2003. in *Ionic Liquids in Synthesis*, P. Wasserscheid and T. Welton, Editors, Wiley-VCH, Verlag, p. 20.

HOLBREY, J.D., R. D. Rogers, 2003. 3.1 Melting Points and Phase Diagrams. *In:* P. Wasserscheid, T. Weldon eds., *Ionic Liquids in Synthesis*, Wiley-VCH, 41-55.

HOLLECK, G.L., J. Giner, 1972. *The* Aluminum Electrode in $AlCl_3$-Alkali-Halide Melts, *J. Electrochem. Soc.*, Vol. 119, No. 9, 1161-1166.

HUDSON, R. F., 1968. Structure and Mechanism in Organo Phosphorus Chemistry, Academic Press, p. 211.

HURLEY, F. and T. Weir, 1951. *J. Electrochem. Soc.*, 207-212.

HUSSEY, C. L., 1983. Room Temperature Molten Salt Systems *In:* G. Mamantov, Ed. *Advances in Molten Salt Chemistry 5*, New York: Elsevier, 185-230.

HUSSEY, C.L., 1985. Transport Numbers in the Basic Aluminum Chloride-1-Methyl-3-Ethylimidazolium Chloride Ionic Liquid. *J. Electrochem. Soc.*, Vol. 132, No. 9 p. 2156.

HUSSEY, C.L., 1986. Chloroaluminate Equilibria in the Aluminum Chloride-1-Methyl-3-ethylimidazolium Chloride Ionic Liquid. *J. Electrochem. Soc.*, Vol. 133, No. 7, p.1389-1391.

HUSSEY, C.L. and J.R. Sanders 1987. Aluminum Bromide-1-Methyl-3-Ethylimidazolium Bromide Ionic Liquids II. Transport Numbers, *J. Electrochem. Soc.*, Vol. 134, No. 8 p. 1977.

HUSSEY, C., 1988. Room Temperature Haloaluminate Ionic Liquids. Novel Solvents for Transition Metal Solution Chemistry, *Pure & Appl. Chem.* Vol. 60, No. 12, p. 1763-1772.

HYDRO MAGNESIUM, 1995. Magnesium in Automotive: An Environmentally Sound Solution.

ISSACS, A., 1979. *The Penguin Dictionary of Science, 5th Edition,* E.B. Uvarov, D.R. Chapman, eds. Markham, Canada: Penguin Books Ltd.

JACOBS, S.C. and R.C. Schoener, 1975. Effluent gas recycling and recovery in electrolytic cells for production of aluminum from aluminum chloride. U.S. Patent 3,904,494.

JENKINS, H.D.B., H.K. Roobottom, J. Passmore, L. Glasser, 1999, *Inorg. Chem.,* 38, 3609.

JENKINS, H.D.B., 2005. Personal Communications.

JI, J., 1994. Fundamental Aspects of Nickel Electrowinning from Chloride Electrolytes. PhD Thesis. The University of British Columbia.

JOHNSON, W.A., 1993. *Ylids and Imines of Phosphorus*, John Wiley and Sons Inc. New York, USA.

JONES, S.D. and G.E. Blomgren, 1989. Low-Temperature Molten Salt Electrolytes Based on Aralkyl Quaternary or Ternary Onium Salts. *J. Electrochem. Soc.*, Vol. 136, No. 2, p. 424-427.

KAMAVARAM, V. and R.G. Reddy, 2005. Thermal Stabilities and Viscosities of Low Temperature Aluminum Electrorefining Electrolytes: Di-Alkyl Imidazolium Chloride Ionic Liquids. *Light Metals 2005.* Halvor Kvande, Ed. TMS, p. 501-505.

KAMAVARAM, V. 2004. Novel Electrochemical Refining of Aluminum Based Materials in Low Temperature Ionic Liquid Electrolytes. PhD Thesis, The University of Alabama.

KAMAVARAM, V. and R.G. Reddy, 2002. Electrochemical Studies of Aluminum Deposition in Ionic Liquids at Ambient Temperatures. *Proceedings of Light Metals 2002, at the 131st TMS Annual Meeting.* Wolfgang Schneider, Editor, p. 253.

KAWASE, M., 2005. in *Metal Electrodeposition*, M. Nunez, Editor, Nova Science Publishers Inc., p. 129-149.

KEYES, D.B., S. Swan, 1933. Process of Electrodeposition of Aluminum, US Patent 1,939,397.

KNOVEL, 2005. Online Chemical Database Available from: www.knovel.com
[Accessed 2005]

KOLTHOFF, I.M. and F.G. Thomas, 1964. Polarography in Acetonitrile of Titanium Tetrachloride and Tetraiodide in Various Supporting Electrolytes. *J. Electrochem. Soc.*, Vol. 111, No. 9, p. 1065-1073.

KORBEL, P. and M. Novák, 1999. *The Complete Encyclopedia of Minerals*, Lisse, the Netherlands: Rebo International.

KORNYSHEV, A. A., 2007. Double-Layer in Ionic Liquids: Paradigm Change? *J. Phys. Chem. B*, 111, (5545-5557).

KORONAIOS, P. and R.A. Osteryoung, 2001. Buffering of 1-Ethyl-3-methylimidazolium Chloride/Aluminum Chloride Ionic Liquids Using Alkali Metal Bromides and Iodides. *J. Electrochem. Soc.*, 148(12) E483-E488.

KRAMER, 2004. Magnesium Metal *In: U.S. Geological Survey, Mineral Commodity Summaries,* U.S. Department of the Interior, VA, U.S.A. Available from:
http://minerals.usgs.gov/minerals/pubs/mcs/2004/mcs2004.pdf (104-105).
[Accessed 10 December 2004]

KROLL, W. J., 1965. A Contribution to the History of Ductile Titanium and Zirconium. *J. Less-Common Metals*, 8, 361-367.

KURAYASU, H., Y. Inokkuma, 1993. Determination of Oxide Ions in Aluminum Chloride-Alkali Chloride Melts by Karl Fisher Titration. *Anal. Chem.* 65, p. 1210-1212.

LABLIN, E.L., 1917. British Patent 106,400 Cf. C.A. 14, 3200.

LAI, P.K. and M. Skyllas-Kazacos, 1987. Aluminium Deposition and Dissolution in Aluminium Chloride-n-Butylpyridinium Chloride Melts. *Electrochim. Acta.,* Vol. 32. p. 1443-1449.

LEGRAND, L., A. Tranchant, R. Messina, 1994. Behaviour of Aluminum as Anode in Dimethylsulfone-Based Electrolytes. *Electrochimica. Acta.*, 39, No. 10, p. 1427-1431.

LIAO, Q., W. R. Pitner, G. Stewart, C. L. Hussey, G. R. Stafford, 1997. *J. Electrochem. Soc.*, Vol. 144, No. 3 March.

LINGA, H., Z. Stojek, R.A. Osteryoung, 1981. *J. Am. Chem. Soc.*, 103, 3754.

LIPSZTAJN, M., R.A. Osteryoung, 1983. Increased Electrochemical Window in Ambient Temperature Neutral Ionic Liquids. *J. Electrochem. Soc.*, Vol. 130 p. 1968-69.

LIPSZTAJN, M., R.A. Osteryoung, 1985. On Ionic Association in Ambient Temperature Chloroaluminate Molten Salts, *J. Electrochem. Soc.,* Vol. 132, No. 5, p. 1126-1130.

LU, J., and D. Dreisinger, 2003. in *Ionic Liquids as Green Solvents Progress and Prospects*, R. Rogers and K. Seddon, Editors, American Chemical Society, Boston p. 495.

LYSENKO, A. P. et al., 1987. Tsvetn. Met. no. 8, 53-55.

MALLOUK, T.E., G.L. Rosenthal, G. Muller, R. Busasco, N. Bartlett, 1984. *Inorg. Chem.* 23, 3167-3173.

MANTZ, R., J. Summers, R.A. Osteryoung, 1998. Behaviour of Oxide Containing Chloroaluminate Molten Salts, *11th International Symposium on Molten Salts, Electrochemical Society Proceedings*, San Diego, 231-243.

MANTZ, R. and P. Trulove, 2003. in *Ionic Liquids in Synthesis,* P. Wasserscheid and T. Welton, Editors, Wiley-VCH p. 62.

MAYER, A., 1990. Electrodeposition of Aluminum, Aluminum/Magnesium Alloys and Magnesium from Organometallic Electrolytes. *J. Electrochem. Soc.*, Vol. 137, No. 9. p. 2806-2809.

MCEWEN, A.B., H.L. Ngo, K. Lecompte, J.L. Goldman, 1999. *Journal of the Electrochemical Society*, 146(5), 1687-1695.

MEHNERT, C.P, N.C. Dispenziere, R.A. Cook, 2005. Method for preparing high-purity ionic liquids. U.S. Patent 6,852,229.

MURESAN, L.M., and S.C. Varvara, 2005. Levelling and Brightening Mechanisms in Metal Electrodeposition, *In: Metal Electrodeposition*, M. Nunez, Editor. Nova Science Publishers Inc. New York, p. 1-45.

MUZHZHAVLEV, K. D. and O. A. Lebedev, 1964. Trudy Vsesoyuznogo Alyuminievo – Magnievogo Instituta, No. 53:65.

NAGAMORI, M., and A. J. Plumpton, 1999. Thermodynamic and technico-economic analysis of the HCl-leach of magnesite and serpentine. *CIM Bulletin*, Vol. 92, N° 103, 64-71.

NAGESH, CH. R. V. S., CH. S. Rao, N.B. Ballal, and P. K. Rao, 2004. Mechanism of Titanium Sponge Formation in the Kroll Reduction Reactor. *Metallurgical and Materials Transactions B*, 35B, Feb, 65-74.

NOBUAKI, I., M. Yamaguchi, K. Kato, S. Ampo, 2005. Process for producing metallic titanium. U.S. Patent 6,942,715.

NODA T., 1988. Recent progress in Ti sponge production in OTC (Part 2) *In:* L.G. Oxall ed. *Light Metals*, 759-768.

NOEL, M.A., P.C. Trulove, R.A. Osteryoung, 1991. *Anal. Chem.*, 63, 2892.

O'GRADY, W.E. and G.T. Cheek, 2007. Low temperature refining and formation of refractory metals. U.S. Patent 7,169,285.

OVERCASH, D.M. and F.C. Mathers, 1933. *Trans. Electrochem. Soc.,* 64, p. 305.

ØYE, H.A., M. Jagtoyen, T. Oksefjell, J.S. Wilkes, 1991. Vapour Pressure and Thermodynamics of the System 1-Methyl-3-ethyl-imidazolium chloride-aluminium chloride. *Materials Science Forum*. Vol. 73-75, p. 183-190.

ØYE, H.A., N. Mason, R.D. Peterson, *et al.*, 1999. Aluminum: Approaching the New Millennium, *JOM*, 51 (2) 29-42.

PAUNOVIC, M., M. Schlesinger, 1998. *Fundamentals of Electrochemical Deposition.* Toronto: John Wiley & Sons, Inc.

PELED, E., E. Gileadi, 1976. The Electrodeposition of Aluminium from Aromatic Hydrocarbon, *J. Electrochem. Soc.*, January, p. 15-19.

PLUNKERT, P.A., 2004. Bauxite and Alumina *In: U.S. Geological Survey, Mineral Commodity Summaries,* U.S. Department of the Interior, VA, U.S.A. Available from: http://minerals.usgs.gov/minerals/pubs/mcs/2004/mcs2004.pdf (31-32). [Accessed 25 November 2004]

PLUNKERT, P.A., 2007. Bauxite and Alumina *In: U.S. Geological Survey, Mineral Commodity Summaries,* U.S. Department of the Interior, VA, U.S.A. Available from: http://minerals.usgs.gov/minerals/pubs/commodity/bauxite/bauximcs07.pdf [Accessed 18 April 2007]

POPOV, K.I., S.S. Djokić, B.N. Grgur, 2002. Fundamental Aspects of Electrometallurgy. Kluwer Academic / Plenum Publishers, New York.

QUANG-MIN, H. N. and Neng-Ping Y., 1983. The Extraction of Metals by Molten Salt Eleectrolysis of Sulfides *In:* G. Mamantov, Ed. *Advances in Molten Salt Chemistry 5*, New York: Elsevier, 231-276.

QUINN, B.M., Z. Ding, R. Moulton, A.J. Bard, 2001. Novel Electrochemical Studies of Ionic Liquids. *J. Am. Chem. Soc.* Langmuir A-I.

RAMAKRISHNAN, S. and P. Koltun, 2004. A Comparison of the Greenhouse Impacts of Magnesium Produced by Electrolytic and Pidgeon Processes, In: A. A. Luo Ed. Magnesium Technology 2004, TMS, 173-178.

REID, W.E. Jr., J.M. Bish, A. Brenner, 1957. Electrodeposition of Metals from Organic Solutions. *J. Electrochem. Soc.* January, p. 21-29.

RICHARDS, N.E., 1994. Strategies for Decreasing the Unit Energy and Environmental Impact of Hall Heroult Cells, U. Mannwiler ed. *Light Metals* Warrendale, PA, U.S., 393-402.

RIOPELLE, L., 1996. The Recycling of Magnesium Makes Cents. *JOM*, 48(10), 44-51.

ROBINSON, J. and R.A. Osteryoung, 1980. *J. Electrochem. Soc.* 127, p. 122.

ROLLAND, P., and G. Mamantov, 1976. Electrochemical Reduction of $Al_2Cl_7^-$ Ions in Chloroaluminate Melts. *J.Electrochem. Soc.,* September, p. 1299-1303.

ROOBOTTOM, H.K. and H.D.B. Jenkins, 1999. Thermochemical Radii of Complex Ions. *Journal of Chemical Education*, Vol. 76. No. 11, p. 1570-1573.

SAFRANEK, W.H., W.C. Schickner and C.L. Faust, 1952. Electroforming Aluminum Waveguides Using Organo-Aluminum Plating Baths. *J. Electrochem. Soc.* Feb, p. 53-59.

SAFRANEK, W.H., W.C. Schickner, C.L. Fraust, 1954. Aluminum Electroforming. US Patent 2,692,850.

SAHAMI, S., and R.A. Osteryoung, 1983. Voltammetric Determination of Water in an Aluminum Chloride-N-n-Butylpyridinium Chloride Ionic Liquid. *Analytical Chemistry*, Vol. 55, No. 12, October, p. 1970.

SANDERS, J., E. Ward, C. Hussey, 1986. *J. Electrochem. Soc.*, 133, 325.

SCHEFFLER, T. B, S.M. Thomson, 1990. Proceedings - Electrochemical Society, 90-17 Proc. Int. Symp. Molten Salts, 7th, 281-9.

SCHICKNER, W.C., 1960. Process of Electroplating Metals with Aluminum. US Patent 2,934,478.

SCHOEBRECHTS, J.P. and B.P. Gilbert, 1981. On the Tetrachloroaluminate Dissociation in Aluminum Chloride-1-n Butylpyridinium Chloride Mixtures. *J. Electrochem. Soc.*, December, p. 2679-2684.

SEDDON, K.R., A. Stark, M.-J. Torres, 2000. Influence of chloride, water and organic solvents on the physical properties of ionic liquids. *Pure Appl. Chem.*, Vol. 72, p. 2275-2287.

SHAVKUNOV, S.P., and T.L. Strugova, 2003. Electrode Processes during Aluminum Electrodeposition on Aromatic Solvent. *Russian Journal of Eelectrochemistry*, Vol. 39, No. 6, p. 642-649.

SIBUM, H., 2003. Titanium and Titanium Alloys – From Raw Material to Semi-finished Products. *Advanced Engineering Materials*, 5, No. 6, 393-398.

SIBUM, H., Westerhaus A., Woditsch P. *et al.*, 1997. 22 Titanium *In:* F. Habashi, ed. *Volume II - Handbook of Extractive Metallurgy*, Toronto: Wiley-VCH, Toronto, 1129-1180.

SIMANAVICIUS, S., 1990. Chemija, 178, 3.

SIVILOTTI, O.G., 1988. Operating Performance of the Alcan Multipolar Magnesium Cell In: L.G. Oxall ed. Light Metals, 817-822.

SMEDLEY, S., 1980. The Interpretation of Ionic Conductivity in Liquids, Plenum, New York.

STAFFORD, G.R., V.D. Jovic, C.L. Hussey, 2000. Electrodeposition of Cu-Al Alloys and Underpotential Deposition of Al onto Cu Single Crystals from a Room-Temperature Chloroaluminate Molten Salt, Materials Science Forum, Vol. 352, p. 49-56.

STRELETS, Kh. L., 1977. Electrolytic production of magnesium. Translated from Russian by J. Schmorak, Jerusalem: Keterpress Enterprises.

SUN, I-W., J.R. Sanders, C.L. Hussey, 1989. Electrochemistry of Iron(III) and Titanium(IV) in the Basic $AlBr_3$-1-Methyl-3-ethylimidazolium Bromide Ionic Liquid. *J. Electrochem. Soc.*, Vol. 136, No. 5, p. 1415-1419.

SVERDLIN, A., 2003. Introduction to Aluminum In: G. E. Totten and D. S. MacKenzie eds. Handbook of Aluminum, Marcel Dekker Inc., 1-31.

TAIT, S. and R.A. Osteryoung, 1984. *Inorg. Chem.* 23, p. 4353.

TAKAHASHI, S., K. Ida, S. Mori, 1990. Electroplating of Aluminum from Room Temperature Molten Salt Baths. *Proc. Electrochem. Soc.* Vol. 90-17, p. 661-670.

TAKAHASHI, S., N. Koura, S. Kohara, M.-L. Saboungi, L.A. Curtiss, 1999. Technological and scientific issues of room-temperature molten salts. *Plasmas & Ions*, 2, p. 91-105.

TAULELLE, F. and I. Popv, 1983. *Polyhedron* 2, p. 889.

TROCMÉ, F., 1971. The Development of the "Magnetherm" Process. *In:* T.G. Edgeworth ed. *Light Metals*, 669-677.

TSUDA, T., C.L. Hussey, G.R. Stafford, J.E. Bonevich, 2003. Electrochemistry of Titanium and the Electrodeposition of Al-Ti Alloys in the Lewis Acidic Aluminum Chloride–1-Ethyl-3-methylimidazolium Chloride Melt. *J. Electrochem. Soc.*, 150 (4) p. 234.

US Bureau of Mines, 1963. Magnesium & Magnesium compounds, Report #IC 8201.

U.S. Environmental Protection Agency, 1995. Compilation of Air Pollutant Emission Factors AP-42, Fifth Edition, Volume I: Stationary Point and Area Sources, Research Triangle Park, NC. Available from: http://www.epa.gov/ttn/chief/ap42/ [Accessed 25 November 2004].

U.S. Department of Energy, 2003, U.S. Climate Change Technology Program – Research and Current Activities, (DOE/PI0001). Available from: http://www.climatetechnology.gov/library/2003/currentactivities/car24nov03.pdf [Accessed 25 November 2004].

WARD-CLOSE, C.M., A.B. Godfrey, 2005. Electrolytic reduction of metal oxides such as titanium dioxide and process applications. U.S. Patent 6,921,473.

WERNICK, I.K., N.J. Themelis, 1998. Recycling Metals for the Environment. *Annu. Rev. Energy Environ.*, 23, 465-497. Available from: http://arjournals.annualreviews.org/doi/pdf/10.1146/annurev.energy.23.1.465 [Accessed 18 March 2005]

WELCH, B. J., 1999. Aluminum Production Paths in the New Millennium. *JOM, 51 (5), 24-28.* Available from: http://www.tms.org/pubs/journals/JOM/9905/Welch-9905.html [Accessed 26 January 2005]

WILKES, J., J. Levisky, R. Wilson, C. Hussey, 1982. *Inorg. Chem.* 21, 1263-1264.

WILLIAMS, G.L. 1920. Electrodeposition of Aluminum. U.S. Patent No. 1,351,144.

WINAND, R., 1992. Electrocrystallization – theory and applications. *Hydrometallurgy*, 29, p. 567-598.

WU, B., R.G. Reddy and R.D. Rogers, 2005. Production, refining and recycling of lightweight and reactive metals in ionic liquids. U.S. Patent 6,881,321.

YE, C. and J.M. Shreeve, 2007. Rapid and accurate estimation of densities of room-temperature ionic liquids and salts. *J. Phys. Chem. A.* 111, 1456-1461.

YUYAMA K., R. Nozu, G. Masuda, T. Sato, 2007. Ionic liquid, method of dehydration, electrical double layer capacitor, and secondary battery U.S. Patent 7,167,353.

ZANELLO P., 2003. *Inorganic Electrochemistry*, The Royal Society of Chemistry, UK.

ZAWODZINSKI, T.A. Jr., R.T. Carlin, R.A. Osteryoung, 1987. *Anal. Chem.*, 59, 2639.

ZHANG, M., V. Kamavaram, R. G. Reddy, 2003. New Electrolytes for Aluminum Production: Ionic Liquids. *JOM*, Nov, 54-57.

ZHANG, M., V. Kamavaram and R. G. Reddy, 2004. Application of Fluorinated Ionic Liquids in the Extraction of Aluminium. TMS - Light Metals 2004, A.T. Tabereaux Editor, 315-318.

ZHANG, M. and R. G. Reddy, 2006. Advanced Processing of Metals and Materials, F. Kongoli and R.G. Reddy, Editors, TMS - Sohn International Symposium, Vol. 4, p. 237-246.

ZHAO, Y. and T.J. VanderNoot, 1997. Review: Electrodeposition of aluminium from nonaqueous organic electrolytic systems and room temperature molten salts. *Electrochimica Acta*, Vol. 42, No.1, p. 3-13.

List of Websites

http://www.webelements.com [Accessed May 23 2007]
http://webmineral.com/ [Accessed May 23 2007]
http://www.world-aluminium.org [Accessed May 23 2007] (International Al Institute)
http://www.magnesium.com/ [Accessed May 23 2007]
http://www.britannica.com/ [Accessed May 23 2007]
http://www.slv2000.qc.ca/bibliotheque/centre_docum/protection/028_a.pdf [Accessed May 23 2007]
http://www.crct.polymtl.ca/fact/index.php [Accessed May 23 2007] (FACT Software)
http://www.container_recycling.org [no longer available]
http://www.aluminiumcanrecycling.co.uk/plant_tour.php# [no longer available] (Alcan UK)